Modulation of the intraocular immune environment by viral gene transfer in mouse models of uveitis

Colin Chu

University College London

Submission for the degree of Doctor of Philosophy

‘I, Colin Chu confirm that the work presented in this thesis is my own. Where information has been derived from other sources, I confirm that this has been indicated in the thesis.'

8th September 2014

Abstract

Treatment options for severe uveitis are predominantly limited to systemic immunosuppressants, which are often accompanied by significant side effects. Ocular gene transfer, though, may serve as a sustained local immunomodulating therapy. New adeno-associated virus (AAV) serotypes were used to investigate gene therapy for uveitis in mouse models. Experimental autoimmune uveoretinitis (EAU) was used to model human disease; whilst endotoxin induced uveitis (EIU) was employed to dissect factors affecting immune suppression by AAV.

Refinement of AAV production processes improved the quality of vectors including AAV8, AAV9 and ShH10. Technical issues were assessed, confirming apical transgene secretion from RPE and examining the effects of endotoxin contamination.

New methods for the evaluation and quantitative scoring of disease severity in both animal models were developed, based on flow cytometry and optical coherence tomography (OCT) for EIU and EAU in *C57BL/6J* mice, respectively.

The complexity of the role of IL-10 in EAU became evident, and pronounced species differences between murine and human IL-10 were identified in EIU. Despite generating intraocular levels comparable to those of recombinant protein known to be effective, AAV-derived human IL-10 did not suppress EIU.

Gene delivery of soluble monomeric TNF receptors did not suppress EAU or EIU, and *in vitro* exhibited less TNF neutralising effects than an equivalent dimeric Fc-fusion protein. Local expression of this dimeric protein from different vectors however was also unable to attenuate EAU.

An NFκB-motif based promoter to regulate the expression of AAV-delivered transgenes in uveitis was developed in parallel. It demonstrated activation only in the presence of, and in proportion to the degree of inflammation in EAU.

Despite these advances, neither IL-10 nor TNF-inhibitors proved optimal targets for local suppression of intraocular inflammation by AAV. Further work is needed to assess the response of the eye to viral gene transfer in the context of uveitis.

Acknowledgments

I wish to firstly thank Pete Gardner, as my supervising post-doc, for his invaluable technical assistance, support and training throughout this project.

I am grateful to all senior members of the lab for their expertise and encouragement particularly Sander Smith and Ulrich Luhmann, as well as my supervisors Robin Ali and Andrew Dick.

James Bainbridge, Richard Lee and Samia Yazid have all provided excellent suggestions for improvement throughout, whilst Heather Kneale has been peerless in keeping everything running smoothly in every administrative aspect.

Selina Azam, Rand Al-Nackkash, Areta Michacz and Stuart Beattie have been instrumental members of the viral production laboratory. I am particularly grateful for their understanding throughout the instigation of my changes to AAV production.

Yanai Duran helped with subretinal injections, whilst Joana Ribeiro and Laura Abelleira Hervas provided expert technical help. Livia Carvalho and Sophia kleine Holthaus provided assistance and training with ERG, Claire Hippert provided Muller glia cultures, whilst stem cell derived RPE was investigated with the help of Anai Gonzalez-Cordero. I am particularly grateful to Anai for her constant support, friendship and unending enthusiasm!

It is not possible to thank all the many other members of the lab by name, but all have made my time not only one of great training and learning, but hugely enjoyable.

Table of Contents

Abstract **3**

Acknowledgments **4**

Table of Contents **5**

Abbreviations **11**

1 Introduction **12**

1.1 The burden of disease and unmet therapeutic needs for uveitis 12

1.2 Animal models of Uveitis 14

1.2.1 Experimental autoimmune uveoretinitis 14

1.2.2 Endotoxin induced uveitis 17

1.3 Pathogenesis and effector mechanisms in posterior uveitis 18

1.4 Ocular gene therapy and its application to treat uveitis 22

1.5 Adeno-associated virus 25

1.6 The immune response to AAV 28

1.7 Bacterial endotoxin and its implications for gene therapy 30

1.8 The approach of gene therapy for uveitis 31

1.9 Inflammation-regulated promoters 34

1.10 Systematic review of published pre-clinical studies of gene therapy for uveitis: translating knowledge of immunological mechanism into therapy 36

1.10.1 Interleukin-10 38

1.10.2 Tumour Necrosis Factor-α 40

1.10.3 Interferons 44

1.10.4 Interleukin-1 receptor antagonist (IL-1ra) 45

1.10.5 α-melanocyte stimulating hormone (α-MSH) 46

1.10.6 Interleukin-27 46

1.10.7 Antigen based therapies 47

1.11 Aims and Objectives 49

2 Materials & Methods **50**

2.1 Animal procedures 50

2.1.1 Animal strains and husbandry 50

2.1.2 Mouse anaesthesia 50

2.1.3 Ocular injections 50

1.1.1.1 Sub-retinal and intravitreal injection 51

1.1.1.2 Intra-cameral injection *51*
2.1.4 Induction of Experimental Autoimmune Uveoretinitis (EAU) *51*
2.1.5 Induction of Endotoxin induced uveitis (EIU) *52*
2.1.6 Dissection and extraction of non-ocular mouse tissues *52*
2.1.7 Topical Endoscopic Fundus Imaging (TEFI) *52*
2.1.8 OCT imaging and fundus fluorescein angiography *53*
2.1.9 Slit-lamp fluorescence fundal imaging of GFP *53*
2.1.10 Mouse electroretinography *53*
2.1.11 Dexamethasone treatment *54*
2.2 Initial AAV production 54
2.2.1 Plasmid production *54*
2.2.2 Recombinant AAV2/9 production *54*
2.2.3 FPLC purification of AAV2/9 using Sephacryl and Poros columns *55*
2.2.4 Recombinant AAV2 production *55*
2.2.5 SYPRO Ruby Gel analysis of AAV preps *56*
2.2.6 Dot blot based AAV prep titre determination *56*
2.3 Refined AAV production process 57
2.3.1 Recombinant AAV8 and ShH10 production process *57*
2.3.2 Recombinant AAV8 and ShH10 production *57*
2.3.3 Purification of AAV8 and ShH10 vectors *57*
2.3.4 Limulus Amoebocyte Lysate assay *58*
2.3.5 Viral titre calculation using qPCR *58*
2.3.6 Capsid separation process *58*
2.3.7 Electron microscopy of AAV *59*
2.3.8 AAV neutralising antibody and ELISPOT assays *59*
2.4 Lentivirus preparations 60
2.5 Molecular biological techniques 60
2.5.1 Basic cloning techniques *60*
2.5.2 Synthesis of mouse p75-Ig, viral and human IL-10 ..... *61*
2.5.3 Interferon gamma inducible promoter and NFκB constructs *61*
2.5.4 Luciferase assessment of promoter activity *62*
2.5.5 RNA extraction and cDNA synthesis for RT-PCR *62*
2.5.6 Quantitative PCR (qPCR) *63*
2.6 Histology and immunohistochemistry 63
2.6.1 Frozen sectioning *63*
2.6.2 Histological scoring of EAU using anti-CD45 ..... *63*
2.6.3 Retinal flat-mount dissection *65*

2.6.4 Frozen section and flat-mount immunohistochemistry *65*
2.6.5 Paraffin sections *66*
2.6.6 Microscopy *67*
2.7 Detection of cytokines 67
2.7.1 Enzyme linked immunosorbant assay (ELISA) *67*
2.7.2 BCA total protein assay *67*
2.7.3 Proteome Profiler *68*
2.8 Tissue culture 68
2.8.1 Maintainance cultures *68*
2.8.2 Recombinant cytokines *68*
2.8.3 Transfection of plasmids and transduction by AAV *68*
2.8.4 NFKB-eGFP based in vitro testing of TNF neutralising activity *69*
2.8.5 WEHI-164 cytotoxicity assay *69*
2.8.6 Muller-glia cultures *69*
2.8.7 Human ES and iPS cell derived RPE transwell cultures *70*
2.9 Preparation and analysis of eyes by flow cytometry 70
2.9.1 Tissue dissection *70*
2.9.2 Preparation of ocular tissues for analysis by flow cytometry *71*
2.9.3 Flow cytometers *71*
2.9.4 Absolute cell count using flow cytometry *72*
2.9.5 Primary conjugated antibodies used for flow cytometry *72*

3 Results 1: Optical Coherence Tomography can be used to characterise and define the severity of murine Experimental Autoimmune Uveoretinitis 74

3.1 Optical Coherence Tomography has the potential to surmount the limitations of current methods of EAU scoring 75
3.2 Pilot studies demonstrate the potential of OCT to detect pathology in the C57BL/6 mouse model of EAU 76
3.3 The development of key features of EAU can be systematically detected by OCT 77
3.4 The development of retinal features during EAU can be tracked by OCT 84
3.5 A minimally subjective OCT-based EAU scoring system correlates well with conventional histological assessment 85
3.6 OCT-based EAU scores were validated in an interventional experiment 90
3.7 Electroretinography of EAU in the C57BL/6 mouse is confounded by the induction protocol 91
3.8 OCT is possible, but not as suited to the *B10.RIII* model of EAU 93
3.9 Chapter summary 94

4 Results 2: Flow cytometry as a quantitative scoring system for endotoxin induced uveitis 95

4.1 Defining the standard EIU model using a flow cytometry based approach 96
4.2 Timecourse and compartmental analysis of EIU 99
4.3 Validation of flow cytometry for EIU from interventional experiments 101
4.4 Chapter summary 102

5 Results 3: Refinement of vectors and AAV production for ocular immunomodulation 103

5.1 Improving the AAV production and purification process 103
5.2 Injecting endotoxin contaminated material has detectable effects upon the eye 110
5.3 Testing a novel AAV genome-containing capsid enrichment technique 116
5.4 Perioperative high-dose corticosteroid does not affect the subsequent success of EIU suppression 120
5.5 EAU does not trigger a systemic response against subretinal delivered AAV8 122
5.6 Soluble transgene-encoded proteins are likely to be delivered into the eye, rather than secreted into the choroidal circulation 123
5.7 Chapter summary 128

6 Results 4: Gene transfer of IL-10 into experimental models of intraocular inflammation using modern AAV serotypes 129

6.1 Defining the parameters of the EAU model for modulation by gene therapy 129
6.2 Murine IL-10 supplementation by AAV9 in EAU 133
6.3 Refined production generated AAV8-mIL-10 avoids overt retinal toxicity but does not suppress EAU 137
6.4 EIU can be used to efficiently screen factors affecting effective suppression by viral gene transfer 141
6.5 Recombinant protein confirms the efficacy of human but not murine IL-10 in EIU 148
6.6 The suppressive effects of IL-10 upon EIU may be affected by the timing after induction 153
6.7 Levels of ShH10-derived human IL-10, comparable to those of suppressive recombinant protein fail to attenuate EIU 156
6.8 IL-10 is not an optimal target for the suppression of intraocular inflammation by gene transfer 159
6.9 Chapter summary 161

7 Results 5: Targeting TNF to suppress ocular inflammation by AAV-mediated gene transfer of soluble receptors 162

7.1 Gene transfer of monomeric soluble TNF receptors by AAV8 fails to attenuate EAU 163

7.2 Neither immunological differences between eGFP and hrGFP, nor the presence of the IRES construct explains the failure to suppress EAU 166

7.3 Avoiding retinal detachment by using ShH10 vector still does not permit the suppression of EAU by monomeric p55 168

7.4 Endotoxin-induced uveitis is not suppressed by ShH10-mediated soluble p55 and TNF inhibition can cause worsened infiltration 170

7.5 In vitro assessment confirms the superior efficacy of soluble p75-Ig fusion dimer over the monomeric form 173

7.6 Prophylactic AAV8 mediated p75-Ig dimer delivery to the eye still fails to detectably suppress EAU 175

7.7 Using the highly TNF driven *B10.RIII* strain model of EAU does not improve suppression by gene delivery of p75-Ig 176

7.8 Gene delivery of p75-Ig during established EAU demonstrates a trend towards reduced structural damage 177

7.9 Chapter summary 179

8 Results 6: An inflammation-responsive promoter can intrinsically regulate AAV-mediated transgene expression in the eye 180

8.1 Interferon Regulatory Factor 1 promoter 182

8.2 NFκB-motif promoter 185

8.3 Flow cytometric quantification establishes the dose-response of the NFκB-promoter in EAU 191

8.4 The NFκB promoter can be used as an *in vivo* reporter to examine aspects of the EAU model itself 194

8.5 Chapter summary 196

9 Discussion 198

9.1 OCT can be used to assess and score EAU 198

9.1.1 OCT Correlates with current EAU scoring methods and has distinct advantages 199

9.1.2 OCT can guide the discovery and characterisation of novel retinal features 200

9.1.3 OCT scoring and future directions 201

9.1.4 Interpreting OCT changes in human intraocular inflammatory disease by correlation of histopathology and OCT in murine EAU *202*
9.2 Flow cytometry provides a more comprehensive and quantitative assessment of the EIU model 203
9.3 Refinement of AAV production and the effect of Endotoxin contamination 206
9.4 Suppressing autoimmunity using interleukin-10 is complex 208
9.5 Local inhibition of TNF by p75-Ig may have a mild effect upon EAU 211
9.6 The NFκB-motif promoter drives inflammation-responsive transcription in proportion to the severity of EAU 214
9.7 Reconciling the failure to suppress intraocular inflammation and implications to future gene therapy for uveitis 216
9.7.1 Vectors *217*
9.7.2 Dose *218*
9.7.3 Therapeutic transgenes *219*
9.7.4 Local versus systemic therapy *219*
9.7.5 Animal models *221*
9.7.6 Immune privilege and implications for ocular gene therapy *221*
9.8 Conclusion 222
10 Figure and table titles 223
11 References 227
12 Published papers 250

Abbreviations

AAV	Adeno-associated virus
APC	Antigen presenting cell
BSA	Bovine serum albumin
CMV	Cytomegalovirus
CNV	Choroidal neovascularisation
DMSO	Dimethyl sulphoxide
EAE	Experimental allergic encephalomyelitis
EAU	Experimental autoimmune uveoretinitis
EIU	Endotoxin-induced uveitis
FBS	Fetal bovine serum
FCS	Fetal calf serum
gc	Genome copies
IFNγ	Interferon gamma
IRBP	Interphotoreceptor binding protein
ITR	Inverted terminal repeat
OCT	Optical coherence tomography
p.i.	Post-induction (of EAU)
PBS	Phosphate buffered saline
PCR	Polymerase chain reaction
TNF	Tumour necrosis factor

1 Introduction

Parts of this chapter have been published as a review:

Chu CJ, Barker SE, Dick AD & Ali RR.
Gene Therapy for Noninfectious Uveitis
Ocular Immunology and Inflammation (2012) 20(6), 394–405.

CJ Chu performed the literature search and wrote the draft manuscript. Other authors provided senior review and suggested revisions where appropriate.

1.1 The burden of disease and unmet therapeutic needs for uveitis

Uveitis is defined as inflammation of the uveal tract. This consists of the iris anteriorly, the ciliary body and then the choroid posteriorly. In clinical practice, a broad anatomical division has proven more relevant to patient management and international consensus was standardised in 2005.[1] The division similarly includes anterior (iris and ciliary body), intermediate and posterior uveitis (retina and choroid) or panuveitis if the whole eye is involved. Whilst anterior disease can be treated with drops, posterior disease often requires systemic medication. The majority of uveitis is caused by either direct infection (bacteria, virus, parasite), autoimmunity or a combined abnormal immune reaction to infectious agents. Common infectious causes include tuberculosis, syphilis, herpetic viruses and parasitic diseases such as toxoplasmosis. Commonly associated systemic autoimmune disorders include SLE, sarcoidosis, HLA-B27+ spondyloarthropathies, psoriasis, Behçet's and inflammatory bowel disease.[2]

Uveitis is a significant ocular disease, accounting for 10% of blindness in the working age population with a disproportionately large economic burden for its prevalence. Direct costs alone have been estimated at $242 million per year in the US.[3,4] Estimated to affect 115 per 100,000 of the Western

population, it typically follows a chronic relapsing course and can occur at any age.[5] There is wide international variation however, with prevalence rates of up to 310 per 100,000 in developing countries such as India, where infectious causes occur more frequently.[6] In the most recent published study the division was into 72% anterior, 6% intermediate and 22% posterior/panuveitis. Associated causes were established in only 37% of cases with the remainder classed as idiopathic.[7]

Current therapies for uveitis are not optimal and around 35% of patients remain visually disabled with a demonstrably poor quality of life.[8] Even in the mildest forms of uveitis such as the distinct group of anterior uveitis, treatment with topical corticosteroid demands often intolerably frequent drop regimes and many hospital visits around each attack. Steroid side-effects such as glaucoma and cataract can be more visually disabling than the disease being treated – particularly if chronic or recurrent therapy is required. Recently the introduction of depot formulations of corticosteroid for posterior disease (Ozurdex) have been shown to be a useful tool, but again require repeat administration and can result in the same complications.[9] For severe forms of uveitis with chronic posterior segment involvement, the mainstay of current therapy is based upon systemic immunosuppression, which now also includes the use of biological therapies such as antibody based anti-TNF agents.[10,11]

In many cases, patients have either isolated intraocular inflammation, or ocular involvement is the single manifestation of otherwise satisfactorily controlled multi-organ disease. The accompanying serious side effects of systemic immunosuppression are accepted in order to control local ocular disease and preserve vision. Current widely used second line agents after oral corticosteroids include T-cell inhibitors (tacrolimus and ciclosporin), anti-metabolites (methotrexate, mycophenolate mofetil, azathioprine) and alkylating agents (cyclophosphamide, chlorambucil).[12] Even with these potent immunosuppressants remission is not attained in 20-30% of patients at one year with long-term outcomes remaining poor in certain subgroups of

uveitis patients.[13,14]

Whilst novel treatments such as tumour necrosis factor-α (TNF) inhibitors have entered widespread use and are effective, they have the disadvantages of high cost, need for regular administration and significant systemic side effects.[15] All of the local (intraocular) treatments emerging from pharmaceutical pipelines are corticosteroid based, recombinant cytokines or monoclonal antibodies. Again, inherent limitations exist including uncertainty how best to select specific biologic therapy for individual patient groups, as well as risks associated with repeated intraocular injection for local therapy. Other therapeutic paradigms are clearly needed and gene therapy may provide a solution.

1.2 Animal models of Uveitis

1.2.1 Experimental autoimmune uveoretinitis

Experimental autoimmune uveoretinitis (EAU) is an animal model that phenotypically and biochemically mirrors human posterior uveitis. It has been central to our understanding of disease pathogenesis and the development and introduction of new therapies into clinical practice.[10,15] Spontaneous and inducible EAU can be obtained using a variety of wildtype animals and transgenic mouse strains to achieve different disease kinetics, severity and T-cell polarity of immune response. Common to all is the initiation of an antigen-specific immune response to retinal proteins. In the Lewis rat S-antigen is used, whilst different fragments of retinol-binding protein-3 (Rbp3 or IRBP) are used in mice. EAU can also be induced in rabbit, guinea pig and non-human primates.[16] The mouse has been the most widely used, due to the capacity for transgenic manipulation, relative availability of reagents and range of subtypes of EAU possible. Details of the different mouse models currently available are summarised in **table 1**.

Strain	Form	Year introduced
C57BL/6 mouse	Induced mild EAU with RBP-3 (1-20 residues).	1992[17]
B10.RIII mouse	Induced severe EAU with RBP-3 (161-180 residues).	1995[18]
Humanised HLA-DR transgenic mouse	Inducible EAU using human S-Antigen.	2003[19]
Aire-knockout mouse	Spontaneous EAU from failure of thymic selection.	2002[20]
TrP-HEL transgenic mouse	Spontaneous EAU designed to model Vogt-Koyanagi-Harada syndrome.	2006[21]
HEL-transgenic mouse	Spontaneous EAU by crossing IRBP-HEL mice with HEL-specific-TCR CD4+ cells.	2007[22]
IRBP R161H Transgenic *B10.RIII* mouse	Spontaneous EAU in mice with auto-reactive CD4+ T-cells to RBP-3.	2013[23]

Table 1. Common mouse models of inducible and spontaneous experimental autoimmune uveoretinitis.

EAU primarily causes posterior uveitis with marked chorioretinitis and minimal anterior segment involvement. In this project the *C57BL/6* strain has been predominantly used with the *B10.RIII* strain employed for selected experiments. *B10.RIII* mice mount a proportionately stronger reaction to the pathogenic RBP-$3_{164\text{-}180}$ peptide than *C57BL/6* strain mice do to their own most pathogenic RBP-$3_{1\text{-}20}$ peptide.[18] The result is both a more rapid and severe disease, with time from induction to peak around 12 days. Retinal detachments, extensive photoreceptor loss and posterior synaechae are common. In contrast, the *C57BL/6* strain does not reach peak disease until over 20 days and develops only moderate photoreceptor destruction.

Both inducible models are unrepresentative of human disease in that they are monophasic in nature with a single acute peak, followed by apparent resolution of inflammation. Most human posterior uveitis is chronic with periodic exacerbations. Recent work has however illustrated the more dynamic nature of post-peak EAU in the *C57BL/6* mouse, with accumulation of an exhausted phenotype CD8+ T-cell population.[24] Tissue and vascular

remodelling also occur and can be clearly identified in this phase by a variety of techniques.[25] As such, this model may be more appropriately chronic and less monophasic than first apparent.

Both inducible models require subcutaneous peptide delivery emulsified in complete Freund's adjuvant. This is predominantly a mineral oil and Mycobacterium tuberculosis mixture, which provides a strong and indispensable innate stimulus. This has however been shown to drive CD4+ T-cell polarisation towards a T_H17 dominant phenotype, compared to T_H1 in disease induced by adoptive transfer.[26] Additionally both - with a lower amount required in B10.RIII mice - need cotemporaneous systemic administration of Bordetella pertussis toxin for full expression of disease. Evidence shows that this not only weakens blood-retinal barrier integrity, but can also polarise T-cells towards a pathogenic Th1 phenotype.[27] These limitations of the induction process must be considered in any successful modulation of disease.

Whilst spontaneous models are ideally suited for testing therapeutic intervention in active disease, all publications using gene therapy to date have treated prophylactically. Spontaneous models of murine EAU arguably better reflect the true pathogenesis of uveitis, but are not widely available. *Aire*-deficient mice lack thymic expression of RBP-3 and develop spontaneous uveitis as autoreactive T-cells are not clonally deleted.[20] Transgenic mice with Hen egg lysozyme (HEL) expressed under the RBP-3 promoter are crossed with mice expressing HEL specific T-cell receptors on CD4+ cells. They develop severe spontaneous EAU by postnatal day 22 on average.[22] The same approach can be used with the Tyrosinase-related protein-2 promoter to give the mice an appearance similar to that seen in Vogt-Koyanagi-Harada syndrome.[21] With an 87% penetrance, mice developed characteristic vitiligo and uveitis. The most recent model is one generated in the *B10.RIII* strain that possesses a transgenic T-cell receptor specific for RBP-3. All mice develop detectable EAU by 12 weeks of age.[23]

A cautionary note arises from use of the HLA-A29 transgenic mouse line, generated as a model for the associated uveitic disease of Birdshot retinochoroidopathy.[28] A phenotype was seen only after one year and later suspected to be the *rd8* mutation found to contaminate all *C57BL/6N* lines.[29] For testing our gene therapy approach we used the *C57BL/6J* strain, confirmed free of the rd8$^{Crb1/Crb1}$ mutation that has confounded so many ocular studies to date.[30]

1.2.2 Endotoxin induced uveitis

Endotoxin-induced uveitis (EIU) as a surrogate model of human anterior uveitis was first described as part of a systemic response to the gram-negative bacterial cell wall component lipopolysaccharide (LPS).[31] It can be induced by peritoneal or footpad injections in rodents, as well as by direct intravitreal injection. Whilst predominantly an acute innate response to the presence of LPS, the rationale derives from the strong association of anterior uveitis and the HLA-B27 haplotype. Patients with this haplotype have long been characterised as more susceptible to gram-negative bacteria and chlamydial infections. Theories of molecular mimicry have been proposed, but the evidence is still inconclusive.[32]

In the mouse EIU is characterized by blood-aqueous barrier breakdown, activation of innate immunity and an ocular infiltrate predominantly comprised of polymorphonuclear leukocytes. Historically this has only been defined using immunohistochemistry with OX-42 staining for neutrophils. A smaller number of monocytes enter the eye in the later stages of EIU, which have only been identified using the ED1 marker. Changes in other cells types including T-cells have not been widely observed, though it is suspected that a decrease in the number of resident mast cells reflects activation and degranulation.[32]

After systemic induction, barrier breakdown can be detected after two hours, with leukocytes infiltrating the ciliary body and iris by 12 hours. Maximum cell

counts peak around 24 hours, with some optic disc infiltration, however the absolute number is fairly low. Due to mild severity local intravitreal injection of LPS has been used and results in over a hundred-fold greater number of infiltrating cells over a more rapid timecourse.[33] It is still unclear why the disparity exists between the two routes and in practice they are treated as separate entities. Both are believed to self-resolve without tissue damage though over unclear timespans. Severity has classically only been assessed by either paraffin histology and semi-quantitative cell counts of haematoxylin-stained cells, or with total protein assays on aqueous humour.[34]

1.3 Pathogenesis and effector mechanisms in posterior uveitis

Uveitis is typically considered as an autoimmune disease to retinal proteins including S-antigen and RBP-3, orchestrated by $CD4^+$ T cells that secrete signature cytokines - either interferon gamma ($IFN\gamma$) from T_H1 or interleukin-17 from T_H17 cells. Concurrent activation of the innate immune response occurs and is also central to the overlap between the autoimmune, autoinflammatory and infectious aetiology of this heterogeneous disease.[16]

Mechanisms of thymic escape of autoreactive T-cells and a breakdown in peripheral tolerance are thought to partly underlie the initiation of the disease in humans. Supportive evidence of the importance of thymic deletion comes from studies of animal models of uveitis. Only strains lacking thymic expression of IRBP are susceptible to the induction, whilst AIRE-knockout mice develop spontaneous disease.[16,35] FoxP3+CD25+ T_{reg} cells form part of the peripheral tolerance mechanism and are able to suppress pathogenic auto-reactive T-cell activation. They are likely to be important as genetic inactivation of *FOXP3* by mutation leads to extensive systemic autoimmunity and uveitis in humans.[36] Whilst the exact triggers leading to the initiation of uveitis remain unclear, the effector pathways and cell types have been interrogated using animal models of EAU (Summarised in **Figure 1**).

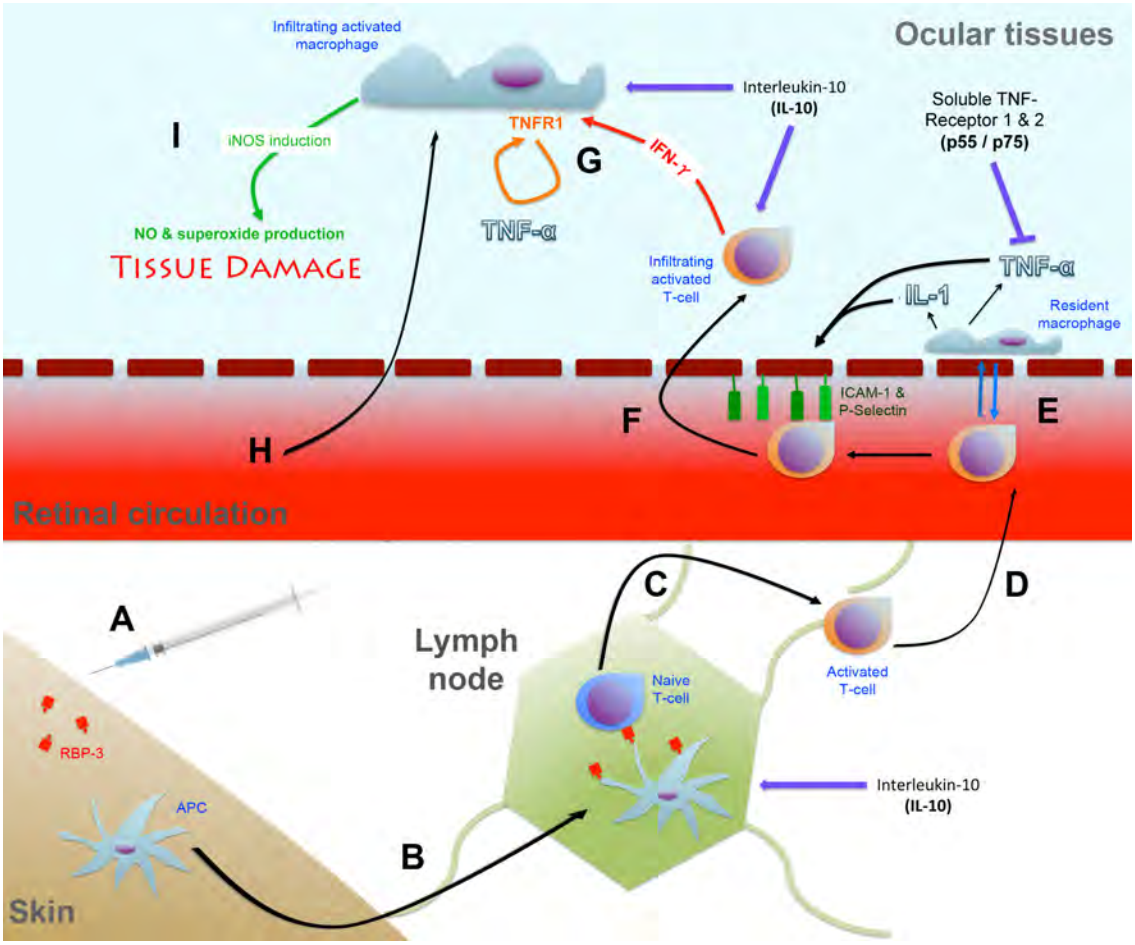

Figure 1. Immunological mechanisms of initiation and effector pathways active in the inducible EAU model. Subcutaneous injection of RBP-3 in complete Freund's adjuvant **A)** activates resident APCs such as dendritic cells, which take up the antigen and **B)** traffic to regional lymph nodes. There RBP-3 fragments are eventually presented **C)** to naive auto-reactive T-cells, which become activated and **D)** home to the blood-ocular barrier. **E)** Early interaction occurs with resident perivascular myeloid cells. The resulting production of pro-inflammatory cytokines such as IL-1 and TNF leads to multiple effects. **F)** This includes the upregulation of ICAM-1 and P-selectin, and degradation of the integrity of the blood-ocular barriers that leads to further infiltration of the eye with activated lymphocytes and monocytes. **G)** In the tissue, predominantly T_H1 polarised T-cells produce IFNγ, which activates myeloid cells. **H)** These then produce TNF to further increase infiltration into the eye. TNF also acts via TNFR1, to cause further activation and the induction of nitric oxide synthetase. **I)** It is the resulting peroxinitrite radicals that lead to photoreceptor loss and tissue damage. Potential anti-inflammatory targets such as soluble receptors might inhibit the effects of TNF at multiple stages (purple bar). Evidence suggests that IL-10 can suppress T-cell and macrophage activation, as well as preventing initial antigen presentation (purple arrows).

In inducible strains such as *C57BL/6* mice their permissive H-2^K MHC haplotype is required to respond to subcutaneous RBP-3 mixed with complete Freund's adjuvant.[17] Antigen-presenting cells traffic to lymph nodes

and establish a CD4+ T-cell antigen specific immune response against RBP-3. These CD4+ cells have been shown to be sufficient alone to establish EAU using adoptive transfer experiments.[37] Acitvated CD4+ cells enter the eye and establish disease through the recruitment of myeloid cells. CD4+ cells have been shown to be of mixed T_H1 and T_H17 polarity when recovered from the eye dependent upon the method of induction. They are capable of secreting high levels of IFNγ or IL-17 respectively, which lead to inflammation of the intraocular environment.[38] IFNγ specifically has been implicated as a key cytokine, licencing myeloid cells to produce TNF. In an autocrine manner, TNF upregulates nitric oxide synthetase to produce destructive peroxinitrite radicals that ultimately cause tissue damage and photoreceptor loss.[39]

The clinical phenotype of this underlying process can be followed *in vivo* in *C57BL/6* mice.[40] Whilst timing varies slightly, typically fundal changes begin around day 14 with optic disc swelling and infiltrate around peripheral collecting ducts. At peak disease around day 25 disc swelling has extended into vasculitis and intraretinal lesions are seen. Post-peak, progressive apparent scaring occurs, with disc swelling resolving.

Flow cytometry has identified the cell types involved during EAU across the same timepoints.[41] A summary of the key markers used for assessment of EAU and EIU are listed in **Table 2**. In the *B10.RIII* strain, three stages of disease can be appreciated in the retina. Before disease occurs, there are negligible numbers of CD4+ T-cells and the small CD11b+ cell count is contributed by the resident parenchymal and perivascular microglial population. In the prodromal phase at 5 days small increases are seen, but it is at peak disease that an explosion in CD4+ and CD11b+ cell counts occurs. Characterisation of the CD11b+ population with Ly6G confirmed a large neutrophil component.[42] The remainder of the CD11b+ population may comprise myeloid derived suppressor cells (MDSCs), as activated CD4+ cells are suppressed following co-culture with this population. The post-peak phase of secondary regulation was typified by globally reduced cell counts,

with an increase in the percentage of FoxP3+CD4+ Tregs and the accumulation of an exhausted phenotype CD8+ population occurs.[24]

Marker	Description	Cell types
CD45	Surface glycoprotein known also known as leukocyte common antigen.	White blood cells (all haematopoietic cells except platelets and mature erythrocytes)
CD11b	Cell surface integrin (αM) involved in adhesion and trafficking.	Predominantly on cells of the myeloid lineage.
Ly6G (1A8 clone)	Component of the myeloid differentiation antigen Gr-1.	Predominantly present on peripheral neutrophils.
Ly6C (HK1.4 clone)	Component of the myeloid differentiation antigen Gr-1.	Predominantly present on inflammatory monocytes.
Gr1 (RB6-8C5 clone)	A glycosylphosphatidylinositol-linked protein and composite epitope of Ly6G and Ly6C.	Expressed on granulocytes and macrophages.
CD4	Immunoglobulin superfamily member TCR co-receptor.	Predominantly thymocytes and helper T-cells
CD8	Immunoglobulin superfamily member TCR co-receptor.	Predominantly thymocytes and cytotoxic T-cells
CD94	C-type lectin involved in control of NK cell activation.	Present on all NK and NKT cells

Table 2. Immunological cell surface markers used in flow cytometry of mouse EAU.[42-44]

In terms of the cytokine environment within the eye during EAU, multiple pro-inflammatory proteins other than IFNγ and IL-17 have been detected. IL-1, IL-2 and IL-6 as well as TNF play critical roles and are elevated during disease initiation and peak inflammation.[45] During later phases of disease levels of these cytokines fall and those associated with resolution such as IL-10 increase.[26] This partly reflects changes in cell populations, not only T-cells but myeloid cells. Depletion of monocytes using the antibody MC-21 after peak disease in *C57BL/6* mice leads reduces Treg numbers in the eye and worsens histological damage.[46,47]

1.4 Ocular gene therapy and its application to treat uveitis

Gene therapy is the strategy of exogenously producing a target protein encoded by DNA (known as the transgene) in selected cells. The mechanism of DNA transfer is broadly divided into those implemented by viral and non-viral vectors. Various non-viral gene transfer techniques have been used in the eye, but thus far they are without exception, inefficient and limited in duration compared with effective viral vectors. The most promising viral vectors to date for use in the eye are those based on adeno-associated virus (AAV) and lentiviruses. Both are currently being used in clinical trials of ocular gene therapy and their use has been recently reviewed.[46] Details of the key vectors used for gene transfer are summarised in **Table 3**.

Results from three independent clinical trials of ocular gene supplementation therapy for a form of early-onset retinal dystrophy suggest that AAV-based gene therapy can result in improved vision in patients.[48-50] These promising trials have thrust the eye into the limelight as one of the most promising target tissues for gene therapy, and as a result, the research effort into ocular gene therapy has expanded, both in academic and commercial settings. The rapid progress of gene therapy for ocular disorders, compared to therapy for many other conditions, highlights the suitability of the eye as a target for gene therapy.

The eye is compartmentalised, small and isolated from the rest of the body by the blood–retinal barrier. Cells can be targeted effectively either by intravitreal injection or subretinal delivery of relatively modest doses of vector. Another advantage of ocular gene therapy, and retinal gene therapy in particular, is that the target cell populations are typically very stable. The lack of cell division allows the use of non-integrating vector systems for sustained transgene expression and also reduces the risk of malignant transformation of cells following the use of integrating vector systems. The age and disease status of the retina itself can also affect transduction patterns. For example, lentiviral vectors can transduce photoreceptors only in early post-natal stages but fail to do so in the presence of the *rd1*

degeneration.[51]

Vector	Posterior segment cells transduced		Anterior segment cells transduced	Duration of gene expression	Comments
	Intravitreal injection	Subretinal injection			
AAV2	Ganglion cells	Photoreceptors and RPE[52]	Trabecular meshwork[53]	Long-term	
Pseudotyped AAV2/8	None	Photoreceptors and RPE[54]	Minimal unless self-complementary genome[54]	Long-term	Faster onset, less vector-directed immune responses and stronger expression than rAAV2
Pseudotyped AAV2/9	Ganglion cells[55]	Photoreceptors, RPE and Muller cells[56]	Photoreceptors and RPE only	Long-term	Muller cell transduction at high titre only
AAV ShH10	Muller and ganglion cells[57]	Unpublished to date	Unpublished to date	Long-term	Engineered by *in vivo* evolution to target Muller cells
Lentivirus (HIV1)	None	RPE	Corneal endothelium, iris and trabecular meshwork[58]	Long-term	
Adenovirus	Ganglion cells	RPE	Trabecular meshwork[59]	Short duration due to immune mediated clearance	Use of this vector has been limited by strong inflammatory responses
Ciliary muscle electro-	None		Ciliary muscle[60]	Short-term	

transfer				
Naked plasmid DNA	Unknown	Unclear	Short-term	Expression only confirmed by detection of transgene products in the aqueous fluid and retina[61]
Nanoparticles	RPE[62]	Unknown	At least 3 months	Various approaches and formulations

Table 3. Comparison of the different methods of gene transfer used in ocular gene therapy. *Adapted from Chu CJ et al. (2012). Gene Therapy for Noninfectious Uveitis. Ocular Immunology and Inflammation, 20(6), 394–405.*

Non-viral electrotransfer of plasmids into the ciliary muscle is rapid and repeatable, but transgene expression is transient and at relatively low levels.[60,63] This technique has been used to reduce disease severity following delivery of plasmids encoding chimeric TNFα-receptors in the rat EAU model. However, the beneficial effect appeared to be rapidly lost and translation into human therapy for chronic disease is unlikely due to the frequent need for repeat injection.

A number of viral vectors have been used to deliver immunomodulatory genes in various animal models of uveitis. Although the first reported study on the development of gene therapy for uveitis utilised a second generation adenoviral vector to treat EAU in rodents, the utility of adenoviral vectors for this purpose is limited by the strong immune responses they elicit.[59] Lentiviral vectors are able to mediate long-term and efficient gene delivery to cells in the anterior chamber and the retinal pigment epithelium, with limited immune responses compared to adenoviral vectors and are thus potentially usefully for the treatment of uveitis. HIV-1 based vectors have been used to

transduce anterior segment structures in order to treat EIU.[34]

1.5 Adeno-associated virus

Vectors based on AAV, a single stranded DNA parvovirus of the genus *Dependovirus*, are now the most commonly used type of vector for ocular gene transfer. This small (25nm diameter) non-pathogenic virus was first identified as a contaminant in isolates of adenovirus and is currently the most promising vehicle for gene delivery to the retina and photoreceptors in particular. Identification of a large number of serotypes has further enhanced the utility of AAV as a vector platform. Many of these variants have unique transduction characteristics defined by their capsid, that can be used to target different ocular cell types.[64]

Production of recombinant AAV for research and therapeutic purposes is based upon the AAV2 genome, though often packaged within the capsid of another serotype in a process known as capsid pseudotyping. For example, wildtype AAV2 could be referred to as AAV2/2, whilst capsid psuedotyped AAV8 serotype would be AAV2/8.[54] In common usage and within this thesis, vectors labelled as AAV2, AAV8, AAV9, and ShH10 should be assumed to contain the recombinant AAV2 genome.

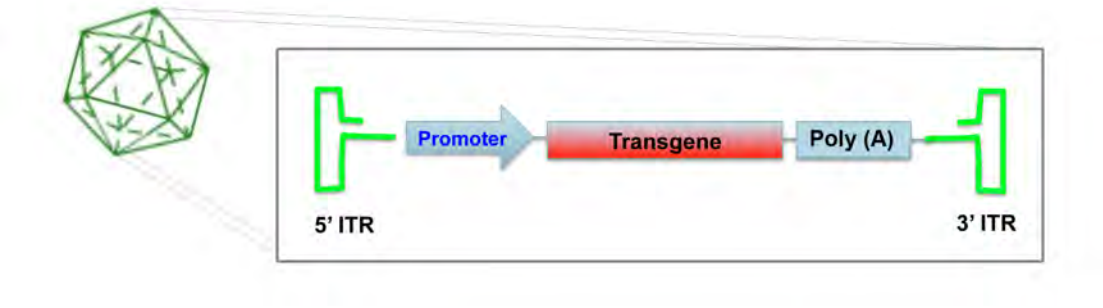

Figure 2. Schematic of recombinant AAV. Note the icosahedral capsid arrangement that contains the genomic construct highlighted. The transgene follows the promoter and is typically followed by a SV40 poly-adenylation site.

The key component of the AAV genome, responsible for most of its biological function once inside a target cell, is the two diametrically positioned inverted-terminal repeats (ITRs). These 125bp palindromic repeats of single stranded

DNA form secondary structures at both the 5' and 3' ends and enclose the viral genes *Rep* and *Cap* required for the native lifecycle.[65] In recombinant AAV, these genes have been removed and the desired promoter and target transgene can be inserted, usually followed by an SV40 poly-adenylation site **(Figure 2)**. AAV lacks an envelope, but has an icosahedral capsid formed of sixty proteins of three varieties – VP1, 2 and 3 in a 1:1:10 ratio respectively. These enclose the genomic construct and the ITRs have been shown to be crucial to efficient packaging. Many capsids will spontaneously assemble and lack a viral genome. They are known as 'empty' or 'unpackaged' capsids and during recombinant AAV2 production can account for over 90% of the population.[66] They lack the ability to effect gene expression but can still trigger antiviral immune responses.

AAV enters cells using receptor-mediated endocytosis, the target of which varies with serotype. For example, wildtype AAV2 predominantly binds to surface Heparan-sulphate proteoglycan whilst AAV9 binds N-linked galactose.[67] Low pH then allows endosomal escape, the single-stranded genome enters the nucleus and second-strand synthesis occurs. The genome then remains as long-lasting episomal concatemers, which enable expression in non-dividing cells. AAV otherwise will only replicate itself in the presence of active adenoviral infection.[65]

New serotypes are still being characterised and refinements in vector efficiency have been engineered by mutating capsid surface tyrosine residues.[55] Further optimisation by engineering a self-complementary viral genome has been shown to increase the level and speed of transgene expression by eliminating the requirement for intracellular conversion into double-stranded DNA.[68] One significant limitation is AAV packaging capacity, which is limited to 4.9kb of DNA - significantly less than adenoviral or lentiviral vectors. Groups have extended this to 9kb using a *trans*-splicing approach, splitting the transgene across two AAV vectors with appropriate splice donor and acceptor sites. This results in lower efficiency of expression however.[69]

AAV has historically been defined as non-integrating, however wildtype AAV2 does undergo relatively site-specific integration in a region known as AAVS1 on human chromosome 19 in up to 70% of integrations. Whilst the recombinant forms of AAV used lack the required Rep78, Rep68 and IEE elements for integration, emerging evidence is that largely random genomic integration does occur.[70] The frequency is very low however, estimated at less than 0.1% of infections in systemic studies. Significant carcinogenesis has not been associated with these events in long-term mouse, dog or non-human primate studies.[71,72] In over two hundred patients treated with rAAV in clinical trials to date, no tumours have been reported.[65]

In the eye, the transgene and its target cell type, determine the choice of AAV serotype and administration site. For instance, AAV2 transduces ganglion cells following intravitreal injection whereas sub-retinal administration results in transduction of photoreceptors and RPE cells. Intracameral administration with a self-complementary genome variant permits transduction of the trabecular meshwork, iris, corneal epithelium and ciliary body.[53] Whilst expression of anti-inflammatory proteins from the RPE may treat retinitis, it is not certain if diffusion might occur to affect the anterior chamber, or if anterior structure transduction would affect retinal disease.

Several serotypes have been used in the course of this project **(Table 2)**. AAV2 is the most extensively characterised, the first to be discovered and the first serotype used in an ocular clinical trial.[73] As highlighted, its transduction characteristics are dependent upon site of delivery within the eye. The main limitation is the slow speed of onset, requiring over three weeks to approach near peak levels of expression. To improve upon these characteristics searches for other naturally occurring serotypes was undertaken. Both AAV8 and AAV9 serotypes were isolated from non-human primate tissue.[74] When generated as AAV2/8 and injected into the subretinal space of mice, strong RPE and photoreceptor expression was seen after even one week. Furthermore, final peak levels at four weeks appeared to be higher in photoreceptors with AAV8 than with AAV2.[54] A similar profile was

seen with AAV2/9, though additional Muller cell transduction was seen following subretinal injection.[56] AAV9, unlike AAV8 can also transduce ganglion cells after intravitreal injection.[55] ShH10 is a newly created artificial AAV serotype based upon AAV6. It was generated by a technique of directed *in vivo* evolution, in an attempt to transduce Muller cells efficiently following intravitreal injection. Combined with a tyrosine to phenylalanine mutation in the capsid, has been claimed as able to generate widespread transduction of Muller cells in a single injection.[57]

1.6 The immune response to AAV

AAV generally elicits minimal immune responses in an un-inflamed eye compared to vectors such as adenovirus and most do not efficiently transduce antigen presenting cells, making them potentially ideal for gene transfer in a uveitic eye.[75] Whilst it might be justifiable to treat posterior uveitis by subretinal injection of vector, isolated anterior uveitis would probably require delivery either by intracameral or intravitreal injection. These routes of administration would also be usable for the treatment of posterior uveitis, but they may not be as optimal as subretinal administration since the anatomical site of injection appears to influence vector-directed immune responses.

Studies in mice suggest that subretinal administration of high doses of AAV vectors can be achieved without developing a neutralising antibody response to capsid antigens.[76] This has also been observed in clinical trials, although transient immunosuppression was used to minimise the risk of immune responses in patients.[48-50] In contrast, the more clinically desirable route of intravitreal administration can result in systemic capsid-directed immune responses in animal models, which generate serum neutralising antibody levels nearly equivalent to intramuscular injection. Although initial administration does result in transgene expression, this response negates therapy in the contralateral eye or repeat ipsilateral treatment.[77] Using different capsid serotypes and transient immunosuppression may partly

circumvent this problem in patients, but immunologically intravitreal administration remains a greater challenge.

Other factors affect the immune response to gene transfer including the vector, dose, the transgene itself and the local inflammatory state. Common concerns are that pre-existing inflammation from chronic uveitis could counter effective transgene expression whilst vector directed responses might exacerbate the degree of intraocular inflammation. Indeed gene therapy for systemic disease, where large intravenous doses of AAV are given has been particularly hampered by vector-induced immune reaction.[78] Initially, this is due to complement activation and capsid-directed neutralising antibodies from prior exposure to wildtype AAV. Whilst 60% of the general population are seropositive for AAV2, other serotypes such as AAV8 are less prevalent and pre-existing antibodies are detected in only 20% of individuals.[79]

The foreign protein of AAV capsids is not the only target of immune responses. Transgenes producing neo-antigens, such as the monogenic replacement of wildtype protein into a completely deficient host, trigger adaptive immune mechanisms as thymic deletion of autoreactive T-cells would not have occurred. This has been well documented in systemic applications such as for Duchenne muscular dystrophy.[80] Following subretinal administration of RPE65 protein into deficient patients, no RPE65-specific responses have been seen, presumed secondary to the immune deviant properties of the subretinal space.[48-50]

Differences with human immunology need to be considered. Systemic AAV used in human clinical trials generates robust cytotoxic CD8+ T-cell responses that clear transduced cells.[81] Mouse models do not reflect this and mice rarely develop T-cell responses to AAV, unless persistently re-challenged. Even if a CD8+ T-cell response can be detected, significant clearance of transduced cells is not seen.[82] Effective humoral neutralising antibody responses however are seen.

The innate immune response to AAV is more poorly characterised. There are clearly acute contributions by the complement system and Muller glia have been observed to express the activation marker GFAP in response to AAV.[83] Resident retinal microglia clearly have a role to play and indications are that activation occurs after subretinal injection of AAV above PBS control (Ulrich Luhmann, personal communication). The effects of innate ligands, such as unmethylated CpG islands in AAV genomes have been also investigated and shown to be one anti-viral component through the activation of endosomal TLR9, such that both transgene and capsid contribute to any immune response.[84] Endotoxin contamination during AAV production is likely and not routinely tested for. It is unclear if this may be important when using AAV for immunomodulation.

1.7 Bacterial endotoxin and its implications for gene therapy

Endotoxin was first described by Richard Pfeiffer in 1894, as a heat-stable toxin discovered in *V.cholerae*. Later work confirmed the pyrogenic properties of this compound and its origin as a component of the outer leaflet of the outer cell membrane of Gram-negative bacteria. It was not until 1947 that endotoxin was discovered to be bacterial lipopolysaccharide (LPS).[85] The primary structure is comprised of variable length O-antigen polysaccharide chains linked to a lipid A core. The spontaneous mouse mutant line *lps* allowed the exact signalling pathway to be discerned, as it was found that a single point mutation led to complete unresponsiveness to endotoxin. In 1998 the mutation was localised to the TLR4 receptor.[86] It is now known that the main mechanism of endotoxin-induced fever is through the triggered release of TNF from TLR4 activated macrophages.

The toxin is extremely resistant to removal and is not cleared by standard autoclaving procedures. These are likely to only increase the degree of contamination through lysis of environmental gram-negative bacteria. Dry heat at 180°C for three hours is typically required for inactivation. Unless specific steps are taken all standard laboratory experiments should be assumed to have endotoxin contamination. The main FDA approved testing

method is based on extracts from the horseshoe crab – the Limulus amoebocyte lysate (LAL) assay. LPS reacts with the lysate to trigger a clotting cascade-like process that results in a gel clot formation. Serial dilutions and calibration against a standard curve can allow the level of quantification, typically expressed as endotoxin units (EU/ml).[87]

Whilst known to be a potent inflammatory stimulus, no studies examining the effect of endotoxin upon AAV-mediated gene transfer have been published and no consensus exists on acceptable research grade levels. Tolerable levels are currently determined by individual judgement based upon target organ and condition. GMP produced clinical grade AAV is typically assured to below 10EU/ml, but this is not an internationally agreed standard.[88] In the eye, the response to LPS has been studied in the acute form of EIU. The focus has been upon the acute recruitment of neutrophils and transient degradation of blood-ocular barriers, but long-lasting sequelae have not been examined.[32] In terms of retinal cells, both Muller glia and photoreceptors have been observed to express TLR4. In culture activation by LPS has been shown to reduce photoreceptor survival after oxidative stress, in line with similar observations of CNS neuron-induced damage.[89] Worsened intraocular inflammation is also possible, as resident microglia have been shown to respond to LPS in a dose-dependent fashion, progressively activating and generating pro-inflammatory cytokines in concert with Muller cells.[90] In the context of an adaptive inflammatory response such as in uveitis, it is also important to consider that LPS through TLR4 signalling has the potential to alter CD4+ T-cell polarisation, preferentially inducing IL-17 production. If unrecognised, this could potentially confound any therapeutic manipulation of the immune environment.[91]

1.8 The approach of gene therapy for uveitis

While still early in development, gene therapy approaches have the potential to provide constitutive, self-regulating, and enduring suppression of intraocular inflammation following a single treatment. The potential advantages and limitations are summarized in **Table 4**.

Advantages	Disadvantages
Long-term production of therapeutic protein following a single treatment.	Initial need for intraocular injection.
Local therapy with no systemic immunosuppression.	Difficult to reverse without tissue destruction.
Combined injection of multiple vectors encoding different therapeutic transgenes is possible.	Transgene and vector-directed immune responses can occur.
Inflammation-regulated promoter control is possible, to restore a form of homeostasis.	

Table 4. A comparison of gene therapy against other treatment approaches for uveitis.

Current approaches in experimental animal models involve intraocular delivery of vectors encoding anti-inflammatory molecules in order to modulate disease and restore homeostasis. This might be achieved by delivering molecules that either have a direct anti-inflammatory effect or neutralise circulating pro-inflammatory cytokines. To date, potential therapeutic strategies have utilised recombinant cytokines, a soluble pro-inflammatory cytokine receptor or a natural antagonist. Strategic approaches using virus-based gene therapy are summarised in **Figure 3**. Selection of transgene has been based primarily on targets believed to be critical in animal models such as murine experimental autoimmune uveoretinitis (EAU), endotoxin-induced uveitis (EIU) and experimental autoimmune anterior uveitis (EAAU). Although the exact cause of human uveitis is unknown, animal models inducing an immune response towards retinal antigens have proven an invaluable starting point.

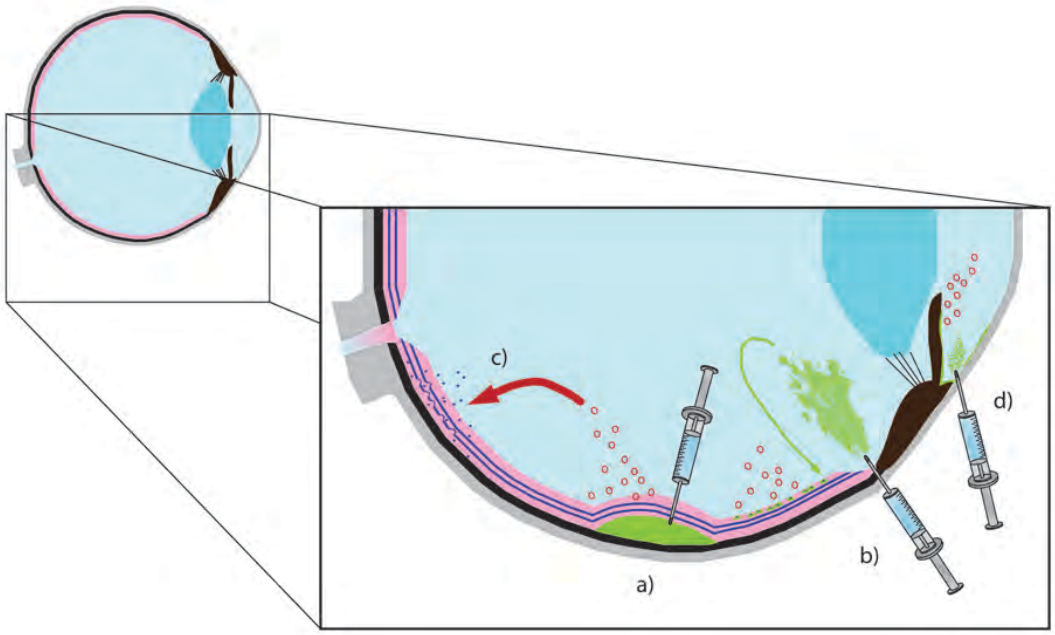

Figure 3. Strategy of viral vector-mediated gene therapy for uveitis. a) Subretinal injection of AAV vectors results in photoreceptor and/or RPE transduction. **b)** Intravitreal administration of AAV2 transduces only ganglion cells. **c)** Attenuation of EAU has been demonstrated following AAV vector-mediated expression of soluble anti-inflammatory proteins such as IL-10, IFN-α, and IL-1ra. **d)** AC injection of lentivirus results in transduction of iris, corneal endothelium and trabecular meshwork. Suppression of EIU has been demonstrated following lentiviral-mediated expression of IL-1ra and IL-10. *Adapted from Chu CJ et al. (2012). Gene Therapy for Noninfectious Uveitis. Ocular Immunology and Inflammation, 20(6), 394–405.*

Although gene therapy may eventually be used to treat relapsing anterior uveitis, the major impact clinically and therefore likely to be used initially in trials, is for the treatment of posterior uveitis. Posterior segment involvement accounts for the greatest burden of visual disability, even with optimal biologic treatment. Initial control of inflammation will inevitably continue to use conventional immunomodulatory therapies, but once in a chronic indolent phase, gene transfer may provide superior long-term control. Patients who have persistent inflammation on maximal therapy, visual decline and isolated ocular involvement would be ideal candidates for proof-of-principle human studies.

There are, however, still a number of challenges in order to take gene therapy for uveitis through to clinical application. These include determining

which approach (combination of vector, gene(s), promoter and route of administration) might be most effective in animal models, whose appropriateness, particularly given the heterogeneous nature of uveitis, is unclear. The effect of gene transfer into an already inflamed environment, particularly if the blood-retinal barrier is not intact, must also be determined.[92] Finally, long-term animal studies are also required in order to determine whether the constitutive expression of specific immunomodulatory molecules may eventually lead to toxicity. Alternatively, to address this final issue and as a final technical refinement, the use of inducible promoters responsive to inflammation were examined.

1.9 Inflammation-regulated promoters

All promoters used so far in gene therapy for uveitis have been essentially constitutive. Whilst one study used a tetracycline-inducible system, it required constant administration of exogenous Doxycycline to activate.[93] This 'Tet-on' promoter is described as leaky, in that basal transcription occurs in the absence of tetracycline. Furthermore it is based upon prokaryotic sequences and so unlikely to be approved for human use.

The ideal promoter would be self-regulatory, activating transcription of the anti-inflammatory transgene only in the presence of and in proportion to local inflammation. In other organ systems, promoters based upon pro-inflammatory cytokine promoters have been used, and these are summarised in **Table 5**. No publications have yet employed a self-regulating promoter in the eye.

Promoter details	Vector and transgene	Target tissue	Year published
Hybrid IL-1/IL-6 promoter	Adenovirus-IL-4	Articular chondrocytes	2007[94]
	Lentivirus-IL-10		2011[95]
Human neurotropic	AAV1 Glial-cell	Hippocampal	2013[96]

polyoma virus NFκB segments	line derived neutrotropic factor (GDNF)	neurons	
IL-6 promoter	Adenovirus LacZ and hIL-10	Lung parenchyma	2010[97]
HIV derived NFκB repeats	AAV5 Human sTNR1-Fc fusion protein	Articular chondrocytes	2007[98]
Intermediate-early CMV promoter (spontaneously disease inducible)	rAAV2 LacZ	Articular chondrocytes	1999[99]
Complement component C3 & HIV promoter fusion	Adenovirus-hIL-10	Articular chondrocytes	2002[100]
E-selectin promoter	Lentivirus-IL-10	Articular chondrocytes	2012[101]

Table 5. Inflammation-regulated promoters published for use in gene therapy.

It was felt the most appropriate strategy to employ in gene therapy for uveitis would use promoters responsive to IFNγ and TNF. Both these pro-inflammatory cytokines are known to be pivotal to EAU pathogenesis, are almost undetectable in the absence of disease, and fall rapidly during resolution of inflammation.

IFNγ signals via the Janus-activated-kinase (JAK/STAT) system. When it binds to its surface receptor IFNγ-receptor 1, this associates with *JAK1* and then recruits IFNγ-receptor 2. This co-receptor is constitutively associated with *JAK2* and receptor convergence leads to auto-phosphorylation and activation of both *JAKs*. These then phosphorylate STAT1 on the 701-tyrosine residue which triggers homodimerisation and translocation into the nucleus. Only STAT1-STAT1 dimers bind to conserved regions called gamma-activated sequences (GAS) to trigger IFNγ-specific transcription. The DNA consensus sequence has been defined as TTC/ANNNG/TAA.[102] Activation is regulated by negative feedback from SOCS1, itself transcribed in response to STAT1 signalling which can bind and directly inhibit JAK

enzymatic activity at the IFNγ-receptor complex by acting as a pseudo-substrate.[103]

TNF predominantly acts through the canonical-NFκB signalling system. Soluble trimeric TNF binding to TNFR1(p55) triggers conformational changes leading to the recruitment of the TRADD-adaptor protein.[104] This in turn recruits TRAF2 and RIP, which activate the IKK complex. This complex phosphorylates IκBα targeting it for ubiquitin-mediated proteosomal degradation and liberating NFκB dimerization partners such as RelA and p50. These enter the nucleus and bind to NFκB response element motifs (e.g. GGGAATTTCC) to drive transcription of a wide array of genes. MAPK signalling is also triggered by TNF. Negative regulators are active such as the de-ubiquitinase A20, which is induced by NFκB and inhibits IKK complex activation via effects upon RIP.[105]

Any attempt to produce an inflammation responsive promoter for use in uveitis, should investigate promoters responsive to both or either NFκB and STAT1 signalling. These signalling pathways are known to be rapid in onset, but whether the levels of expression achieved will be sufficient in a therapeutic setting is still unknown. As well as use in gene therapy, an inflammation-responsive promoter delivered by AAV could also be used as an *in vivo* reporter of tissue inflammation, to further examine mechanisms in EAU.

1.10 Systematic review of published pre-clinical studies of gene therapy for uveitis: translating knowledge of immunological mechanism into therapy

For the purposes of this introduction, studies addressing intraocular inflammation with either direct gene therapy or cell based treatments using *ex vivo* genetic manipulation have been included (**Table 6**). Although the use of siRNA is a form of downstream genetic modification, these studies have not been included as they involve repeated administration of siRNA molecules rather than gene delivery. To date several biological pathways

have been targeted using gene transfer. Although self-reactive T_H1 and T_H17 $CD4^+$ cells are thought to initiate EAU, it is the subsequent infiltration of myeloid cells, coordinated through macrophage signalling that cause structural and functional damage to the eye. Deviation of this final effector pathway has been the predominant target of many recent studies.[106]

Gene transferred	Mechanism of transfer	Site of transfer	Disease model	Year
Human sTNFR1-mIgG1	Plasmid electrotransfer	Ciliary muscle	EIU in Lewis rat	2005[63]
			EAU (S-Ag induced) in Lewis rat	2009[107]
Human sTNFR1 p55 variants			EIU in Lewis rat	2009[60]
Viral IL-10	Adenovirus	Subconjunctival, retro-orbital sinus and systemic injection	EAU (S-Ag induced) in Lewis rat and B10-A mouse	2002[59]
	Ex vivo adenoviral transfected retinal Muller glial cells or raw adenovirus	Intravitreal injection	EAU (S-Ag induced) in Lewis rat	2003[108]
	rAAV2 with and without *tet-on* promoter.		EAU (S-Ag induced) in Lewis rat	2005[93]
Murine IL-10	Adenovirus	Intraperitoneal injection	EAAU in Lewis rat	2005[109]
	rAAV-2	Subretinal injection	EAU (IRBP induced) in C57BL/6 mice	2005[110]
Murine IL-10, IL-1ra and in combination	Lentivirus	Intracameral	EIU in C57BL/6 mice	2008[34]
Human IL-1ra	rAAV2	Intravitreal injection	IL-1 mediated EAU in New Zealand white rabbits	2009[111]

α-MSH (as precursor ACTH1-17)	Naked plasmid	Subconjunctival injection	EAU (IRBP induced) in C57BL/6 and B10.RIII mice	2009[61]
Human IFN-α 2a	rAAV2	Subretinal injection	EAU (IRBP induced) in B10.RIII mice	2011[112]
Human IFN-α2a & murine IL-4				2012[113]
Murine IL-27p28	rAAV2	Subretinal injection	EAU (IRBP induced) in B10.RIII mice	2012[114]
gp100 (to immunise against EMIU)	Adenovirus	Systemic injection	Experimental melanin-protein induced uveitis (EMIU) in Lewis rat	1998[115]

Table 6. Published preclinical studies of gene therapy for uveitis. Adapted and updated from *Chu CJ et al. (2012). Gene Therapy for Noninfectious Uveitis. Ocular Immunology and Inflammation, 20(6), 394–405.*

1.10.1 Interleukin-10

Mouse Interleukin-10 was first termed cytokine synthesis inhibitor factor and identified as a critical factor produced by mouse T_H2 CD4+ T-cells that could suppress the activation of T_H1 cells. IL-$10^{-/-}$ knockout mouse lines highlighted its critical regulatory role, as they developed spontaneous inflammatory colitis and an enhanced severity of induced autoimmune disease.[116] Linkage to genetic polymorphisms in IL-10 has now been identified in multiple human autoimmune diseases including uveitis.[117]

IL-10 is well characterised in human and mouse, with both encoded on chromosome 1 and consisting of five exons. The two proteins possess 73% amino acid homology and though mouse IL-10 is N-glycosylated, this is not thought to alter function. Human IL-10 is recognised to be active on mouse cells, but mouse IL-10 has no effect upon human cells.[118]

A protein isolated from Epstein-Barr virus known as BCRF-1, was found to be highly similar to mouse and human IL-10 and re-named viral IL-10. This has

an 84% amino acid homology to the human protein, with differences primarily occurring at the N-terminus at a key isoleucine/alanine exchange at position 87. It is thought to have evolved to lose many of its pro-inflammatory characteristics, as it lacks the ability to activate B-cells and Mast cells.[119,120]

IL-10 forms a homodimeric protein complex and binds to IL-10 receptor-1. The IL-10 receptor-2 co-receptor is then recruited engaging Jak/Stat family tyrosine kinases Jak1 and Tyk2. These lead to phosphorylation and activation of Stat1, 3 and 5, which lead to the changes in transcription responsible for most of the effects of IL-10. Whilst the exact mechanisms are unclear, rapid and high levels of SOCS3 are generated, that is suspected not only to be a form of negative feedback for IL-10, but also may enact its anti-inflammatory effects.[119]

IL-10 can be produced by almost any cell of the immune system, but is predominantly derived from activated macrophages and T-cells.[121] It is critically involved in the effector function of regulatory T-cells.[122] IL-10 down-regulates MHCII and co-stimulatory molecule expression as well as inhibiting the production of many pro-inflammatory cytokines including TNFα, interferon-γ (IFNγ), interleukin-1 (IL-1) and interleukin-12.[119] Reduced levels of these cytokines in particular, impair the generation of superoxide anions and nitric oxide, limiting the destructive potential of myeloid cells in the retina during EAU.[123]

The importance of IL-10 is supported by studies that have shown that levels of IL-10 in ocular fluids is lower from patients with idiopathic uveitis than from controls[124] and that EAU-susceptible rat strains show lower basal levels of IL-10 expression than their resistant counterparts.[125] IL-10 levels increase during the spontaneous resolution phase of EAU, indicating a crucial role in reasserting control over the inflammatory process.[41] Furthermore, intraperitoneal injection of recombinant IL-10 for five days after the induction of murine EAU has been shown to reduce IFNγ production and disease scores, though this is likely through inhibition of disease initiation.[126]

One of the earliest approaches for gene therapy for uveitis involved sub-conjunctival injection of an adenoviral vector expressing viral IL-10. This approximately halved histological EAU scores in both rats and mice when given one day before induction.[59] Another group used intraperitoneal administration of an adenoviral vector expressing murine IL-10, to prophylactically treat a rat model of anterior uveitis (EAAU). Although they reported a ten-fold reduction in anterior chamber leukocyte infiltration, the indirect effect of systemic immunosuppression was not quantified and IL-10 production appeared to be lost by two weeks.[109] Whilst intraocular administration of adenoviral vectors is not beneficial since the vectors elicit such a strong immune response, Lentiviral and AAV vectors in particular, generate relatively minimal immune responses. Sub-retinal injection of AAV2 encoding murine IL-10 two weeks before induction of disease has been shown to reduce the histological EAU disease score in C57BL/6 mice by 40%, without evidence of systemic immunosuppression. A reduction in co-stimulatory molecule expression on $CD11b^+$ cells isolated from the retina and reduced levels of peroxynitrite damage were also observed.[110] Similar results have been obtained in a rat EAU model using tetracycline-inducible viral IL-10 delivered by an AAV2 vector. A comparable 40% reduction in histological scores was obtained in the group where oral Doxycycline was administered.[93] Anterior chamber administration of an HIV-1 vector expressing murine IL-10, fourteen days prior to the induction of EIU has been shown to reduce the degree of anterior chamber infiltration by 74%, but this effect was not maintained upon re-challenge.[34]

1.10.2 Tumour Necrosis Factor-α

Most of the inflammatory damage responsible for visual loss in uveitis is mediated through macrophage activity when destructive superoxide radicals and nitric oxide are generated primarily in response to the high levels of IFNγ. The induction of nitric oxide synthase in macrophages is crucially dependent upon the autocrine action of tumour necrosis factor alpha (TNF) in response to IFNγ.[127]

TNF itself is synthesised as a 26kDa pro-TNF protein, which assembles into trimers on the cell membrane. This transmembrane complex is active and capable of binding and stimulating TNF receptors. Following processing and cleavage by the matrix metalloproteinase TACE (known also as ADAM-17), the active soluble form is released.[128] Soluble and transmembrane forms of TNF are produced by leukocytes, fibroblasts or smooth muscle cells and signal differentially through two receptor pathways. Activation of TNF-Receptor 1 (TNFR1/p55) on macrophages is necessary for the pro-inflammatory phenotype seen in EAU, is involved in cell infiltration and the receptor has a greater affinity for soluble TNF. TNF-receptor 2 (TNFR2/p75) preferentially binds transmembrane TNF and has been implicated in modulating angiogenesis and tissue repair **(Figure 4)**.[104,129] Soluble forms of TNFR1 and 2 also exist and may form part of a homeostatic mechanism, by competitively regulating the amount of free soluble TNFα. There is some evidence however that at low concentrations they may in fact stabilise TNF trimers and potentiate their effect.[130]

TNF levels are normally undetectable. It is elevated in the blood and aqueous of patients with active uveitis, where it stimulates the production of cytokines including IL-6 and IL-12, and promotes tissue infiltration through endothelial ICAM-1 and ELAM-1 adhesion molecule up-regulation and blood-retinal barrier degradation.[131] In TNFR1 knockout mice, nitric oxide production is prevented and there is both resistance to the induction of EAU and reduced myeloid infiltration.[132] Consequently, neutralising systemic TNFα activity in EAU prevents end organ damage, despite the presence of a significant cellular infiltrate.[133]

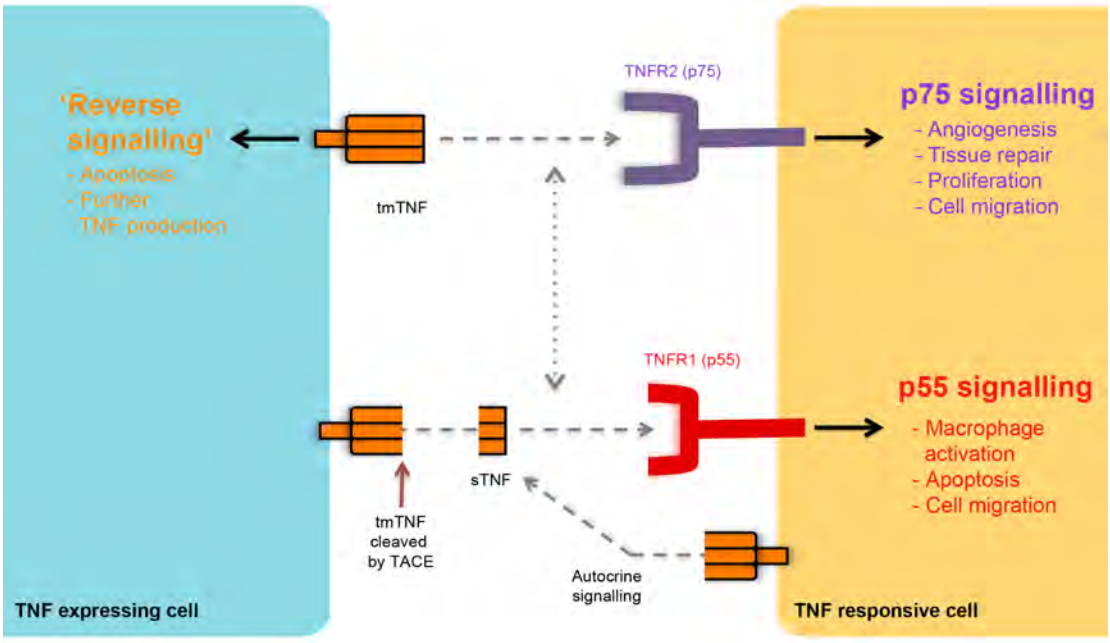

Figure 4. TNF forms and their binding receptors. Two TNF receptors exist, TNFR1 (p55) and TNFR2 (p75). p75 preferentially binds to transmembrane TNF (tmTNF) whilst p55 preferentially binds to soluble TNF (sTNF). Both however can bind either form. sTNF is generated by cleavage of transmembrane TNF by the matrix metalloprotease ADAM17. Each receptor results in different downstream effects as summarised above. Autocrine signalling is an important mechanism in macrophages. The phenomenon of 'reverse signalling' can also occur, where receptor bound tmTNF can lead to intracellular signal transduction and changes in the tmTNF expressing cell. Adapted from Khera et al, 2010.[104]

Anti-TNF therapy, using drugs developed for systemic autoimmune diseases such as rheumatoid arthritis and ankylosing spondylitis, has been employed increasingly over the last decade for the treatment of refractory uveitis. It is now even recommended by consensus as first line treatments for ocular Behçet's disease.[134] The most commonly prescribed agents are chimeric (Infliximab) or fully humanized (Adalimumab) monoclonal antibodies to TNF itself. With systemic administration, promising results have been attained in cases resistant to standard immunosuppressive drugs, with reported response rates, between 78-100% across different age groups and subtypes of uveitis depending on definition of response.[10,15,135] Despite these benefits there are significant side effects due to systemic administration of these anti-TNFα agents, including reactivation of latent tuberculosis, predisposition to

opportunistic infection and a theoretical increase in malignancy. The development of multiple sclerosis has also been reported.[136] Local inhibition of TNFα activity by gene therapy may provide the same degree of disease suppression, without these adverse effects. A single gene treatment would additionally deliver long-term benefit, avoiding the need for weekly subcutaneous injections or monthly intravenous infusions.

It is still unclear if local TNF inhibition alone is sufficient to attenuate EAU. Whilst intravitreal delivery of a TNFR1 fusion protein suppresses EAU induced structural damage in mice by two-thirds, the effect of local TNF inhibition upon acute intraocular inflammation in humans remains unknown.[129] Intravitreal administration of anti-TNF antibodies has no effect on macular oedema in otherwise quiescent eyes. In one clinical study, intravitreal Infliximab for non-uveitic macular oedema actually induced severe inflammation in 42% of eyes, although this may have been due to the chimeric nature of the molecule leading to non-specific myeloid activation via Fc binding. Inflammation was not seen at a lower dose, or when Adalimumab was used.[137,138]

Several studies have investigated the potential of local inhibition of TNF activity by gene therapy. Plasmid DNA electrotransfer to ciliary muscle has been used to deliver chimeric soluble TNFα receptor. This resulted in reduced inflammation in concurrently induced EIU in Lewis rats, but when assessed using luciferase, transgene expression was all but lost by three weeks.[63] Using various monomeric variants of the soluble p55 TNFα receptor, prolonged transgene production was obtained at 3 months, which reduced the clinical score of EIU.[107] A similar approach was used to delay onset and attenuate the severity of EAU in the rat, but the effect appeared to reduce by day 17 and did not completely prevent structural damage.[60] This technique has certainly shown potential as a treatment for acute anterior uveitis, but may not last long enough to treat posterior uveitis, which often runs a protracted course of many years.

1.10.3 Interferons

Interferon-alpha (IFNα) and Interferon-beta (IFNβ) are human cytokines typically induced as an innate immune response to viral infection. Both are classed at Type I interferons and distinct from the Type II member IFNγ. They have the capacity to be both suppressive and stimulatory, depending on the context of the surrounding cytokine environment and the interferon subtype. Their exact mechanism of action is still unclear, but they may exert their anti-inflammatory effects by suppressing Th17 responses and stimulating the production of IL-10.[139]

Many groups have examined the potential of IFNα administration as a treatment for posterior uveitis, particularly in Behçet's disease. One rationale for this approach is that when stimulated *in vitro*, plasmacytoid dendritic cells from uveitis patients have been observed to produce less IFNα than controls.[140] Several studies have shown that subcutaneous injection of recombinant IFNα-2a may have a beneficial effect on refractory uveitis and chronic cystoid macular oedema (CMO).[141,142] In one group of 37 patients with Behçet related panuveitis resistant to conventional immunosuppression, 95% achieved quiescence and the rate of relapse was reduced four-fold at 24 months. However, weight loss occurred in 24% of subjects and all were affected by transient flu-like symptoms. Alopecia, dermatitis and leucopaenia also occurred in a significant number of patients.[143] Localised delivery of IFNα by a gene therapy vector could potentially avoid these side effects and the need for subcutaneous injections three times a week.

Tian *et al*.[112] have shown that subretinal AAV2-mediated transfer of human IFNα can decrease IL-17 production and lymphocyte proliferation and attenuate clinical and histological scores in murine B10.RIII EAU. Peak expression of IFNα did not occur, however, until 42 days after injection and as the effects of IFNα expression were only assessed up to 3 months, further evaluation is required. Combined therapy delivering murine Interleukin-4 (IL-4) alongside IFNα by AAV2 was also trialled, but failed to show any additional benefit over IL-4 or IFNα alone.[113] A clinical study to investigate

intravitreal injection of recombinant IFN-α2b for neovascular macular degeneration reported a transient reduction in ERG responses and this may need to be addressed before pursuing IFN-α therapy further.[144]

Intraocular inflammation has been reported to occur in 15% of patients with multiple sclerosis (MS) and often manifests as intermediate uveitis.[145] IFNβ therapy is licensed as a disease modifying treatment for MS and increasing evidence suggests it may also have an effect upon MS-associated uveitis. One retrospective study of 24 eyes after systemic IFNβ therapy, reported improvement in disease activity in 71% of eyes and resolution of pre-existing CMO in 82%.[146] Although the use of IFNβ appears promising, interferon treatment for isolated ocular inflammation has to be balanced against the significant reported side effects. Persistent flu-like symptoms may account for the average compliance rate of only 50% at two years when IFNβ-1a is used for treatment of MS.[147] However, the prospect of using gene therapy to express IFNβ within the local intraocular environment may provide therapeutic benefit without unwanted systemic side effects. One study has used AAV8-mediated transfer of IFNβ to treat a mouse model of retinoblastoma,[148] but this approach has yet to be tested in a model of uveitis.

1.10.4 Interleukin-1 receptor antagonist (IL-1ra)

IL-1 is a key mediator in both EIU and EAU. It promotes breakdown of the blood-retinal barrier, leukocyte infiltration through the expression of ICAM-1 and the production of pro-inflammatory cytokines including IL-8 and IL-6 by RPE.[149,150] IL-1ra is a naturally occurring structural variant that competitively inhibits the activation of IL-1 receptors.[151] Attenuation of EAU in mice was demonstrated following subcutaneous injections of recombinant IL-1ra (Anakinra) and subsequent case reports have suggested benefit following systemic administration in CINCA syndrome and Behçet disease.[1,152-154] One study has investigated the potential of local IL-1ra gene transfer in mouse EIU. Following anterior chamber administration of a lentiviral vector expressing IL-1ra, there was a reduction of protein leakage into the anterior

chamber after EIU induction, suggesting that there was partial preservation of the blood-aqueous barrier. Concurrent neutrophil infiltration was also reduced significantly. After re-challenge 12 weeks later, there was no statistically significant reduction in protein leakage, which may be explained by successive loss of vascular integrity after the second episode of EIU.[34] Combination therapy with IL-10 and IL-1ra gene transfer did not result in greater efficacy over either gene in isolation.

1.10.5 α-melanocyte stimulating hormone (α-MSH)

α-MSH, an endogenous derivative of pro-opiomelanocortin (POMC), is an immunosuppressive molecule with a diverse mode of action. It is constitutively present in the anterior chamber where it inhibits IFNγ release from primed T-cells. It is also implicated in the generation of locally derived T regulatory cells thought to be responsible for the resolution of ocular inflammation in mice.[155] Effects upon other types of cells may contribute to resolution of inflammation, with reduced levels of NF-κB and phosphorylated p38 MAPK observed in macrophages after exposure to α-MSH.[156] Direct plasmid transfer of ACTH1-17, converted in ciliary and retinal pigment epithelial cells to α-MSH, has been used to suppress murine EAU in both B10.RIII and C57BL/6 models.[61] Following gene transfer the histological EAU disease scores were around a third lower than in empty plasmid controls. The specificity of the therapy was confirmed, as there was loss of the protective effect when EAU was induced in melanocortin 5 receptor deficient mice.

1.10.6 Interleukin-27

The importance of the T_H17 polarity of CD4+ T-cells has become increasingly recognised in multiple autoimmune diseases, including uveitis.[157] IL-27 is part of the IL-12/IL-6 family of cytokines and is a heterodimer of EBI3 and IL-27p28 subunits. IL-27 and even the IL-27p28 subunit alone are able to suppress both T_H17 and T_H1 responses. Transgenic IL-27p28 expression was observed to attenuate EAU induced three-weeks after subretinal

injection of AAV2 in *B10.RIII* mice. A mild reduction in intraocular IL-17 and an increase in IL-10 were seen at peak disease, compared to AAV2-GFP controls.[114]

1.10.7 Antigen based therapies

Gp100 is a melanocyte differentiation antigen recognised by HLA-A2 restricted $CD8^+$ cells. Adenoviral-mediated transfer of gp100 has been used as pro-immunogenic treatment for malignant melanoma. Chan and colleagues used a similar approach to attenuate the induction of experimental melanin-protein induced uveitis (EMIU) seven days after prophylactic systemic administration of adenovirus encoding gp100.[115]

B cells have the capacity to act as tolerogenic antigen presenting cells. Retroviral vectors expressing $IRBP_{161-180}$ in frame with the mouse IgG1 heavy chain have been used to transduce B cells *ex vivo*. Ten days after intraperitoneal infusion back into syngeneic *B10.RIII* mice, EAU was induced, but showed significantly reduced levels of disease compared with controls. Of greater clinical relevance, the disease course was unaltered when a single infusion was given seven days after the induction of EAU. However, following repeated alternate day dosing from day 7, a significant reduction in disease score was obtained, implying a potentially different mechanism of action.[158]

Almost all published experimental studies have used a prophylactic approach, that is, treating before the induction of EAU. While such an approach is a logical first step for proof of concept, intervention during established disease in a chronic model is more clinically relevant. Refinement of animal models of EAU may help to achieve this. Standard inoculation of rats with S-antigen results in aggressive, short-lived, monophasic disease, terminating when complete retinal destruction removes the source of antigen. Inducing *B10.RIII* mice with IRBP peptides causes an acute and damaging peak of disease followed by a form of resolution, but continued retinal infiltration.[159] Reducing the dose of peptide can alter disease dynamics, but alternatively a different model can be used. *C57BL/6* mice develop milder,

slower and persistent disease, with evidence of retinal angiogenesis and continued changes four months after initiation.[160] Aside from spontaneous models, this would therefore be the most appropriate model to use in the interrogation of gene therapy for uveitis.

1.11 Aims and Objectives

The main project aim was to build upon previous published work that used AAV2 to suppress EAU. Provisional objectives at the outset were:

1. To improve assessment of the EAU model where possible, adopting the routine use of flow cytometry and TEFI, and examining new modalities such as OCT or scanning-laser ophthalmoscopy.
2. To test if expressing IL-10 initially using the modern serotype AAV2/8 would lead to superior suppression of EAU in the C57BL/6 model. This would include assessment of severity of disease using histology and flow cytometry. Levels of IL-10 achieved would be determined by ELISA.
3. To examine the effectiveness of other anti-inflammatory transgenes delivered by gene transfer particularly including soluble TNF receptors 1 and 2. Other options could include TGF-β, IL-4 or CD200. If these were all successful, combinations could be tried to see if there was a synergistic effect.
4. Other modern serotypes apart from AAV2/8 could be trialled and techniques for AAV production and purification examined to ascertain if a refined process can improve therapy further.
5. To assess the feasibility of an intrinsic inflammation-regulated promoter to control the expression of anti-inflammatory transgenes. Selection of the promoter would be based upon pro-inflammatory mediators known to be critical in the EAU model, such as IFNγ and TNF.

2 Materials & Methods

2.1 Animal procedures

2.1.1 Animal strains and husbandry

Unless stated otherwise, all mice used were female *C57BL/6J* (Harlan, UK), brought into the animal facility at 4-6 weeks of age and maintained on the open shelf, with food and water *ad libitum*. B10.RIII mice were obtained from the Animal Services Unit at Bristol University, Bristol, UK a minimum of one week prior to procedure.

All procedures were performed under the UK Home office project licence PPL 70/1279 and conformed to the Association of Research in Vision and Ophthalmology (ARVO) statement for the use of animals in ophthalmic and vision research.

2.1.2 Mouse anaesthesia

Adult mice were anaesthetised with a bolus intraperitoneal injection of 200µl of a mixture of medetomidine hydrochloride (1 mg/ml), 100 mg/ml ketamine (Orion pharmaceuticals, Helskinki, Finland), and water in the ratio 5:3:42. Post-procedure, anaesthesia was reversed by peritoneal injection of an equal volume of AntiSedan (Pfizer pharmaceuticals, USA). Mice were recovered overnight on heat mats and supplied with hydrated chow.

2.1.3 Ocular injections

Under reversible anaesthesia, pupils were dilated with a single drop of tropicamide 1% (Chauvin Pharmaceuticals, Romford, UK) prior to the application of Viscotears (Novartis Pharmaceuticals, UK) and a small glass coverslip to the ocular surface. A standard ophthalmic operating microscope (Carl Zeiss, Jena, Germany) and a 34-gauge needle (Hamilton, Switzerland) attached to a 5µl glass syringe was used for all injections. At the end of all procedures, 1% Chloramphenicol ointment was applied to the eye (Martindale Pharma, UK).

1.1.1.1 Sub-retinal and intravitreal injection

Using an operating microscope (Carl Zeiss, Jena, Germany) a 34-gauge needle (Hamilton, Switzerland) was passed posterior to the equator into the subretinal space via the sclera and 2μl of viral suspension or other agent injected. For intravitreal injection, the needle was passed perpendicular to the sclera, approximately 0.6mm from the corneal limbus, then angled posteriorly to avoid the lens and enter the vitreous cavity. Up to 2μl of agent was subsequently injected.

1.1.1.2 Intra-cameral injection

A 34-gauge needle was advanced horizontally 0.5mm anterior the to the corneal limbus, to enter the anterior chamber. Posterior pressure was applied to vent a small amount of aqueous from the eye, prior to the injection of 4μl of agent. The needle was held in place for 10seconds and then withdrawn.

2.1.4 Induction of Experimental Autoimmune Uveoretinitis (EAU)

For the induction of EAU in C57BL/6J mice, human $IRBP_{1-20}$ peptide (GPTHLFQPSLVLDMAKVLLD) was synthesised (Cambridge Peptides, UK) and reconstituted in 10% DMSO/PBS (Sigma Aldrich, Dorset, UK) to a concentration of 20mg/ml. The stock was subjected to five freeze-thaw cycles and stored at -80°C.

On the day of injection the stock solution was diluted with PBS to a concentration of 10mg/ml and mixed with an equal volume of Complete Freund's Adjuvant (Sigma Aldrich, Dorset, UK) supplemented with 1.5mg/ml of *Mycobacterium tuberculosis* H37Ra (Difco laboratories, BD, Oxford, UK). The solution was vigorously mixed to obtain a white emulsion and 50μl was subcutaneously injected into each flank to give a total dose of 500μg per mouse. 1.5μg of Bordetella Pertussis toxin (Tocris Bioscience, Bristol, UK) per mouse was injected into the peritoneum, from a 0.1mg/ml stock diluted in PBS.

B10.RIII mice were injected in an identical fashion, but substituting 300μg of Human $IRBP_{161-180}$ (SGIPYIISYLHPGNTILHVD) from Cambridge Peptides and injecting only 0.4μg Bordetella pertussis toxin (Sigma Aldrich, Dorset, UK) intraperitoneally.

2.1.5 Induction of Endotoxin induced uveitis (EIU)

1ng of LPS from E.coli 055:B5 (Sigma Aldrich, Dorset, UK) was injected in a volume of 2μl from a stock dissolved in PBS at 0.5ng/μl into the vitreous cavity as described. A dedicated Hamilton needle and syringe was used and the working solution made freshly prior to injection.

2.1.6 Dissection and extraction of non-ocular mouse tissues

Serum was obtained as a terminal procedure only. Mice were injected with 250μl of 200mg/ml Euthatal (Merial Animal Health, UK). When the pain reflex was confirmed absent, a 23-gauge needle was passed trans-thoracically into the heart and an average 500μl blood withdrawn. This was placed into an Eppendorf tube and allowed to clot at 4°C. Following centrifugation at 13,000rpm, the serum was aspirated into a fresh tube and stored at -20°C until use.

Lymph nodes were dissected from the cervical and inguinal regions using blunt, curved forceps and placed into D10 medium on ice. Spleens were dissected and collected in the same way. Homogenisation was performed with the plunger of a 2ml disposable syringe, washed through a 70μm filter with PBS. Dependent upon subsequent application, red cell lysis was performed with red-cell lysing buffer (Sigma Aldrich, Dorset, UK) according to the manufacturer's instructions.

2.1.7 Topical Endoscopic Fundus Imaging (TEFI)

Adapting a published method, a 5cm endoscope 3 mm in outer diameter (1218AA; Karl Storz, Tuttlingen, Germany), was connected by fibre-optic cable to a Nikon D80 digital camera with a 10-million pixel charge-coupled device image sensor. Pupils were dilated for 8 minutes with topical tropicamide 1%, phenylephrine 2.5%, oxybuprocaine 0.4% (Chauvin

Pharmaceuticals, Romford, UK) and finally Viscotears (Novartis Pharmaceuticals, UK) as a coupling agent for corneal contact. Using an adapted clinical grading system, fundal images were scored masked according to changes in the optic disc, vessels and surrounding retina.[40,159]

2.1.8 OCT imaging and fundus fluorescein angiography

Spectralis™ HRA and OCT (Heidelberg Engineering, Heidelberg, Germany) with an aspheric, 80mm focal length, near-infra-red lens adaptator (Linos, Qioptiq, Luxembourg) was used to capture images. The OCT+IR channel was used to correlate the retinal position with the obtained OCT optical section. Animals were injected in the peritoneal space with 200µl of 2% fluorescein in PBS. Fundus fluorescein angiography was obtained using the autofluorescent channel of the Spectralis™ HRA. Images were then exported and processed in Adobe Photoshop CS5.1 (Adobe Systems Incorporated, San Jose, USA). Images using the HRA2 scanning laser ophthalmoscope, were obtained and analysed in an identical manner.

2.1.9 Slit-lamp fluorescence fundal imaging of GFP

Following anaesthesia and dilation with 1% Tropicamide, mice were imaged using the standard fluorescein excitation filter on an SL-16 slit-lamp (Keeler, Windsor, UK). The optic disc was focussed centrally, with Viscotears as a coupling agent and a glass coverslip. Images were captured using the attached Leica DC500 camera, with a 30.5s exposure time for GFP and 200.5ms for brightfield images.

2.1.10 Mouse electroretinography

Animals underwent overnight dark adaptation prior to ERG. Anaesthesia was used as described above and eyes dilated with 1% Tropicamide and 2.5% Phenylephrine. ERGs were recorded using commercially produced equipment (Espion E2, Diagnosys LLC, MA, USA). The bandpass filter cut-off frequencies used were 0.312 Hz for the low and 1000 Hz for the high-frequency cut-off. Scotopic recordings were obtained from dark-adapted animals at the following increasing light intensities: 0.003, 0.007, 0.03 and

0.5 cd.s/m^2. The recordings used 15 responses per intensity with a 10 second dark adaptation interval between each set. The final response was then averaged for each intensity and analysed at 0.03 cd.s/m^2. Photopic recordings were performed following a 10-minute light adaptation interval on a background light intensity of 20 cd/m^2, which was then used as background illumination for the duration of photopic flash and flicker recordings. Photopic flash recordings consisted of the average of 25 responses for each intensity with a 60s light adaptation interval between each step. Light intensities used were 0.1, 1, 3, 5, 10 and 20 cd.s/m^2.

2.1.11 Dexamethasone treatment

A stock solution of 2mg/ml Dexamethasone (Sigma Aldrich, Dorset, UK) was made in endotoxin free PBS. This was diluted 1:10 and 100µl injected i.p. 24 hours before, after and contemporaneously as the sub-retinal injection.

2.2 Initial AAV production

2.2.1 Plasmid production

The pD10 vector backbone containing CMV-mIL-10-IRES-eGFP and CMV-hrGFP between two ITR regions were provided by Dr Susie Barker. AAV9 capsid and pHGTI helper plasmids were already generated. Plasmids were grown in DH5α bacteria, cultured for 16 hours in Miller's LB broth (Merck, UK) with ampicillin selectivity and DNA isolated using a PureLink HiPure Plasmid Megaprep Kit (Invitrogen life technologies, Paisley, UK).

2.2.2 Recombinant AAV2/9 production

Twenty 15cm diameter Nunclon plates (Nunc, Thermo Fisher Scientific, Rochester, USA) were prepared per viral batch and seeded with HEK-293T cells at 4.5x10^6 in Dublecco's modified eagle medium (DMEM) with 10% Fetal Calf Serum and 1x Anti-Anti (Invitrogen, life technologies, Paisley, UK). These were simultaneously transfected with 10µg of PD10 genomic plasmid, 10µg of AAV9 capsid plasmid and 30µg of pHGTI helper plasmid per plate using Polyethylenimine (PEI). The plates were incubated at 37°C. Fresh media was replaced after 18 hours and the cells were harvested 72 hours

after transfection by scraping, suspension in TD Buffer and frozen at -80°C. Prior to purification three-freeze that cycles are performed.

2.2.3 FPLC purification of AAV2/9 using Sephacryl and Poros columns

On the day of purification, the viral lysate was defrosted and 50 units of Benzonase nuclease (Sigma Aldrich, Dorset, UK) per ml of lysate incubated for 30 minutes at 37°C. Multiple spins at 5000g for 20 minutes and 0.22µm filtration were performed to achieve debris-free supernatant. Using an AKTA prime plus FPLC machine the supernatant was passed over sequential Sephacryl and Poros columns (GE healthcare, Little Chalfont, UK). Sephacryl S-300 FPLC medium separates on the basis of size, retarding larger proteins less. AAV is thus eluted earlier than contaminant debris. Subsequently the elute is further purified by quaternary amine anionic exchange using Poros HQ50 medium, eluted in high salt buffer, collected and concentrated with a Vivaspin 40 column (Sartorius, Germany) to a volume of 200µl. Aliquots of virus are frozen at -80°C.

2.2.4 Recombinant AAV2 production

Twenty 15cm diameter plates (Nunc, Thermo Fisher Scientific, Rochester, USA) of BHK cells seeded at $4.5x10^6$ were prepared per viral batch. Feeding medium for these cells consists of 500ml Glasgow MEM BHK-21 media (Gibco, Grand Island, NY, USA) is supplemented with 50ml Fetal Calf Serum (First Link, UK), 25ml of 1x Tryptose Phosphate broth (Gibco, USA). The BHK cells were transfected with 30µg per plate of the pD10-CMV-IL-10-IRES-eGFP construct plasmid and an equal amount of pHAV7.3 (rep/cap helper) plasmid. This was combined with 45µg of Lipofectin reagent (Invitrogen life technologies, Paisley, UK) and 200µg Peptide 6 (Insight Biotechnology, Wembley, UK) per plate. After 72 hours incubation at 37°C, cells were harvested, re-suspended and freeze-thawed three times. On the day of purification, 50 units of Benzonase (Sigma Aldrich, Dorset, UK) per ml of lysate were incubated for 30 minutes at 37°C. The mixture is then spun at 5000g for five minutes and the supernatant brought to a 0.5% final concentration of deoxycholic acid (Sigma Aldrich, Dorset, UK). Following a further 30-minute incubation, the mixture is passed through a 0.8µm filter.

Purification was carried out using a Heparin packed column (Sigma Aldrich, Dorset, UK), which specifically binds the AAV2 capsid. The column is washed with 0.1M NaCl and the virus then eluted with 0.4M NaCl and concentrated in a Vivaspin 40 column (Sartorius, Germany) to a volume of 200μl. Aliquots of virus are frozen at -80°C.

2.2.5 SYPRO Ruby Gel analysis of AAV preps

Two dilutions of each AAV prep were incubated with Laemmli buffer (4%SDS, 20%glycerol, 0.004% Bromophenol blue, 0.125M Tris HCl, 0.2M DTT) and incubated at 95°C for 5 minutes. Samples were run on a 10% acrylamide gel to completion. The gel was fixed with 7% acetic acid in 50% v/v methanol, then stained overnight with SYPRO Ruby total protein stain (Invitrogen life sciences, Paisley, UK). Following two washes with 7% acetic acid in 10% methanol v/v the gel was imaged on a standard UV gel imager (Syngene, UK).

2.2.6 Dot blot based AAV prep titre determination

Different dilutions of AAV prep were incubated with Proteinase K (Sigma Aldrich, UK) for 30 mins at 56°C. The DNA was precipitated then dissolved in the working buffer of 0.4M NaOH 10mM EDTA. A known standard curve of linearised plasmid was created in the same buffer. All samples were denatured at 95°C for 2 minutes, then transferred on to a Hybond-N+ membrane (GE Healthcare) in a 96-well plate vacuum transfer apparatus (BioRad, Hemel Hempsted, UK). The membrane is then dried and hybridised in a rotisserie oven at 65°C overnight with a biotinylated DNA probe to the region of interest, eg. CMV promoter. Multiple washes first with 5%SDS/ 125mM NaCl/ 25mM sodium phosophate, then with a 1:10 dilution are performed. Streptavidin-Alkaline phosphatase labelling with Phototope-Star detection kit (NEB, Hitchin, UK) A solution containing 0.79g Tris-HCl/ 0.29g NaCl/ 0.048g MgCl in 500ml distilled water is used for washing, before chemiluminescent development and photography on a Nikon LAS4000 CCD imager. Image J was used for densitometry and the titres calculated against the standard curve of plasmid.

2.3 Refined AAV production process

2.3.1 Recombinant AAV8 and ShH10 production process

The pDP8.ape plasmid was obtained from PlasmidFactory GmbH & Co. KG (Bielefeld, Germany) at 1mg/ml concentration, produced in endotoxin-free conditions. Genomic plasmids, the ShH10 capsid plasmid and pHGTI helper were grown in DH5α bacteria, cultured for 16 hours in Miller's LB broth (Merck, UK) with ampicillin selectivity. DNA was isolated using an EndoFree Plasmid Mega Kit (Qiagen, Valencia, USA).

2.3.2 Recombinant AAV8 and ShH10 production

Twenty 15cm diameter Nunclon plates (Nunc, Thermo Fisher Scientific, Rochester, USA) were prepared per viral batch and seeded with HEK-293T cells at $4.5x10^6$ in Dublecco's modified eagle medium (DMEM) with 10% Performance Plus Fetal Bovine Serum and 1x Anti-Anti (Invitrogen, life technologies, Paisley, UK). These were simultaneously transfected with 10μg of pD10 genomic plasmid, 10μg of ShH10 capsid plasmid and 30μg of pHGTI helper plasmid per plate using Polyethylenimine (PEI). For AAV8 10μg of pD10 plasmid was combined with 30μg of pDP8.ape. Plates were incubated at 37°C. Medium was aspirated after 18 hours and replaced with DMEM and Anti-Anti alone. The cells were harvested 72 hours after transfection by scraping, suspension in TD Buffer and frozen at -80°C. Prior to purification three-freeze that cycles are performed and lysates were assured at below 2.5EU/ml endotoxin.

2.3.3 Purification of AAV8 and ShH10 vectors

On the day of purification, the viral lysate was defrosted and 50 units of Benzonase nuclease (Sigma Aldrich, Dorset, UK) per ml of lysate incubated for 30 minutes at 37°C. A single spin at 18000g for 30 minutes and 0.22μm filtration were performed to achieve debris-free supernatant. Lysate is diluted to 45ml with endotoxin-free PBS and passed into a disposable 1ml AVB affinity column (GE Healthcare, UK) at 2ml/min on a 0.5M Sodium hydroxide sanitised AKTA prime plus FPLC machine. AAV is eluted with a solution of 50mM Glycine (pH2) into 1.5ml tubes containing 30μl 1M Tris pH8.8 from

Trizma base (Sigma Aldrich, Dorset, UK). The pooled aliquots corresponding to the peak of viral elution are diluted 1 in 2 with PBS and concentrated with a Vivaspin 40 column (Sartorius, Germany) to a volume of 200µl. Aliquots of virus are frozen at -80°C.

2.3.4 Limulus Amoebocyte Lysate assay

Single use gel-clot limulus amebocyte lysate assay tubes of 0.03EU/ml sensitivity (Pyrotell, Associates of Cape Cod, USA) were used to test samples for endotoxin. Briefly, samples were diluted with endotoxin-free PBS to achieve the desired threshold for testing e.g. 1:83 to test at 2.5EU/ml. 200ul were added to each tube and incubated undisturbed for one hour at 37°C. A positive result is confirmed by static clot formation, despite inversion of the tube. Positive control tubes were used to detect the presence of any test inhibitors in all samples (Charles River, France).

2.3.5 Viral titre calculation using qPCR

Custom ITR primers (see **Table 7**) were used with a bespoke FAM probe based assay (Sigma Aldrich, UK) to determine genomic titre with a quantitative PCR thermal cycler 7900HT (Applied Biosciences, USA). Following initial denaturation at 95°C for 10minutes all AAV capsids are lysed, exposing DNA to direct primer annealing. 40 cycles of 15sec at 95°C and 1min at 60°C annealing extension are used. From linearised pD10 plasmid of known concentration a standard curve was generated. Master mix was from Roche Diagnostics, UK. For each sample, technical triplicates were performed over a four two-fold dilutions.

2.3.6 Capsid separation process

Following standard production and AVB purification, fractions are pooled and diluted in MilliQ water in a 1:10 ratio. A 1ml Sepharose Q_{XL} column (GE Healthcare, UK) is equilibrated with 10mM NaCl solution. The vector is loaded and washed with 5 column volumes. Using a 250mM NaCl solution as the second buffer, a step to 30% mix was performed, before a gradient from 30%-100% over 50ml. 1ml fractions were retained separately for analysis.

2.3.7 Electron microscopy of AAV

AAV fractions were washed with distilled water and concentrated using a Vivaspin 40 column (Sartorius, Germany). 8μl is placed upon a glow discharged EM grid. Following two PBS washes, 2% Uranyl acetate is applied for 1 minute. A single wash with distilled water is then performed. Grids were imaged by Dr Hannah Armer from the Institute of Ophthalmology imaging core facility on a JEOL 1010 100kV Transmission electron microscope with a Gatan Orius digital camera.

2.3.8 AAV neutralising antibody and ELISPOT assays

30,000 HEK-293T cells were plated in each well of a 96-well plate and expanded over 24hr. Serial dilutions of serum to be tested were made with a minimum of neat and 1:100 dilutions. $5x10^8$gc AAV8-CMV-hrGFP per well diluted in 20μl DMEM was combined with 20μl of diluted serum and incubated at 37°C for 10minutes. 110μl of D10 medium was added and the combined volume of 150μl added to each well of 293T cells. After 72hrs cells were dissociated with 0.05% Trypsin and 10,000 events acquired on a BD FACScalibur flow cytometer. Technical triplicates were performed and the percentage of GFP+ cells enumerated.

Mouse ELISPOTs were performed with Dr Pete Gardner. Briefly, a 96-well Immobilon-P plate (Merck Millipore, Watford, UK) was prepared and coated with rat anti-mouse anti-IFNγ antibody plate (clone R4-6A2, eBioscience, San Diego, USA) at 10μg/ml in 100μl PBS. After incubation at 4°C overnight, the plate was washed four times with PBS, blocked for an hour at 37°C with neat FBS (Invitrogen life technologies, Paisley, UK) and then washed again with PBS. Cryopreserved splenocytes were recovered and diluted to a concentration of $2.5x10^6$ cells/ml in D10 medium. 100μl of cells were added to each well, including positive and negative control wells. Finally, to test directly against viral capsid protein, AAV-CMV-eGFP was added to each well to achieve a final concentration of 10^8gc/ml. The plate was incubated at 37°C for 48 hours, before removal of cells and washing with PBS. 100μl secondary biotinylated anti-mouse IFNγ (clone XMG1.2, eBioscience, San Diego, USA)

was applied at 1µg/ml and incubated for 2 hours at room temperature. Following PBS washing, 1:1000 dilution of ExtrAvidin (Sigma Aldrich, Dorset, UK) in PBS is incubated for 30mins at room temperature, before repeat washing and development using AP-substrate buffer (AP-conjugate substrate kit, BioRad, Hemel Hempsted, UK) at working dilution. This takes approximately 30 minutes and is quenched by washing with tap water. The membrane is dried overnight and subsequently punched out from the plate, and spot counts calculated using ImmunoScan (C.T.L. Bonn, Germany).

2.4 Lentivirus preparations

Lentivirus SFFV.mIL-10 and SFFV.eGFP were a kind gift of Dr Susie Barker and Dr Anastasios Georgiadis. Briefly, vectors were produced using transient triple transfection of 293T cells. At 28–72 h post-transfection, supernatant was harvested and filtered through a 0.45µm filter. The virus particles were concentrated using a Resource Q anionic exchange column (Amersham, UK) and eluted using a sodium chloride gradient. The eluted fractions were placed in an ultra centrifuge at 90000g for 2h. The pelleted virus was re-suspended in OptiMEM medium and stored at -80°C.

2.5 Molecular biological techniques

2.5.1 Basic cloning techniques

All restriction enzymes were from New England Biosciences or Promega. T4 ligase was used for ligation (Promega). DH5α competent cells were from Bioline, UK. Gel electrophoresis was performed with 1-2% Agarose (Invitrogen Life Sciences) and run with TE buffer (Invitrogen Life Sciences) in the Mini-Sub cell system (Biorad laboratories, Hemel Hempsted, UK). DNA and RNA quantification employed spectrophotometry on a Nanodrop ND-1000 (Thermo Scientific, UK). PureLink HiPure Plasmid Mini-prep Kit (Invitrogen life technologies, Paisley, UK).

2.5.2 Synthesis of mouse p75-Ig, viral and human IL-10

All synthesis was performed by GenScript, Piscataway, USA. The open reading frame of BCRF1 from Human Herpes Virus 4, type 1 (NCBI Reference Sequence: NC_007605.1) was synthesized after human codon optimization (USA) and ligated into pD10 under the control of the immediate-early CMV promoter. The human IL-10 sequence (NM_000572.2) was synthesized with flanking restriction enzyme sites and also ligated into the pD10-CMV plasmid. The mouse p75-Ig (TNF receptor 2 Fc-fusion protein) was synthesized according to the sequence obtained from *Doll et al.* [161] This was also ligated into pD10-CMV.

2.5.3 Interferon gamma inducible promoter and NFκB constructs

The sequence for human Interferon Regulatory Factor 1 (IRF1) was obtained from the ENSEMBL database (ENSG_00000125347) and a previously identified enhancer region was amplified using PCR.[162] The primer sequences are shown in **Table 7**. Promoter fragments were cloned into the commercially available pGL4-Luc2 construct (Promega, USA). The minimal SV40 promoter was synthesised and cloned downstream of the short IRF1 enhancer fragment (Genscript, Piscataway, USA). A five-repeat NFκB enhancer sequence $(GGGAATTTCC)_5$ in front of a minimal SV40 promoter in the pGL4 plasmid was commercially available (Promega, UK). This was in turn cloned in place of the CMV promoter in pD10.

Name	Sequence	Use
Short IRF1-F	GTCGACGCGCCCGGCCGGAGAG	PCR
Short IRF1-R	AGATCTCGAGCAGCGGCGCCACCGA	PCR
ITR_F	GGAACCCCTAGTGATGGAGTT	qPCR AAV titre
ITR_R	CGGCCTCAGTGAGCGA	qPCR AAV titre
FAM-ITR probe	[6FAM]-CACTCCCTCTCTGCGCG	qPCR AAV titre

IFNγR1-F	CATAACCGGAGTGGGGAGA	RT-PCR
IFNγR1-R	TCCGTCTACTGAAATACAATATCTGG	RT-PCR
KC_F	AGACTCCAGCCACACTCCAA	qPCR
KC_R	TGACAGCGCAGCTCATTG	qPCR
CCL2_F	CATCCACGTGTTGGCTCA	qPCR
CCL2_R	GATCATCTTGCTGGTGAATGAGT	qPCR
TNF_F	CTGTAGCCCACGTCGTAGC	qPCR
TNF_R	TTGAGATCCATGCCGTTG	qPCR
Mouse β–actin F	AAGGCCAACCGTGAAAAGA	qPCR
Mouse β–actin R	GTGGTACGACCAGAGGCAT	qPCR

Table 7. All oligonucleotides were synthesised by Sigma Aldrich, Dorset, UK.

2.5.4 Luciferase assessment of promoter activity

Candidate pGL4 constructs were transfected into HEK-293T cells using 0.75µl Lipofectin (Sigma Aldrich, Dorset, UK) suspended in Optimem medium (Gibco, Invitrogen life technologies, Paisley, UK) and 1µg of plasmid per 50,000 cells for four hours. A pTK-Renilla control plasmid was co-transfected at a ratio of 1:50. After 40 hours, the medium was supplemented with different concentrations of recombinant human IFNγ or TNF (Invitrogen life technologies, Paisley, UK). Four hours later cells were harvested in 30µl/well 1x Passive Lysis Buffer (PLB) and then tested using the Dual-Luciferase Reporter assay system (Promega, Madison, USA). 1µl of PLB was combined with 15µl LARII reagent, then 15µl Stop & Glo® buffer as directed. Luminescence was detected using a single sample TD-20/20 luminometer (Turner Designs, Steptech, Stevenage, UK) with a two second delay and 15-second integration time. All tests were performed in triplicate with controls for background levels.

2.5.5 RNA extraction and cDNA synthesis for RT-PCR

RNA was extracted using RNeasy Mini Kit (Qiagen, USA) according to manufacturer's instructions following tissue homogenization in mortar and pestle eppendorf tubes (VWR International, Dublin, Ireland). RNA was

reverse-transcribed using the QuantiTect Reverse Transcription Kit (Qiagen, USA). Ambion RNA-ZAP was used for decontamination of surfaces (Invitrogen life technologies, Paisley, UK).

2.5.6 Quantitative PCR (qPCR)

For simple RT-PCR such as IFNγR1 detection, hot start master mix (Promega, USA) was used with 1µl cDNA and primers at 10µM (detailed in **Table 7**). A standard program of 40 cycles at 60°C annealing extension was used.

Relative real-time quantitative RT-PCR was performed using the Universal Probe Library system and master mix (Roche diagnostics, UK). An Applied Biosciences 7900HT thermal cycler and SDS software was employed. Following initial denaturation at 95°C for 10min, 40 to 50 cycles of 15sec at 95°C and 1min at 60°C annealing extension were used. Samples were run in triplicate and analysed using the 2^{-ddCT} method.

2.6 Histology and immunohistochemistry

2.6.1 Frozen sectioning

Enucleated eyes were snap frozen with liquid nitrogen in Optimal Cutting Temperature (OCT) medium (Fisher scientific, Loughborough, UK). 12µm cryosections were placed on Superfrost plus ultra slides (VWR International, Dublin, Ireland), using a manual cryostat (OTF5000, Bright Instruments, Huntingdon, UK) If not used immediately, the slides were kept at -20°C for up to 3 months.

2.6.2 Histological scoring of EAU using anti-CD45

Slides were thawed, before fixation for 10 minutes at 4°C in 99.5% Acetone (Sigma Aldrich, Dorset, UK). Endogenous peroxidase activity was blocked with 0.3% Hydrogen Peroxide diluted in Methanol (Sigma Aldrich, Dorset, UK) for 15 minutes. Non-specific binding was blocked with 7.5% rabbit serum in 2% BSA/PBS for an hour and incubated overnight at 4°C with a CD45 rat anti-mouse primary antibody (Clone IBL-3/16, AbD Serotec, Kidlington, UK). Biotinylated rabbit anti-rat secondary antibody (Dako UK Ltd, Ely, UK) was

applied, diluted 1:200 in 0.1% BSA/PBS, before using Vectastain elite ABC kit (Vector laboratories, Peterborough, UK) according to manufacturer's instructions to conjugate horseradish peroxidase to the secondary antibody. Between all of the above steps, two washes with PBS were performed on each slide. Chromogenic staining was performed using a 3, 3'-diaminobenzidine (DAB) substrate kit (Vector laboratories, Peterborough, UK) for three minutes duration and counterstained with Haematoxylin (Vector laboratories, Burlingham, USA). Scoring was performed across the whole slide, selecting the most severe example of disease possible and marked according to a previously described system.[163] A summary table of the scoring system is reproduced here for clarity.

Cellular infiltration		
Anterior segment		
Iris	Infiltrating cells	1
	Mild thickening of iris	2
	Moderate thickening of iris	3
	Gross thickening of iris	4
Anterior chamber	Cells <10	1
	Cells 10–30	2
	Cells 30–100	3
	Cells > 100	4
Cornea	Infiltrating cell	1
	Corneal thickening/oedema	2
Posterior segment		
Ciliary body	Cell infiltrate <5 cells	1
	Mild thickening	2
	Moderate thickening	3
	Gross thickening	4
Vitreous	Cells <5	1
	Cells 5–25	2
	Cells 25–50	3
	Cells 50–100	4
	Cells >100	5
Vasculitis (mural or extravascular cells)	<10% vessels involved	1
	10–25%	2
	25–50%	3
	50–75%	4
	>75%	5
	Cells in or around wall	1
	Mild perivascular cuffing	2
	Moderate cuffing	3
	Gross cuffing	4
Rod outer segments	Cell infiltrate	1
	Partial loss	2
	Moderate loss	3
	Subtotal loss	4
	Total loss	5
Choroid	Cell infiltrate	1
	Mild thickening	2
	Moderate thickening	3
	Gross thickening	4
	Granulomas 1	1
	Granulomas 2–5	2
	Granulomas >5	3

Structural/morphological changes		
Posterior segment		
Rod outer segments	Cell infiltrate	1
	Partial loss	2
	Moderate loss	3
	Subtotal loss	4
Neuronal layers	Cell infiltrate	1
	Partial loss	2
	Moderate loss	3
	Subtotal loss	4
	Total loss	5
Retinal morphology	Folds	1
	Focal detachment	2
	Subtotal detachment	3
	Total detachment	4
SRNVM	1–3	1
	>3	2

TOTAL	
Infiltrative	40
Stuctural	16

Grading: Infiltrative	
1	<10
2	10–15
3	15–20
4	20–30
5	30–35
6	>35
Grading: Structural	
1	<2
2	2–6
3	6–10
4	10–14
5	>14

SRNVM, subretinal neovascular membrane.

2.6.3 Retinal flat-mount dissection

Following enucleation, eyes were fixed in 4% PFA for 2 minutes then placed in 100µl PBS and dissected under an operating microscope (Zeiss, Jena, Germany). Briefly, a 28G needle is passed through the corneal limbus and then curved Vanna scissors used to remove the cornea and iris. The lens is carefully dislodged and removed, before four evenly spaced full-thickness cuts from limbus to near the optic disc are performed. The retina is mobilised from the RPE/choroid complex at each petal now formed and a cut made at the fusion around the region of the vitreous base. A final cut through the optic nerve head immediately under the retina is performed. Tissues are then fixed with 100% methanol and stored at -20°C.

2.6.4 Frozen section and flat-mount immunohistochemistry

Slides were defrosted and post-fixed with 4% PFA for 15minutes. Two PBS washes are followed by blocking with 1%BSA in PBS (Sigma Aldrich, Dorset, UK) and 5% normal goat serum (AbD serotec, Kidlington, UK) for one hour at room temperature. Primary antibodies were applied at concentrations described in **Table 8** overnight at 4°C. After two PBS washes secondary antibodies were applied in 1%BSA in PBS in a 1 in 500 dilution at room temperature for two hours. Following two further PBS washes, slides were mounted in Fluorescent mounting medium (Dako, Ely, UK) containing 1:1000 dilution of DAPI.

Flat-mounts were placed into 1%BSA in PBS supplemented with 5% Triton as a detergent. 5% Normal goat serum is added and incubated at room temperature for two hours. Following three PBS washes, flat mounts were incubated overnight at 4°C in 1%BSA/PBS/5%Triton with primary antibodies at dilutions listed in **Table 8**. A further three PBS washes are performed and then incubated for another 24hr at 4°C in 1%BSA/PBS/5%Triton with secondary antibodies. Two PBS washes are performed before a 1:1000 dilution of DAPI in PBS is applied for 1 hour. Three PBS washes precede mounting between two coverslips in Fluorescent mounting medium (Dako, Ely, UK).

Reactivity	Host species	Concentration	Manufacturer	Catalogue number
CD45	Rat	1 in 200	AbD Serotec	MCA1388
CD4	Rat	1 in 200	BD Bioscience	553043
CD8	Rat	1 in 200	BD Bioscience	553027
IFNγR1	Armenian hamster	1 in 300	BD Bioscience	559911
Nitrotyrosine	Rabbit	1 in 400	Sigma	N0409
Isolectin-B4	Biotin	1 in 200	Sigma	L2140
CD11b	Rat	1 in 200	BD Bioscience	553308
Iba-1	Rabbit	1 in 200	Wako	01-19741
Collagen IV	Rabbit	1 in 200	AbD Serotec	2150-1470
Human Ezrin	Rabbit	1 in 200	Cell Signalling	31545
Human Phalloidin	TRITC-conjugate	1 in 500	Sigma	P1951

Table 8. Primary antibodies used in immunohistochemistry. Unless stated all antibodies are raised against mouse tissues. All secondary antibodies used Goat anti-rat/rabbit/streptavidin - Alexa Fluor 488/546/633 from Invitrogen live sciences.

2.6.5 Paraffin sections

Eyes were fixed in Serras fixative (60% Ethanol, 30% Buffered 37% Formalin, 10% Acetic acid, Sigma Aldrich, Dorset, UK) for 3 hours. This was then changed into 70% isopropanol and refreshed over 24hrs. Standard processing sequence was then performed and then embedded into paraffin wax. A microtome (Leica RM2235) was used to cut 6µm sections placed on to Polysine coated slides (VWR International, Dublin, Ireland). Slides were dewaxed and stained with haematoxylin and eosin. EAU scoring of these sections used a published method.[164]. Briefly, vitreous cells only = 1,

vasculitis = 2, retinal folds >10% retina = 3, moderate photoreceptor loss = 4, extensive retinal destruction = 5.

2.6.6 Microscopy

Brightfield and simple fluorescence microscopy was performed using an Axio Observer.Z1 (Carl Zeiss Microimaging, Jena, Germany). High magnification immunofluorescent histology and retinal flat-mounts were imaged with a Leica DM5500Q confocal laser-scanning microscope (Leica Microsystems, Wetzlar, Germany). Z-stacks were obtained at 1µm intervals. 3D reconstruction was performed using Imaris software (Bitplane, Zurich, Switzerland).

2.7 Detection of cytokines

2.7.1 Enzyme linked immunosorbant assay (ELISA)

R&D Duoset ELISAs (R&D systems, Minneapolis, USA) were used to quantify all soluble cytokines and transgenes except Human IL-10 Deluxe (Biolegend, San Diego, USA) and human VEGF Quantikine ELISAs (R&D systems). All were used according to manufacturer's instructions. Cell culture supernatants were diluted 1:10 and 1:100. Homogenised ocular samples were spun at 13,000 rpm for 10 minutes and the supernatant typically diluted between 1:10 to 1:1000 prior to testing. Samples were analysed with technical triplicates unless limited material precluded this. Only results within the linear range of the standard curve were used.

2.7.2 BCA total protein assay

Following the manufacturer guidelines, 5ul of sample was measured against a standard curve constructed from BSA of known concentration (Bio-Rad laboratories, Hemel Hempsted, UK). After a 20 minute incubation the result was read at 650nm on a plate spectrophotometer (Molecular devices Emax, Sunnyvale, USA).

2.7.3 Proteome Profiler

Pooled supernatants from 5 eyes, obtained through the standard EIU quantification protocol were combined and used for each membrane. The assay was otherwise carried out according to the manufacturer's guidelines (R&D systems, Minneapolis, USA). Chemiluminescent imaging was performed with a Nikon LAS4000 CCD imager and saved as an 8-bit TIFF file. Densitometry was calculated with Image-J and each membrane was normalised to another using all six positive control spots and a background reading.

2.8 Tissue culture

2.8.1 Maintainance cultures

All HEK-293T and WEHI-164 cell cultures used D10 medium, composed of 10% Fetal bovine serum and 1x Anti-anti in DMEM (Gibco, Invitrogen life sciences, UK). Cell were maintained in 50ml tissue culture treated flasks (Cellstar, Greiner bioscience, Frickenhausen, Germany), until plated as required into 48- or 96-well flat bottom plates (Costar, Corning, NY, USA)

2.8.2 Recombinant cytokines

Recombinant cytokines were stored and used according to manufacturers' instructions and purchased in lyophilised aliquots of 10µg. Mouse TNF (Invitrogen life technologies, Paisley, UK), human TNF (Invitrogen life technologies, Paisley, UK), human IFNγ (Invitrogen life technologies, Paisley, UK and Biolegend, San Diego, USA), mouse IL-10 (Biolegend, San Diego, USA and Cell Signalling technologies, Danvers, USA) and human IL-10 (Invitrogen life technologies, Paisley, UK) were used.

2.8.3 Transfection of plasmids and transduction by AAV

The following day the cells were transfected using Lipofectin (Sigma Aldrich, Dorset, UK) and Peptide 6, suspended in Optimem medium (Gibco, Invitrogen life sciences, UK) and 0.3µg per well of pD10-NFKB-eGFP plasmid for four hours. After this the medium was replaced with D10.

2.8.4 NFKB-eGFP based in vitro testing of TNF neutralising activity

30,000 HEK-293T cells were plated overnight into a flat-bottomed 96-well tissue culture treated plate and incubated in standard 37 degree 5% CO2 conditions. The following day the cells were transfected using Lipofectin (Sigma Aldrich, Dorset, UK) and Peptide 6, suspended in Optimem medium and 0.3μg per well of pD10-NFKB-eGFP plasmid for four hours. After this the medium was replaced with D10.

5ng/ml human TNF in D10 was mixed with the test sample (cell culture supernatants or recombinant antibody) and incubated at room temperature for 15 minutes. Cells were then culture in this mix for 16 hours before the media was aspirated, 100μl 0.05% Trypsin-EDTA added to each well and

2.8.5 WEHI-164 cytotoxicity assay

Cells were cultured in D10 medium and with 30,000 per well plated in a 48-well plate for 3 days. 10ng/ml mTNF (Invitrogen Life Sciences) was added to Optimem and combined 1:1 v/v with 0.22um filtered 293T supernatants containing different proteins at room temperature for 30 minutes. D10 was aspirated from the WEHI-164 cells and replaced with the TNF-Inhibitor mix. After 18 hours in standard culture conditions (5% CO_2. 37°C) the cells were trypsinised, spun down at 300g for 5 minutes before resuspension in 7AAD. (Sigma Aldrich, Dorset, UK) Cells were analysed for 10000 events on a FACScalibur analyser (BD Biosciences, Oxford, UK).

2.8.6 Muller-glia cultures

These were a kind gift of Dr Claire Hippert. Briefly retinae from the CRALBP-GFP reporter mouse line were dissected and dissociated in 20U/ml Papain. Cells were sorted for GFP+ signal using FACS (MoFlow XDP, Beckman Coulter, UK) and plated on laminin coated 8-well tissue culture plates. Standard D10 medium was used. After 1 week of culture at 37°C cells elongate processes and are ready for analysis. They have been previously characterised as possessing a Muller cell phenotype.

2.8.7 Human ES and iPS cell derived RPE transwell cultures

Stem-cell cultures were a kind gift of Dr Anai Gonzalez-Cordero. Briefly, human embryonic stem (ES) and induced pluripotent stem (iPS) cells were differentiated into RPE using suspension conditions, which aid the formation of embryoid bodies (EBs). From day 2-4 SMAD inhibition of Wnt and BMP signalling was used to promote an anterior telencephalic phenotype. On day 6, EBs were plated on laminin-coated 6-well flat-bottom plates and cultured at 37°C/5% CO_2 in neural induction media until day 15. At this point retinal differentiation medium (RDM), but supplemented with activin A was used to induce RPE maturation and pigmentation.

Patches of pigmented RPE were observed from day 30 in culture. These were dissected out using a 21G needle and expanded in a laminin coated 24-well plate transwells of 0.22µm diameter pore size. These were cultured in the presence of FBS until confluence, when they were maintained in FBS free-RDM. ShH10 vector was added at an MOI of 15000 diluted in 300µl medium the apical compartment. 24 hours later 500µl of medium was added to each compartment. Viral expression was checked for GFP fluorescence and confirmed at 5 days. Media was sampled and exchanged at different timepoints from 5 days onwards.

2.9 Preparation and analysis of eyes by flow cytometry

2.9.1 Tissue dissection

Following enucleation, each eye was dissected in 100µl of PBS. Using a limbal incision the vitreous and retina were extracted. The anterior chamber was also opened and the contents washed into the dissecting fluid. The retina and PBS were completely aspirated and placed into a 1.5ml eppendorf tube. If AC and posterior chamber separation was required, the AC was opened by clear corneal incision first, PBS removed, then replaced before the retina and vitreous were dissected. RPE samples were dissociated initially by scraping with curved forceps in 100µl of PBS until only bare sclera is seen. The fluid is then transferred to a 1.5ml eppendorf tube.

2.9.2 Preparation of ocular tissues for analysis by flow cytometry

Mechanical cell dissociation was performed by rapping the eppendorf tubes containing the retinal or RPE sample across a standard tube rack ten times. The whole sample was placed into a 96-well 60µm cell strainer plate (Merck Millipore, Watford, UK) and washed with 100µl of PBS. The plate was centrifuged at 300g for 5 minutes, 'retinal supernatants' collected, with the remaining cell pellet transferred into a 96-well V-bottom plate. Where appropriate, cells were incubated in 100µl of working dilution fixable viability dye eFluor780 (eBioscience, San Diego, USA) for 30 minutes at room temperature. Cells were washed in the plate with 0.1% BSA in PBS before resuspension in 0.5µl of neat Fc-block rat anti-mouse CD16/CD32 (BD Biosciences, Oxford, UK) diluted in 50µl 0.1% BSA in PBS. After 5 minutes, another 50µl was added containing 0.5µl of each neat primary conjugated antibody (See **Table 9**). Following staining on ice for 20 minutes, the cells were washed twice then placed into 200µl 0.1% BSA in PBS in FACS tubes. Intracellular cytokine staining of retinal T-cells was performed by re-stimulating for 2 hours with 50 ng/ml PMA and 500 ng/ml Ionomycin then 1 mg/ml Brefeldin (all from Sigma Aldrich, Dorset, UK) in complete IMDM. Transcription Factor Buffer Set (BD Biosciences, Oxford, UK) was used according to the manufacturer's protocol for intracellular staining.

2.9.3 Flow cytometers

Three flow cytometers (FACScalibur, LSRII, Fortessa X-20) all from BD Biosciences were used during the project, dependent upon experiment. Each was regularly maintained and used according to manufacturers' instructions. Medium or High flow rates were used. Compensation was performed using OneComp eBeads (eBioscience, San Diego, USA, 01-1111-42) and an ArC Amine reactive Compensation bead kit (Invitrogen Life Sciences, A10346) for the live-dead stain. Fluorescence-minus-one (FMO) controls were used to determine gate position. Analysis was performed using FlowJo (Treestar, Ashland, OR, USA).

2.9.4 Absolute cell count using flow cytometry

50,580 Sphero AccuCount Blank polystyrene beads of 7.28µm diameter (Spherotech Inc, Chigaco, USA) were diluted into 300µl of 0.1% BSA in PBS and eight, two-fold serial dilutions were made. These were acquired on the flow cytometer at on the same occasion as samples. Settings were kept the same, with the highest flow rate for a fixed duration - typically 45 seconds. By gating around the bead region and taking an absolute count (FlowJo, Tree star), a standard curve was constructed in relation to the number of expected beads, using a linear regression constrained through zero. (Graphpad Prism, La Jolla, USA). This method was used to estimate the absolute number of cells in each flow cytometry experiment.

2.9.5 Primary conjugated antibodies used for flow cytometry

Reactivity	Clone	Conjugate	Company	Catalogue number
CD45	30-F11	FITC	eBioscience	11-0451-85
CD45	30-F11	BV 421	Biolegend	103133
CD11b	M1/70	PE-Cy7	eBioscience	25-0112-82
CD4	L3T4	PE	BD Bioscience	557308
Ly6G	1A8	APC	Biolegend	127614
Ly6C	HK1.4	PE	eBioscience	12-5932-80
CD8b	H35-17.2	eFluor 450	eBioscience	48-0083-82
Ly6C	HK1.4	PerCP	Biolegend	128027
IL-4	11B11	BV605	Biolegend	504125
Gr1	RB6-8C5	APC	eBioscience	17-5931-82
FoxP3	MF23	Alexa 488	BD Bioscience	560403
Ly6C	HK1.4	BV605	Biolegend	128035
CD11b	M1/70	PerCP	Biolegend	101230
CD4	GK1.5	PE-Cy7	eBioscience	25-0041-82
CD45	30-F11	BUV395	BD Bioscience	564279
CD94	18d3	PE	eBioscience	12-0941-81

IL-17A	17B7	eFluor 450	eBioscience	48-7177-82
IFNγ	XMG1.2	APC	eBioscience	17-7311-82
I-A[b]	AF6-120.1	PE	BD Bioscience	553552
Fixable viability dye	N/A	eFluor 780	eBioscience	65-0865-14

Table 9. Primary conjugated antibodies used for flow cytometry. Unless stated otherwise all antibodies were raised against mouse tissues.

3 Results 1: Optical Coherence Tomography can be used to characterise and define the severity of murine Experimental Autoimmune Uveoretinitis

Work presented in this chapter has been published as:

Chu CJ, Herrmann P, Carvalho LS, Liyanage SE, Bainbridge JWB, Ali RR, Dick AD & Luhmann UFO

Assessment and *In Vivo* Scoring of Murine Experimental Autoimmune Uveoretinitis Using Optical Coherence Tomography.

PLoS ONE (2013) 8(5): e63002.

CJ Chu performed the majority of the work and manuscript preparation. P. Herrmann provided technical assistance with OCT image capture. LS Carvalho and SE Liyanage provided independent EAU disease scores using the different systems. All other authors provided supervision, advice on experimental design and data interpretation.

Before starting interventional studies to suppress EAU, it was apparent that the tools used for assessing disease severity and progression could be improved. The utility of conventional readouts for EAU such as histology, fundal photography and flow cytometry are each limited by either their inability to provide repeated *in vivo* assessment, their semi-quantitative nature or the lack of corresponding structural information. To surmount many of these limitations, a novel scoring system for EAU using optical coherence tomography was explored.

3.1 Optical Coherence Tomography has the potential to surmount the limitations of current methods of EAU scoring

Central to the application of any animal model of human pathology, is the ability to follow the course of disease and assess the result of therapeutic intervention. In experimental autoimmune uveoretinitis (EAU) in *C57BL/6* mice, the gold standard for determining disease severity is with histology and several scoring systems have been validated.[165,166] Obtaining post-mortem histology however necessitates large numbers of animals and precludes repeated examination or multiple terminal analyses upon the same eye.

These limitations prompted the introduction of topical endoscopic fundus imaging (TEFI), which whilst a useful technique also has limitations. Based on a fundal image it only provides a surrogate measure of histological pathology. It additionally uses an extremely bright light source, which can induce confounding light damage across repeated examinations.[167] Furthermore, scoring of TEFI images (and histology using current scoring methods) features subjective measures that result in large inter-observer variation, in part due to the difficulty in distinguishing between scarring, infiltrate and resolving disc changes.

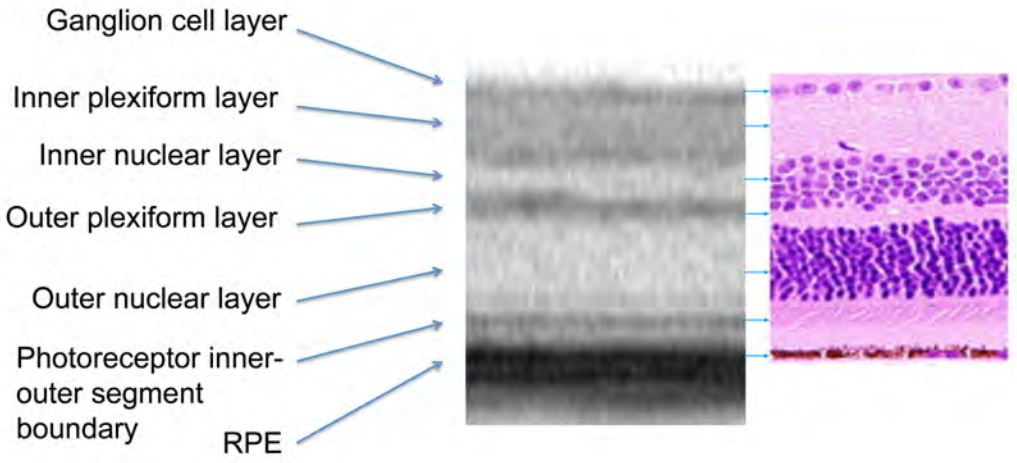

Figure 5. An anatomical comparison between an OCT optical section and histology. Retina from a wildtype *C57BL/6J* mouse is shown next to a matched OCT scan.

Optical coherence tomography (OCT) is analogously described as optical ultrasound scanning. By measuring changes in the coherence of light reflected from ocular tissues, a near histological level of detail can be obtained. The technology is now routinely employed in clinical practice for imaging the fundus.[168,169] It is only recently however, that technological adaptations have permitted examination of the mouse eye.[170] An example of the correlation between an OCT-derived 'optical section' and paraffin histology of the retina is shown in **Figure 5**. An early study had used a simple handheld OCT to examine EAU in the rat, but the signal quality obtained was poor, partly due to the severity of inflammation.[171] No publications existed where OCT had been used to evaluate EAU pathology in the more widely used mouse model. Thus, a pilot study was launched to assess the utility of OCT imaging as an alternative for histology and TEFI.

3.2 Pilot studies demonstrate the potential of OCT to detect pathology in the C57BL/6 mouse model of EAU

We used our in-house Spectralis HRA and OCT from Heidelberg Engineering with an aspheric, 80mm focal length, near infrared lens to capture 30-degree angle images. It was possible to obtain adequate quality OCT images of the mouse fundus during EAU and they could be correlated with images obtained by TEFI (**Figure 6**). Changes in the disc, vitreous and retinal layers appeared to reflect changes seen on fundal images through the course of the disease.

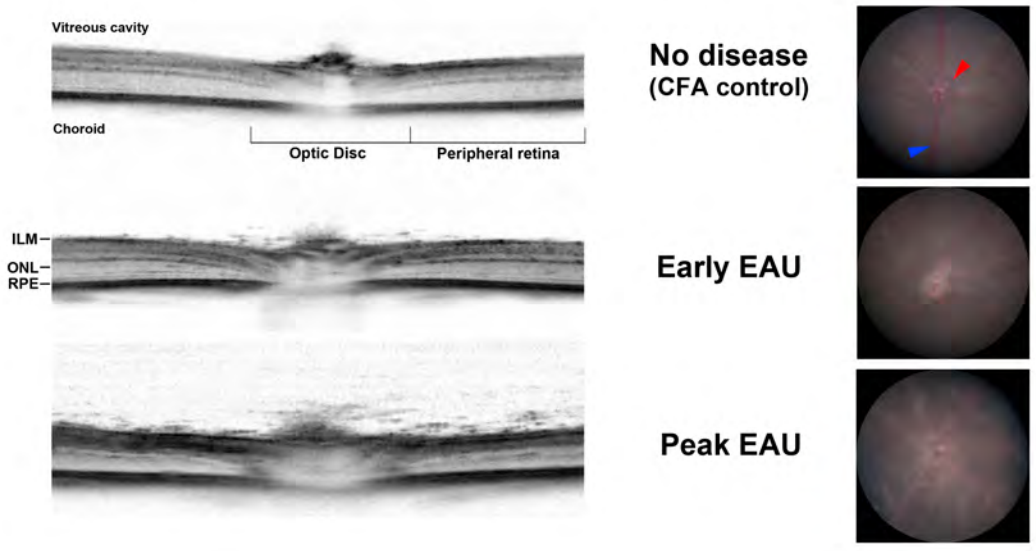

Figure 6. Pilot OCT images of mouse EAU and matched TEFI photographs. OCT scans centred on the optic disc (*left*) from different mice with matched TEFI images (*right*). An un-induced CFA control animal and scans from early (day 15 post-induction) and peak (day 26) EAU are shown. Note with EAU progression on OCT, black flecks appear in the vitreous and the signal corresponding to the optic disc enlarges. ILM: Inner limiting membrane, ONL: Outer nuclear layer, RPE: Retinal pigment epithelium. The optic disc (red arrowhead) and a retinal vein (blue arrowhead) are indicated on the top TEFI image.

Following these promising findings, a full timecourse of EAU in *C57BL/6J* female mice was started. OCT, fundus fluorescein angiography and TEFI were performed synchronously and a cohort also underwent electroretinography (ERG) to supplement the structural assessment with functional information. Several eyes were selected for retinal flat-mount immunohistochemistry and 3D reconstruction. Assessment was performed at 15, 26, 36 and 60 days post-induction of EAU, with CFA (induced with complete Freund's adjuvant and pertussis toxin only) control animals as a comparison. TEFI, histological and OCT scoring, the latter developed during the project, were all performed masked by three assessors.

3.3 The development of key features of EAU can be systematically detected by OCT

We initially aimed to confirm that all features of EAU could be detected using OCT. Firstly a spectrum of changes in the vitreous could be seen and

appeared to correspond with other structural changes. Whilst discrete lesions could be seen, it is likely that these represented clusters of infiltrate, rather than single cells **(Figure 7)**.

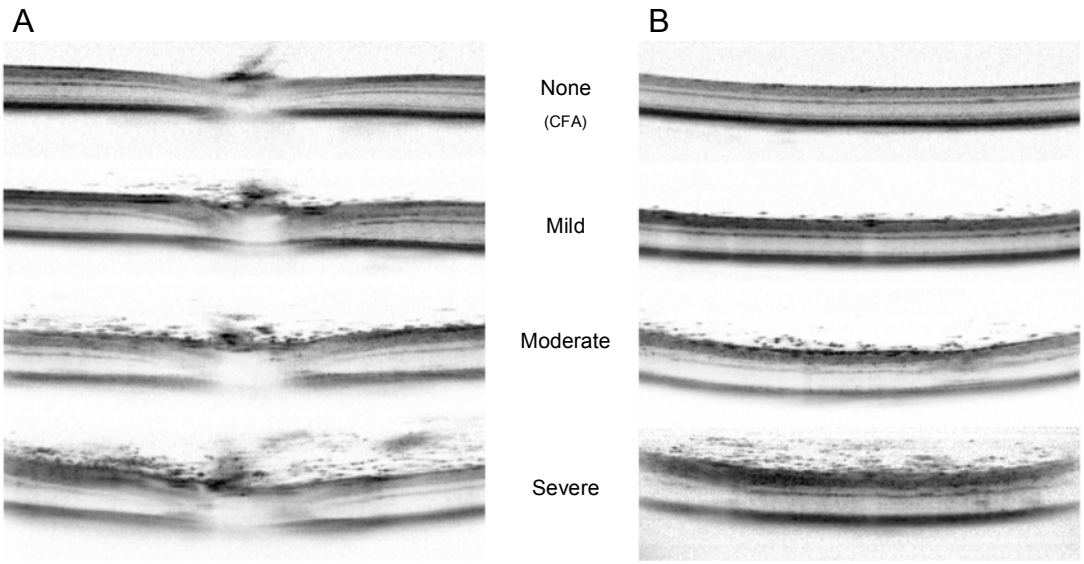

Figure 7. Vitreous condensation at the interface between the posterior hyaloid face and inner retinal surface is consistent with clinical vitritis. OCT scans centred on **A)** the optic disc and **B)** periphery are shown for a range of EAU severities compared to a CFA control eye.

It is known that one of the earliest sites of infiltration is at the optic disc.[172] Even at day 15 post-induction, alterations in signal at the optic nerve head could be distinguished. **Figure 8** shows representative examples that illustrate several differences between the imaging techniques. With TEFI alone, it is hard to distinguish early disease, as the angle and depth of focus affect the disc appearance and size **(Figure 8A)**. Fluorescein angiography (FFA) is possible, but time consuming, and early leakage of fluorescein at the disc margin can be subtle. OCT allows an assessment of disc enlargement, presumed secondary to infiltration, most easily measured between marks placed at the limits of the OPL signal identified as a change in tissue reflectance **(Figure 8C)**. Vitreous changes, presumed to be clusters of infiltrating cells are frequently seen at the optic disc.

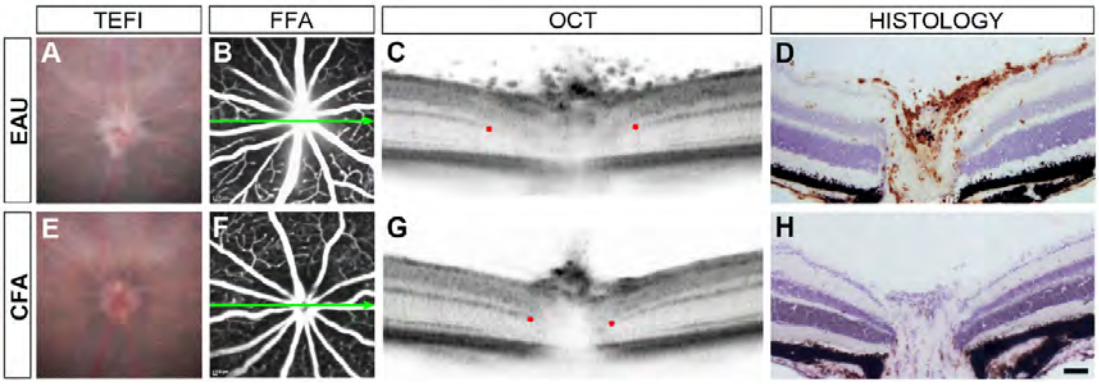

Figure 8. EAU induces distinct optic nerve head changes on OCT. Representative images from the same eyes, one at day 15 post-induction of EAU **(A–D)** and a matched CFA control **(E–H)**. Blurred optic disc margins on TEFI **(A)** and disc hyperfluorescence by FFA **(B)** are observed during EAU. The green arrows show the orientation and position of the OCT scans. Red dots indicate where the discrete signal from the outer plexiform layer becomes obscured by disc enlargement, as a landmark for comparison between eyes. Note the wider separation and vitreous opacities in EAU **(C)**. Matched histology demonstrates CD45+ infiltration (DAB in brown with haematoxylin counterstain) during EAU only **(D)**. Disc enlargement is not seen as it is likely a result of oedema which would be lots during histological processing. With TEFI alone **(E)**, it is possible that changes in disc appearance would erroneously be identified as disease with infiltration in the CFA control. Scale bar = 25μm.

The detection of intraretinal structural change is one of the main clinical applications of OCT. Photoreceptor loss and the development of 'retinal folds' are described as a consequence of EAU. We wished to detect and characterise this latter feature, typically seen with an onset late in the disease course. An example **(Figure 9)** reveals that these lesions can be imaged and correlated with histology on retinal flat-mounts. 3D reconstruction confirms that the retinal folds project arise from photoreceptor displacement away from the subretinal space, which is full with microglia, myeloid and lymphoid cells. Within the displaced ONL, these cells protrude inwards. A video of the 3D reconstruction highlighting the retinal folds can be viewed online at: (http://www.plosone.org/article/info%3Adoi%2F10.1371%2Fjournal.pone.0063002)

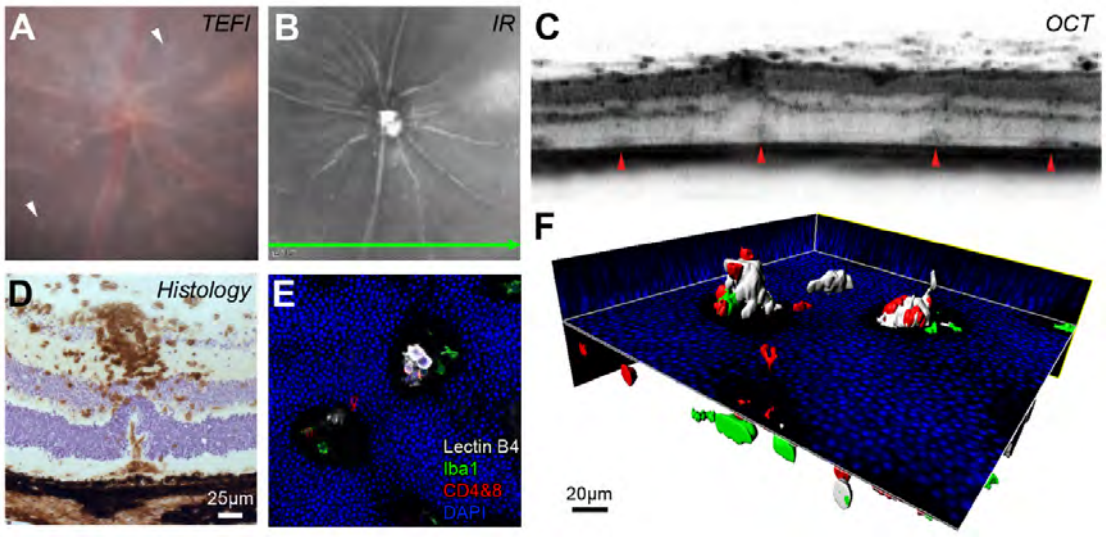

Figure 9. OCT imaging and matched histology identify deep retinal structural changes and an associated cellular infiltrate. Images from an eye at day 80 post-induction of EAU (**A–C)** was analysed with matched *ex vivo* histology **(D–F)**. By TEFI **(A)** multiple pale retinal lesions (white arrowheads) are present. The infrared (IR) image **(B)** marks the position and orientation of the simultaneously obtained OCT scan. **C)** Focal changes at the level of the subretinal space/deep retina approximately correspond to observed lesions (red arrowheads). **D)** Note the CD45+ cellular infiltrate (DAB in brown with Haematoxylin counterstain) around the superficial vessel and under the displaced outer nuclear layer. **E)** A limited projection image and 3D-reconstruction **(F)** of the stained retinal flat-mount identifies these lesions as folds in the outer nuclear layer containing T cell - CD4+ & CD8+ (red), myeloid - isolectin B4 binding (white) and Iba1+ (green) cell populations protruding from the subretinal space (DAPI in blue).

Vasculitis or perivascular immune infiltrate is a predominant feature in murine EAU.[37] To assess vascular changes *in vivo* and *ex vivo*, we compared TEFI, FFA and OCT images of CFA control **(Figure 10A–C)** and EAU **(Figure 10D–G, I)** animals with corresponding immunohistochemistry for vascular and inflammatory cell markers on retinal flat-mounts **(Figure 10H & J)**.

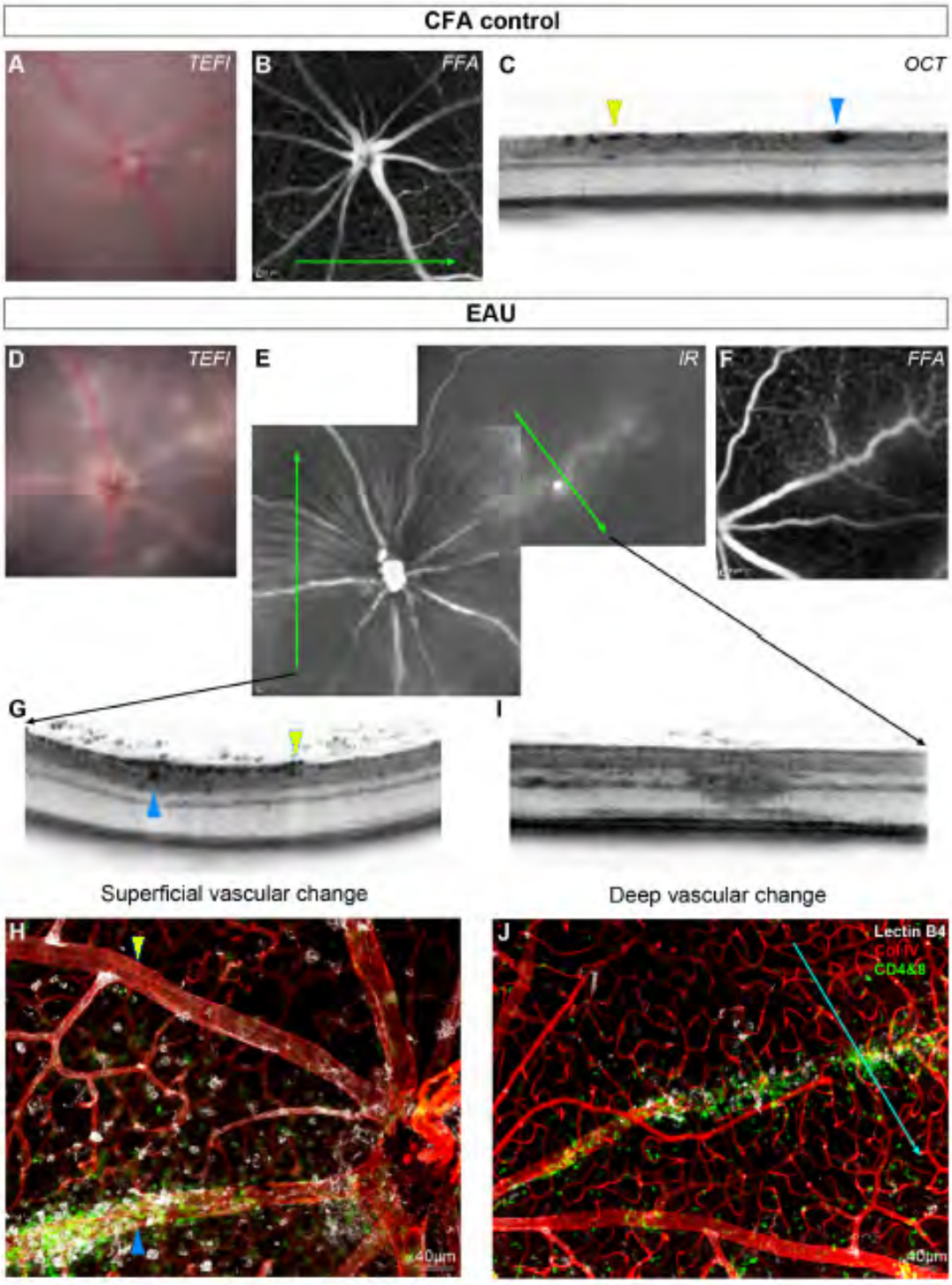

Figure 10. OCT identifies vascular changes in EAU with appearances altered by depth and degree of infiltration. The CFA control eye has normal TEFI **(A)** and FFA **(B)** appearances. The green arrow indicates the orientation and position of the OCT scan **(C)** that transects a superficial retinal arteriole (yellow arrowhead) and vein (blue arrowhead). Matched images from an eye at day 36 post-induction of EAU demonstrate the range of changes **(D–J)**. Corresponding disc swelling and vascular changes are seen on TEFI **(D)** and infrared SLO **(E)**, with mild leakage on FFA **(F)**. One OCT scan transects two large vessels travelling near the retinal surface **(G)**. The vessel (collagen IV in red) with altered OCT signal in the perivascular tissue (upward pointing blue arrowheads) is densely infiltrated with

myeloid - lectin B4 binding (white) and T cell - CD4+ & CD8+ (green) cells as shown by immunohistochemistry on retinal flat mount **(H)**. This is in contrast to the retinal arteriole (downward pointing yellow arrowheads), which lacks any localised infiltrate. Diffuse hyper-reflective signal on OCT **(I)** corresponds to a deep retinal vein, with associated cellular infiltrate **(J)**. The blue line indicates alignment with the OCT scan.

In CFA control mice, vessels assessed by TEFI, FFA and OCT showed a normal, non-inflamed appearance. In contrast in the EAU eyes, TEFI detected several abnormal, inflamed vessels that were also identified on the corresponding infrared SLO image, FFA and OCT. Two large superficial retinal vessels were observed on the OCT scan **(Figure 10G-H)** and their corresponding appearance assessed on flat-mount. Interestingly, the abnormal vascular signal, enlargement and distortion of surrounding retinal tissue on OCT correlated with a dense perivascular infiltrate that surrounded the vessel, whilst the vessel lacking substantial perivascular accumulation of cells was small, dense and had preserved adjacent layers on OCT.

In many mice, including wildtypes, retinal vessels were occasionally observed running below the inner nuclear layer. Involvement of these vessels in EAU resulted in a dramatically different appearance on OCT **(Figure 10I-J)**, with attenuation of signal in most of the thickness of the retinal tissue with evidence of fluorescein leakage on FFA. Whilst it is not possible to detect oedema on retinal flat-mounts, myeloid and T-cells were found to be closely associated with these vessels. Given that such changes can be detected on OCT, the evolution of vasculitis and its effects upon surrounding retina might be further delineated *in vivo* using this technique.

Interesting other features, not recognised as classically part of EAU were observed. One example is of a vascular abnormality that looked similar to the intraretinal neovascularisation observed in chronic retinal degenerations.[30] Noticed during FFA imaging of a mouse at day 36 post-induction, the lesion had both an atypical angiographic and OCT appearance **(Figure 11)**. A video of the 3D reconstruction of this lesion, demonstrating the vascular arrangement can also be seen at:

(http://www.plosone.org/article/info%3Adoi%2F10.1371%2Fjournal.pone.0063002)

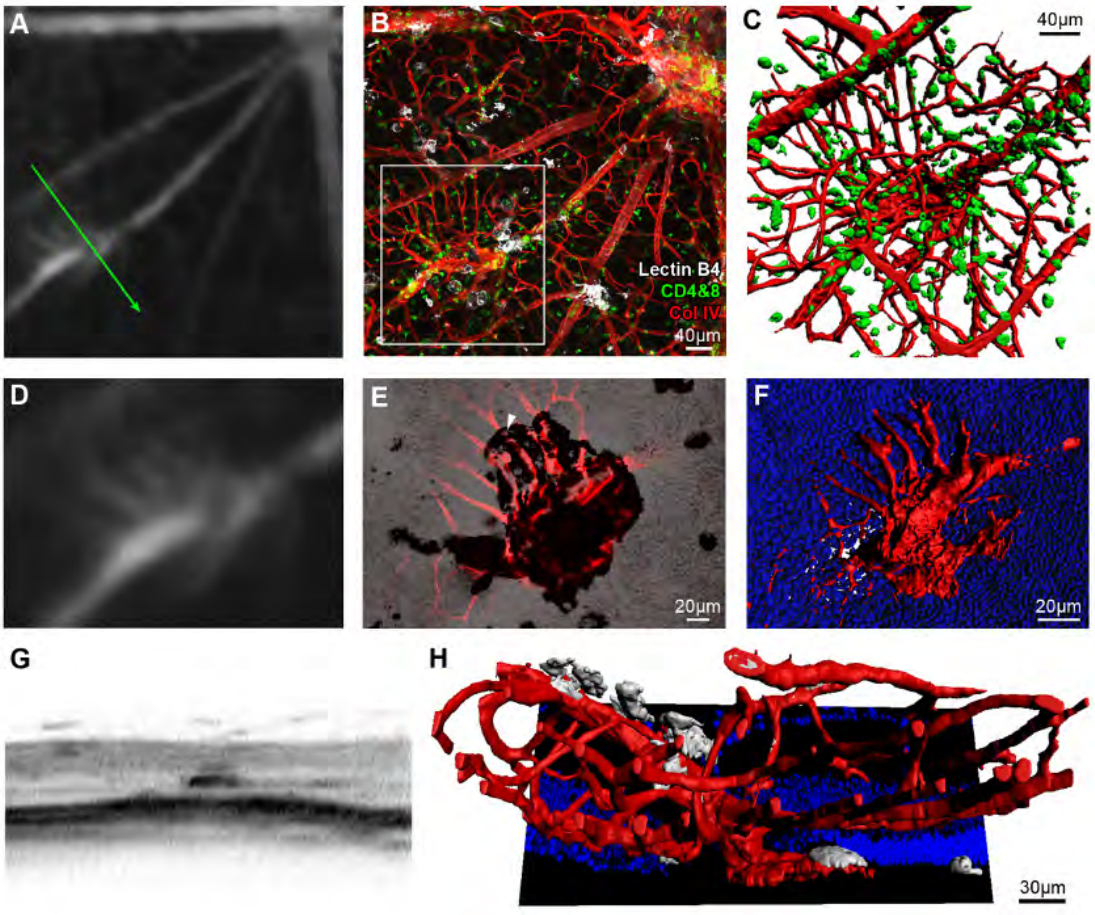

Figure 11. OCT imaging assists the identification and characterisation of novel features developed during the EAU model. Fundus fluorescein angiography (FFA) on an eye at 36 days post-induction of EAU revealed an abnormality initially believed to lie within the spectrum of vasculitis **(A)**. Retinal flat-mount revealed an atypical vascular lesion arising along the course of a large vessel **(B)**. 3D reconstruction of the region (enclosed by the white box), with CD4+ & CD8+ cells (green) displayed **(C)**. Magnified view of the FFA **(D)** correlates with a combined collagen IV (red) and brightfield projection image viewed from the subretinal space towards the vitreous **(E)**. The black patch corresponds to RPE adherence during retinal separation and vessels pass through this region (example indicated by white arrowhead) having arisen from the retina after penetrating the outer nuclear layer (in blue) - highlighted in the reconstruction **(F)**. OCT demonstrates a unique, dense signal appearance **(G)**, inconsistent with more widely observed vasculitic changes in EAU. The green arrow in **(A)** indicates the location and orientation of the OCT scan The arrangement seen on sagittal reconstruction **(H)** might partly explain the appearance, which could be consistent with inflammatory-induced intraretinal telangiectasia, vascular reorganisation or neovascular buds. Lectin B4 staining is displayed (white).

3.4 The development of retinal features during EAU can be tracked by OCT

Whilst in humans, repeated Spectralis OCT scans can be locked to an identical location, this process proves difficult as a result of optical constraints in the mouse. However, features can be manually followed in a single eye and OCT holds the potential to follow the dynamic intraretinal changes during EAU **(Figure 12)**.

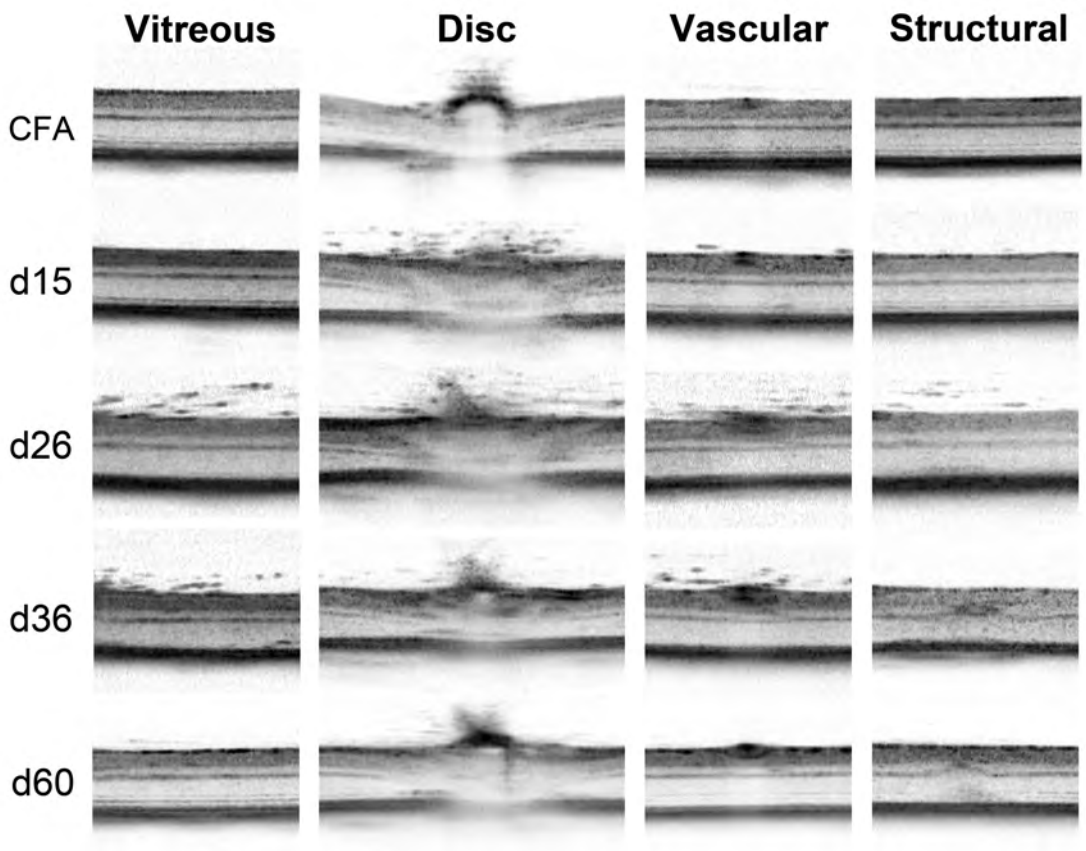

Figure 12. OCT can track the development of tissue changes over time during the course of EAU. Each column illustrates the development of a feature from the same eye of an animal at a constant, manually located region on OCT for all four main features. Timepoints at 15, 26, 36 and 60 days post-induction of EAU are shown.

Due to the intrinsic variability of the model, the timing and severity of changes varies between animals, but a general trend to early inflammation and late reduction in disease is evident. Following peak disease at day 26, vitreous opacities appear to clear, as do perivascular changes. Deep retinal

folds only develop late, are associated with vessels and do not appear to regress in the timeframe examined. The changes at the optic disc are dynamic and also regress following peak disease. Note that it would be impossible to directly quantify the degree of vitreous or intraretinal involvement using TEFI and it is likely that histology would lose the component of disc enlargement secondary to oedema.

3.5 A minimally subjective OCT-based EAU scoring system correlates well with conventional histological assessment

A scoring system was developed which required a standardised method of imaging. Each eye underwent eight scans - two transecting the disc perpendicular to each other, four at the 30-degree edges whilst centred on the optic disc, one far superior and one far inferior shot. This was felt to be the optimal balance between a comprehensive and yet feasible assessment. One example is shown in **Figure 13**. Whilst this set of scans requires around ten minutes per animal and an equivalent amount to process, this is far less than processing, sectioning, staining and scoring histological specimens.

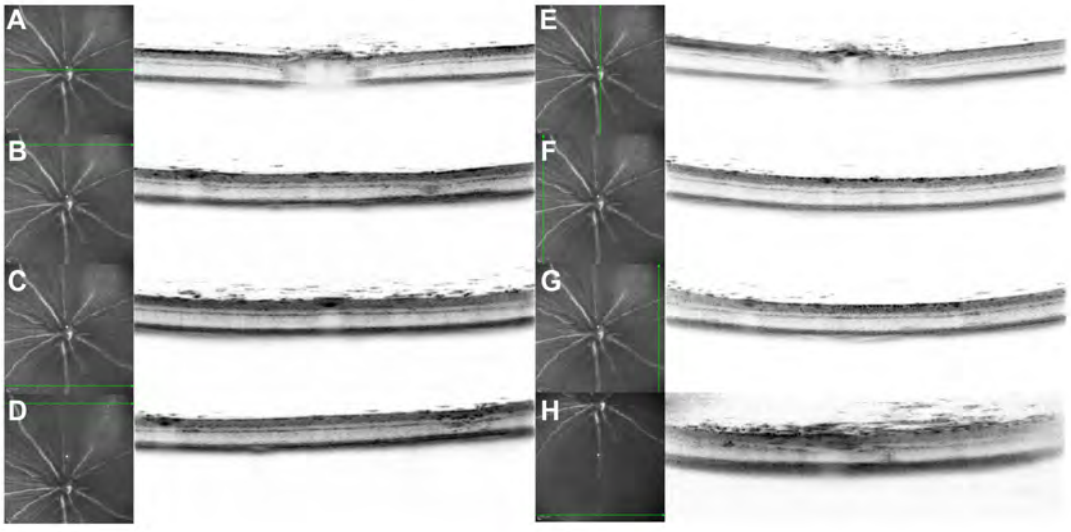

Figure 13. An example of the standard scoring series. Eight shots were obtained from an eye at d26 EAU. Horizontal **(A)** and vertical **(E)** scans through the optic disc, one scan at each of the four edges centred on the disc **(B-C, F-G)** and far superior **(D)** and inferior **(H)** scans were captured.

The OCT scoring system was derived from an analysis of current histological schemes and an appreciation for the developmental time course of OCT changes **(Figure 12)**. The system was constructed to remove subjectivity where possible and thus reduce inter-observer variation. The result involves measuring four variables – vitreous change, disc swelling, large vessel involvement and structural reflective changes. A worked example is shown in **Figure 14**.

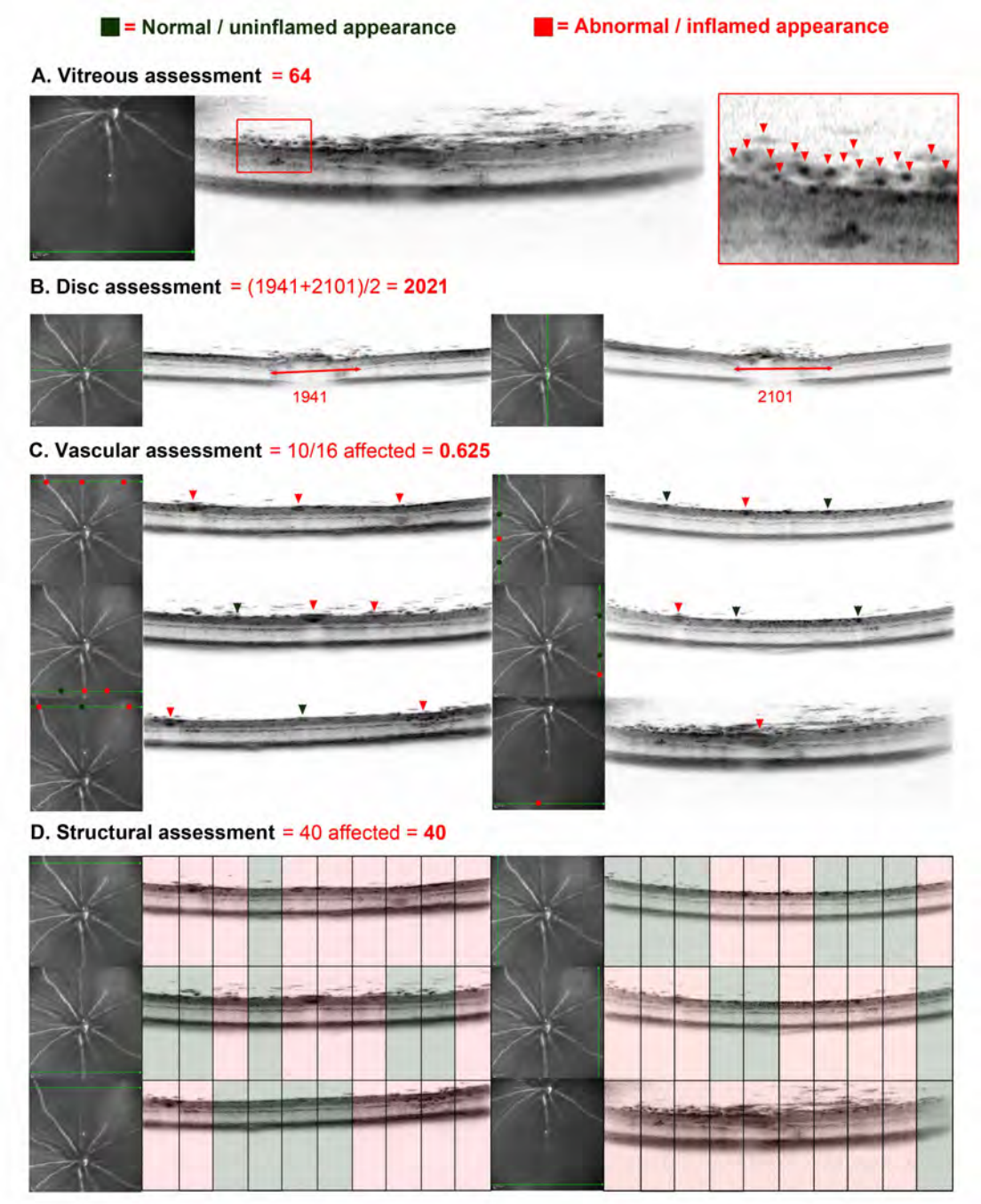

Figure 14. A worked example of the OCT-based scoring system. Using all eight scans, each eye is scored across four domains and the raw results displayed. The number of discrete vitreous opacities separate from the retina is counted in the scan that shows the largest number (**A**). Clusters that would receive scores are illustrated in the red box. A vertical and horizontal average of disc swelling is measured using the on-machine software between the terminations of the layer corresponding to the outer plexiform layer (**B**). Across the six non-disc scans, the proportion of all abnormal vessels of the total transected by all scans is calculated (**C**). The infrared scan can guide vessel location on the OCT B-scan (green arrow indicates position) Non-disc scans are finally divided into ten equal vertical segments and the proportion containing any abnormality (including inflamed vessels, excluding vitreous changes) are counted out of a total of 60 (**D**).

It was necessary to transform the raw scores, to provide a sensible working range and weight each characteristic to provide the greatest correlation between histological and OCT scores **(Table 10)**. This was derived empirically by examining scores in the initial pilot cohort **(Figure 6)**. Additionally, analysis of disc swelling using on-machine measurements is complicated. As each machine and optical adaptation will alter, the disc enlargement score is expressed relative to a cohort of CFA control mice. This cohort would only need to be run once, to calibrate the baseline for the particular machine. Other scores assessing the vitreous, vessels and structure were created to be minimally subjective. Whilst much information could be extracted from a detailed sub-analysis of the intraretinal changes in structure, this was not thought to be practical during application as a scoring tool.

SUB-SCORING CATEGORY	DESCRIPTION	RAW SCORE RANGE PER EYE	ALTERATION FACTOR	EAU SCORE RANGE
Vitreous involvement	Absolute count of discrete opacities in the vitreous space up to a maximum of 150. The count from the worst affected scan is used.	0–150	None	0–150
Disc enlargement	On-machine measure of the linear distance between the termination of the outer plexiform layer equivalent on either side of the disc. For each eye, average the results of the horizontal and vertical disc scans.	Relative value to control CFA group	(Measure/average CFA control group measurement)^2 then multiplied by 35	25.6–92.0 (CFA control group average of 1695 units in this cohort)
Vascular involvement	Number of abnormal vessels as a ratio of total vessels scanned based on OCT appearance. Two disc centred scans excluded.	0–1	Multiply by 300	0–300
Structural change	Using six scans (non-disc centred) only, each is divided into 10 equal vertical segments. The total number not completely normal are counted, ignoring vitreous changes.	0–60	Multiply by 1.5	0–90
			Maximum final EAU score range for this cohort:	**25.6–632**

Table 10. Range and processing of final OCT scores. Weighting was determined by correlation to histology, of which vascular change was most parallel. On average most scores will lie between 20 and 600 points, dependent upon calibration of the disc score. The range for the cohort in these experiments is presented.

Quantitative analysis was possible by combining data from all three cohorts to show the time-course of EAU scores generated using OCT, TEFI and CD45 immunolabelled histology **(Figure 15A-C)**. Scoring was performed by three masked assessors and the averaged results are displayed. The data from each system are presented in raw form and not normalised to one scheme. All three reflect the expected course of EAU and correlate significantly with each other **(Figure 15D–F)**. OCT scores correlated well with histology (Pearson R^2 = 0.6392, P<0.0001, n =31 eyes), affirming the hypothesis that inflammatory changes in the limited 30-degree field of OCT are directly proportional to whole eye changes sampled by histology.

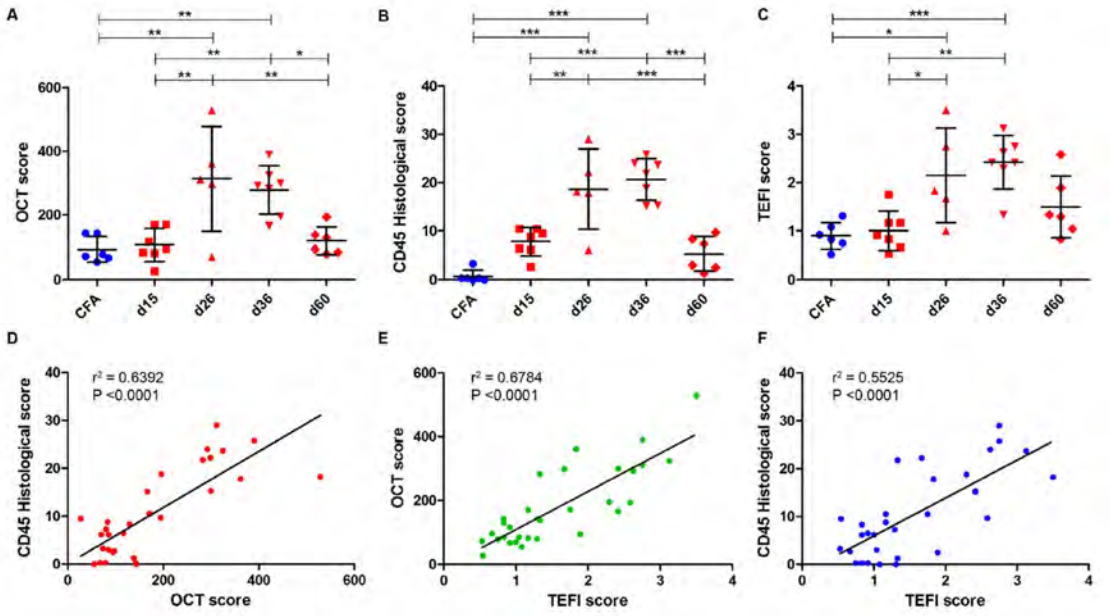

Figure 15. OCT-based scoring correlates well with established measures. Combined data from the cohorts across the entire time-course for **A)** OCT, **B)** histological and **C)** TEFI disease scores. **D)** Correlation between OCT and histology is present. **E-F)** Other correlations between OCT, TEFI and histology. Mean + SD shown. One-way ANOVA (P<0.0002 for each), with Tukey post hoc test for multiple comparison (* = P<0.05, ** = P<0.01, *** = P<0.001). Pearson correlation and linear regression of the values are displayed.

The overall conclusion was that the OCT scoring system correlated well with the gold standard of histology for EAU. There are several advantages to the technique as mentioned, including the possibility for repeated examination of intraretinal changes in the same eye. By removing the need for a parallel cohort for the assessment of disease severity when other analyses such as flow cytometry or Western blot are required, OCT also permits a reduction in animal numbers in line with the principle of the 3R's of animal experimentation. Additionally a severity score matched to the very eye used for such subsequent analysis, can partly mitigate the wide variation in severity between animals with EAU.

3.6 OCT-based EAU scores were validated in an interventional experiment

Whilst the scoring system has been shown to correlate during an observational series, it was unknown whether this would hold true during an independent and interventional experiment. As part of the main project, a head-to-head study was performed, injecting AAV8 expressing either murine IL-10 or GFP control. Nine *C57BL/6J* mice were injected with either vector randomised to an eye. One week later, EAU was induced and the OCT scoring series acquired at day 26, before histological processing of the eyes.

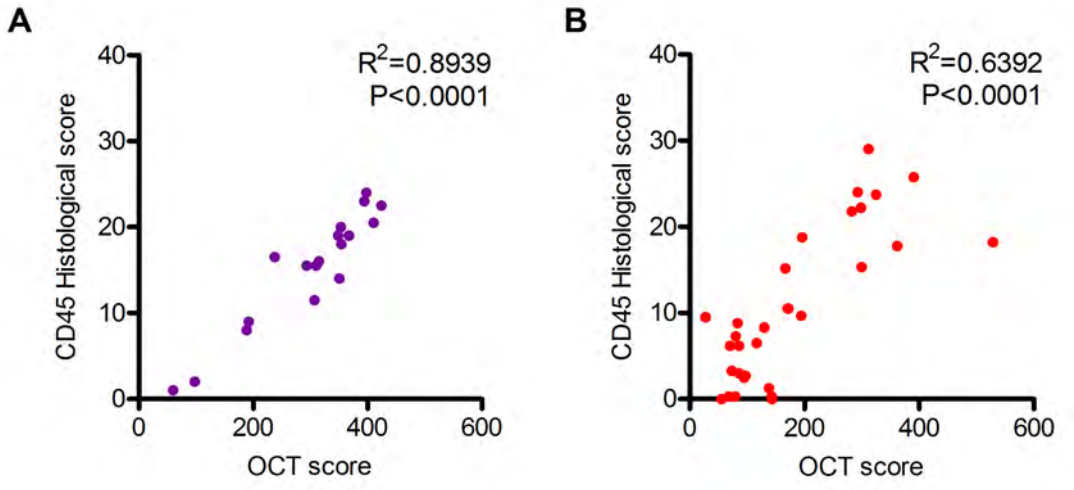

Figure 16. The OCT-based scoring system was validated in an interventional experiment. Comparison between the calibration cohort and an experiment injecting AAV8-CMV-mIL-10-IRES-eGFP and AAV8-CMV-hrGFP control vector one week prior to the induction of EAU. OCT imaging was performed at day 26 and the same eyes taken for histological CD45 scoring. **A)** The correlation from this experiment reveals a significant and even better fit between the OCT and histological scores than the correlation in the initial calibration experiments **(B)**. Pearson correlation shown. Each point represents one eye.

Disease was scored by two masked assessors **(Figure 16)**. The previously observed correlation was seen and was even tighter, perhaps due to less inter-observer variation or as a function of the intervention. This provided confirmation that the system was valid over a range of applications and was suitable for further use.

3.7 Electroretinography of EAU in the C57BL/6 mouse is confounded by the induction protocol

Electroretinography was performed in collaboration with Dr Livia Carvalho. A pilot study showed electroretinogram (ERG) changes at day 40 post-induction of EAU **(Figure 17A-B)**, with reduced b-wave amplitude compared to wildtype mice (n=7 EAU, 3 control). As an ERG defect was identified, the OCT cohorts were assessed by ERG and also demonstrated progressive loss of b-wave amplitude, indicating possible photoreceptor or bipolar cell dysfunction from 15 days post-induction onwards **(Figure 17C)**. Surprisingly, the control cohort that received the same dose of subcutaneous CFA and intraperitoneal pertussis toxin only developed comparable ERG changes **(Figure 17D)**. Whilst the mean b-wave amplitudes of the CFA controls were always higher than the EAU cohort, there was no statistical difference at any timepoint. Expressing the values as a percentage of the original baseline ERG did not provide any additional insight **(Figure 17E)**. Photopic readings showed an identical pattern to the scotopic throughout (data not shown).

The progressive amplitude suppression in the control group was unforeseen. Structural appearances of the retina by OCT, TEFI and histology were as expected. It is possible that either the CFA, or the Pertussis toxin was leading to inhibition of the ERG. As Pertussis toxin *in vitro* can inhibit G-protein signalling, it was felt to be the most likely candidate, by directly inhibiting phototransduction components such as Transducin[173] but no studies have previously documented the effects upon the retina *in vivo*. It is unusual though that the effects persisted to 36 days after injection. Due to time constraints, a repeat study with a Pertussis toxin alone cohort has not been performed. The implications of this study will be discussed in later chapters.

As b-wave amplitudes began to resolve at day 60pi, it was possible that a window of opportunity existed, where the side effects of the induction were resolving and the persistent ERG reduction from structural damage in EAU was evident. ERG was performed on three additional WT mice and the mean plotted against the raw values of the other cohorts **(Figure 17F)**. As complete

groups there was no statistical difference, but compared to this reference, 67% of the CFA group eyes were equal to or greater than the WT mean, against 17% with EAU. This suggests that if repeated or with greater animal numbers a difference might be seen, at a timepoint when it is likely the effects of the induction have ceased, particularly if the low values in the CFA group are erroneous outliers.

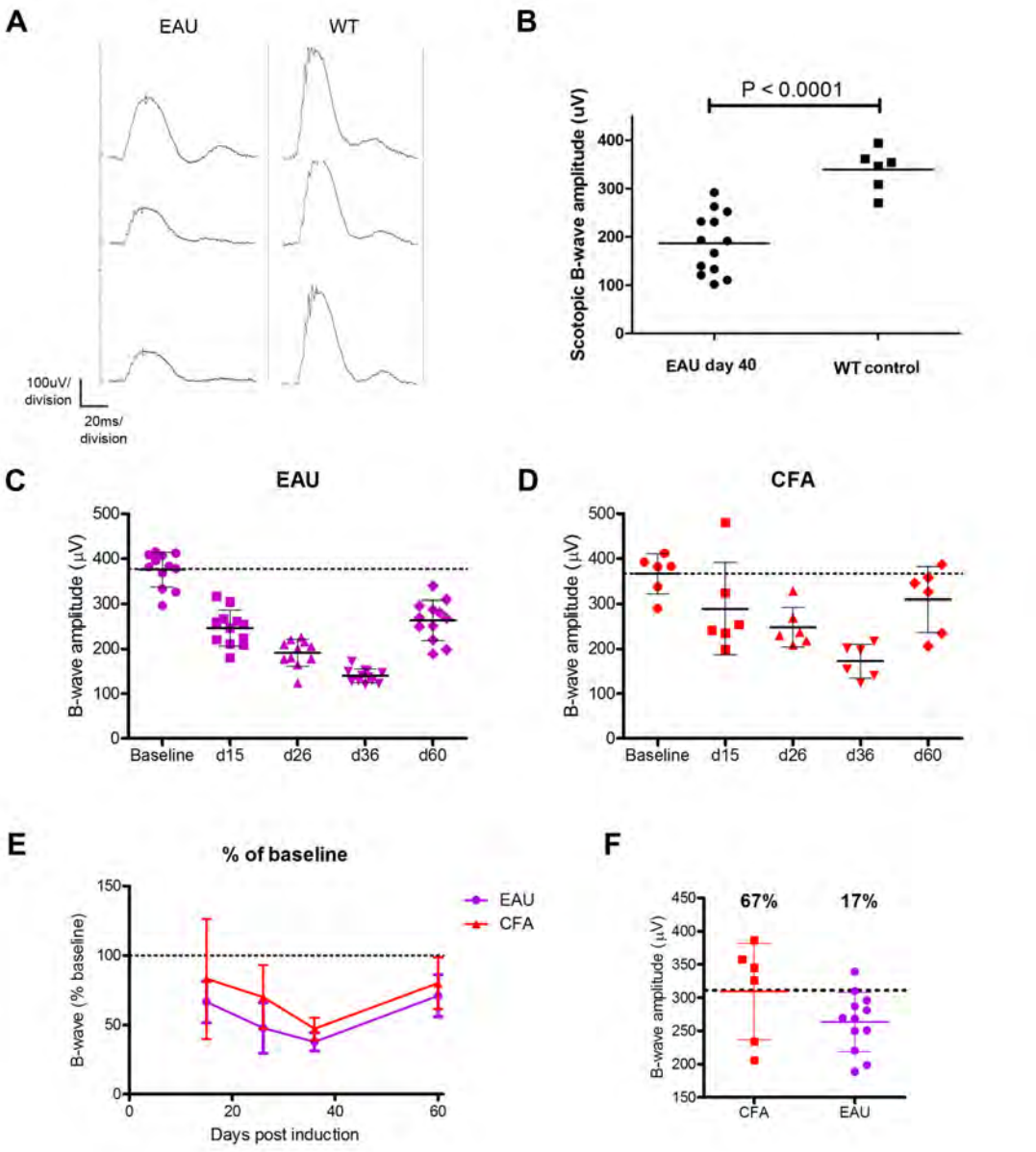

Figure 17. The scotopic electroretinogram shows reduced b-wave amplitude during *C57BL/6* EAU, but this may be a result of the induction protocol. A cohort of mice at day 40 post-induction of EAU was compared to wildtype (WT) mice. **A)** Representative averaged scotopic traces are shown for three individual animals, illustrating reduced amplitude in EAU. **B)** Pooled results for the cohort show a significant difference. Each point represents one eye. Mann-Whitney U test used. The OCT cohort underwent ERG at each timepoint and **C)** scotopic

ERG b-wave amplitudes show a progressive reduction over time, with partial recovery by day 60pi. **D)** The cotemporaneous CFA (+Pertussis toxin) control cohort also showed similar reduction in the b-wave. This could not be corrected for by plotting as a change from baseline ERG **(E)**. Three WT mice underwent ERG contemporaneously with day 60pi mice **(F)** and the mean b-wave amplitude of 311μV is shown as a dotted line. As groups there was no statistical difference between EAU and CFA, although a greater percentage of the latter reached the mean WT value or above. Means + SD shown. All traces were analysed at a scotopic flash intensity of 0.03cd.s/m^2.

3.8 OCT is possible, but not as suited to the *B10.RIII* model of EAU

It was uncertain if OCT was a possible assessment method in the *B10.RIII* strain model of EAU, which develops severe vitritis, retinal detachments and posterior synechiae - all of which would be expected to affect OCT scan quality. Of six eyes examined, only one eye had posterior synechiae that precluded examination. A representative example of a mouse without posterior synechiae is shown below **(Figure 18).** All three modalities of OCT, TEFI and histology correlate with large retinal folds clearly imaged. Uniquely, OCT reveals the presence of subretinal fluid - known to occur in this model. This feature **(Figure 18E**, **red arrow)** is typically lost during histological processing, but is an important marker of severe disease.

In view of the perceived limitations and low use of the strain in this project, no further work was performed. Two years later an OCT based grading system was published by another group.[174] The difficulties of imaging this model were evident, as distinct features were not incorporated into the scoring system. Overall retinal thickness was used as a gross measure instead. It would be possible to examine the model in post-peak disease when the vitritis has resolved. The technique would then be highly pertinent to investigating severe chronic inflammatory changes are known to result in tissue remodelling and angiogenesis.[24]

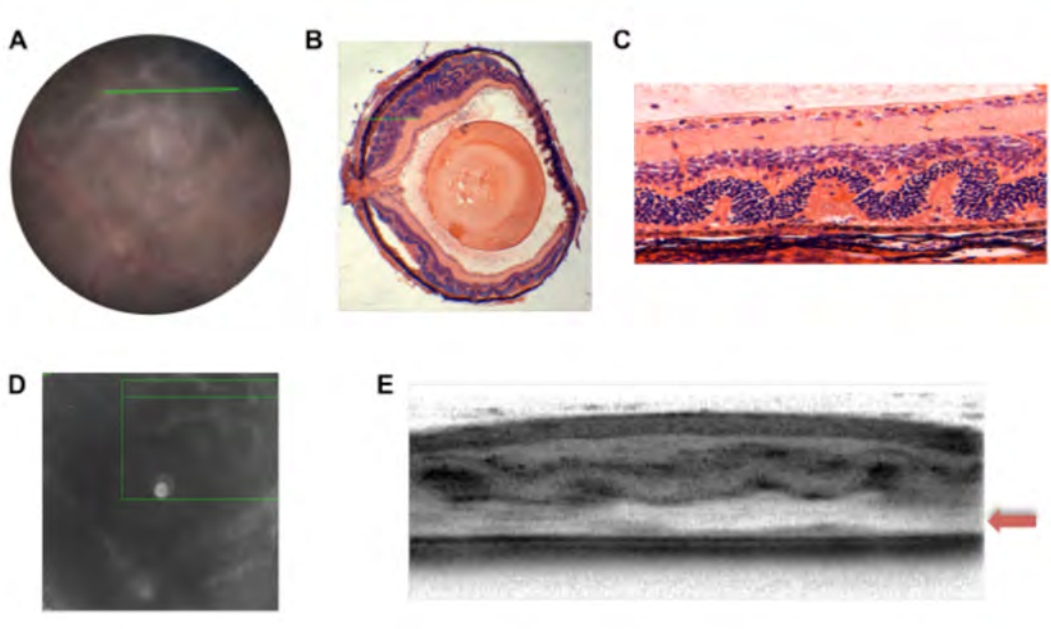

Figure 18. OCT can detect pathology during the severe form of EAU induced in the *B10.RIII* mouse strain. Despite marked vitritis and extensive retinal disruption, it was still possible to obtain reasonable scans in the B10.RIII strain model. Widespread retinal folds confirmed by TEFI **(A)** and histology **(B and C)** could be identified on the infrared scout image **(D)** and imaged by OCT in cross-section **(E).** The folds correspond to changes in the outer nuclear layer in both tissue sections **(C)** and OCT **(E)**, with only the latter demonstrating likely subretinal fluid (red arrow), which would be lost during fixation and histological processing.

3.9 Chapter summary

The detection and analysis of key features during EAU in the *C57BL/6* mouse is possible using OCT. Vitreous infiltration can be quantified and does not significantly degrade the quality of the retinal images. Optic disc enlargement can be measured and is a dynamic feature over the course of the disease. Deep retinal features, such as folds are demonstrable and matched histology on flat-mounts used to dissect their associated cellular phenotype. Vasculitis can also be imaged, with the appearance dependent upon vessel depth within the tissue. Incorporating all of these features, a scoring system has been created and shown to significantly correlate with established histological disease scores. This scoring system was subsequently validated in an interventional experiment.

4 Results 2: Flow cytometry as a quantitative scoring system for endotoxin induced uveitis

Endotoxin-induced uveitis (EIU) is primarily an acute response to injected lipopolysaccharide (LPS) and as a model of human uveitis *per se*, it serves best to elucidate mechanisms rather than as a direct clinico-pathological correlate. It has however been used to emulate mechanisms of human anterior uveitis, particularly following the known association with gram-negative bacterial infection and predominant anterior segment infiltration.[32] Unlike EAU, there is minimal tissue damage and disease is self-resolving.

In this project EIU was employed as it provides several advantages over EAU, namely it elicits a narrower range of pro-inflammatory signals and it is rapid. It takes up to 24 hours to reach peak disease, compared to 26 days, so different therapeutic approaches could be tested more swiftly. Although the immunological mechanisms are not identical, it has been shown that many EAU therapeutic agents such as IL-10 and TNF receptor fusion proteins can also suppress EIU.[34,107] With this in mind, once basic parameters are optimized in EIU, they can be applied back to the EAU model.

To date in the literature, whilst flow cytometry has been used for investigating some features of the model, only histology has been routinely used to assess the outcome (scoring) of murine EIU. As with most semi-quantitative analyses, studies have typically used limited numbers of semi-thin paraffin sections taken across each eye and then performed subjective cell counts of haematoxylin-staining cells in a random selection of only the aqueous or vitreous spaces. Building on the experience of flow cytometry for EAU, it was decided to investigate the technique as a routine outcome measure for EIU.[42,159]

We decided to induce EIU by intravitreal injection of 1ng LPS from E.coli which generated larger numbers of infiltrating CD11b+Ly6G+ cells than systemic induction. The severity of this procedure is less, as acute peritonitis

and septic shock are not induced in the mice. Animals were culled 16-18 hours later and this will be referred to subsequently in the text as 'standard EIU induction.'

Briefly, eyes with EIU are dissected in 50µl PBS, the aqueous humour is washed out and the retina and enclosed vitreous removed. These are aspirated into a tube and mechanically dissociated, before being spun through a specific 60µm pore diameter 96-well filter plate. The cornea, iris, ciliary body, lens and RPE/choroid are not needed and can be used for matched alternative analyses, such as ELISA or qPCR. Dissociated cells are retained in the 96-well plate and form a cell pellet after the first spin. The supernatant can also be removed at this stage for other analyses and matched to the subsequent EIU score. Antibody staining and washes are performed in the same 96-well plate. Anti-CD11b and anti-Ly6G are the minimum recommended choice of antibodies. Where possible anti-Ly6C and a live-dead stain are included. We use a flow cytometer with a compatible automated plate loader, which also improves the efficiency of the technique. A standard curve of polystyrene beads is run for each experiment, which allows the calculation of an absolute cell count for the whole sample. The absolute count of CD11b+Ly6G+ cells was used as the single routine outcome score, as it is known that these neutrophils are the predominant and key cell type in EIU.[32]

4.1 Defining the standard EIU model using a flow cytometry based approach

Hypopyon was routinely obtained using this EIU technique, which reflects the severe end of the disease spectrum when compared to the equivalent clinical observation of anterior uveitis in humans **(Figure 19A)**. The gating strategy included sequential gating on CD11b+ then Ly6G+ and Ly6C+, permitting enumeration of neutrophils and monocytes respectively.[43] Flow cytometry plots are displayed for an eye undergoing 'standard EIU induction' of 1ng LPS in 2µl, culled after 18hrs. **(Figure 19B)**. In the normal mouse eye there are few CD11b+Ly6G+ cells. Following standard EIU induction, a mean of

around 20,000 cells is detected per eye at 18 hours **(Figure 19C)**. Technical refinements to the model itself can also be assessed, as many groups use different injection volumes and doses of LPS.[33,175,176] As part of our own evaluations, the delivery volume and dose of LPS was varied. Reducing the delivery volume to 1µl led to reduced disease, but increasing the dose to 200ng LPS with a constant volume of 2µl did not result in an increase in infiltrate **(Figure 19C)**.

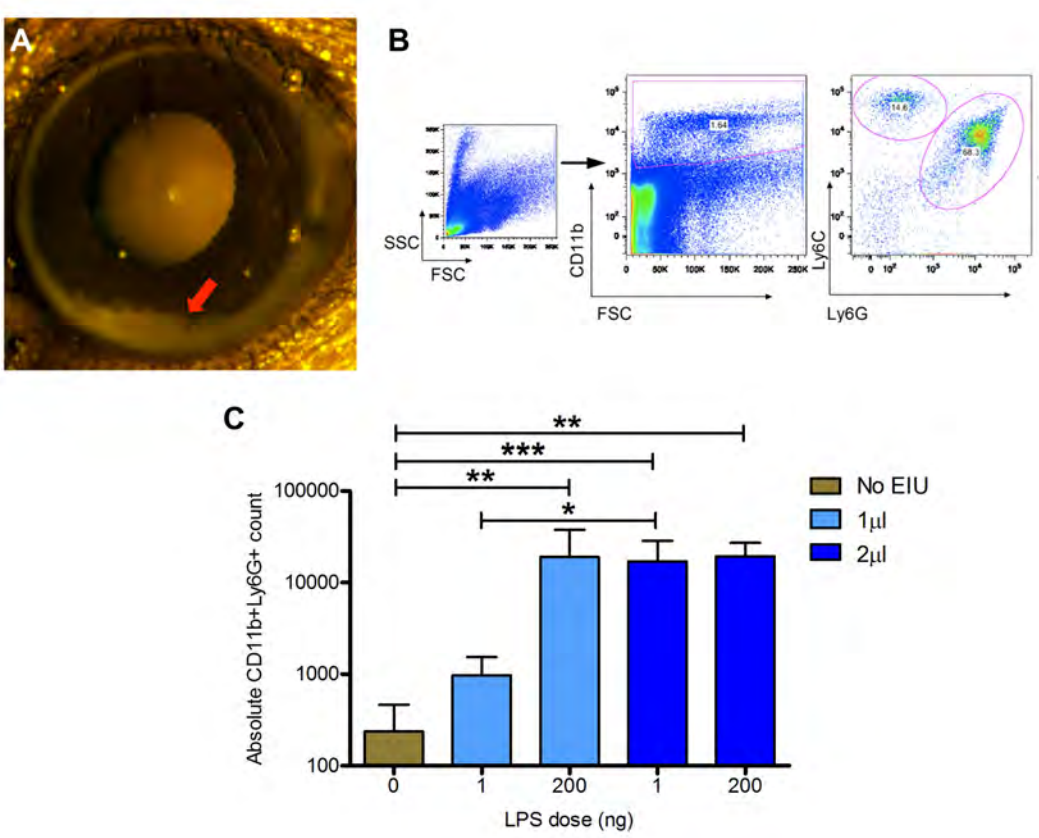

Figure 19. Characterisation of EIU using quantitative flow cytometry. Following standard EIU induction with a 2µl intravitreal injection of 1ng LPS from E.coli, by 18-hours **A)** most eyes have developed hypopyon (sedimented leukocytes in the anterior chamber; red arrow) similar to that seen in severe human anterior uveitis. **B)** The AC, retina and vitreous can be dissociated for combined analysis by flow cytometry. A representative example of flow plots shows that sequential gating by CD11b staining allows the identification of distinct Ly6G+ and Ly6C+ populations. Calculation of an absolute cell count is possible using a standard curve. **C)** Taking this CD11b+Ly6G+ cell count (neutrophils) as the measure of EIU severity, an average count of 20,000 is obtained following standard EIU induction with 1ng LPS in 2µl, and is clearly differentiated from eyes not receiving LPS. Altering conditions of the EIU model itself can be assessed. At the standard 2µl volume, increasing the dose of LPS further to 200ng has minimal effect. Delivering 1ng in 1µl however leads to reduced disease, overcome

by using 200ng in 1 µl. Kruskal-Wallis test with Dunn's multiple comparison test. *=P<0.05, **=P<0.01, ***=P<0.001. n=5-6 per group.

Whilst CD11b and Ly6G are the only phenotypic markers required for simple assessment, the flow cytometry panel can be extended. An expanded composition within standard EIU was determined, showing that CD4 and CD8 T-cell content was negligible and only a small number of CD94+ cells were identified, which should represent NK and NKT cells. The population classified as CD45+ but negative for additional markers and labelled as 'other' may comprise resident microglial cells **(Figure 20A-B)**.

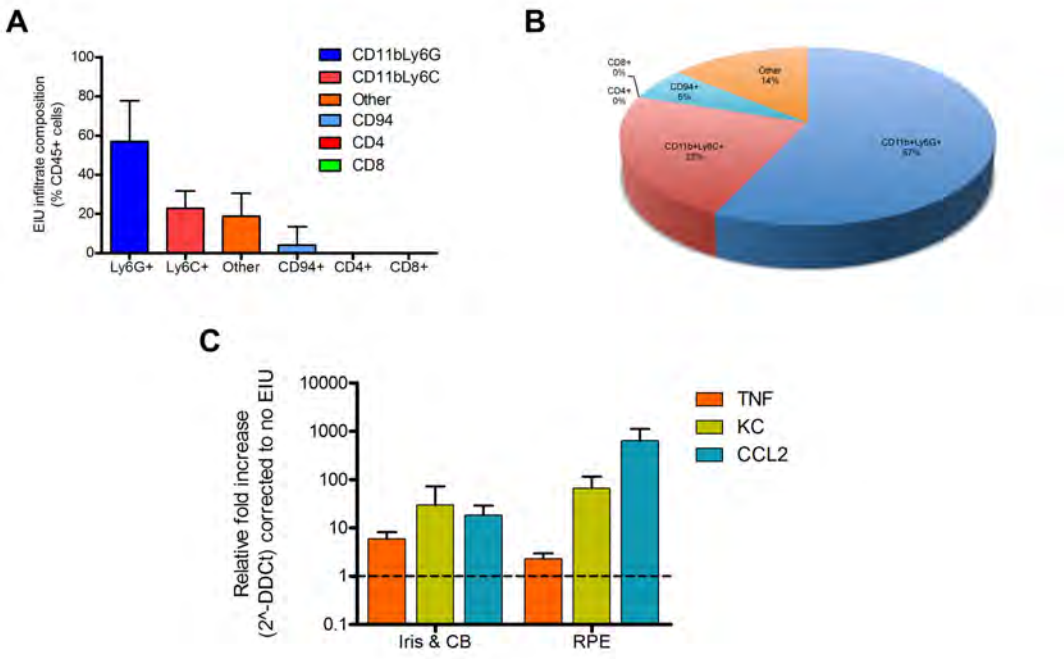

Figure 20. Composition of the infiltrate in EIU can be distinguished by flow cytometry whilst qPCR on matched tissues can assess the transcription of multiple chemokines. Flow cytometry allows the simultaneous analysis of subtypes, identifying mainly CD11b+Ly6G+, CD11b+Ly6C and CD94+ cells. **A)** Samples were first gated on CD45+, and then expressed as percentage of this population. n=6. **B)** The same data displayed as a pie chart, to highlight the predominant CD11b+Ly6G+ population. As only the AC, retina and vitreous are used for cell counts, the remaining iris, ciliary body (CB) and RPE/choroid were used for **C)** quantitative RT-PCR for key chemokines in EIU relative to β-actin and normalised to eyes with no disease. n=3 per group, with technical triplicates. Means + SD shown.

Finally by using matched iris, ciliary body and RPE from eyes analysed by flow cytometry, RNA transcripts for TNF, KC and CCL2 could be detected by

quantitative RT-PCR. All three were elevated and are known to contribute to cellular recruitment and blood-ocular breakdown **(Figure 20C)**.

4.2 Timecourse and compartmental analysis of EIU

The infiltrate in EIU can be further scrutinised by keeping the anterior chamber infiltrate separate from the retina/vitreous. This is performed by careful dissection, puncturing the cornea and evacuating the aqueous humour separately, before extracting the retina. Similar appearances by flow cytometry are seen **(Figure 21A)**. Following standard EIU induction a near equal division of numbers is seen, with a trend towards a greater CD11b+Ly6G+ count in the AC **(Figure 21B)**.

Live-Dead discrimination is routinely performed in flow cytometry using dyes such as DAPI, 7AAD or propidium iodide. We used proprietary fixable live-dead 780nm stain to examine the viability of cells detected in EIU. One caveat is that dead cells can non-specifically stain with antibody, however this was not observed to be substantial after comparing samples tested with and without live-dead discrimination, where no dead cells were seen to stain for multiple incompatible markers as might be expected. Subsequently, live-dead staining was used routinely to look at the viability of subsets. To observe if changes in cellular viability occurred over the duration of recruitment into the eye, an early timepoint of 6-hours was also included. Interestingly a greater number of CD11b+Ly6G+ cells in the retina were dead than in the AC and the percentage was higher at 18-hours, though it is possible that the increased processing time might affect this **(Figure 21C)**. With monocytes a similar pattern was seen, however a higher proportion of cells were dead in the retina at 6 hours **(Figure 21D)**.

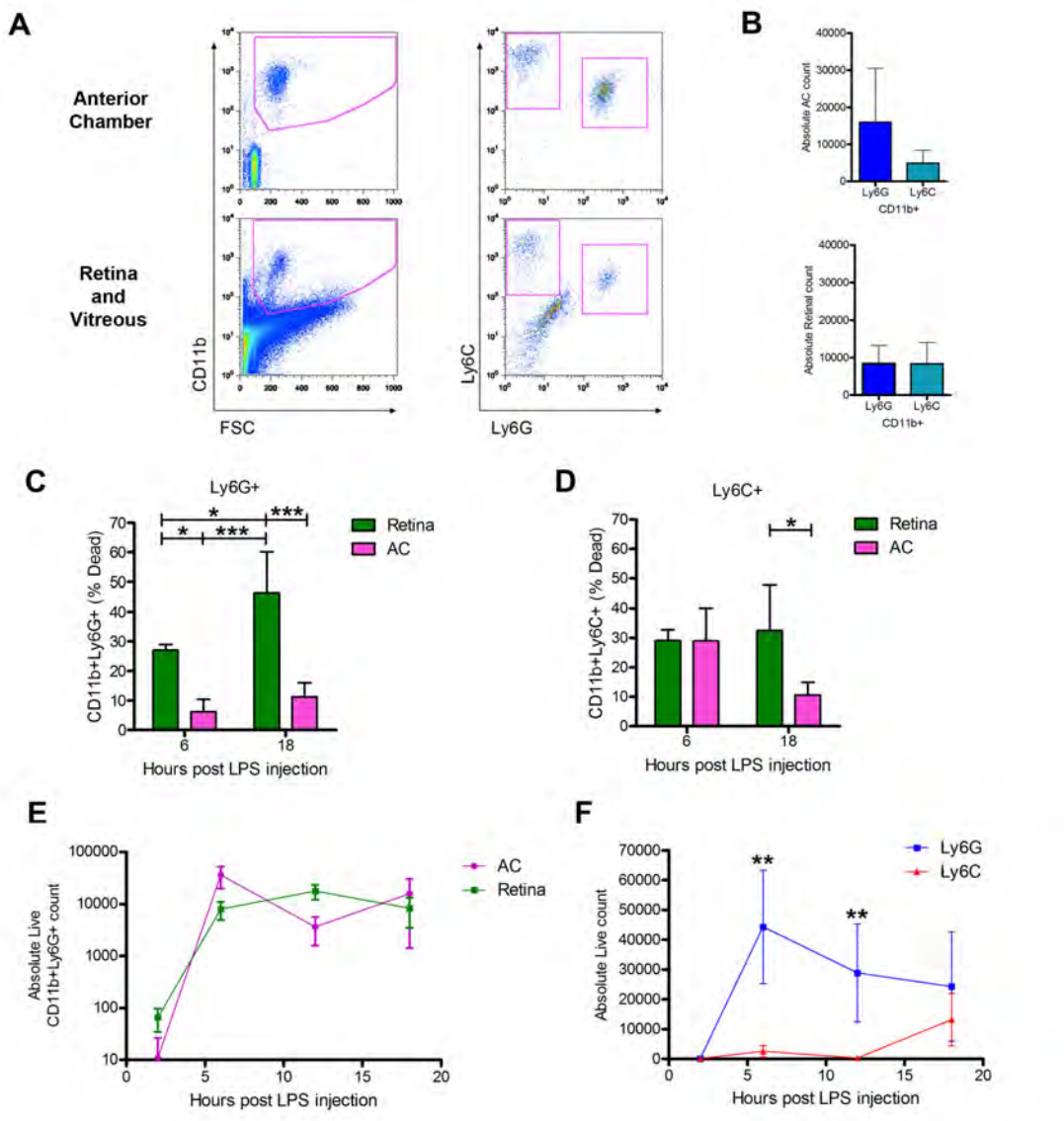

Figure 21. Compartmental sub-analysis of the EIU model is possible using flow cytometry. Standard EIU was induced with a 2µl intravitreal injection of 1ng LPS from E.coli. When dissected at 18-hours for analysis, the AC was kept separate from the vitreous and retina. **A)** Representative flow plots showing gating for CD11b then Ly6G or Ly6C, display each population clearly identified in both compartments. **B)** Absolute AC and retina/vitreous counts of individual eyes from two separate experiments for CD11b+Ly6G+ and CD11b+Ly6C+ cells. There is an approximately even split between compartments. n=6. Vital dyes can be uniquely used with flow cytometry to gauge the live and dead status of cells in the infiltrate. **C)** Relative comparison between the percentage of dead CD11b+Ly6G+ cells in the AC and retina at an early and standard timepoint. More dead cells are seen in the retinal compartment. **D)** There is a more even pattern for CD11b+Ly6C+ cells, but greater viability in the AC at 18-hours. **E)** An extended timecourse of live CD11b+Ly6G+ cells at 2, 6, 12 and 18-hours post-induction for the two compartments. This demonstrates a rapid increase, with negligible cell numbers at 2-hours, but a near plateau by 6-hours. **F)** Whole eye counts for simplicity illustrate the relative change with Ly6G+ cell infiltration early and increasing

numbers of Ly6C+ cells towards a later stage, in line with the known pattern of monocyte accumulation in EIU. Means + SD shown. Kruskal-Wallis test with Dunn's multiple comparisons. *=P<0.05, **=P<0.01, ***=P<0.001.

A timecourse was undertaken to understand the effect of time upon EIU dynamics and cellular composition. At 2-hours no infiltrate could be detected, but by 6-hours, near-maximal numbers of CD11b+Ly6G+ cells were present in both the AC and retinal compartments **(Figure 21E)**. Looking at combined counts, from 6 hours onwards, the overall number of CD11b+Ly6G+ cells does not markedly change, but the CD11b+Ly6C+ cell number dramatically increases by 18-hours **(Figure 21F)**. This is consistent with previous published studies and proposed to be monocytes entering to clear dying neutrophils.[175]

4.3 Validation of flow cytometry for EIU from interventional experiments

This EIU scoring protocol has been applied extensively to work detailed in subsequent chapters. As examples to support the validity of the approach, three different experiments are outlined in **Figure 22**. In the first, the effect of systemic Dexamethasone upon subretinal detachment alone prior to EIU was tested and found not to affect the degree of infiltration. The lack of a significant difference is clearly seen, alongside an accurate description of the wide biological and technical variation that exists **(Figure 22A)**.

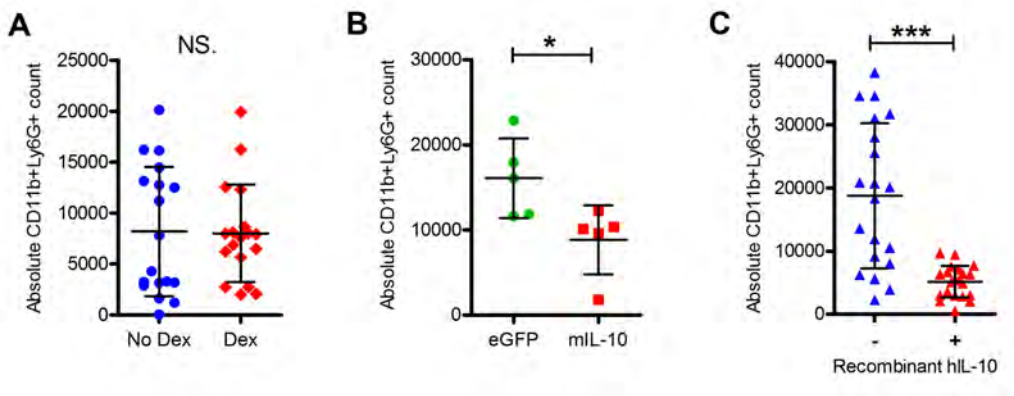

Figure 22. Examples of flow cytometry applied to interventional EIU experiments. 2mg/kg systemic Dexamethasone was administered at the time of subretinal injection of a mixture of

PBS and AAV8-hrGFP to determine if it affects the degree of EIU induced a week later. **A)** Flow cytometry quantitatively confirmed it had no effect, nor was one apparent during subgroup analysis. **B)** Another experiment assessed the effect of intracameral administration of Lentivirus expressing either GFP or murine IL-10 upon EIU. Flow cytometry reproduced the expected result obtained previously conventional histology. **C)** An interventional experiment administered concurrent doses 200ng of recombinant human IL-10 at the time of EIU induction. Suppression of both the mean value and biological variation of infiltrating cell counts was demonstrated. Mann-Whitney U test, *=P<0.05, ***=P<0.001. Means + SD shown.

The second experiment was a repeat of published work suppressing EIU by gene transfer of murine IL-10 by intracameral delivery of Lentivirus.[34] As seen when assessed by histology in the published paper, a significant reduction in cells was seen in the AC **(Figure 22B)**. Finally, the effect upon EIU of direct administration of recombinant human IL-10 into the AC was investigated. Marked suppression with reduced neutrophil numbers was seen, again in line with published data obtained using histology **(Figure 22C)**.[177]

4.4 Chapter summary

Flow cytometry can be used to score the severity of EIU in place of conventional histological counts. A quantitative assessment is possible and using CD11b+Ly6G+ gating, the exact number of neutrophils ascertained. The standard range of disease for EIU was characterised, with a mean infiltrate of 20,000 neutrophils at 18-hours. Key cellular populations were identified as Ly6G+ neutrophils, Ly6C+ monocytes and CD94+ cells such as NK and NKT cells. The benefit of matched residual tissues was demonstrated through the detection of TNF, KC and CCL2 upregulation in RPE and iris/ciliary body homogenates. Live-dead discrimination revealed greater viability of cells in the anterior chamber compared to the posterior compartment. A timecourse demonstrated the rapid ingress of neutrophils from 6-hours post induction, with numbers of Ly6C+ monocytes only increasing by 18-hours. Finally, three interventional experiments demonstrated the successful application of this technique.

5 Results 3: Refinement of vectors and AAV production for ocular immunomodulation

Ocular gene therapy as a field and the development of AAV vectors have been geared towards the correction of inherited monogenic disorders. The first clinical trials in the eye used AAV2 to replace the RPE65 gene in deficient patients.[48-50] None of the patients had significant pre-existing ocular inflammation and no obvious immune-related complications developed during the trials. However, during early experiments looking at modulating of models of ocular inflammation such as EAU, it became apparent that the AAV vector preparations generated, whilst adequate for monogenic gene therapy rescues, were not optimal for immunomodulation.

Several refinements were investigated, such as changing production procedures to obtain cleaner and more pure AAV preparations. The consequences of endotoxin contamination were explored and new vector production methods were developed to address the endotoxin issue. Avoiding the subretinal route was one aim, achieved by introducing the use of an engineered AAV serotype into the lab. Finally some key assumptions, such as the direction of secretion of transgenes from the RPE and the benefit of Dexamethasone treatment were examined. The intention was that these refinements would make successful suppression of intraocular inflammation more likely.

5.1 Improving the AAV production and purification process

Following the failure of mIL-10 to supress EAU after expression using subretinal AAV9, a reassessment of the quality of AAV preps was made (see **results chapter 4**, **Figure 36**). A trial run using a new AVB-medium based column seemed to lead to less toxic retinal changes, though the titre and efficiency of production was less. This relatively simple change appeared to be beneficial and so other issues were identified and changes instigated. For exact details of the production and purification process see **Materials & Methods**.

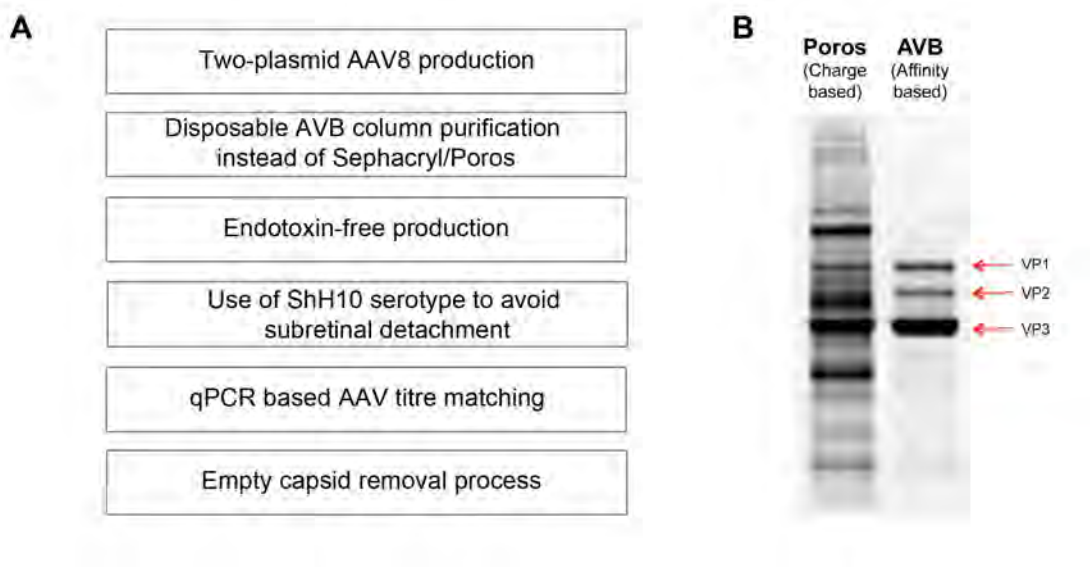

Figure 23. Alterations leading to the refined AAV production process. Key changes instigated are **A)** listed for reference. **B)** An example of titre-matched AAV8-CMV-mIL-10-IRES-eGFP analysed by SYPRO Ruby gel. The three viral capsid proteins VP1-3 are indicated. Other sized bands represent non-viral protein contaminants.

Several of the refinements to the production process for AAV manufacture in the lab are summarised in **Figure 23A**. The decision was made to switch to using the AVB column permanently. Previously AAV9 was purified using sequential Sephacryl (size separation) and then Poros (anion-exchange) medium based columns. Whilst these lead to high titre preps, the relatively unselective and crude separation based only on size and a broad window of protein charge results in multiple contaminating proteins. The majority of these are likely to derive from HEK-293T cell components used to generate the AAV and would be expected to be highly immunogenic and biologically active. Additionally, columns would be reused around thirty times, which whilst regenerated with buffer and washed at each stage, is still likely to accumulate contaminants.

AVB-medium is a commercially available compound by GE Healthcare engineered to bind the AAV2 capsid with high affinity, but is not antibody based. Whilst the exact binding residues are commercially sensitive, it has been stated as also able to bind AAV1 and AAV5. In our hands AAV8 binds well and AAV9 less so, though still to a usable degree. Having trialled a pre-

packed 5ml column, disposable 1ml sized columns were settled upon for use a maximum of three times. When compared by SYPRO Ruby total protein stain on a denaturing polyacrylamide gel, the greater purity - with essentially only the VP1-3 AAV capsid proteins visible – can be seen compared to Poros/Sephacryl separation **(Figure 23B)**.

To enable efficient purification without loss of titre, it was decided to change to using AAV8. In terms of speed and cellular transduction profiles, it is very similar to AAV9, except it is not known to infect Muller cells. A two-plasmid system was possible using the commercially available pDP8.ape plasmid. Traditional three-plasmid transfection – genomic, capsid and helper – requires three separate plasmid preparations, each with the risk of contamination or plasmid mutation at each stage. Requiring one plasmid fewer not only reduces these issues, but there is evidence that improved viral titres are achieved due to optimised ratios of components.[178] Furthermore pDP8.ape can be relatively cheaply purchased at high GLP grade quality, superior to any achievable in the lab and was done so from Plasmid Factory GmBH, Germany.

At the same time as AAV9-mIL-10 was observed to lead to retinal loss, the issue of possible endotoxin contamination arose. Endotoxin, or lipopolysaccharide is a cell wall component derived from Gram-negative bacteria and a common environmental contaminant. The AAV9 viral preparations were tested and whilst the non-toxic AAV9-CMV-hrGFP prep was positive at 300 EU/ml, the toxic AAV9-CMV-mIL-10 was heavily contaminated at over 100,000 EU/ml. It is possible this may have led to the changes observed and the immune status of the eye is likely to be altered by LPS.

It was decided to alter the production process so all AAV preps used for *in vivo* work would test below 2.5EU/ml. This limit was empirically chosen, based on an extrapolation of the FDA maximum permitted levels on devices used upon humans. It should therefore be suitably low. All testing was performed using the Limulus Amoebocyte Lysate (LAL) method, which is the

industry gold standard. An assessment of the endotoxin contamination status of viral preps and key reagents used in the facility was made **(Table 11)**.

Sample type	Subtype	Number tested	Above 2.5 EU/ml
AAV	AAV9 (Poros purified)	4	+
	AAV8 (Poros purified)	4	+
	AAV2 (Heparin column purified)	1	+
	AAV2 (clinical grade)	1	-
Lentivirus	Standard ultracentrifugation purified	3	+
Water	Milli-Q water	2	-
	Simple distilled water	2	+
	Tap water	1	+
PBS	Standard tablet produced	1	+
	Gibco tissue culture	1	-
Mega-preps	Invitrogen standard kit	2	+
	Qiagen standard kit	3	+
	Qiagen endofree kit	2	-
Reagents	PEI	2	-
	PBS-MK buffer	2	-
	Standard Fetal Bovine Serum	3	+
	Gibco Performance Plus Fetal Bovine Serum	1	-
Purification equipment	Akta FPLC machine washings	2	+
	AVB column flow-through – 10 volumes	2	+

Table 11. Endotoxin status of several vectors, reagents and equipment used for AAV production in the lab. Different numbers of each sample type was tested using Charles River Endosafe single-use tubes at a cut off of 2.5EU/ml. Results were consistent in each group and it is indicated if the results were positive or negative at this concentration. Of note all vector preparations were positive, except the GMP-produced clinical vector. Several alternative endotoxin-low reagents were also tested and subsequently integrated into the refined process.

All glass equipment was subsequently dry heat baked for 8 hours at 270°C to inactivate all endotoxin, as standard autoclaving is ineffective. Reagents and buffers were tested by LAL prior to use. 0.5M Sodium hydroxide wash was used to partially sanitise the fast-protein liquid chromatography (FPLC) machine before each run, though the only certain method for prevention of endotoxin contamination is to prevent any initial introduction. Genomic plasmid isolation was altered to use a commercial Endotoxin-free mega-prep

kit (Qiagen) as plasmids were all positive above 2.5EU/ml using standard kits. Standard Fetal bovine serum (FBS) used for tissue culture of HEK-293T cells in AAV production is typically not quality assured for endotoxin, but can be specially obtained as Gibco Performance Plus. This is guaranteed as below 5EU/ml. Following introduction of these measures and disposable AVB columns, viral preps of AAV8 at $1x10^{12}$gc/ml negative for endotoxin at 2.5EU/ml were reliably attained.

One aspect important to the accurate use of AAV is thorough matching of control and intervention preps to the same titre of genome copies. Until this point the 'Dot-blot' protocol using southern blot hybridisation of DNA against a known standard curve was employed. This was widely used but accepted to be crude, with over half an order of magnitude observed in test-retest variation in our hands. To improve upon this, a new protocol was introduced based upon qPCR using primers binding in the ITR region. Using this more robust quantification of titre-matching was possible, with good repeatability observed in extensive subsequent application (Selina Azam, personal communication).

It is well known that subretinal detachment leads to ocular inflammation and can even affect retinal function detected by ERG for several weeks after.[179,180] To circumvent these potential limitations a new AAV vector called ShH10 was investigated, which had recently become available in the lab as a gift from Prof John Flannery of Berkeley University, USA. It was engineered by *in vivo* evolution to primarily target Muller cells following intravitreal injection. Whilst work in the lab confirmed this pattern in mouse pups, the transduction profiles had not been assessed in the adult mouse.

ShH10-CMV-eGFP was produced and purified using the same clean AVB column-based process with good titres of $1x10^{13}$gc/ml obtained. 2µl of vector suspension containing $1x10^{10}$gc ShH10 was injected into either the subretinal space or the vitreous cavity and eyes were sectioned after one day, one week and 3 weeks. Co-staining was performed for CD45 **(Figure 24)**. At one day, no GFP signal is visible, but CD45+ cells are seen around the sclera

after subretinal injection, likely reflecting an acute response to reflux of ShH10 around the eye. At one week following subretinal injection GFP expression can been seen in RPE and photoreceptors around the region of the bleb. No GFP fluorescence was seen in the ciliary epithelium, in contrast to intravitreal injection where the ciliary body is fully transduced, as well as corneal endothelium and an occasional inner retinal cell. By three weeks, occasional columns of GFP positive Muller cells are seen predominantly around retinal vessels, but transduction of Muller cells was not as extensive as described in pups.[57] By three weeks the subretinally injected eyes show higher levels of expression in the RPE and photoreceptors still without any ciliary epithelium involvement. Interestingly CD45+ cells are only evident in the sclera, but were not seen following intravitreal injection.

All these refinements were employed to produce the AAV8 and ShH10 vectors used in work described in all other chapters. In the following sections the effect of ocular endotoxin, a novel technique for removing unpackaged capsids, an assessment of the directionality of viral mediated transgene secretion and the effects of dexamethasone on subretinal injection will be described.

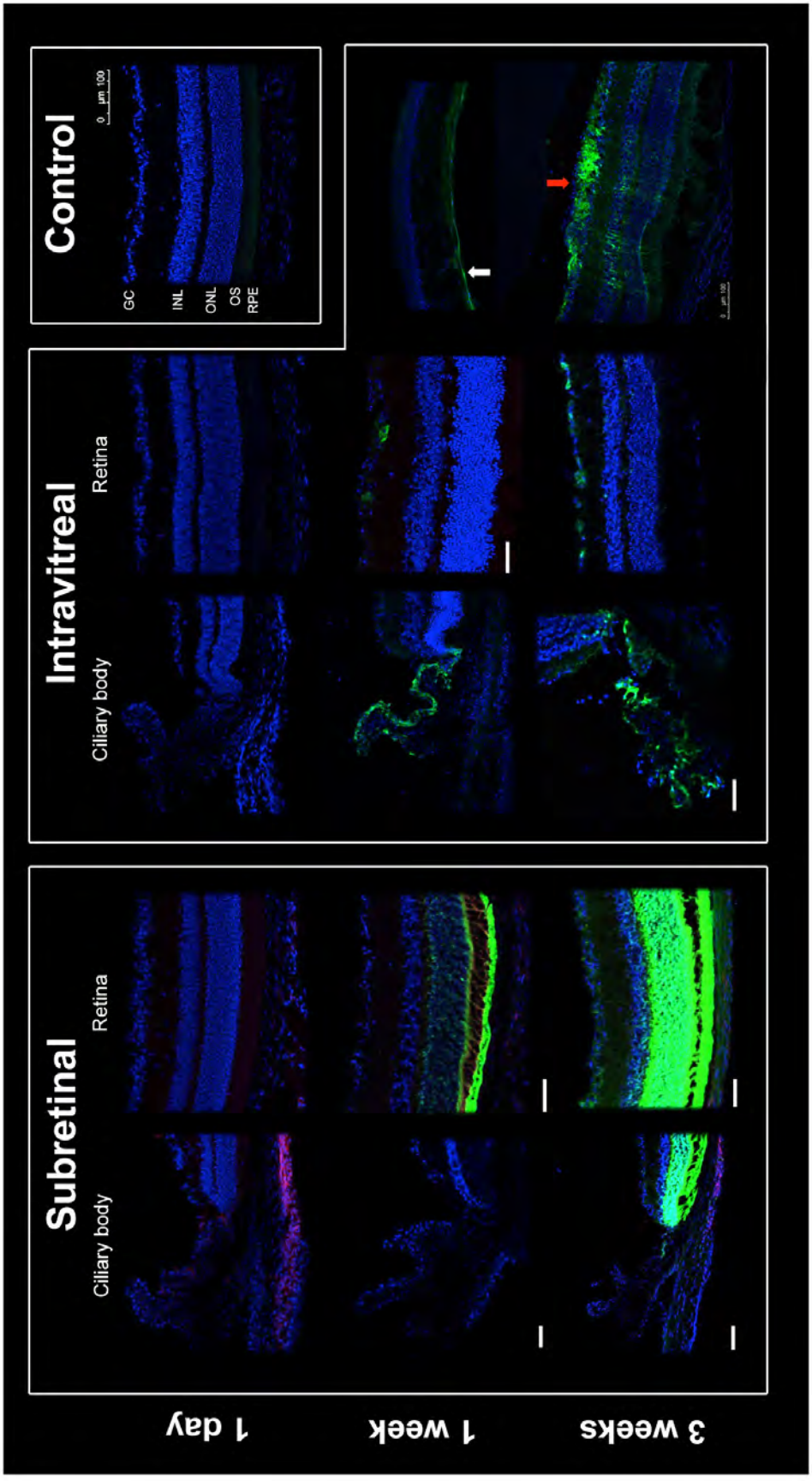

Figure 24. Intravitreal and subretinal delivery of ShH10 lead to different patterns of cell transduction in the adult mouse. Representative examples from a time-course of 1 day, 1

week and 3 weeks following injection of $1x10^{10}$gc of ShH10-CMV-eGFP. All were fixed with 4%PFA, stained with anti CD45-Alexa 546 and imaged by confocal microscopy. At one day post-injection, no GFP expression is seen, but scleral CD45+ cells are seen in the subretinal injected group. At one week, mild photoreceptor and RPE transduction is seen with subretinal delivery, whilst intravitreal injection leads to ciliary epithelium, corneal endothelium (white arrow) and the occasional inner retinal cell becoming GFP+. By three weeks, strong photoreceptor and RPE expression is evident from subretinal injection, with no ciliary epithelial transduction seen at any stage. With intravitreal ShH10-CMV-eGFP at three weeks, the same cell types as at one week are seen, with now occasional columns of Muller cells (red arrow), typically around the location of inner retinal vessels. Scale bars = 100µm. Unmarked are same magnification as control image. DAPI (blue), GFP (green), CD45 (red). GC= Ganglion cell layer, INL-Inner nuclear layer, ONL-outer nuclear layer, OS-photoreceptor outer segments, RPE-retinal pigment epithelium.

5.2 Injecting endotoxin contaminated material has detectable effects upon the eye

Whilst systemic or intraocular injection of refined lipopolysaccharide from E.coli or Salmonela is used to elicit the model of endotoxin-induced uveitis, the effects of typical environmental endotoxins are unknown. Universal standard endotoxin is an internationally agreed mix of different bacterial endotoxins, used to emulate typical contaminants. The National Institute for Biological Standards and Control kindly provided a sample of this. Endotoxin-low (<2.5EU/ml) AAV8-CMV-hrGFP was spiked with 2000 EU universal standard endotoxin or with carrier only and injected into the subretinal space of adult WT mice. TEFI at 24hrs shows subtly different retinal appearances, with a greater degree of possible retinal oedema in the endotoxin group **(Figure 25A)**. Flow cytometry on dissociated retinae confirm elevated numbers of CD11b+Ly6G+ cells, likely to reflect acute neutrophil infiltration **(Figure 25B)**.

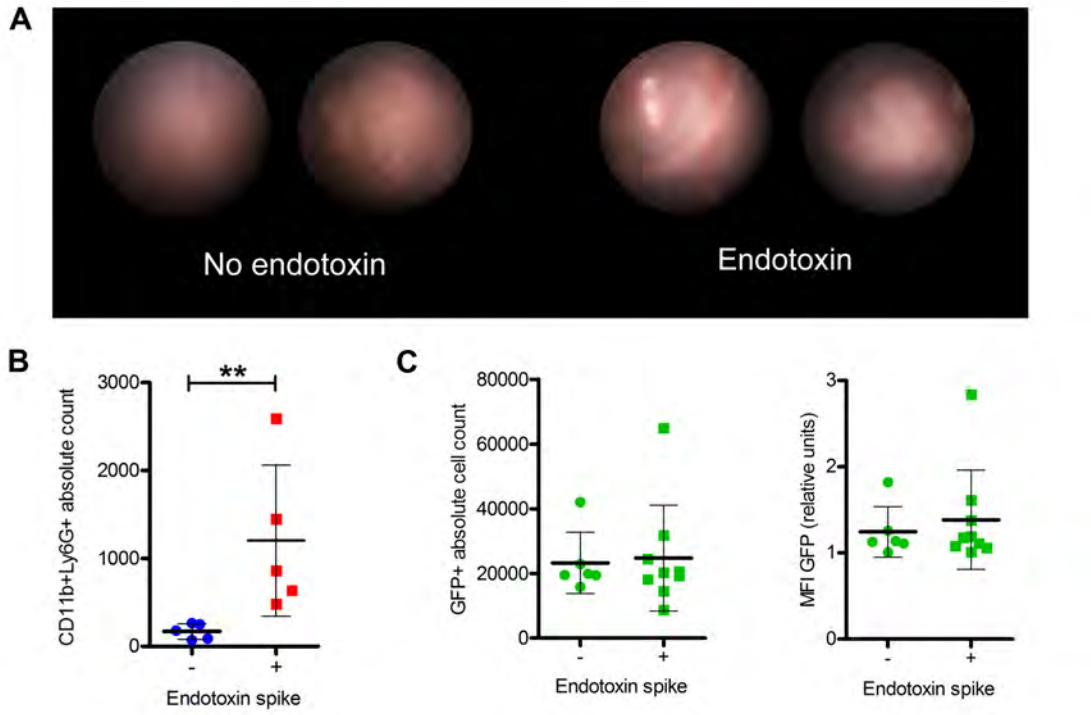

Figure 25. Endotoxin positive AAV8 leads to acute neutrophil infiltration, but no changes in transgene expression. Endotoxin-free AAV8-CMV-hrGFP spiked with PBS or 2000 EU of universal standard endotoxin was injected into the subretinal space. **A)** At 24hr subtle differences in retinal appearance were evident by TEFI. **B)** Flow cytometry showed a statistically significant increase in retinal CD11b+Ly6G+ cells with endotoxin. Mann-Whitney U test, P=0.0022. Another cohort was left for 7 days prior to analysis of GFP signal by flow cytometry. The expectation was for increased levels of expression in the presence of endotoxin. **C)** No differences however were observed for either GFP+ cell count or median fluorescence intensity (MFI). Means +/- SD shown.

It has been reported that the ITR regions of the AAV2 genome used for almost all gene therapy applications has NFκB-binding regions. This means it is potentially responsive to inflammatory signalling, that certainly appears to modestly increase transcription from the ITRs themselves.[181] As TLR4 signalling downstream of LPS can trigger NFκB activation, the effect of endotoxin upon AAV-mediated transgene expression was tested. Subretinal injection of endotoxin spiked AAV8-CMV-hrGFP and control was assessed at one week, where high levels of expression should be occurring **(Figure 25C)**. No difference in either the number of GFP+ cells or the median fluorescence intensity appeared different. Whilst the experimental design might not be optimised to detect a small difference, it is unlikely for a dramatic effect upon transcription to exist.

Previous endotoxin contaminated AAV preparations for gene therapy of monogenic disorders did not lead to obvious inflammation in mice. As all of these were delivered using the subretinal route, no changes may have been seen if there was either a deviant innate response to LPS or sequestration in this space. To investigate this issue, eyes were injected with purified 1ng LPS from E.coli to ensure maximal stimulation and the greatest chance to detect infiltration. The same dose was injected intravitreally as a control. Six hours after injection, eyes were sectioned and stained with anti-CD45. In the intravitreal group, typical changes of EIU were seen, with anterior chamber cells **(Figure 26A)**, which were predominantly polymorphonuclear **(Figure 26B)**. The cells can be seen associated with the iris, having likely emerged from iris vessels **(Figure 26C)** and are also present in the vitreous cavity **(Figure 26D)**, where they are believed to emerge from the region of the optic nerve head **(Figure 26E)**.

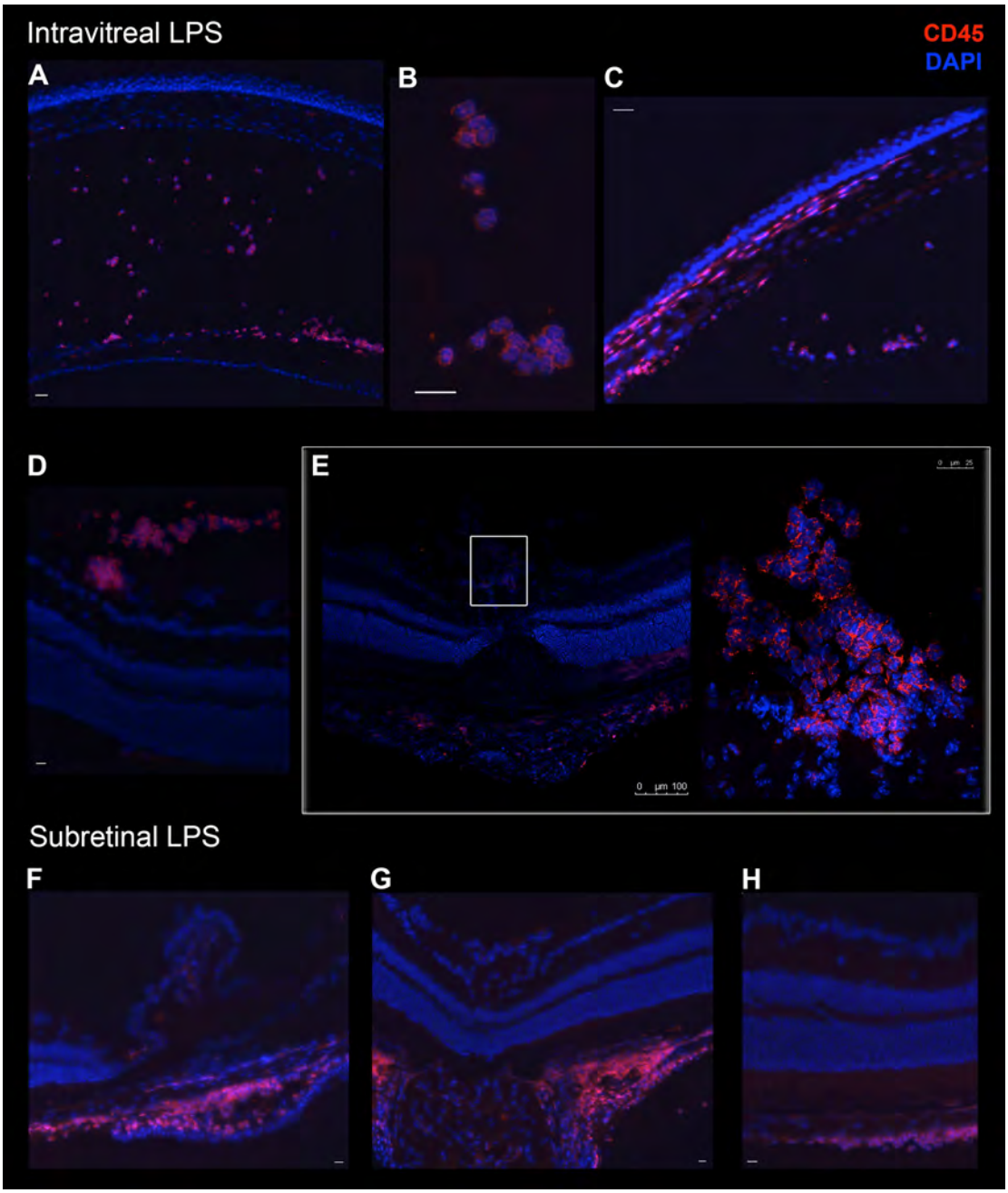

Figure 26. Histological differences are evident between responses to intravitreal and subretinal delivery of endotoxin. Eight eyes were injected with 1ng LPS either via the intravitreal or subretinal route. Six hours later they were cryosectioned, stained with immunofluorescent anti-CD45 antibody and imaged using either confocal or fluorescent light microscopy. As expected, following intravitreal injection **A)** the anterior chamber is filled with CD45+ cells likely emerging from the iris, which is heavily infiltrated. **B)** On higher magnification the polymorphic nuclei are consistent with neutrophils. **C)** Cells are present in the angle and other resident cells are seen at the corneal limbus. **D)** In the posterior chamber, cells are present in the vitreous, adjacent to inner retinal vessels. **E)** At the disc, CD45+ cells were also seen (x40 confocal image inset), as this is a likely region for access into the eye. Following subretinal delivery, no cells were obvious in the AC or vitreous. Consistently, cells were observed instead in the choroidal/scleral complex around the **F)**

ciliary body, **G)** optic nerve head and **H)** posterior retina. Where not annotated, scale bars = 25µm.

In contrast, no CD45+ cells could be seen within the eye in any subretinal LPS injected eyes at the same timepoint. CD45-staining cells were seen in the scleral/choroidal regions in almost every eye, often near the ciliary body **(Figure 26F)**, always around the optic disc **(Figure 26G)** and typically in mid-equatorial regions near the injection site **(Figure 26H)**. Whilst this could purely reflect an acute response to reflux of LPS into the sub-tenon's space following injection, it is interesting that no retinal infiltrate is seen, suggesting that subretinal injection leads to a different response to intravitreal injection. It is possible that there is retardation of exposure and so after a longer delay examination might yield different results. In either instance, it is fair to conclude that the potential to miss subtle responses to endotoxin has been greater due to use of the subretinal route, but it is still unclear what the long-term consequences are.

A small study compared a 2µl subretinal injection with 1ng LPS from E.coli and PBS control (n=4 eyes each group). At one month post-injection eyes were embedded in paraffin, sectioned and stained with haematoxylin and eosin. No gross structural differences could be seen, in terms of outer nuclear layer cell dropout, thinning, retinal folds or photoreceptor outer segment loss. It would have been worth repeating with universal standard endotoxin, which contains a mixed population of LPS more reflective of environmental contamination instead of purified single strain LPS, but supply was limited.

Differences between reported cellular tropism, the distribution and speed of transduction of AAV serotypes exists throughout the field and literature. It might be that unrecognised, but highly variable levels of endotoxin contamination could lead to the observed disparities. For example, ShH10 was originally reported as achieving widespread Muller cell transduction at three weeks. In our hands only sparse islands of transduced cells around vessels are achieved. Differences exist between purification methods – in our lab endotoxin-free AVB column purification is used, as opposed to caesium

chloride gradients, without endotoxin testing. One hypothesis was that endotoxin and/or other cellular contaminants could cause inflammation and degradation of the inner limiting membrane following injection, which would then allow more ShH10 to penetrate the retina and transduce Muller cells.

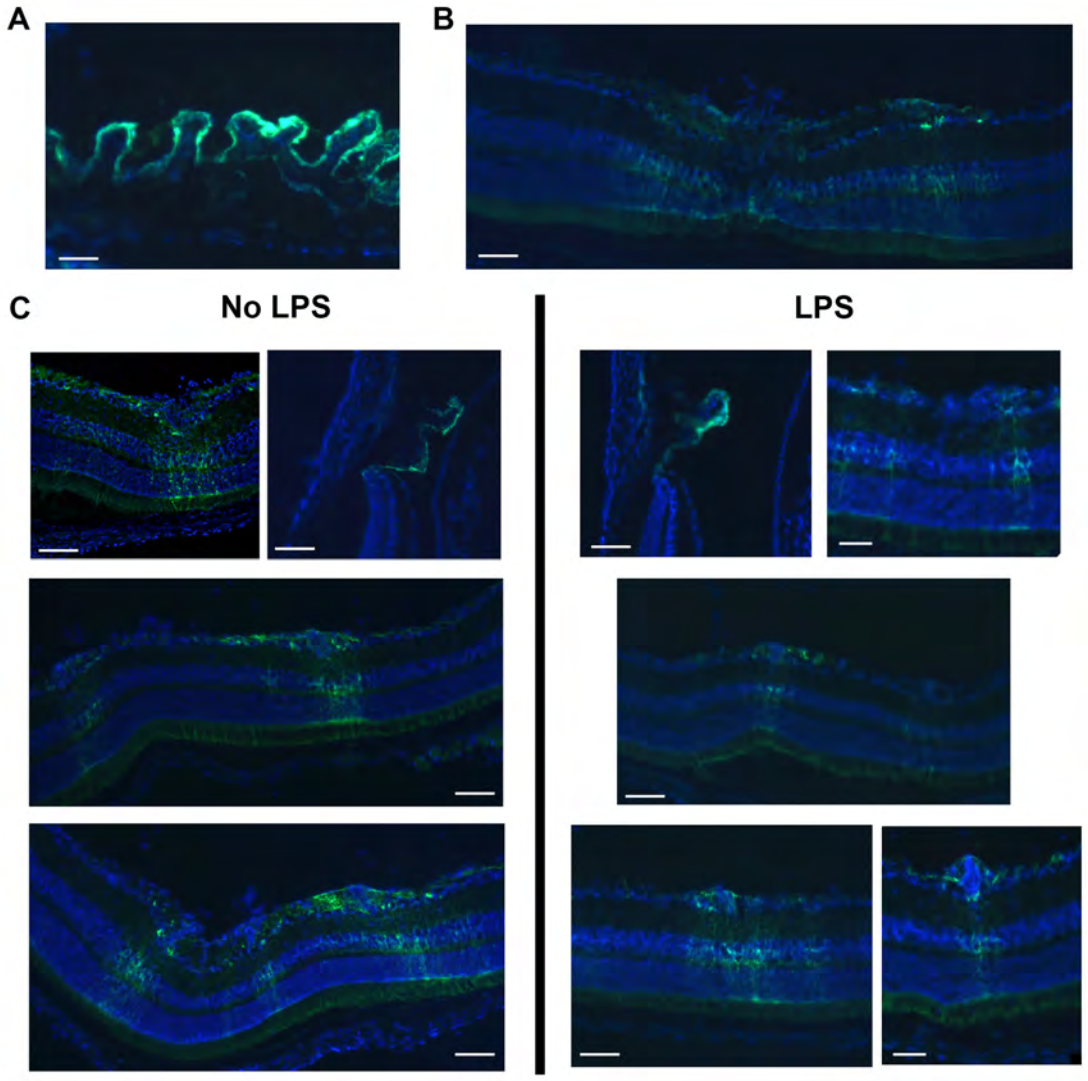

Figure 27. Spiking ShH10-CMV-eGFP with endotoxin does not overtly affect the extent or type of retinal cells expressing GFP. Three weeks following intravitreal delivery of $1x10^{10}$gc ShH10-CMV-eGFP spiked with 1ng LPS from E.coli or PBS carrier control, eyes were enucleated, sectioned and imaged. **A)** In all eyes the ciliary body epithelium was completely transduced, as were **B)** Muller cells in the region of the optic nerve head. **C)** GFP expression was found in Muller cells across the rest of the retina; no obvious differences between groups could be appreciated. n=6 eyes per group. DAPI counterstain (blue). Sectioned at 16µm thickness. Scale bars = 100µm.

To test this hypothesis, ShH10-CMV-eGFP with and without a 1ng LPS spike was delivered by intravitreal injection into C57BL/6 mice. Three weeks later eyes were assessed **(Figure 27)**. No differences in the extent or degree of GFP expression in Muller cells were apparent. Whilst this makes it unlikely that the presence or absence of endotoxin is responsible for the differences in reported ShH10 transduction, it could be that other unidentifiable components such as HEK-293T cell debris could still have an effect. This would be difficult to test in a controlled way.

A final experiment assessed the possibility of long-term structural damage as a result of subretinal delivery of endotoxin. Four eyes were injected with PBS and four with 1ng LPS from E.coli in 2µl. They were examined by paraffin section after six weeks. Minimal structural changes or photoreceptor nuclei loss were seen with H&E staining in either group, suggesting that there is no long-term effect upon cellular viability. One caveat is that eyes were injected with purified LPS that may not reach the same dose or diversity of species as that achieved during standard environmental contamination.

5.3 Testing a novel AAV genome-containing capsid enrichment technique

It has been well established that during recombinant AAV production, many assembled capsids do not contain any genomic insert. For AAV2 it has been calculated that using typical production techniques 96.5% of particles are ‘empty’.[66] In terms of immunomodulation, highly antigenic capsid protein that does not contribute to the therapeutic effect is highly undesirable. Furthermore, evidence suggests that using the subretinal route in the eye, the capacity to prevent systemic response to AAV is dose dependent. At high titres of AAV, systemic responses to capsid proteins can be seen, which prevent effective treatment of the contralateral eye.[76]

Based upon the concept of a difference in surface protein charge between full and empty AAV a technique using a gradient over an anion exchange medium was proposed. AAV5 was trialled first, as personal communication

from another group had claimed some success using this serotype and a similar approach. A 20-plate preparation of AAV5-GFP was made and initially purified using an AVB-column and the endotoxin-free production process **(Figure 28A)**. The entire three fractions from the elution peak were pooled and diluted 1:10 with distilled water. A 5ml Sepharose Q_{XL} column was used and loaded with the AVB-purified vector, washed and then eluted with a gradient of 250mM sodium chloride buffer from 30% to 100% over 50ml **(Figure 28B)**. The absorbance spectrum confirmed one large initial peak and then another two semi-distinct peaks. 1ml fractions from across all three peaks were tested by both qPCR to determine the number of genome copies and SYPRO Ruby gel **(as Figure 23B)** with densitometry restricted to VP1-3 bands as a measure of capsid protein. These two readings had background readings subtracted and were then normalised to a pre-elution fraction. The relative amounts are plotted superimposed over the corresponding fractions where tested **(Figure 28C)**. They indicate that capsid proteins are relatively evenly distributed throughout all three peaks in proportion to the absorbance trace. Genome copies however, are predominantly located in the first peak. This disconnect implies that most full packaged AAV is in the first peak and the empty capsids have been separated to lie mainly in the third peak.

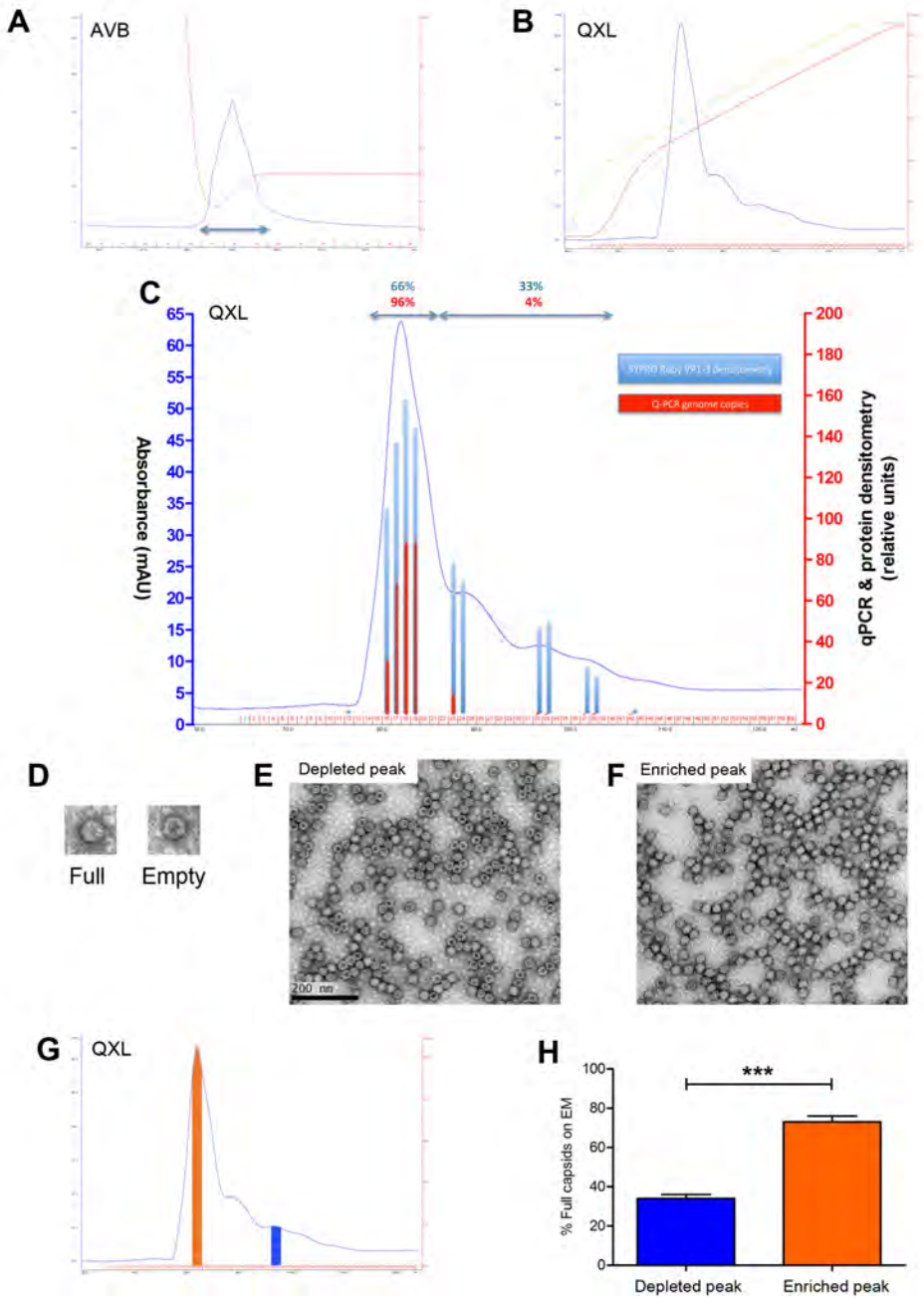

Figure 28. An enrichment of genome-containing capsids is possible using Sepharose Q_{XL} medium and AAV5. Applying the new technique on a twenty 15cm-plate batch of AAV5-CAR-GFP, the first stage is a standard AVB purification. **A)** Three fractions representing the majority of the absorbance peak from the AVB column (blue arrow) are pooled and **B)** run on a GE Sepharose Q_{XL} column and eluted using a salt gradient (red = conductance). **C)** The resulting absorbance trace shows a pattern of three main peaks. Twenty 0.5ml fractions were taken across the run and a subset analysed by both ITR qPCR determination of viral genome number (blue) and SYPRO Ruby protein gel with densitometric quantification of VP1-3 bands (red). The conclusion is that the ratio of genome copies to capsid protein is highest in the first peak, suggesting that a greater number of empty capsids are present in the latter peaks. **D)** Electron microscopy with uranyl acetate counterstain was used as another method to determine the percentage of full capsids. It has previously been shown, as the examples

illustrate, that empty capsids collapse to develop a pit that stains darkly with uranyl acetate. **E)** Representative example taken from the depleted peak (blue) showing predominantly empty capsids. **F)** The equivalent example from the enriched first peak with mainly full capsids (orange). **G)** Sepharose Q_{XL} trace showing the location of fractions pooled for the relevant EM assessments. **H)** A masked count of three random fields from three different images each sample is plotted for the two peaks. Two-tailed unpaired T-test, ***=P<0.001. Mean + SD shown. Blue traces = UV absorbance (mAu), red = conductance (mS/cm), beige = Akta Prime set percentages for B (high salt) buffer.

To confirm these findings, electron microscopy of two pooled fractions from the first and third peaks were analysed. Empty capsids can be distinguished as the concave centre resulting from capsid conformation in the absence of a genomic core stains with Uranyl acetate counterstain **(Figure 28D)**. Representative examples are shown for the depleted **(Figure 28E)** and enriched peaks **(Figure 28F)**. As the first peak could be taken alone for *in vivo* use, separation out of the empty capsids seen in the deplete peak is a form of enrichment. The relative percentages of capsids were enumerated by blinded counts over multiple fields from the two peaks **(Figure 28G)** and a significant difference in the percentage of packaged capsid AAV from 30% to 70% **(Figure 28H)**. This allows an estimate of enrichment of full capsids by 30%. AAV5 transduces RPE and photoreceptors after subretinal detachment, but less efficiently than AAV8, and with a slower onset and a lower final level. As a result, the possibility for a similar enrichment of AAV8 was investigated, as this was the current vector of choice.

A 20-plate preparation of AAV8 was AVB purified and again run through the Sepharose Q_{XL} column using the same protocol. This time only one distinct absorbance peak was acquired, suggesting that no demonstrable separation had occurred **(Figure 29)**. Analysis of fractions by qPCR and SYPRO ruby gel confirmed the finding, with both distributing evenly across the peak. A cotemporaneous publication illustrates the separation of AAV8 using a CIM-QA column, a similar type of medium, but with the smaller size monoliths used to allow finer resolution of protein separation.[182] At the time of writing separation of AAV8 into two peaks corresponding to full and empty capsids has been possible using the developed protocol, but with a GE MonoQ column (Selina Azam, personal communication).

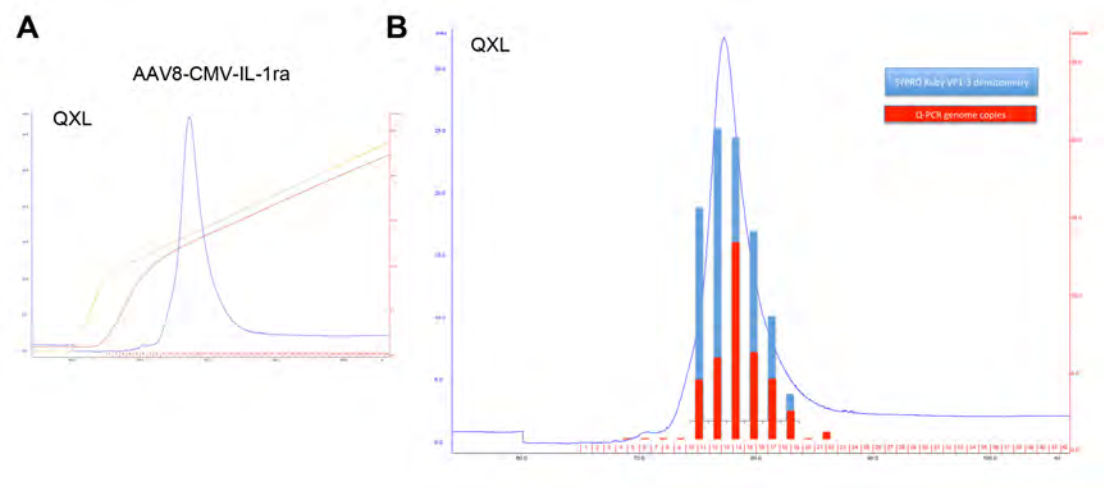

Figure 29. The genome-containing-capsid enrichment process using a Sepharose Q_{XL} column is not able to separate full and empty AAV8 capsids. A twenty 15-cm plate prep of AAV8-CMV-IL-1ra was purified by AVB column and then **A)** run across the gradient program on a GE Sepharose Q_{XL} column. Only one absorbance peak could be seen, implying no significant separation had occurred, or minimal empty capsids were present. **B)** ITR qPCR determination of viral genome number (blue) and SYPRO Ruby protein gel with densitometric quantification of VP1-3 bands (red) confirmed this finding. No obvious enrichment was evident and so electron microscopy assessment was not performed. Blue traces = UV absorbance (mAu), red = conductance (mS/cm), beige = Akta Prime set percentages for B (high salt) buffer.

Due to the time and resource constraints of employing this process, it was not integrated into the routine production scheme, but retained as a final refinement once an optimal suppressive target and method has been developed.

5.4 Perioperative high-dose corticosteroid does not affect the subsequent success of EIU suppression

Previous evidence indicates that subretinal injection alone can cause widespread microglial activation and an increase in detectable myeloperoxidase from the eye (Ulrich Luhmann, unpublished observations). Following the observed trend towards worsening of EAU and EIU after subretinal injection of even control vector, one hypothesis was that the early innate immune responses to retinal detachment were worsening the outcome

and preventing AAV-mediated immunosuppression. During optimisation of the EIU model, it was ascertained whether systemic Dexamethasone administration at the time of vector delivery could attenuate this potentially nullifying effect **(Figure 30)**.

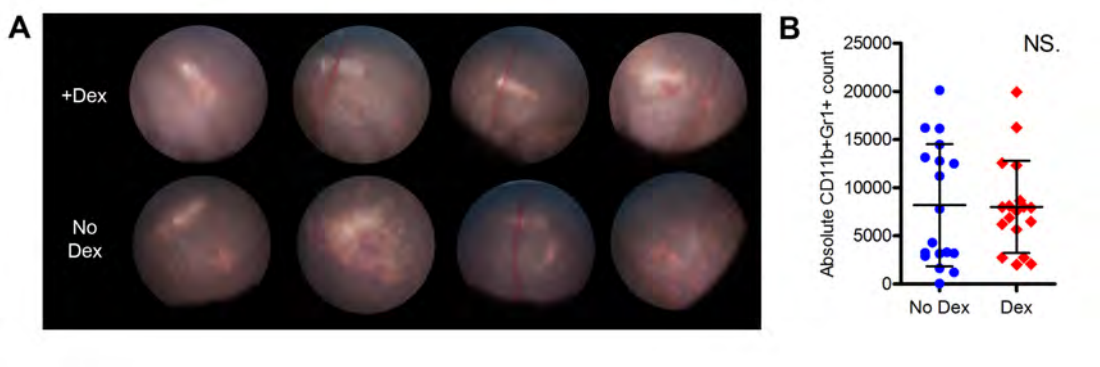

Figure 30. High dose systemic Dexamethasone at the time of subretinal injection does not alter the degree of EIU induced a week later. 2mg/kg water soluble Dexamethasone was administered into the peritoneal space of C57BL/6J mice 24hr before, immediately prior to and 24hr following subretinal injection. **A)** Representative TEFI images of the injection site of PBS subretinal-injected mice receiving Dexamethasone and controls fail to demonstrate any change in retinal appearance at one week. **B)** CD11b+Gr1+ infiltrative cell counts of PBS, AAV8-Null and AAV8-hrGFP injected eyes were unaffected in subsequently induced EIU with 1ng LPS from E.coli. There was no trend upon subgroup analysis. Mean + SD shown.

2mg/kg Dexamethasone was given as an intraperitoneal dose the day before, the time of and the day after subretinal injection. EIU was induced one week later. No obvious change in retinal appearance could be detected by TEFI and flow cytometry of eyes from mice treated with and without Dexamethasone did not differ in CD11b+Ly6G+ cell count. Perioperative corticosteroids are used routinely in clinical practice and are known to suppress active ocular inflammation, but it is not known if they affect the resident rather than infiltrating immune cells, and this may explain the lack of effect in the experiment. Whilst technical refinements in timing and readout might reveal a small benefit, it was felt unlikely to lead to dramatic effect and so not pursued further.

5.5 EAU does not trigger a systemic response against subretinal delivered AAV8

The absence of systemic response to AAV2 when injected into the subretinal space has been well established in both pre-clinical studies and clinical trials.[48-50,76,183] The effect of pre-existing or subsequent independent ocular inflammation upon this poorly understood form of 'immune privilege' is unknown. One hypothesis is that the subretinal space contains viral antigens, preventing systemic exposure, rather than an active immune deviation process. If so, then intraocular inflammation with the accompanying infiltrate, retinal damage and degradation in blood-ocular barriers may lead to exposure and subsequent responses. To model this in mice, EAU was induced following subretinal delivery of AAV8-CMV-mIL-10-IRES-eGFP in one eye and AAV8-CMV-hrGFP in the other. No local suppression of disease had been observed as discussed in **results chapter 4**. Serum and spleens were collected at peak disease on day 26 and analysed for ELISPOT responses to AAV8 capsid and the development of neutralising antibodies **(Figure 31)**.

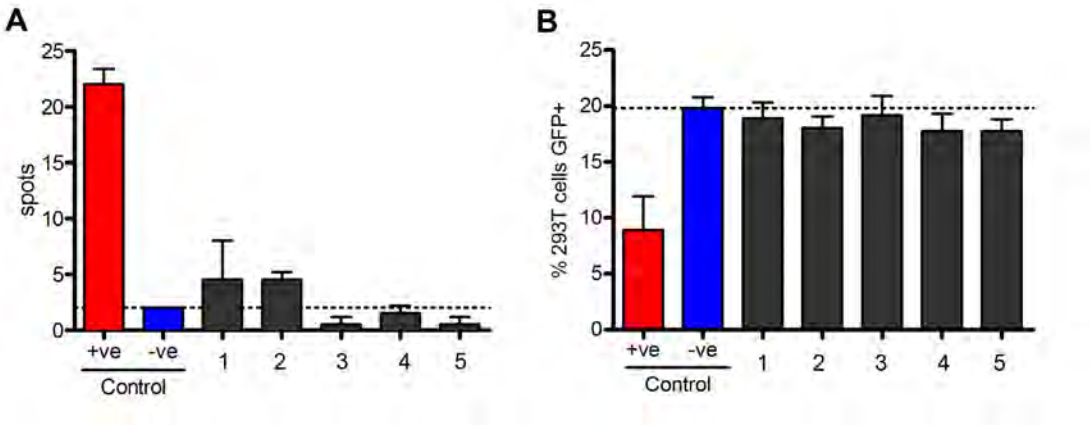

Figure 31. No systemic antigen-specific immune responses are detected after EAU induction following subretinal delivery of AAV8. 1x10^{10}gc AAV8-CMV-mIL-10-IRES-eGFP was injected into the subretinal space of both eyes. A week later EAU was induced and serum and lymph nodes harvested at day 26. **A)** IFNγ-release assay for CD8+ T-cells responsive to AAV8 capsid was performed, with positive and naïve negative controls. The number of discrete spots staining was counted. No significant response was detected for all five animals tested. **B)** Neutralising capsid-directed antibodies from serum were determined by their ability to prevent AAV8-CMV-eGFP from transducing HEK-293T cells *in vitro*. With appropriate positive and negative controls, none of the five mice tested had detectable levels of

neutralising antibody. Three dilution and technical duplicates were performed. 1:100 dilution is illustrated. Means + SD shown.

Positive controls were obtained from mice injected subcutaneously with AAV8-CMV-hrGFP one month earlier, whilst naïve wildtype mice were used as negative controls. ELISPOT responses were tested against re-stimulation with whole virus capsids **(Figure 31A)**. Of the five mice tested from an experiment where eyes were injected alternately with AAV8-CMV-hrGFP and AAV8-CMV-mIL-10, none demonstrated significant responses. It is possible that systemic exposure of IL-10 may have affected responses, but elevated levels have not been detected in the serum of injected mice when cytokines were expressed previously.[110] The ELISPOT result was mirrored by neutralising antibody assessment where serum was incubated with intact AAV8-CMV-hrGFP prior to addition to HEK-293T cells in culture. After three days the percentage of GFP expression was enumerated by flow cytometry **(Figure 31B)**. As mice are known to predominantly develop a humoral response to AAV, this last finding is perhaps more critical than the ELISPOT result.[77]

5.6 Soluble transgene-encoded proteins are likely to be delivered into the eye, rather than secreted into the choroidal circulation

Tracing soluble, secreted proteins delivered by AAV transduction of ocular cells is a problematic but important issue. All AAV serotypes infect RPE after subretinal administration. When using transmembrane or intracellular transgenes it is clear that the transduced cells themselves will develop elevated concentrations. With secreted targets such as IL-10 or soluble TNF-receptors, it is critical that the transgene product leaves the RPE to reach other appropriate sites in the eye. Whilst an effect on the RPE may provide some benefit, it is likely that other cells, such as microglia or infiltrating myeloid cells, will need to be affected to achieve full disease suppression. As most of these inflammatory cells traffic to the retina, vitreous and ciliary body, secretion from the RPE would need to reach these sites and not be directed exclusively basally to be washed rapidly away in the choroidal circulation.

To assess if exclusive basal secretion of viral mediated transgene occurs in the RPE, two experiments provide evidence – *in vivo* and *in vitro* - in mouse and human cells respectively. Firstly, lentivirus carrying murine IL-10 was injected into the subretinal space before induction of EAU a week later. Although no attenuation in infiltrating cell counts was seen **(Figure 32A)**, matched supernatants taken from either homogenised retina and vitreous or RPE/choroidal complex were tested for murine IL-10 by ELISA. Delivered into the subretinal space, lentivirus is well known to infect only RPE. The detectable elevation of mIL-10 in the Lentivirus.mIL-10 injected retina compared to the PBS injected control retina is likely to represent secretion apically from the RPE **(Figure 32B)**. Whilst there may be slight cross-contamination of RPE/choroidal to retinal samples, dissection along the subretinal plane is normally very reliable. Further support arises from homogenisation of the RPE, where levels are approximately equal to that in the retina, implying that a significant proportion of the IL-10 produced ends up secreted apically.

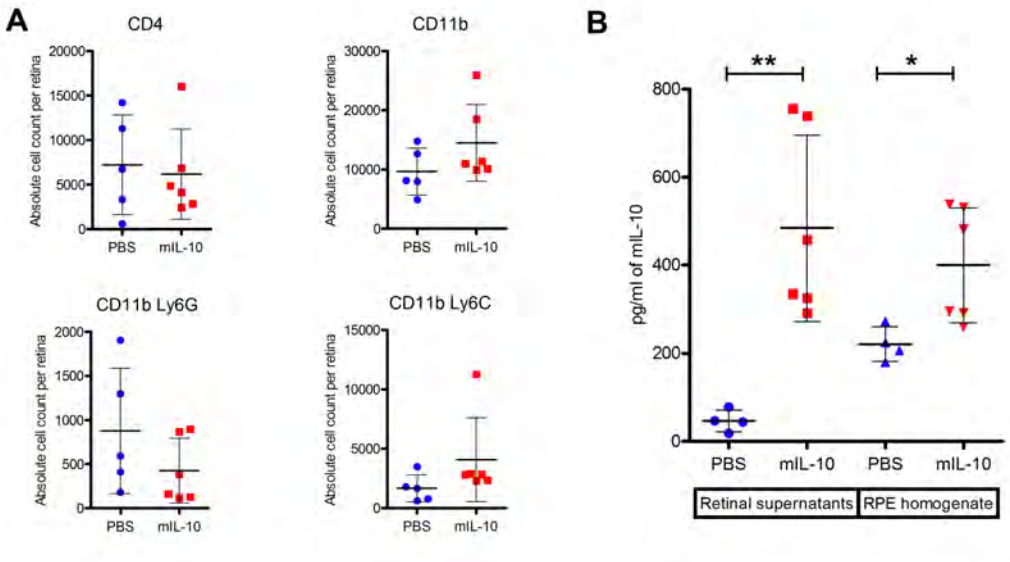

Figure 32. Subretinal Lentivirus-mIL-10 delivery provides support for the successful secretion of transgene product from RPE into retina and vitreous. One week following subretinal injection of neat Lentivirus-SFFV-murine IL-10 or PBS, EAU was induced. At day 26 eyes were carefully separated by dissection into retina, vitreous, AC fluid and RPE-choroidal complex. **A)** Retina, vitreous and AC fluid were pooled and spun down to extract leukocytes. The supernatants were retained for ELISA. Flow cytometry was performed for a

variety of markers. No statistically significant suppression in infiltrate was observed. **B)** Matched retinal supernatants and homogenised RPE/choroid samples underwent ELISA for mIL-10. Lentivirus is known to only transduce RPE, so detectable levels in the retina above the levels in PBS injected eyes can only have originated from the RPE, implying secretion of IL-10 to the apical side. As a comparable, significant increase was seen in both groups treated with Lentivirus, this level of secretion is likely to be substantial. Kruskal-Wallis test with Dunn's multiple comparison **=P<0.01, *=P<0.05. Mean + SD shown.

Further support arises from work performed with human embryonic stem cell and induced pluripotent stem cell-derived RPE cultures. These experiments were performed in collaboration with Dr Anai Gonzalez-Cordero. Differentiated RPE was cultured in transwells with apical and basal reservoirs and grown as monolayers to tight confluence. Examples of the monolayers achieved are shown **(Figure 33A)**. Good polarisation was confirmed by both detecting apical Ezrin staining on immunohistochemistry **(Figure 33B)** and polar secretion of VEGF as expected in a predominantly basal direction by ELISA **(Figure 33C)**.

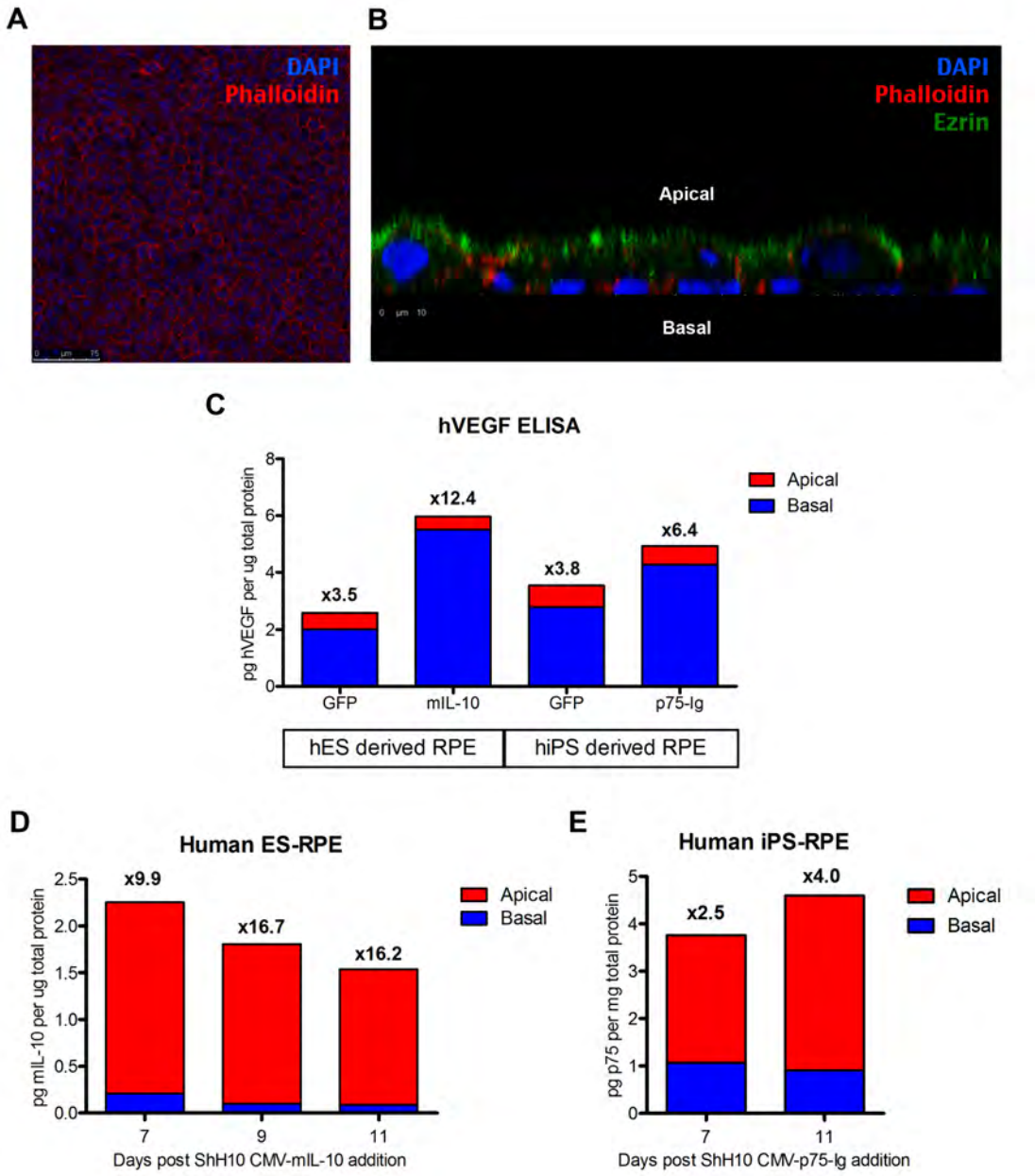

Figure 33. Polarised human ES and iPS-derived RPE confirm apical secretion of murine IL-10 and p75-Ig protein following ShH10 transduction. Human ES-derived and iPS-derived RPE cells were plated in 0.22µm mesh size transwells and grown to confluence. **A)** A representative image of ES-derived RPE stained for the membrane marker Phalloidin, demonstrates polygonal RPE morphology of consistent cell type and confluence. **B)** Confocal imaging of iPS-derived human RPE demonstrates a confluent and polarised monolayer stained for Ezrin - a protein that localises apically to the RPE microvilli. Supernatant from the apical and basal compartments were collected from transwells at a series of timepoints following the addition of ShH10 carrying mIL-10, mouse p75-Ig or eGFP control. **C)** Human VEGF is known to be secreted basally by RPE. This was confirmed using ELISA and results were corrected for total protein to eliminate any generalised effects of dilution. Whilst total amounts varied between transwells, in all samples the apical-basal ratio indicated at least

3.5-fold higher levels in the basal compartment. This is further evidence the cultures were suitably polarised. **D)** ES-derived RPE transduced by ShH10-CMV-mIL-10 generated detectably higher levels of mIL-10 in the apical compared to basal compartment by almost 10-fold at all timepoints post-infection. This was statistically significant by two-way ANOVA, P=0.0075. **E)** A similar result was obtained by ShH10-CMV-p75-Ig, where again, the majority of produced transgene was found in the apical compartment, though this did not quite reach statistical significance by two-way ANOVA, P=0.16. Numbers in bold above bars = ratio of largest to smallest concentration. Species-specific ELISA and BCA determination of total protein were performed at three dilutions and with technical triplicates. GFP controls by ELISA did not differ from background blank wells.

Transwells were infected with ShH10-CMV-eGFP, ShH10-CMV-mIL10 or ShH10-CMV-mouse p75-Ig and medium sampled from both apical and basal compartments across multiple timepoints. ShH10 was used as *in vitro* it appears to result in the highest level of expression in human ES or iPS-derived RPE (Anai Gonzalez-Cordero, personal communication). The use of mouse transgenes ensured minimal complicating background when testing with species specific ELISA. Transwells were filled with an equal volume of medium at each re-feed. In further potential demonstration of polarity however, the volume would distribute so that the basal compartment would accumulate almost double that of the apical. Presumably fluid is pumped through the RPE in a basal direction as occurs *in vivo*.

Both mIL-10 and p75-Ig were detected predominantly in the apical compartments **(Figure 33D-E)**. ELISA readings were corrected for total protein content, in case the changes in volume affected these results. With only two targets it is impossible to confirm if this is a transgene-specific effect dependent upon signal sequence, or less likely a generalised effect of AAV-driven expression. Nevertheless, the previously held hypothesis that all transgene product is lost into the choroid appears unlikely.

5.7 Chapter summary

Multiple refinements to the manufacture and purification of AAV have been introduced, to obtain purer material that should provide the best chance for successful ocular immunomodulation. Endotoxin contamination has been addressed during AAV production and its consequences defined. The lack of systemic responses to AAV8 in the context of EAU was identified. New serotypes of AAV8 and ShH10 have been investigated and a novel technique for removing empty capsids was trialled. Intravitreal ShH10 was shown to transduce ciliary epithelium, corneal endothelium and a reasonable number of Muller cells. This is the most extensive cellular transduction achieved from the intravitreal route used in any study of gene therapy for uveitis to date. Finally, the propensity for AAV-transduced RPE to beneficially secrete soluble transgene proteins apically was confirmed using human stem cell derived cultures.

6 Results 4: Gene transfer of IL-10 into experimental models of intraocular inflammation using modern AAV serotypes

Several publications have shown the suppressive effect of interleukin-10 (IL-10) upon EAU following viral gene transfer[93,110]. To continue the work performed in these earlier studies, the efficacy of more recently developed AAV serotypes was examined. The hypothesis is that the faster onset of transduction, higher levels of expression and wider cellular tropism would prove superior to the previously used AAV2. This original serotype predominantly transduces RPE and takes over three weeks to reach near maximal levels of expression. Serotypes such as AAV8 exceed the levels achieved by AAV2 even by one week. This advantage could allow intervention in active inflammation, rather than prophylactic treatment only when drug-induced remission had been achieved. This is the eventual translational goal and was approached by using animal models of uveitis.

6.1 Defining the parameters of the EAU model for modulation by gene therapy

An initial requirement was to establish the parameters of the *C57BL/6* EAU model in our facility. The severity of the EAU model is affected by many variables, which need to be defined in order to achieve effective induction and as consistent disease as possible. The genetic background of mice, housing conditions, commensal microbiota and dose of RBP-3 peptide can all affect both the severity and timecourse of EAU. Identifying the parameters of disease achieved as a result of these variables was necessary to effectively employ the model. Disease was identified and classified using CD45-immunolabelled histology **(Figure 34A)** and TEFI. Peptide was synthesised and trialled over a range of DMSO concentrations to obtain an optimal mix that provides complete peptide solubility and the greatest amount of disease. Whilst workable, complete dissolution of peptide into a liquid suspension was only consistently achieved at 35%. Below this it remained as a gel which was possible, but technically awkward to work with. Unfortunately

at high levels, the DMSO resulted in minimal EAU potentially due to the inhibitory effects of DMSO upon T-cell activation.[184] Therefore a 10% maximum concentration was used for all subsequent work **(Figure 34B)**. Delineating the exact EAU timecourse achieved is important as both strain variations and microbiome often determined by the local animal facility can affect EAU severity and timing. Without this peak disease might be missed in subsequent experiments. Using TEFI to chart progression, day 26 was chosen as the peak disease timepoint of EAU **(Figure 34C-D)**. Using the same dataset, a correlation was confirmed between the two eyes of each individual animal. Whilst a disparity between eyes was frequent, there was less variation between the two eyes of the same mouse (intra-animal variation) than between eyes of different mice (inter-animal variation). This highlighted that where possible paired analyses between intervention and control are preferable **(Figure 34E)**.

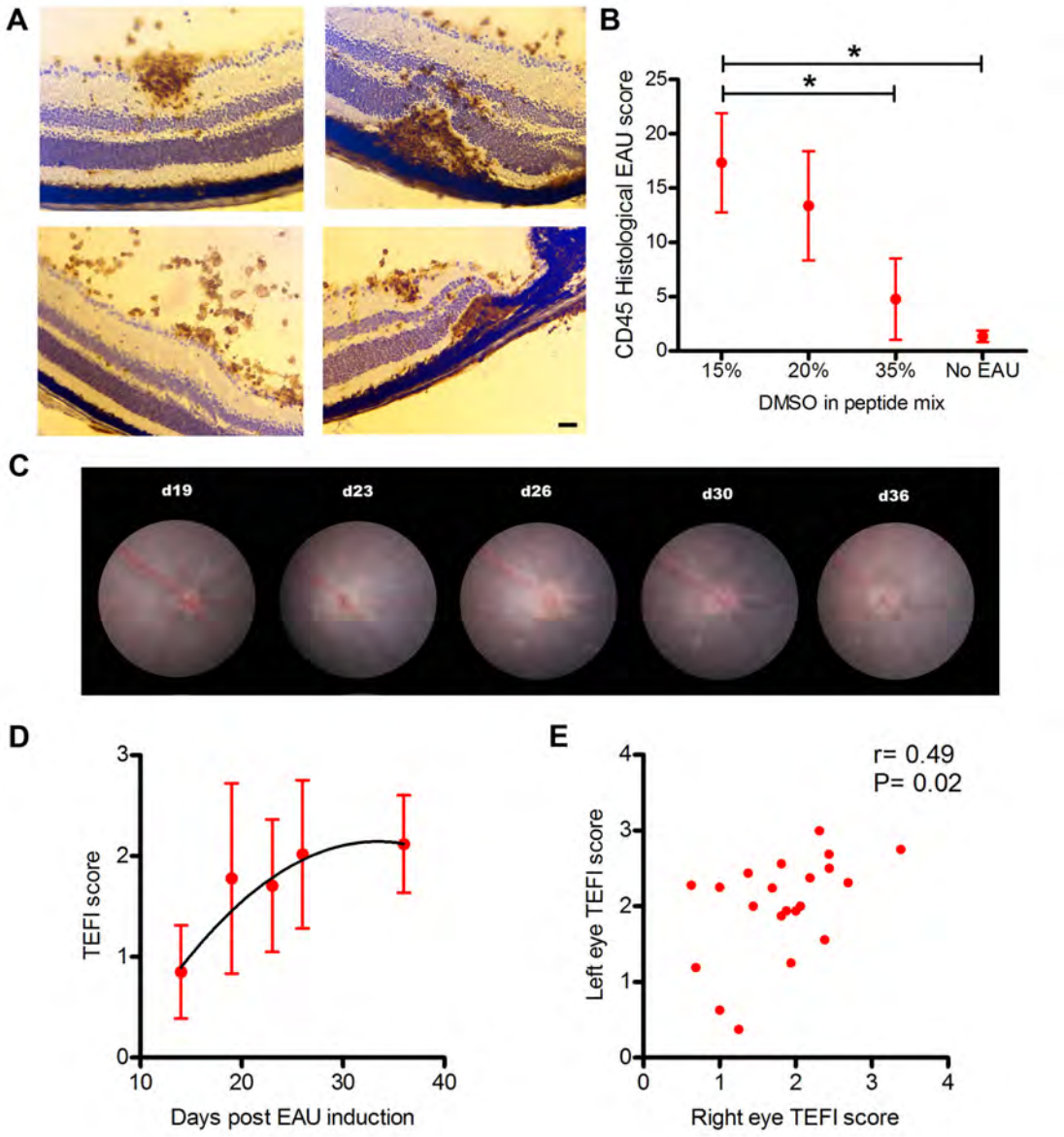

Figure 34. Local parameters of the *C57BL/6* EAU model. Induction of EAU used 500µg $IRBP_{1-20}$ in complete Freund's adjuvant, with 25µg pertussis toxin. **A)** Representative CD45-DAB (brown) and haematoxylin stained sections of eyes at peak EAU demonstrating infiltrate and structural damage. Scale bar = 50µm. The IRBP peptide is typically dissolved in a 10% dilution of DMSO. **B)** Due to solubility issues, a range of DMSO from 15% to 35% was tested and showed reduced disease with increasing DMSO percentage. Kruskal-Wallis test with Dunn's multiple comparison, *=P<0.05, n=3. Topical endoscopic fundal imaging (TEFI) was used to further characterise the EAU model. **C)** A representative timecourse illustrates progression between day 19 and 36 post-induction, with disc swelling, vasculitis and retinal lesions. **D)** Pooled TEFI scores from three masked scorers for multiple eyes followed over the course of EAU. A second-order polynomial fit is shown, which highlights peak disease at day 26. n=10. **E)** Left and right eyes of the same animal during EAU, show a significant correlation implying less intra-animal than inter-animal variation. Spearman correlation. Means + SD shown.

EAU in the presence of AAV transduced retina was assessed to observe if any dramatic loss of transduced cells occurred in this context. Following subretinal AAV8-CMV-hrGFP injection, EAU was induced and eyes examined by a variety of techniques including TEFI, SLO and histology (see **Materials & Methods**). As expected the control eyes without EAU demonstrated normal appearances on TEFI and SLO imaging, with superiorly located GFP signal arising from the RPE and photoreceptors **(Figure 35)**. Histology revealed confluent transduction of the RPE and a majority of the photoreceptors in the region of the subretinal detachment.

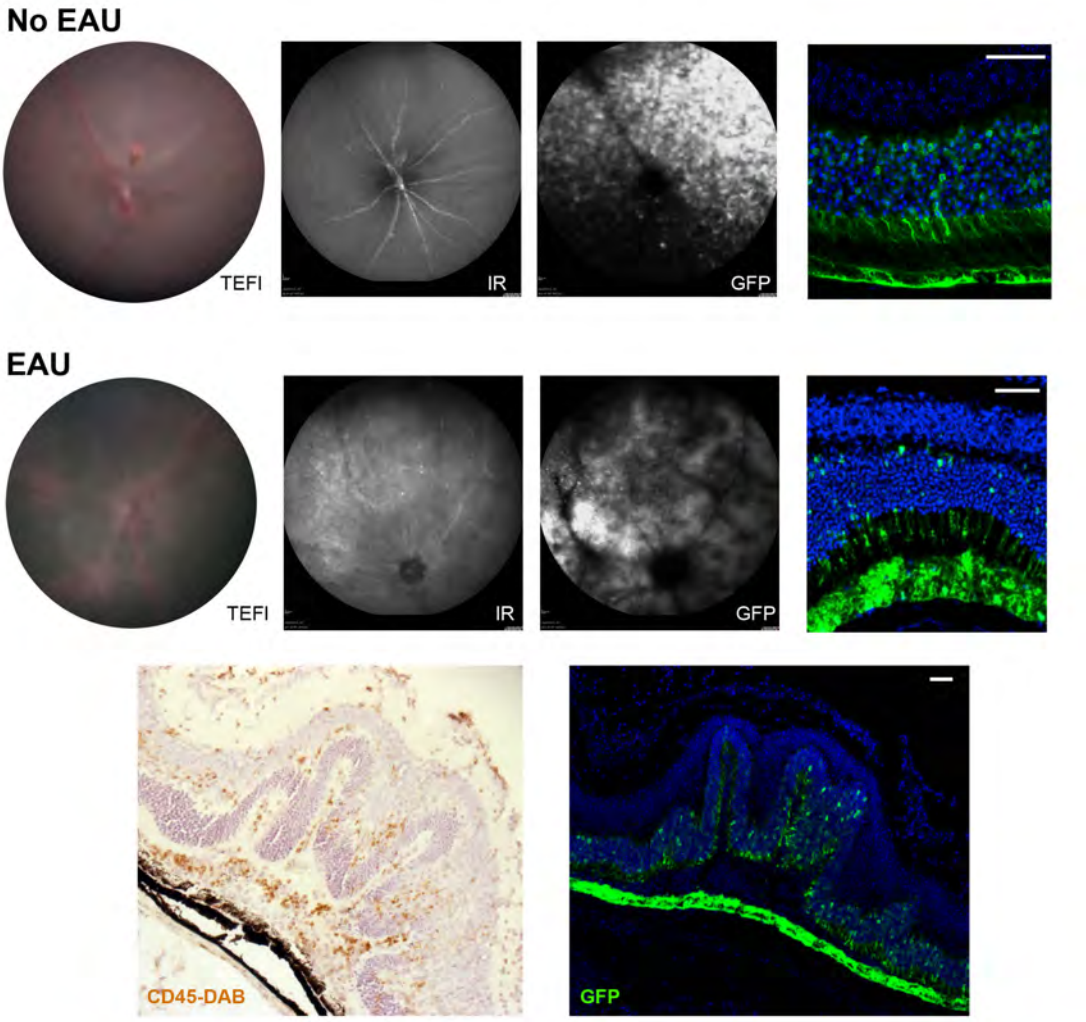

Figure 35. The effect of EAU upon AAV transduced retina. Representative examples of eyes injected superiorly in the subretinal space with 2µl of $1x10^{10}$gc AAV8-CMV-hrGFP. The top row is from an eye 3 weeks post-injection, with a normal TEFI and infrared (IR) appearance. GFP signal can be seen using the 488 channel of the HRA2 scanning laser ophthalmoscope. Matched histology shows the expected and previously reported RPE and

photoreceptor transduction. The lower rows are from eyes 26 days after the induction of EAU. Disc swelling, vasculitis and a green hue can be seen by TEFI. GFP channel shows patches of reduced signal and histology shows loss of the expected number of GFP+ photoreceptors compared to control. Using CD45 labelled histology, another example in a region of extensive structural damage and infiltration again demonstrates some loss of transduced photoreceptors with relatively intact signal from the RPE. Scale bars = 50μm.

In eyes at peak EAU, TEFI demonstrated classical clinical changes of vasculitis (perivascular cuff), disc enlargement and retinal lesions. This corresponded to disruption in GFP signal on SLO. By histology the transduced RPE remains predominantly intact, though the density of GFP+ photoreceptors appears reduced in regions of structural change **(Figure 35)**. Using sequential slides from the same eye, CD45+ cells are visible in the subretinal space, associated with the inflammatory retinal folds where GFP signal in the photoreceptors has been lost. It is unclear if these findings represent preferential loss of transduced rods and cones or only reflects generalised damage to the retina during EAU. Regardless, it appears likely that a potent suppressive effect is required from any target gene delivered, or the disease process may eliminate the very cells responsible for its production.

6.2 Murine IL-10 supplementation by AAV9 in EAU

Subretinally delivered AAV2 carrying murine *IL-10* had been shown to suppress EAU when delivered three weeks prior to the onset of EAU.[110] This period is required as AAV2 takes many weeks to reach maximum expression. AAV9 is a new serotype in use in the lab. It is known to be expressed strongly by one week and transduces RPE, photoreceptors and occasional Muller cells following subretinal injection.[185] As the first experiment, high dose AAV9-mIL-10-IRES-GFP was injected with a AAV9-CMV-hrGFP control. AAV2-CMV-mIL-10-IRES-eGFP was used to compare to previous work. All vectors were left for 3 weeks, to allow a fair comparison with AAV2 before the induction of EAU.

At peak disease on day 26, eyes were examined by TEFI and CD45-labelled immunohistochemistry **(Figure 36A)**. Surprisingly the AAV9-mIL-10 cohort was markedly abnormal, with extensive outer layer retinal loss and choroidal changes, not seen in the GFP control or AAV2 groups. Successful expression had been confirmed by fundal imaging for GFP **(Figure 36B)** after injection, whilst elevated levels of mIL-10 were established using ELISA **(Figure 36C)**. As expected, AAV9 resulted in higher final levels than AAV2 despite the extensive retinal loss. Final histological EAU scoring showed statistically significant worsening in the AAV9-mIL-10 group relative to unprocedured eyes **(Figure 36D)**. AAV2 failed to suppress disease, but in this experiment AAV2-mIL-10 was compared to AAV9-hrGFP and had been delivered at a higher titre than before to maximise any potential effects. Electroretinograms consolidated the findings, with AAV9-mIL-10 injected eyes demonstrating a statistically significant reduction in B-wave amplitude, consistent with tissue damage during EAU giving rise to significant retinal loss **(Figure 36E)**.

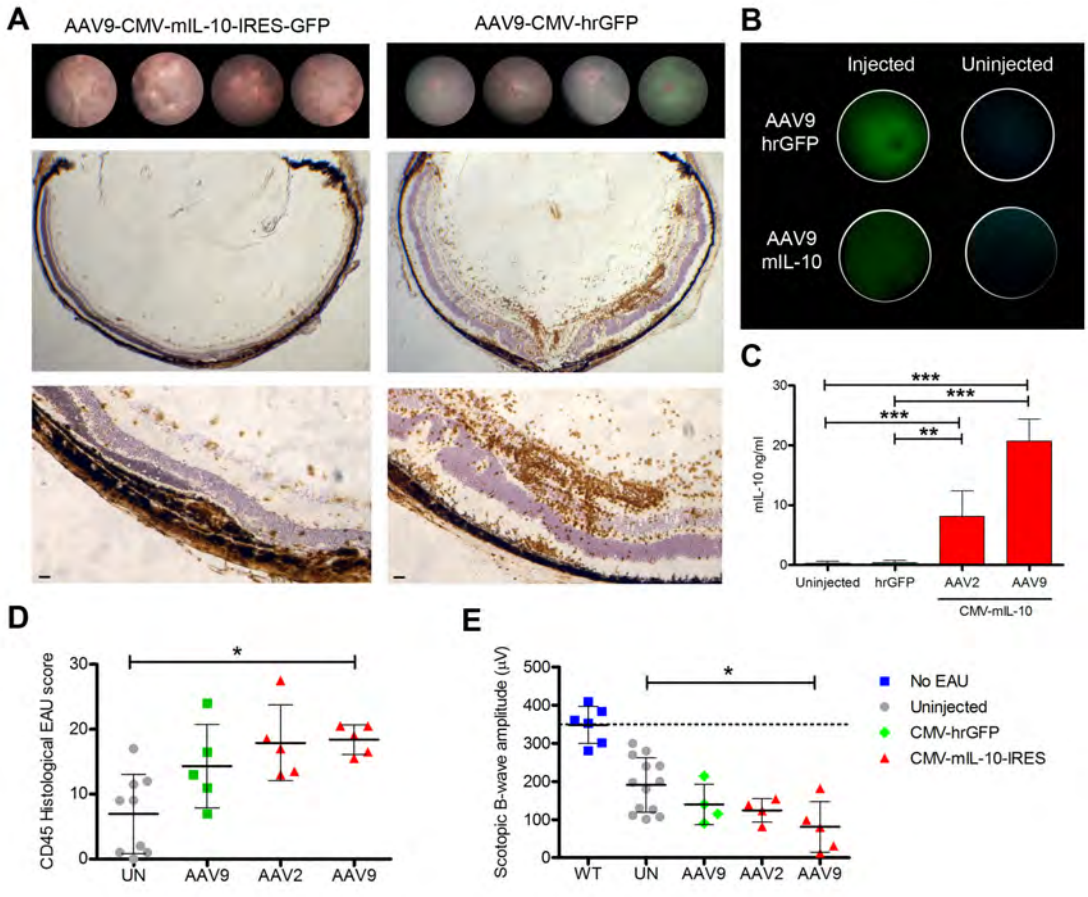

Figure 36. AAV9 mediated expression of *mIL-10* leads to increased severity of EAU and associated retinal cell loss. Double 2µl subretinal injections of $5x10^{11}$gc/ml titre-matched AAV9-CMV-mIL-10-IRES-GFP, AAV9-CMV-hrGFP or AAV2-CMV-mIL-10-IRES-GFP was performed three weeks prior to EAU induction. **A)** Representative images of TEFI and CD45-DAB histology. Extensive retinal loss and abnormal choroidal appearances were seen in the AAV9-mIL-10 cohort, compared to AAV9-hrGFP control. Scale bars = 50µm. **B)** Successful GFP expression was confirmed by slit-lamp fluorescent fundus imaging at day 17 post-injection, whilst ELISA of whole eye homogenates detected elevated levels of mIL-10 from AAV2 and AAV9-mIL-10 vectors. n=3, with technical triplicates. One-way ANOVA and Tukey's multiple comparison test, **=P<0.01, ***=P<0.001. **D)** Final CD45 histological EAU scores demonstrate statistically significant worsening with AAV9-mIL-10 compared to uninjected eyes. A trend towards worsening is seen even with AAV9-hrGFP and AAV2-mIL-10. **E)** Electroretinography demonstrates marked suppression of the scotopic B-wave in the AAV9-mIL-10 cohort, consistent with both EAU and extensive retinal damage. Kruskal-Wallis test with Dunn's multiple comparison, *=P<0.05. Means + SD shown.

Unexpectedly AAV9-mIL-10 was highly detrimental to the eye. Similar findings had not been seen before using AAV9. AAV9-hrGFP and AAV2-mIL-10 did not show the same dramatic appearance though all vectors had a trend towards worsened EAU. The observed changes could be a result of high level expression of *mIL-10* itself causing toxicity, or due to a non-protein specific effect of expressing secreted transgenes from AAV. It was also uncertain if the AAV9-mIL-10 vector specifically was only toxic in the context of simultaneous EAU and so a small dose-titration experiment was performed without disease induction.

TEFI performed on AAV9-mIL-10 injected eyes after one month again revealed similar retinal damage and appeared to be titre-dependent **(Figure 37A)**. Eyes were homogenised and tested by ELISA (see **Materials & Methods**) for mIL-10 and a dose-response was seen dependent upon titre. The onset of retinal changes appeared to coincide with the $1x10^{7}$gc dose – the first where detectable IL-10 production is seen **(Figure 37B)**. Flow cytometry on dissociated retinas was performed and an increase in CD4+ and CD8+ T-cells was also seen with higher titre **(Figure 37C)**.

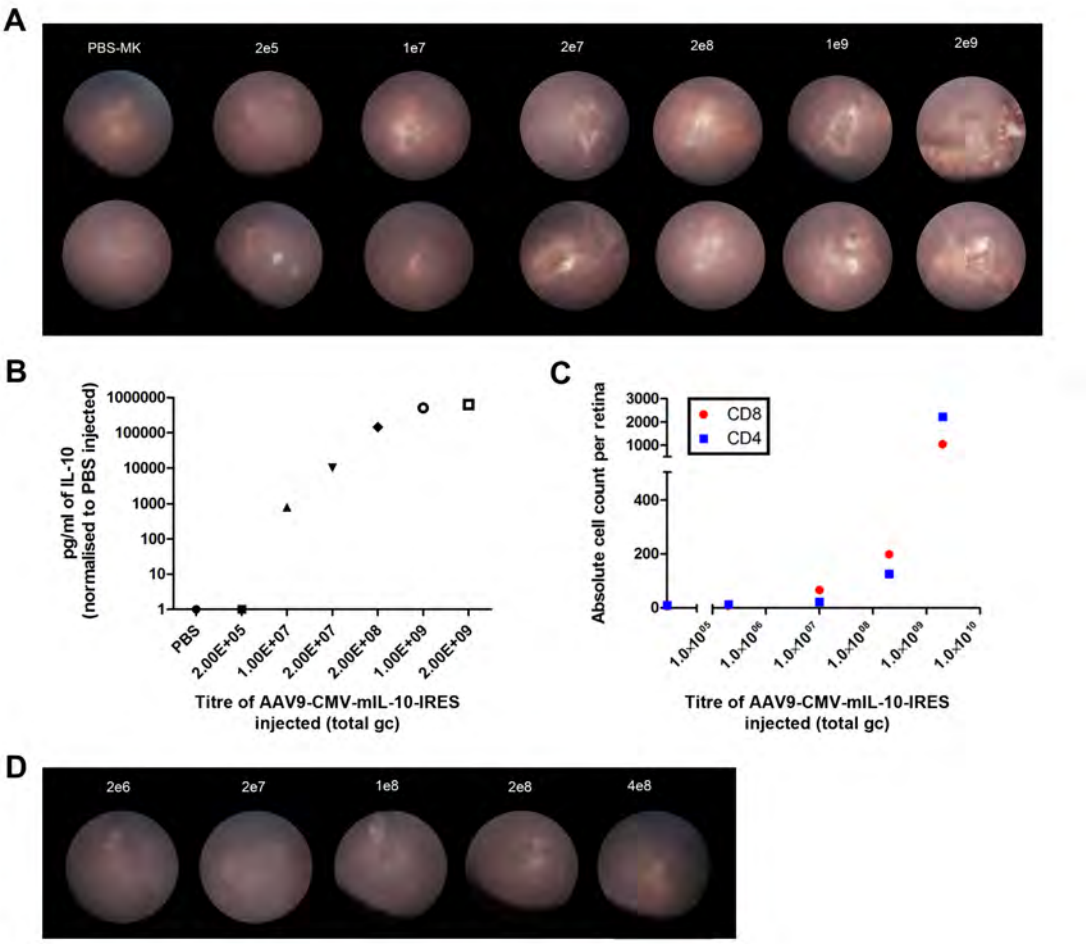

Figure 37. The AAV9-mIL-10 vector induces dose-dependent retinal changes and T-cell infiltration. Double 2µl subretinal injections of varying titre AAV9-CMV-mIL-10-IRES-eGFP purified by Sephacryl and Poros columns were assessed after 32 days. **A)** TEFI shows progressive retinal changes with increasing total genome copies of AAV. PBS is shown to control for the effect of retinal detachment. **B)** Eyes were homogenised and tested for mIL-10 levels by ELISA. This showed an effective elevation in ocular mIL-10, when a 2µl injection of above a $1x10^7$gc/ml titre was performed. **C)** Other eyes underwent flow cytometry after retinal dissociation. A trend towards higher numbers of CD4+ and CD8+ T-cells is seen with increasing titre. **D)** TEFI appearances of eyes injected with different titres of AAV9-mIL-10, purified using an AVB column. This method does not provide as high a titre, but contains less cellular contaminants, resulting in less marked retinal changes.

With possible toxic changes seen in the retina, the quality of AAV preparations being used was examined. The viral facility was optimised for monogenic rescue projects and had not extensively produced AAV for immunomodulation applications that might be more sensitive to contaminants. As an initial trial, purification was performed using an AVB column – an affinity-based separation medium. This is believed to give

cleaner preparations, but was not designed for use with AAV9 and so lower titres were obtained, with a maximum of $2x10^{10}$gc from a 20-plate prep.

Less clinical toxicity was observed, with improved retinal appearances seen on TEFI for equivalent titres **(Figure 37D)**. This manner of production however, was not satisfactory due to the inefficient yield of virus. At this point it was decided to fully re-assess the entire AAV production process and the many resultant changes are detailed in **results chapter 3**.

6.3 Refined production generated AAV8-mIL-10 avoids overt retinal toxicity but does not suppress EAU

As described multiple alterations were made to the viral production facility to enable optimal AAV production. Briefly this included removal of endotoxin contamination, a two-plasmid transfection process, routine purification using disposable AVB columns and improved titre-matching using a PCR based technique. The serotype used was also switched to AAV8. This is because it allows high-titre purification by binding strongly to AVB medium, be generated using a two-plasmid system and has similar transduction characteristics to AAV9. Specifically it is known to transduce RPE and photoreceptors but not Muller cells.

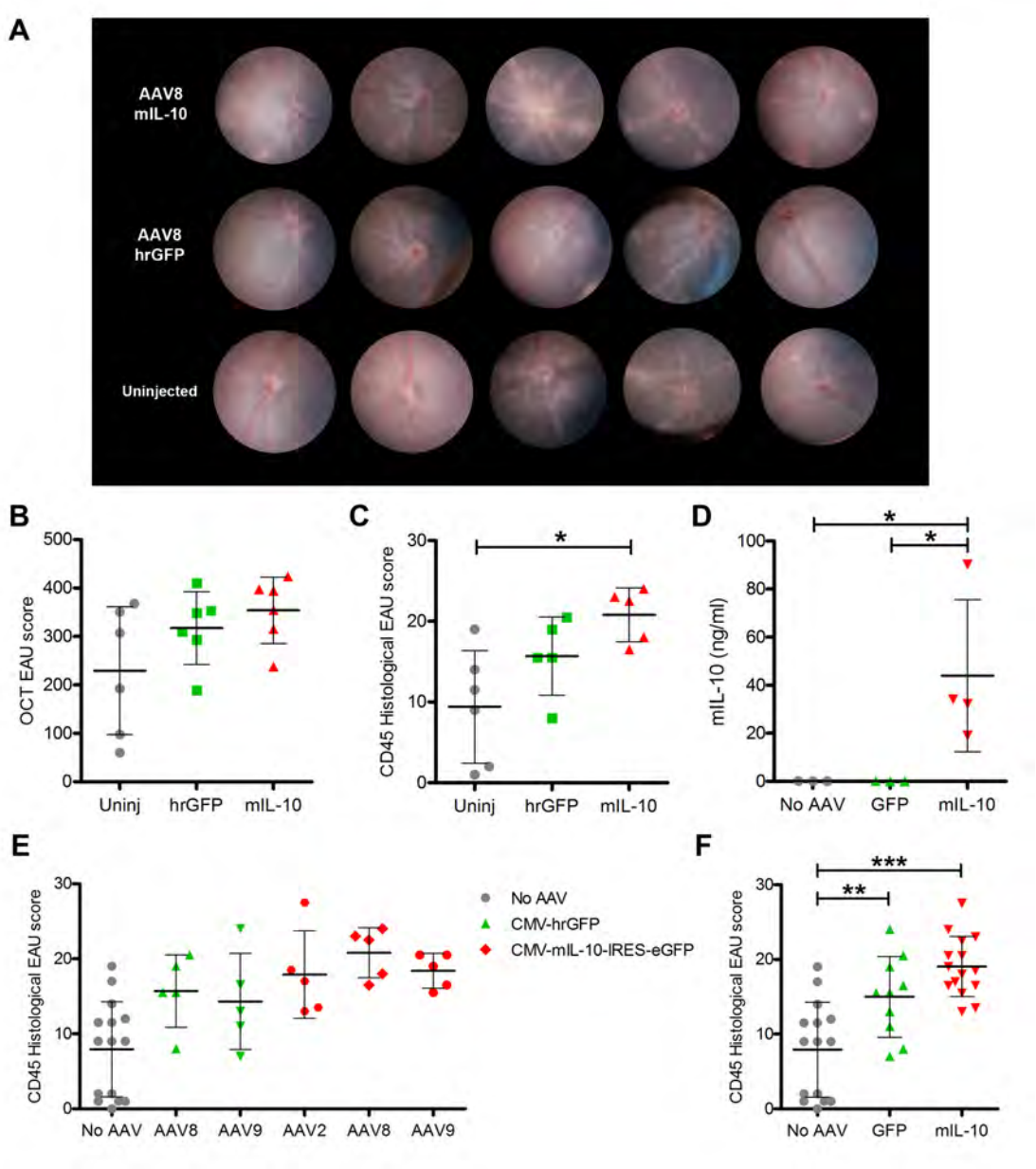

Figure 38. Refined production process AAV8-CMV-mIL-10 still fails to suppress EAU. Following the refined AAV production process described in results chapter 3, AAV8-CMV-mIL-10-IRES-eGFP or AAV8-CMV-hrGFP was produced and 0.5µl of $5x10^{12}$gc/ml injected into the subretinal space. One week later EAU was induced then terminated at peak disease at 26 days later. **A)** Representative TEFI images of eyes from the three intervention groups, shows limited differences between the groups. **B)** *In vivo* scores for the cohort using the OCT-based EAU scoring system developed in results chapter 1 shows a trend towards worsened EAU. **C)** CD45 histological EAU scores show worsened disease in the AAV8-mIL-10 group compared to uninjected eyes. **D)** ELISA of whole eye homogenates from eyes injected in the same cohort confirms elevated levels of mIL-10 in the intervention group only. Kruskal-Wallis test, *=P<0.05. **E)** Summary graph of CD45 histology EAU scores from this and the previous AAV9 experiment, with **F)** pooled data to demonstrate the effect of *mIL-10* overexpression. One-way ANOVA with Tukey's multiple comparison test. **=P<0.01, ***=P<0.001. Means + SD shown.

Using the newly produced vectors, the initial experiment was repeated using AAV8-CMV-mIL-10-IRES-eGFP and AAV8-CMV-hrGFP. TEFI appearances did not reveal the atrophic changes seen before with AAV9, implying previous findings might have been specific to that serotype or contaminants from the original production process **(Figure 38A)**. The newly developed OCT-based EAU scoring system was employed and showed a trend towards worsened disease in AAV8 injected eyes **(Figure 38B)**, confirmed by CD45 histology scores **(Figure 38C)**. Successful supplementation of mIL-10 was identified by ELISA on whole eye homogenates **(Figure 38D)**. Pooling data from both AAV9 and AAV8 experiments, **(Figure 38E-F)** significant worsening of EAU was observed in both GFP and *mIL-10* expressing vectors, compared to uninjected eyes. The difference between GFP and mIL-10 was not statistically significant and so it is not possible to conclude that the effect of mIL-10 is responsible.

It is known that retinal detachment leads to an increase in multiple inflammatory cytokines and microglial activation.[179] One hypothesis at this stage was that the subretinal injection resulted in a larger increase in inflammation than the degree of suppression obtained from mIL-10. Timing of intervention is also important and cytokines such as IL-10 may lead to different effects given prior to established inflammation, rather than during disease. Different forms of IL-10 also exist and three main types have been investigated widely in the literature. Murine, human and viral IL-10 share similar properties, but differ with respect to their potential pro-inflammatory effects. For example, viral IL-10 lacks the predominantly stimulatory regions and is felt to possess superior immunosuppressive qualities.

To address these three issues, a novel engineered serotype known as ShH10 was obtained from Prof. John Flannery (Berkeley, USA). It was characterised as described in **results chapter 3** and produced using the refined production process. ShH10-viral IL-10 was produced and delivered using the intravitreal route, which is suspected to be less destructive than a subretinal injection, albeit at the risk of greater systemic absorption of vector. The relative simplicity of an intravitreal injection also makes it tractable

clinically to intervene in eyes with established EAU, which may otherwise suffer from hypotony and vitritis that would make subretinal injection technically challenging, and would increase adverse outcomes.

EAU was induced in a cohort of *C57BL/6J* mice and at day 14 two doses of ShH10-viral IL-10-IRES-GFP were injected. Eyes were analysed at day 26, by which time expression would be obtained from the ciliary epithelium, corneal endothelium and occasional Muller glia. TEFI did not show differences in retinal appearance compared to PBS injected controls **(Figure 39A)**, despite the presence of 500pg/ml in retinal supernatants **(Figure 39B)**. Flow cytometry confirmed the absence of effect upon changes in key infiltrating cellular populations **(Figure 39C)**.

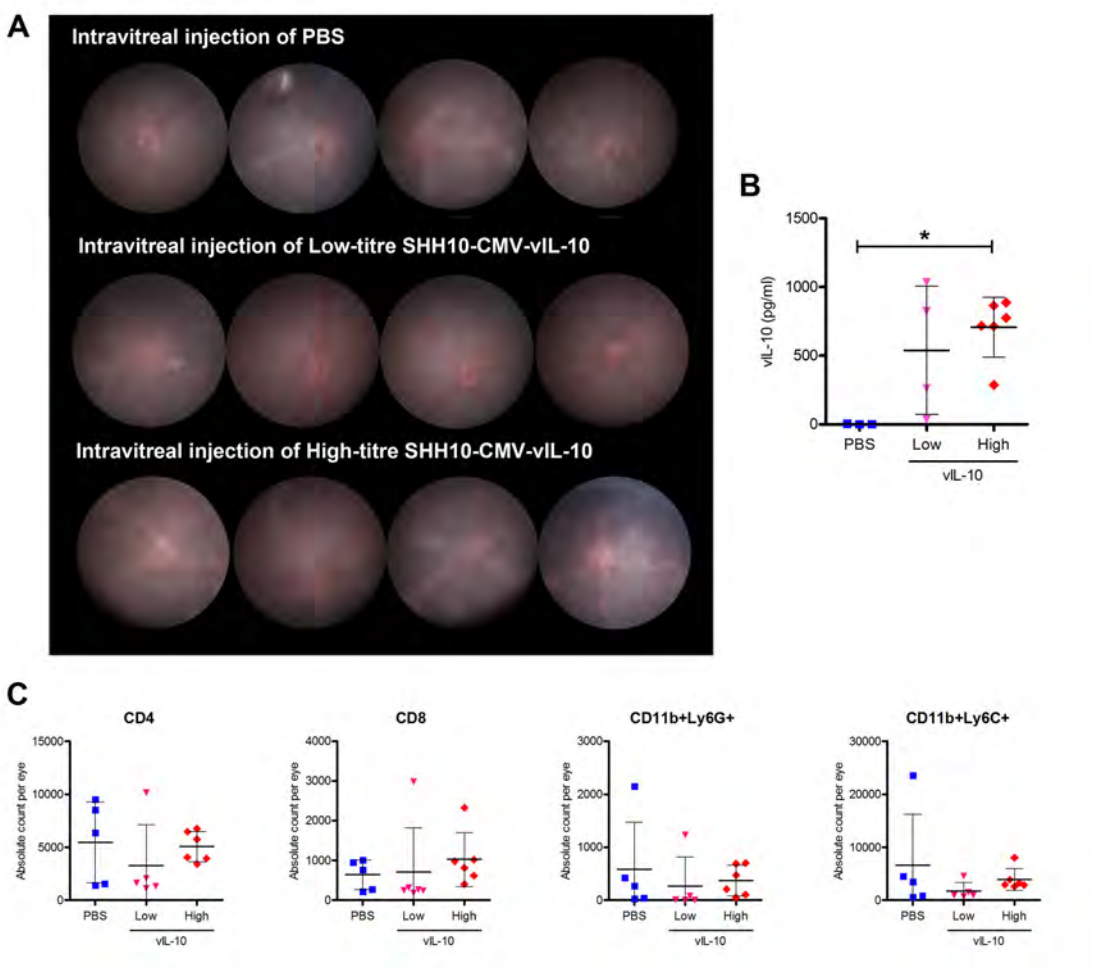

Figure 39. Intravitreal injection of ShH10-viral IL-10 during established EAU does not change final disease outcome. EAU was induced and at day 14, intravitreal injection of 2µl PBS, $2x10^{10}$gc (high dose) or $2x10^{9}$gc (low dose) ShH10-CMV-vIL-10-IRES-GFP was performed. **A)** At peak disease on day 26 TEFI appearances do not show dramatic differences

between groups. Following dissociation retinal samples were analysed by flow cytometry with supernatants used for ELISA. **B)** vIL-10 was detectable in both high and low dose groups. Kruskal-Wallis test with Dunn's multiple comparison, P=0.03. **C)** Flow cytometry shows no significant alteration in cell counts of CD4, CD8 T-cells, CD11b+Ly6G+ (neutrophils or MDSC) or CD11b+Ly6C+ (monocyte) populations. Whilst no suppression of disease was achieved, there was equally no worsening in disease despite intravitreal administration of up to $2x10^{10}$ viral genome copies during acute EAU. Means + SD shown. n=16 eyes.

It was clear that further investigation would be required to identify and correct issues affecting successful suppression of EAU by viral gene transfer of *IL-10*. As the priority was to discern why expressing *IL-10* using newly developed AAV serotypes did not reduce intraocular inflammation, a simpler model was employed to reduce the number of potential variables. Endotoxin-induced uveitis (EIU) is a non-antigen based model of acute ocular inflammation that occurs rapidly, allowing assessment within 24 hours. Triggered by ocular TLR4 ligation, the pro-inflammatory signalling pathways involved are much more narrow than EAU and so arguably the opportunity for successful suppression is greater. This has been corroborated by publications showing attenuation of EIU using lentivirally delivered mIL-10.[34]

6.4 EIU can be used to efficiently screen factors affecting effective suppression by viral gene transfer

Prophylactic delivery of the refined AAV8-mIL-10-IRES-GFP vector was tested first with EIU induced by intravitreal administration of 1ng LPS a week after subretinal injection. No suppression in neutrophil (defined as CD11b+Ly6G+) infiltration was seen, even though detectable supplementation of mIL-10 was identified by ELISA **(Figure 40A-B)**. The lack of correlation between infiltrative cell number and mIL-10 level implies that either mIL-10 has no dose-response effect or levels are outside the therapeutic range **(Figure 40C)**.

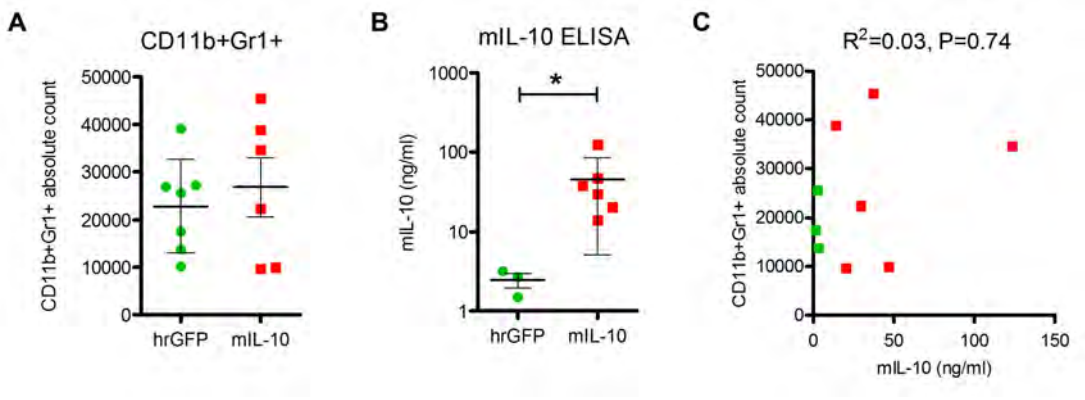

Figure 40. Subretinal administration of AAV8-CMV-mIL-10-IRES-eGFP does not affect EIU. One week following 2µl subretinal injection of titre-matched 2x10^{9}gc refined AAV8, 1ng of LPS was administered into the vitreous cavity and 18hr later, AC, vitreous and retinal cells were dissociated and analysed by flow cytometry. **A)** There was no effect upon EIU severity as measured by granulocyte infiltration, despite **B)** an 18-fold elevation in IL-10 protein level detected by ELISA of matched RPE/choroid homogenate. Mann-Whitney U test, P=0.024. **C)** No significant correlation was detected between mIL-10 levels and degree of infiltration. Pearson correlation. Means + SD shown.

To address the issue of dose, route and vector effects, *mIL-10* was delivered from variety of vectors and routes, including intravitreal ShH10, subretinal AAV8, AAV9 and lentivirus. ShH10-CMV-eGFP was used as a control. EIU was induced a week later and analysed by flow at 18-hours **(Figure 41A)**. No significant differences were seen between numbers of infiltrating neutrophils (CD11b+Ly6G+). A range of concentrations of mIL-10 was recovered from matched retinal supernatants **(Figure 41B)**. Comparing dose to disease severity, there was no correlation, indicating that over a range of doses from 10pg/ml to 10ng/ml mIL-10 has no effect upon EIU, when delivered by a variety of viral routes **(Figure 41C)**.

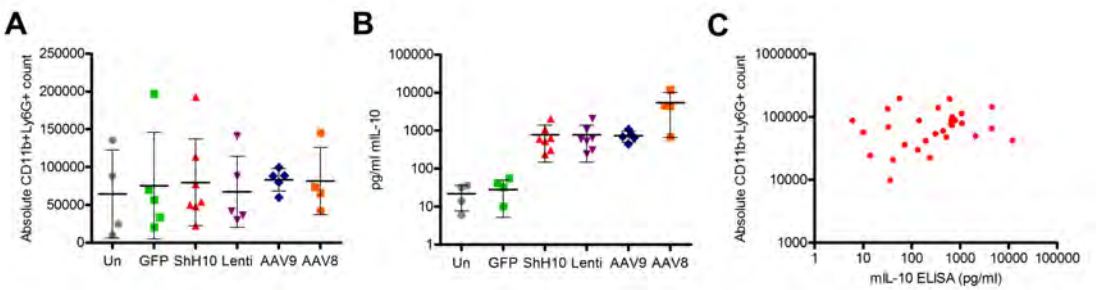

Figure 41. Murine *IL-10* expressed from different AAV serotypes fails to suppress EIU at any dose achieved. A wide range of ocular mIL-10 was achieved by injecting different serotypes, titres and routes. ShH10-CMV-mIL-10 (IV), AAV9 (double subretinal), AAV8 (single subretinal), Lenti-mIL-10 (single subretinal). ShH10-CMV-eGFP (IV) and uninjected eyes were used as a control. **A)** No change in the number of CD11b+Ly6G+ cells was seen between any group. **B)** Elevated levels of mIL-10 were confirmed in all intervention groups by ELISA. Three dilutions and technical duplicates. All OD values were on the linear part of the standard curve. **C)** No correlation was identified between mIL-10 level and cell count, implying lack of efficacy across a range from 10pg/ml to 10ng/ml. Pearson correlation, R^2=0.0005, P=0.91. Means + SD shown.

This result was unexpected and hard to reconcile with previously published work.[34] Before making a conclusion about the effect of mIL-10, the prior experiment of intracameral lentivirus and EIU was repeated exactly, but using the disease readout of flow cytometry developed in **results chapter 2**. Injecting lentivirus in this manner leads to transduction of the corneal endothelium, iris, trabecular meshwork and ciliary body. Suppression was seen in the anterior chamber, but not in the vitreous/retinal compartment **(Figure 42A)**. Additionally no difference in mIL-10 levels could be detected between the therapeutic vector and eGFP control injected eyes **(Figure 42B)**. Diseased eyes were not tested by mIL-10 ELISA during the initial publication and suppression was seen by histology in both compartments **(Figure 42C)**. The potential implication is that either EIU itself or the GFP vector induced endogenous production of mIL-10. Interleukin-10 is known to increase during normal EIU.[186] It could be that the suppressive effects result from conditioning of resident cells in the two weeks prior to EIU induction.

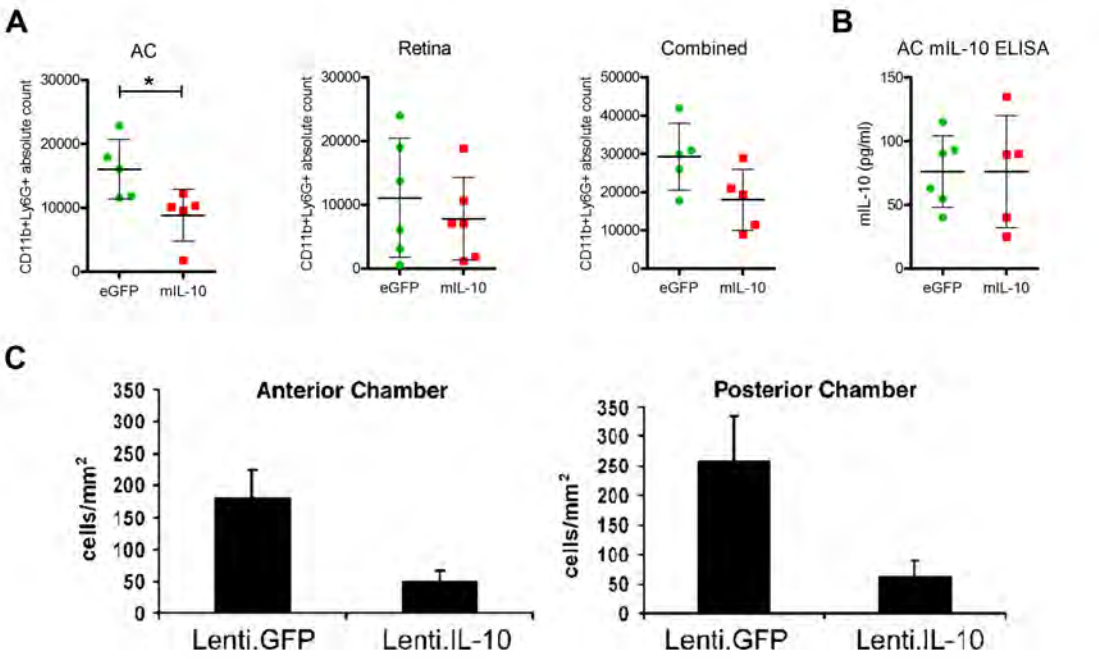

Figure 42. Intracameral Lentivirus expressing murine *IL-10* attenuated AC cell counts only during EIU when analysed by flow cytometry. Eyes received 4µl intracameral injections of Lentivirus expressing GFP or *mIL-10*. Two weeks later EIU was induced and eyes taken for flow cytometry at 12 hours post-injection. **A)** Absolute counts of CD11b+Ly6G+ cells in the AC, Retina/Vitreous and the two-combined demonstrate a reduction in the AC only. Mann-Whitney U test. P=0.03. **B)** This is despite no detectable difference in mIL-10 levels in AC fluid at the end of the experiment. **C)** Histological scores from previously published data for comparison.[34] Mean + SD shown.

To clarify several variables, the experiment was repeated again, but including eyes injected with lentivirus without the induction of EIU. This cohort failed to demonstrate the AC suppression previously seen **(Figure 43A)**. Matched ELISA data for mIL-10 levels reveals details of changes during EIU **(Figure 43B)**. Firstly, prior to the induction of disease a detectable elevation in mIL-10 exists relative to PBS and GFP control at baseline. During EIU levels in the AC do not significantly change in any groups. Larger amounts of IL-10 are observed in the retinal compartment during EIU compared to the matched eye AC samples, with a trend to greater levels in the Lenti.mIL-10 group. Despite now detectable elevations there is no suppression of disease. Pooling data from both experiments confirms no overall effect of *mIL-10* expression **(Figure 43C)**.

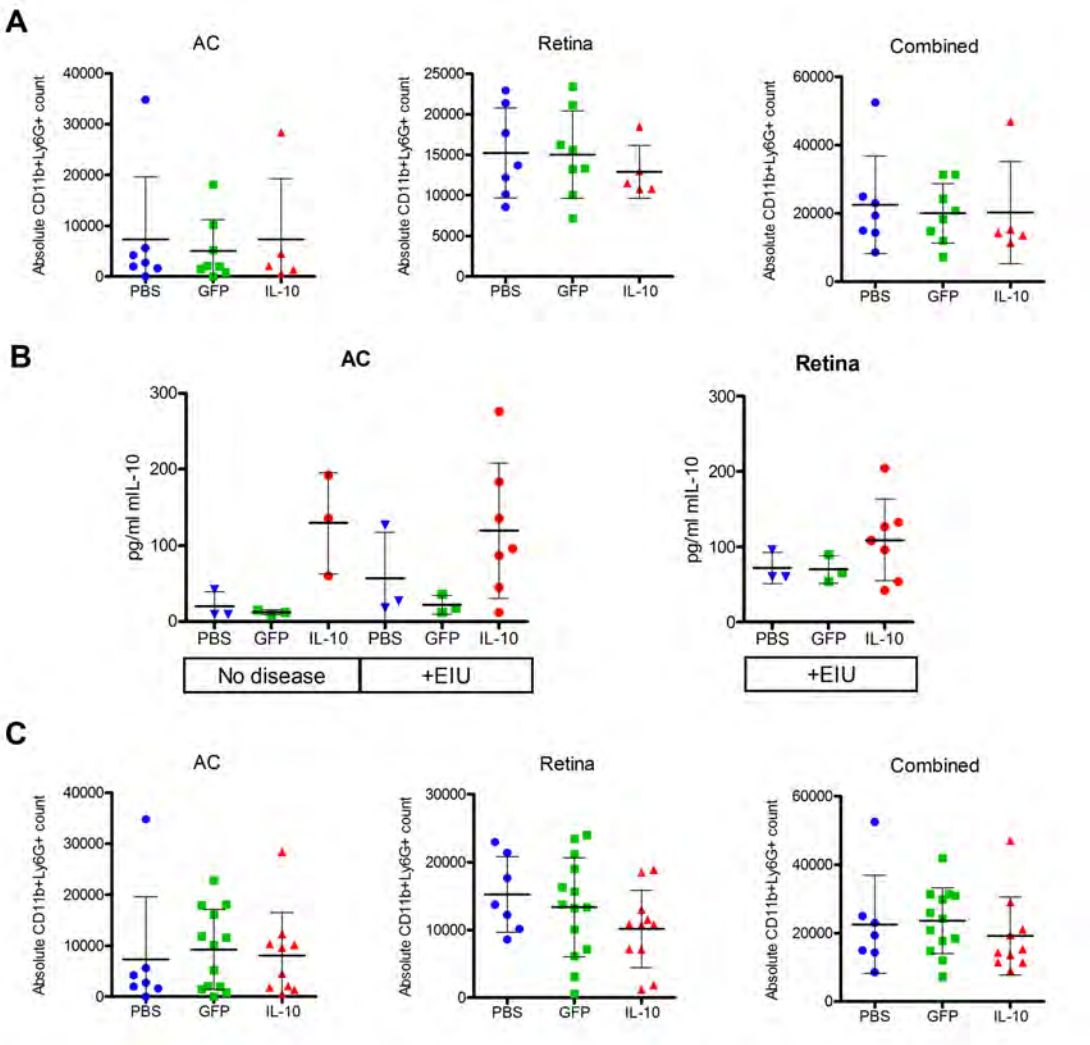

Figure 43. The experimental repeat and addition of a PBS control demonstrates no significant suppression of EIU by Lenti.*mIL-10*, despite detection of elevated mIL-10 protein levels in the eye. Eyes received 4µl intracameral injections of PBS or Lentivirus expressing GFP or mIL-10. Two weeks later EIU was induced and eyes taken for flow cytometry at 12 hours post-injection. **A)** Absolute counts of CD11b+Ly6G+ cells in the AC, Retina/Vitreous and the two-combined shown no significant suppression. Kruskall-Wallace test. P>0.30. **B)** ELISA for mIL-10 on ocular supernatants detects significantly elevated levels after Lenti.mIL-10 in the AC. Kruskall-Wallace test. P=0.02. The induction of EIU appears not to affect levels of mIL-10. **C)** Pooled cell counts including the previous experiment from Figure 42 confirm no significant suppression by Lenti.*mIL-10*. Means + SD shown.

There is clearly large variation between experiments and the previous work was not fully repeatable. As levels were not assessed in that paper, it is hard to compare the required therapeutic dose. Additionally, the caveat of using a different form of assessment – flow cytometry vs histology – should be considered when comparing results. As the first repeat showed AC

suppression without a difference in mIL-10 level, it is possible that mIL-10 requires below-detection concentrations to suppress disease. To investigate the different effects of other species of IL-10, viral IL-10 derived from Epstein-Barr virus was delivered to the eye using ShH10. It was thought possible that the different structure, lacking pro-inflammatory regions might prove superior in efficacy to mouse IL-10.

A week after intravitreal injection of ShH10-CMV-vIL-10-IRES-GFP, EIU was induced and eyes examined 18 hours later by flow cytometry. A reduced CD11b+Ly6G+ count was seen in the AC **(Figure 44A)** but not the retina, accompanied by detectable levels of vIL-10 **(Figure 44B)**. An R&D-manufactured cytokine and chemokine panel proteome profiler was used with pooled AC fluid supernatants from vIL-10 and GFP control groups **(Figure 44C)**. Densitometry of the signals in the detectable range revealed reduced levels of multiple proteins in the vIL-10 group, relative to GFP. Only C5a was increased with treatment **(Figure 44D)**. It is not well established with this technique how the significance of effect size should be estimated. Arising from AC fluid, it is indiscernible which contributions the infiltrating cells or ocular tissues each make. Certainly the near global suppression, rather than a particular pattern of neutrophil specific protein reduction makes this data less convincing.

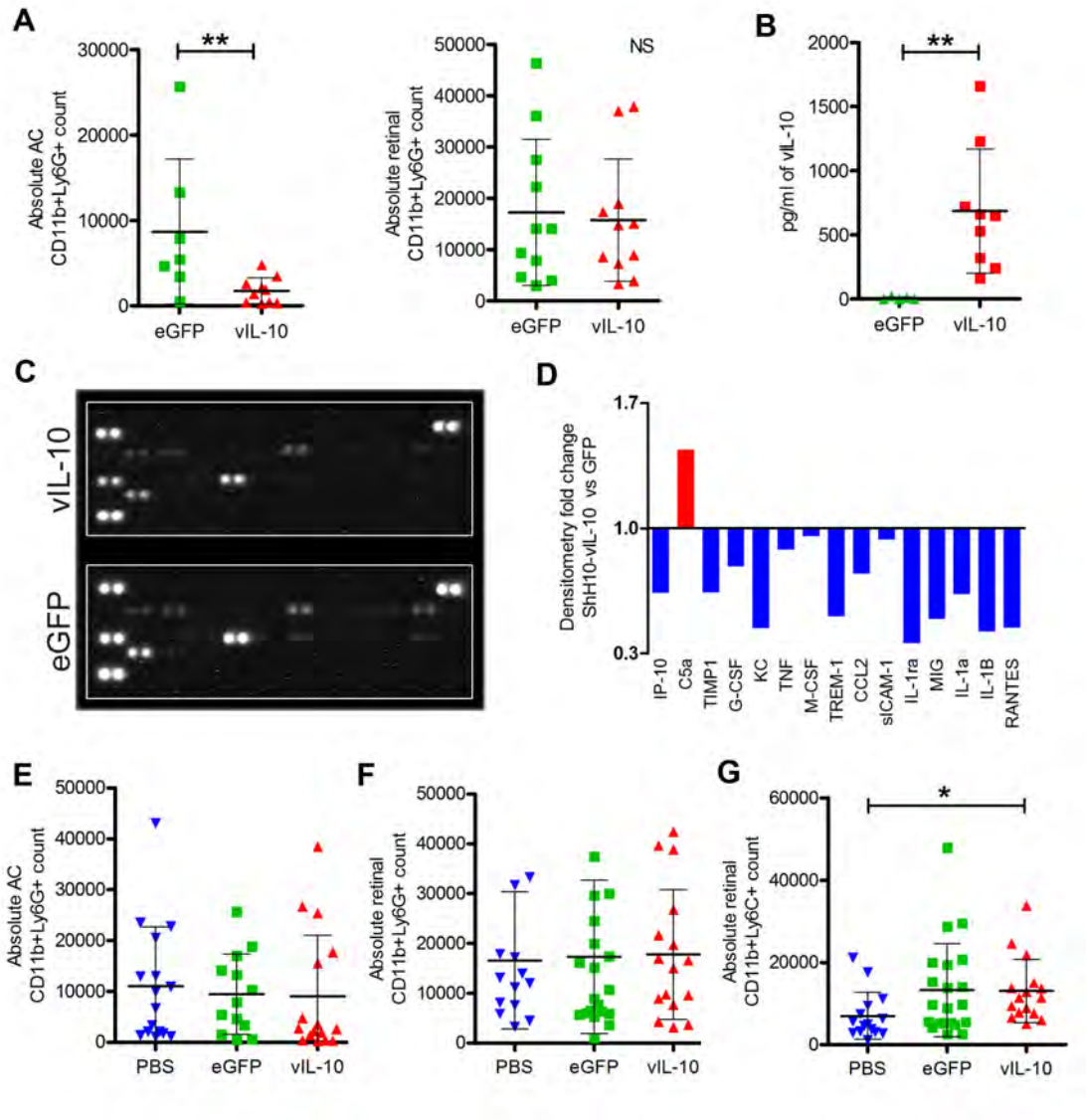

Figure 44. ShH10 delivered viral IL-10 does not reliably suppress EIU. ShH10-CMV-vIL-10-IRES-eGFP was titre matched to ShH10-CMV-eGFP and $1x10^{10}$gc delivered via 2µl intravitreal injection. After one week EIU was induced and eyes analysed 18-hours later. **A)** In the first experiment, suppression was seen in the AC (P=0.009), but not in the retina. Mann-Whitney U test. **B)** This was accompanied by detectably elevated levels of vIL-10 in the AC. **C)** Pooled AC supernatants from five eyes were tested by R&D proteome profiler. **D)** Densitometry was used to assess relative changes between eGFP and vIL-10 groups. All detectable cytokines or chemokines appeared reduced to variable degrees in the vIL-10 cohort, except C5a complement component which was elevated. The experiment was independently repeated, but this time no therapeutic effect was seen. Pooled results including concurrent PBS injected controls confirm no significant effect upon CD11b+Ly6G+ cell number in either the **E)** anterior chamber or **F)** retinal compartment. **G)** A statistically significant elevation in CD11b+Ly6C+ cell number was seen in the retinal compartment in the vIL-10 treated group compared to PBS. Kruskal-Wallis test with Dunn's multiple comparison, P=0.019. Means + SD shown.

The experiment was independently repeated but again the first result could not consistently be reproduced, suggesting a small, negligible or highly variable effect. Data from both experiments was pooled **(Figure 44E-F)**. There was however a significant increase in CD11b+Ly6C+ cells in the retinal compartment, during *vIL-10* expression **(Figure 44G)**. This could reflect a more generalised response against the ShH10 vector transduction and not just an effect of vIL-10 itself, as discussed in **results chapter 3**.

6.5 Recombinant protein confirms the efficacy of human but not murine IL-10 in EIU

A wide range of viral vectors, routes and doses had failed to suppress EAU and EIU using IL-10. Repeating previous published work had also failed to validate the original results consistently. Furthermore, inconsistent data was seen even between sequential repeats of the same recent experiments, implying either the therapeutic effect was small or unknown variables exist. To identify issues, and reduce variables recombinant protein was used to treat EIU. A strong positive control was also required. One key publication had shown the beneficial effect of local delivery of recombinant human IL-10 in EIU, scored by histology.[177] We sought to use flow cytometry and compare these findings to those obtained using murine IL-10.

Different doses of recombinant human and murine IL-10 or PBS control we injected into the vitreous cavity at the same time as EIU induction. Whole eyes were dissociated and analysed 18-hours later **(Figure 45A-C)**. Human IL-10 demonstrated a potent dose-response, significantly suppressing EIU at 200ng and above. Murine IL-10 showed a trend towards suppression, but this was not statistically significant and failed to exhibit any dose-response behaviour. To confirm this was not due to biological inactivity or defect in the recombinant mIL-10 protein, the data shown is pooled from experiments using product from two different manufacturers (Biolegend and Cell Signalling technologies). Subgroup analysis showed no difference between the two, reinforcing the results obtained. Furthermore, elevated levels of mIL-10 could be detected in ocular supernatants from injected eyes at 18-hours

post EIU using a murine IL-10 specific ELISA **(Figure 45D)**. Further evidence that mIL-10 is not suppressive is that increasing mIL-10 concentration is significantly correlated with increasing CD11b+Ly6G+ cell number **(Figure 45E)**. Biological activity of mIL-10 was also confirmed by quantitative RT-PCR, where mIL-10 injected eyes had lower levels of KC transcripts than PBS injected controls **(Figure 45F)**. As this is a prototypic neutrophil chemo-attractant, lower levels should typically result in less infiltration.

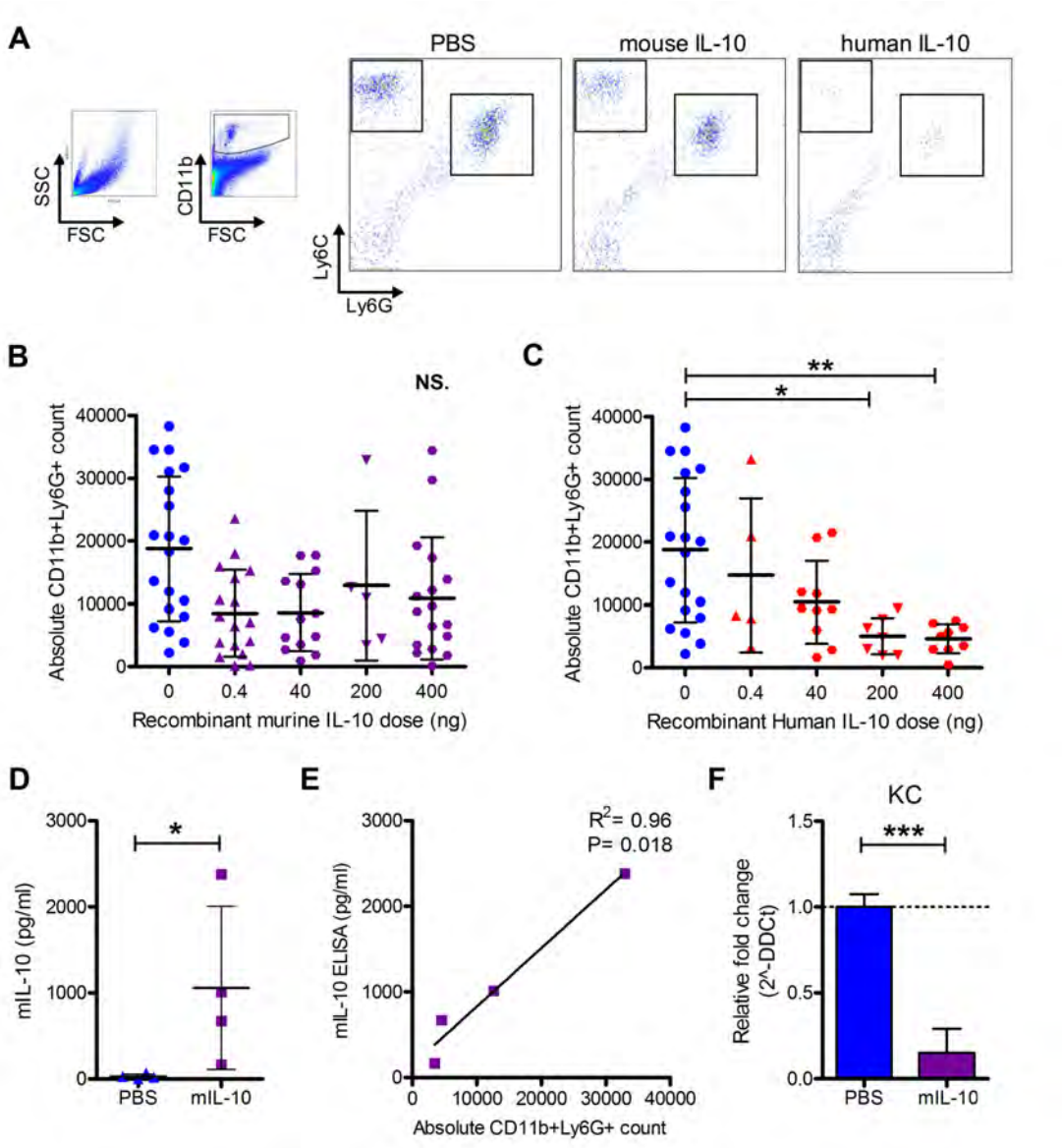

Figure 45. Unlike recombinant murine IL-10, human IL-10 suppresses EIU in a dose-dependent manner. Using flow cytometry as a readout, 1ng LPS was intravitreally injected with PBS or different doses of recombinant murine and human interleukin-10. Eighteen hours later retina, vitreous and aqueous fluid from each eye were dissociated and analysed by flow cytometry. **A)** Representative dot plots of eyes with EIU, gated first by CD11b. Only the 400ng human IL-10 group has marked reduced counts of Ly6G or Ly6C+ cells. **B)** Over a range of

doses murine IL-10 fails to significantly suppress CD11b+Ly6G+ infiltration, though a generalised trend towards lower counts than PBS exists. **C)** Human IL-10 exhibits a strong dose-response suppression of EIU, which is statistically significant at 200 and 400ng. Data shown is pooled from 3 independent experiments, using two different batches of cytokines each from two different manufacturers. Kruskall-Wallace with Dunn's multiple comparison test. *=P<0.05, **=P<0.01. **D)** To confirm the presence of murine IL-10, elevated levels in retinal supernatants from injected eyes were confirmed by ELISA. Mann-Whitney U test, *=P<0.05. **E)** Furthermore, the level of mIL-10 was inversely proportional to the degree of suppression. Pearson correlation. **F)** Relative qPCR for KC normalised to β-actin on whole eye homogenates 18 hours after PBS and mIL-10 injection. Mann-Whitney U test, ***=P<0.001, n=3. Means + SD shown.

These discoveries may begin to reconcile some of the previously observed findings. It is known that human and murine IL-10 differ by 27% amino acid sequence with the latter also N-glycosylated, however they have been broadly regarded as similar in action and used relatively interchangeably in much of the literature.[119] The limited effect, if any of murine IL-10 in EIU may have been responsible for the uncertain and highly variable findings between different experiments. As human IL-10 was clearly effective, it was decided to use this endpoint as a positive control and essentially reverse-engineer successful suppression using AAV. The human IL-10 sequence was cloned behind the CMV promoter and produced as an ShH10 vector.

All three forms of interleukin-10 – human, murine and viral – encoded in ShH10 were delivered by intravitreal injection. A week later EIU was induced and eyes analysed at 18-hours. No statistically significant suppression relative to PBS or ShH10-CMV-eGFP was seen in either the AC or retinal compartments **(Figure 46A-B)**. At one week ShH10 mediated expression is predominantly from the ciliary epithelium and corneal endothelium. Whilst a change would have been likely to be seen in the anterior chamber, it is possible the dose of human IL-10 may have been too low. From the analysis of recombinant protein consistent suppression was only seen after an initial dose of 200ng. Whilst this would have decreased by the 18-hour timepoint, it was uncertain if ShH10 mediated delivery of human IL-10 would ever achieve the same dose range.

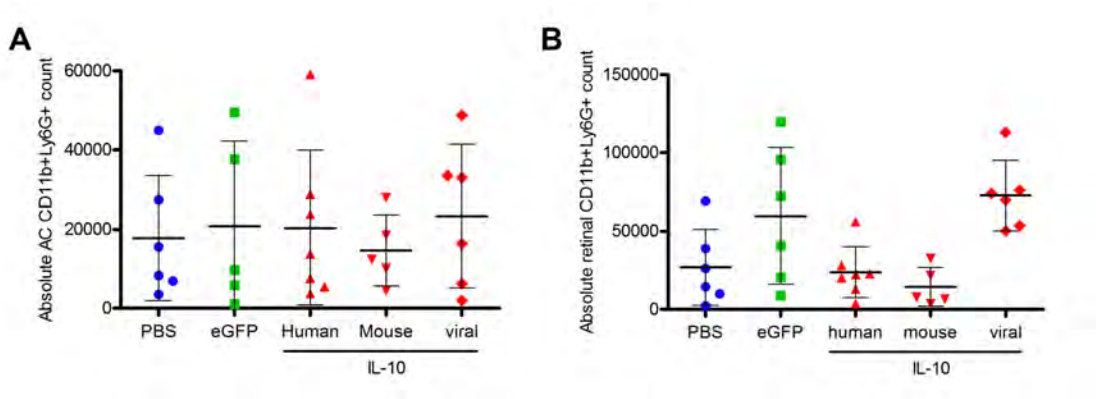

Figure 46. ShH10-mediated transfer of mouse, human or viral *IL-10* does not suppress EIU at 18-hours following injection one-week prior. 2µl intravitreal injection of PBS, 1x10^{9}gc ShH10-CMV-eGFP or titre-matched ShH10-CMV-murine IL-10, human IL-10 or viral IL-10 was performed. One week later EIU was induced and at 18-hours eyes dissected into AC and retina/vitreous. Flow cytometry analysis shows no statistically significant change from PBS or GFP control in **A)** the anterior chamber or **B)** posterior compartment. Means + SD shown.

To gauge the decay and relative changes in concentration following bolus human IL-10 injection in EIU, a kinetic experiment was performed. All samples were standardised and analysed simultaneously to minimise error and variation, with samples split evenly across the same ELISA plates and run on one 96-well plate for flow cytometry. Suppression of CD11b+Ly6G+ cell number by human IL-10 beyond 6 hours was seen **(Figure 47A)**. At 18-hours, AC and retinal compartment supernatants were tested by ELISA for EIU eyes injected with either 200ng recombinant hIL-10 protein or one week post intravitreal ShH10-CMV-hIL-10 administration **(Figure 47B)**. Surprisingly at this point, levels were similar or fractionally higher in the viral derived group. Looking at the ELISA levels over the course of time, initial recovery at 2hours in the AC was around 15ng/ml, so significantly higher, but by 18-hours levels have rapidly decayed to below those obtained from steady ShH10 mediated production **(Figure 47C)**. The trend to higher levels in the AC following both viral delivery and intravitreal recombinant protein delivery may reflect the natural path of fluid egress in the eye. Aqueous humour produced by the ciliary body is likely to wash hIL-10, with some vitreous

contribution, through the pupil, into the AC and out of the eye via either the trabecular meshwork or uveoscleral outflow pathways.

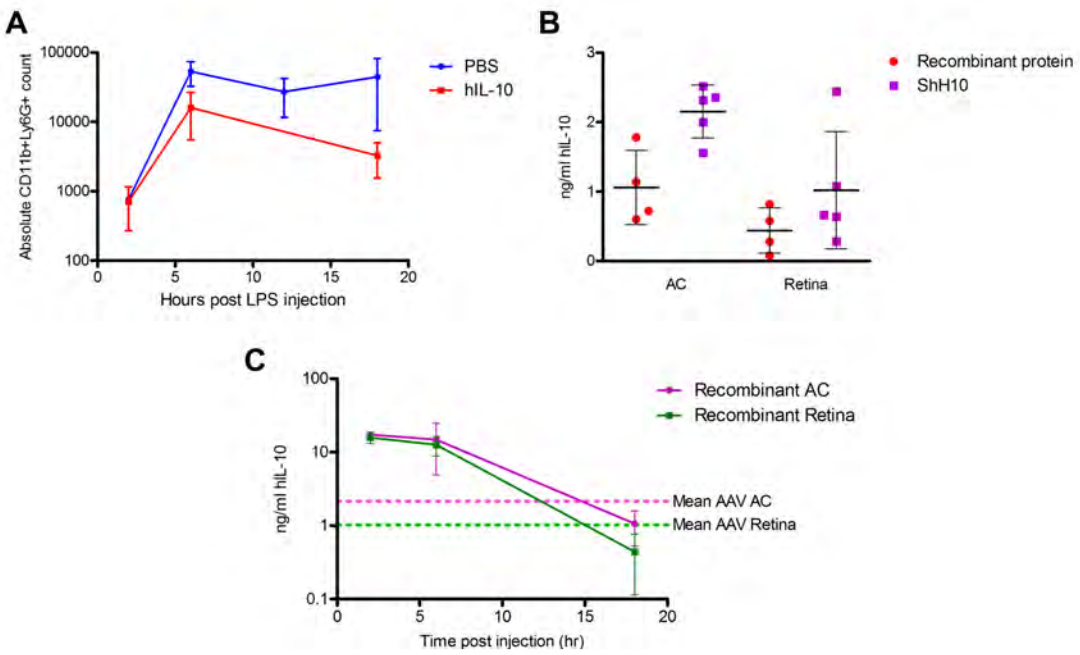

Figure 47. A comparative timecourse of recombinant protein demonstrates comparable levels at 18-hours post injection to ShH10-derived human IL-10 in the eye. Eyes receiving intravitreal injection of $1x10^{10}$gc ShH10-CMV-human IL-10 were induced with EIU after one week. During the same session other eyes induced with EIU and co-injected with either PBS or 200ng recombinant human IL-10. Eyes from this cohort were analysed at 2, 6 and 18-hours. ShH10-injected eyes were terminated at 18-hours post–EIU. Eyes were separated into AC or retina/vitreous compartments. Simultaneously analysis was performed for all samples, split evenly across ELISA plates and stained and analysed by flow cytometry in the same 96-well plate. **A)** Pooling data from two other independent experiments, a timecourse of typical EIU and that treated with intravitreal recombinant human IL-10 is shown. At all timepoints human IL-10 treated eyes show lower cell counts. n=4-6 eyes per point. **B)** Human IL-10 ELISAs at 18-hours for AC and retina/vitreous compartment supernatants. Recombinant protein has decayed to approximately the same level produced by ShH10 delivery. **C)** Compartment separated ELISA data over time, with mean levels from ShH10 production at 18 hours marked. Means + SD shown. ELISAs performed at three dilutions, with technical triplicates.

High levels of human IL-10 are achieved following recombinant protein injection, with little reduction from 2 to 6hrs, but rapid decay such that at 18 hours levels of hIL-10 are significantly lower than that achieved by ShH10 delivery. Clearly viral expression can achieve similar concentrations at this

late stage, but as no suppression of EIU is seen, either the early 2 to 15hr period is the crucial window where high levels of IL-10 are required, or the presence of virally transduced cells attenuates the suppressive effect.

6.6 The suppressive effects of IL-10 upon EIU may be affected by the timing after induction

The kinetic data and progressive characterisation of the EIU model in our hands highlighted the effect of changing cell populations and cell viability over time (see **results chapter 2**) Total numbers of CD11b+Ly6G+ cells were similar between the 6 and 18 hours post EIU induction, with a trend to greater numbers in the 6hr group. CD11b+Ly6C+ cells however, increased dramatically in number by 18 hours. It is possible that different mechanisms and biological interactions are occurring at this late point. Certainly it has been proposed that Ly6C+ monocytes may be recruited as a form of resolution to clear dead neutrophils recruited at peak EIU.[32] In this context, human IL-10 may not be effective. We decided to repeat the initial experiment using ShH10-CMV-human IL-10, but assessed at 6hrs post EIU induction.

Whole eye suppression of CD11b+Ly6G+ and Ly6C+ cells was observed when tested at 6hrs **(Figure 48E-F)**. Elevated levels of human IL-10 were confirmed from ocular supernatants **(Figure 48G)**. To ascertain if the effect was real, supernatants were run on an R&D proteome profiler as before and relative differences to the eGFP group were calculated by densitometry **(Figure 48H)**. Most pro-inflammatory agents were suppressed, but the greatest magnitude of reduction was seen particularly for proteins involved in neutrophil chemotaxis such as IP-10, KC, CCL2, and MIP2.

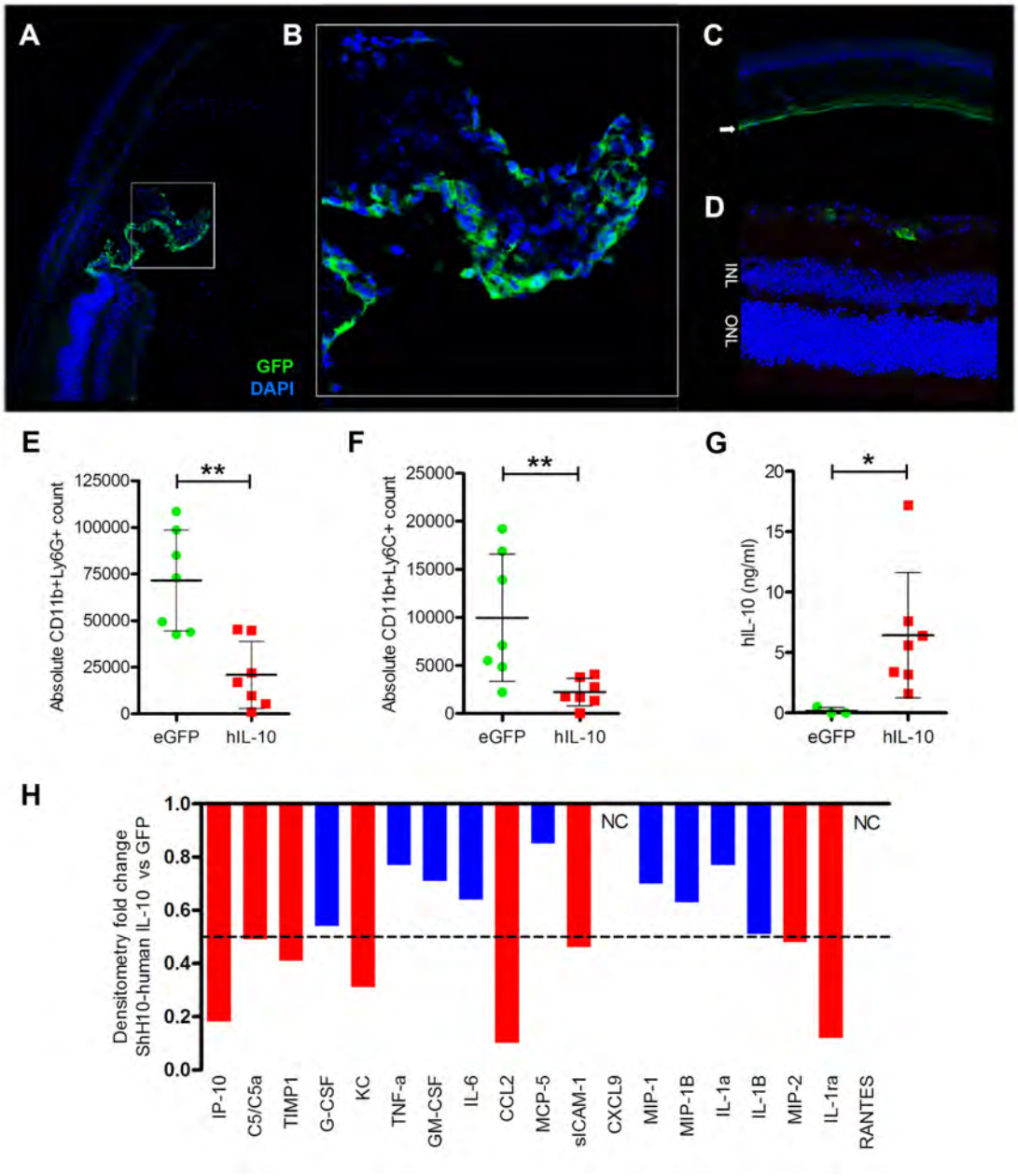

Figure 48. ShH10-derived human IL-10 suppresses EIU at the 6-hour timepoint, with corresponding reduction in key neutrophil chemokines. Intravitreal injection of $1x10^{10}$gc titre-matched ShH10-CMV-hIL-10 or ShH10-CMV-eGFP was performed. One week later EIU was induced and eyes examined 6-hours later. **A)** Representative histology from ShH10-CMV-eGFP injected eyes at 1 week, demonstrating transduced **B)** ciliary epithelium, **C)** corneal endothelium (arrow) and **D)** occasional ganglion cells and astrocytes. Flow cytometry confirms reduced whole eye counts of both **E)** CD11b+Ly6G+ and **F)** CD11b+Ly6C+ cells in the human IL-10 treatment group. **G)** ELISA confirms significantly elevated levels of human IL-10 compared to the GFP control. Mann-Whitney U test, *=P<0.05, **=P<0.01. Means + SD shown. **H)** R&D proteome profiler of pooled whole eye supernatants from five animals, show decreased levels of several detectable chemokines predominantly involved in neutrophil recruitment with ShH10-human IL-10 treatment. A 50% reduction was arbitrarily chosen as significant. NC = No change.

The experiment was independently repeated with additional controls. PBS was used as there may be a worsening with GFP control virus, that might make the intervention look effective. Mouse IL-10 was used to discern if human IL-10 was truly more effective. Unexpectedly, no reduction in the number of CD11b+Ly6C+ or Ly6G+ cells was observed relative to PBS or GFP control **(Figure 49A)**. A similar, if not higher level of human IL-10 was detected by ELISA **(Figure 49B)**, but no correlative effect upon cell count seen **(Figure 49C)**.

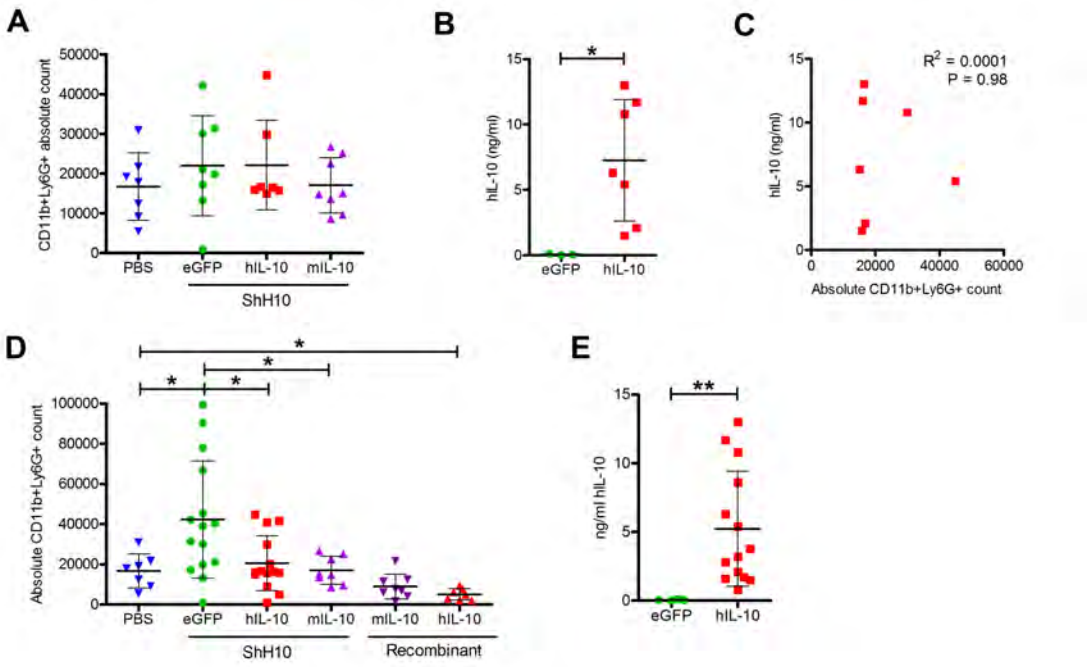

Figure 49. Repeat experiment of ShH10-human IL-10 with additional controls fails to reproduce the suppression of EIU at the 6hr timepoint. 2µl of PBS or $5x10^{12}$gc/ml ShH10 CMV-eGFP, human or mouse IL-10 was delivered into the vitreous cavity. A week later EIU was induced and terminated 6hr post-induction. **A)** Flow cytometric counts of the whole eye are not statistically different between PBS or viral intervention groups. Kruskal-Wallace test P=0.59. Despite **B)** detectably elevated levels of human IL-10, there is also no correlation **C)** between infiltrate and IL-10 levels. Pearson correlation. **D)** Pooled data from both experiments demonstrates that the ShH10-GFP cohort has worse EIU than PBS, such that in isolation ShH10-mIL-10 and hIL-10 would look to be suppressive. Relative to PBS there is no suppression. Only 200ng recombinant human IL-10 suppresses beyond PBS control. **E)** ELISA on retinal supernatants confirms the presence of human IL-10 in treated samples. Mann-Whitney U test, *=P<0.05, **=P<0.01. Means + SD shown.

Combining both data sets, with representative data from recombinant mouse and human IL-10, the initial suppressive effect looks due to the exacerbation

that ShH10-CMV-eGFP appears to have caused **(Figure 49D-E)**. Relative to PBS only recombinant human IL-10 injected eyes reduce disease, whereas both ShH10-derived murine and human IL-10 show reduced disease compared to GFP only.

6.7 Levels of ShH10-derived human IL-10, comparable to those of suppressive recombinant protein fail to attenuate EIU

The absence of effect similar to recombinant protein could still be due to dose if it is the early timepoint where high levels of IL-10 are required. To examine this, two approaches using ShH10-CMV-human IL-10 were taken and compared to a control of PBS. Intravitreal ShH10 was used but left for three weeks to improve the number of Muller cells transduced and improve levels of IL-10. Double subretinal injection was confirmed as leading to RPE and photoreceptor transduction (see **results chapter 3**). Together these account for the largest proportion of ocular cells possible to be transduced with viral gene transfer. The resulting levels of human IL-10 should therefore be the highest possible. If despite this no effect is seen, it may be that constitutive tonic signalling from constitutive virally-mediated IL-10 production may result in different effects to that of a single bolus dose and require complex regulation of expression to succeed. It would then be clear that IL-10 should not be prioritised further in the context of current AAV-based therapy.

No adverse effects at high doses of recombinant protein were seen **(Figure 45C)**. As proof of principle, the highest possible dose of ShH10-CMV-human IL-10 was double injected into the subretinal space and allowed three weeks to reach maximum expression levels. EIU was induced and assessed at the 6hr timepoint **(Figure 50A)**. Compared to PBS, there was no suppression of EIU for both cell types **(Figure 50B-C)**. Levels of human IL-10 achieved by ELISA on ocular supernatants were the highest detected so far, with a mean of 200ng/ml **(Figure 50D)**. No correlation between levels and cell count could be seen however **(Figure 50E)**. This is higher than the recombinant protein

dose known to suppress disease at 6hr, which has a mean of 40ng/ml **(Figure 50F)** with both samples tested in the same volume.

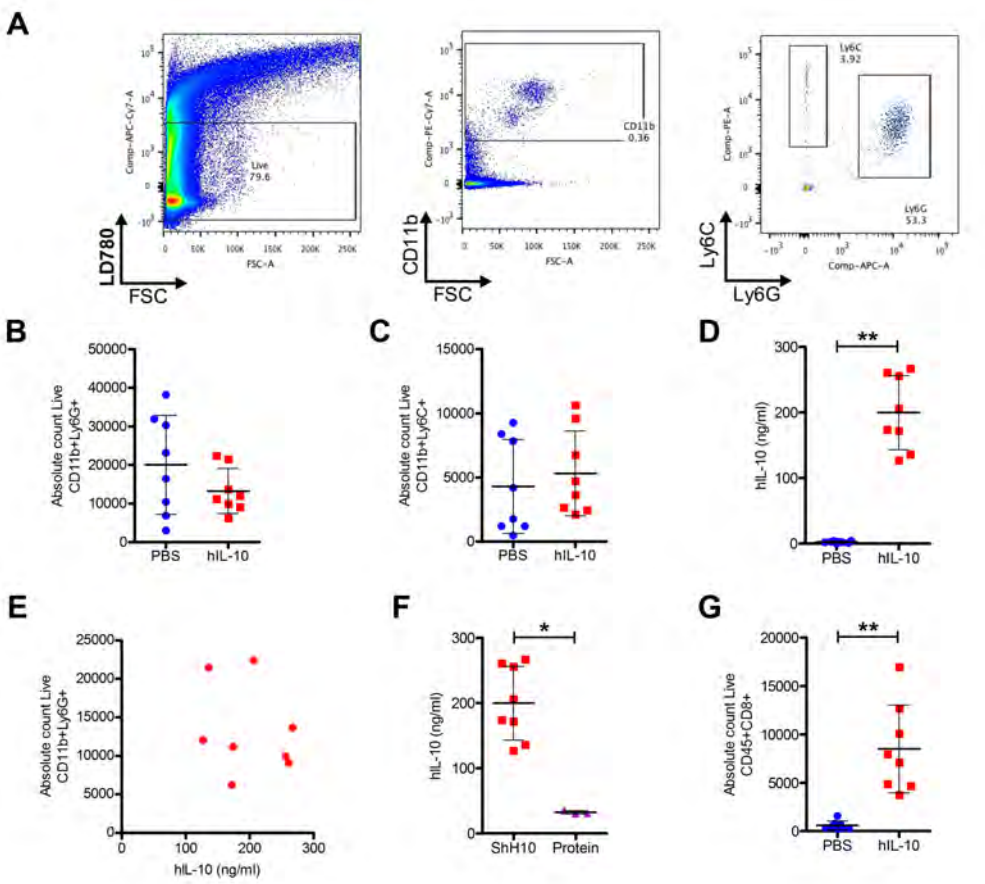

Figure 50. Levels of human IL-10 comparable to suppressive recombinant protein doses can be obtained using subretinal ShH10, but no therapeutic effect is seen upon EIU. Furthermore, a local infiltration of CD8+ cytotoxic T-cells is detected. 3 weeks following paired eye double subretinal injections of PBS or $1x10^{10}$gc ShH10-CMV-human IL-10, EIU was induced and analysed at 6hrs. **A)** Representative flow plots of sequential gating strategy, on live cells then CD11b+ gated, split into Ly6G+ and Ly6C+ populations. **B)** No significant suppression is seen upon CD11b+Ly6G+ or **C)** CD11b+Ly6C+ whole eye cell counts. **D)** hIL-10 ELISA upon supernatants confirms highly elevated levels in the viral delivery group. Wilcoxon signed rank test, P=0.007. **E)** No correlation is seen between levels of hIL-10 and CD11b+Ly6G+ cell counts. 200ng recombinant hIL-10 protein at 6 hours is known to significantly suppress EIU vs. PBS. **F)** Data from a previous experiment are plotted next to the current ELISA results. Whilst some variation exists between ELISA plates, it is clear that viral derived levels are at least as high, if not greater. Mann-Whitney U test, P=0.012. **G)** Of note, a significant elevation in CD45+CD8+ T-cells was seen in the ShH10-hIL-10 group. This is likely to represent an anti-viral or IL-10 specific response. No correlation existed between CD45+CD8+ counts and hIL-10 levels. Wilcoxon signed rank test, P=0.008. Means + SD shown.

A significant infiltration of CD45+CD8+ T-cells was seen in ShH10 injected eyes **(Figure 50G)**. This could be a confounding factor as it may represent a cytotoxic T-cell response to either ShH10 transduced cells or as a function of the effects of hIL-10 signalling.

The experiment was repeated with intravitreal injection of ShH10 but left unmanipulated for three weeks, to improve expression from Muller cells and increase overall levels without introducing additional inflammation from retinal detachment. Again, no suppression of EIU was seen **(Figure 51A-B)**, despite levels of hIL-10 around 40ng/ml in ocular supernatants - compared to the mean of 5ng/ml if left one week **(Figure 51C)**. This is the likely maximum achievable level using ShH10 and the intravitreal route, however is approximately the same level achieved as that of recombinant protein at 6hr **(Figure 51D)**. The implication is that either the tonic nature of continuous production from ShH10 or the very presence of the virus is sufficient to abrogate the suppressive function of human IL-10. In this experiment, no significant CD8+ T-cell infiltration was seen as a confounding factor **(Figure 51D)**.

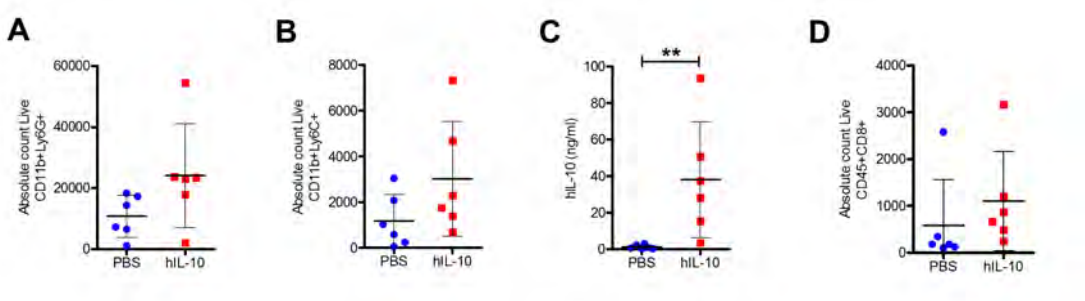

Figure 51. Extending the time to three weeks following intravitreal injection of ShH10-human IL-10 achieves higher transgene levels, but still does not suppress EIU. 2µl PBS or $1x10^{10}$gc ShH10-CMV-human IL-10 was injected into the vitreous cavity. Three weeks later EIU was induced and whole eyes analysed by flow cytometry and ELISA at 6hr. **A)** No suppression was seen in live CD11b+Ly6G+ or **B)** CD11b+Ly6C+ cell counts. **C)** ELISA for human IL-10 on ocular supernatants demonstrates a significant elevation in levels, with a mean of 40ng/ml, compared to 5ng/ml when left one week. Mann-Whitney U test, P=0.005. **D)** No elevation in CD45+CD8+ T-cell counts was seen, implying no significant local cytotoxic T-cell response was evident. Means + SD shown.

In this final experiment, levels of hIL-10 in the eye were matched to a known concentration that suppresses EIU. That no attenuation of disease was seen implies the final dose at 6 hours is not a crucial factor. It is possible that the kinetics of IL-10 signalling is important, or the responses to virus itself may affect the unknown mechanism for suppression of recruitment of CD11b+Ly6G+ cells.

6.8 IL-10 is not an optimal target for the suppression of intraocular inflammation by gene transfer

Due to the of lack of consistent results using IL-10 and the potential differences between mouse and human IL-10, the original experiment that proposed local EAU immunomodulation by AAV transfer of *mIL-10* was repeated.[110] It was possible that as AAV2-mediated gene transfer achieves lower levels of expression, an idiosyncratic property of low-dose mIL-10 might be identified. Alternatively, relatively lower levels of expression using AAV2 might avoid cellular responses that may have confounded successful attenuation of EAU.

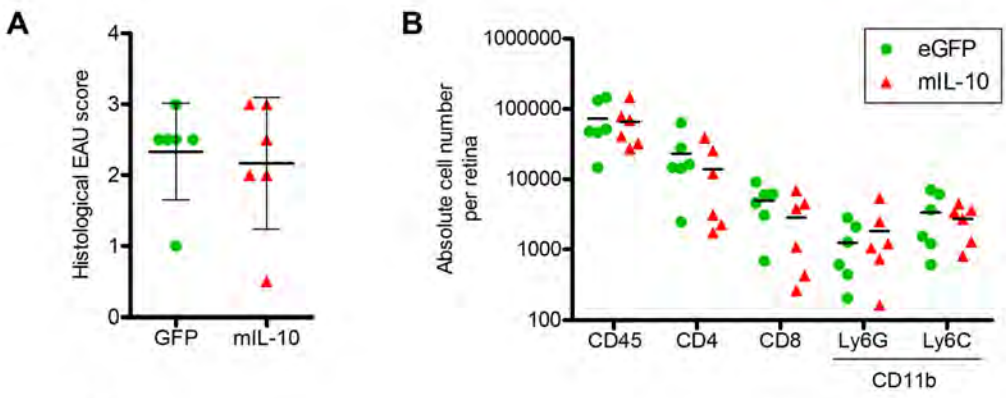

C

(pg/ml)	mIL-10	IL-1β	TNF	IL-17A	IL-12p70
AAV2-IL-10	322.6	18.4	88.6	7.8	12.2
AAV2-GFP	78.0	14.9	ND.	ND.	8.5

Figure 52. Repeat of AAV2 mediated delivery of *mIL-10* with the addition of flow cytometric analysis fails to reproduce the reported suppression. In an exact repeat of published work, double 2µl subretinal injection of $1x10^{10}$gc/ml titre-matched AAV2-CMV-eGFP and AAV2-CMV-mIL-10-IRES-eGFP was performed in *C57BL/6J* mice. After three weeks EAU

was induced and mice culled at day 23. **A)** H&E histology EAU scores, as used in prior assessment, show no statistically significant differences between groups. Scoring was performed masked to treatment group. n=6 mice. Mean + SD shown. **B)** Flow cytometry assessment of dissociated retinae from six eyes of each group confirms the lack of effects upon lymphocyte or myeloid cell infiltration. Means shown. n=6 mice. **C)** Retinal supernatants were pooled from six eyes of each group and run on a multiplex bead array for several mouse cytokines. Whilst only single readings, elevated mIL-10 was detected (red) confirming successful transgene expression. Other pro-inflammatory cytokines are higher in the IL-10 group. ND = Not detected.

Repeating the experiment comparing AAV2-GFP and AAV2-IL-10, no difference in histological EAU scores, or flow cytometric analysis of infiltrating cells could be identified **(Figure 52A-B)**. To confirm successful expression, retinal supernatants from eyes used for flow cytometry were pooled and analysed by multiplex bead array **(Figure 52C)**. Elevated levels of mIL-10 were detected at peak disease relative to AAV2-GFP in the intervention group. Additional pro-inflammatory cytokine measurement identified higher levels in the IL-10 group, which only supports the lack of suppression.

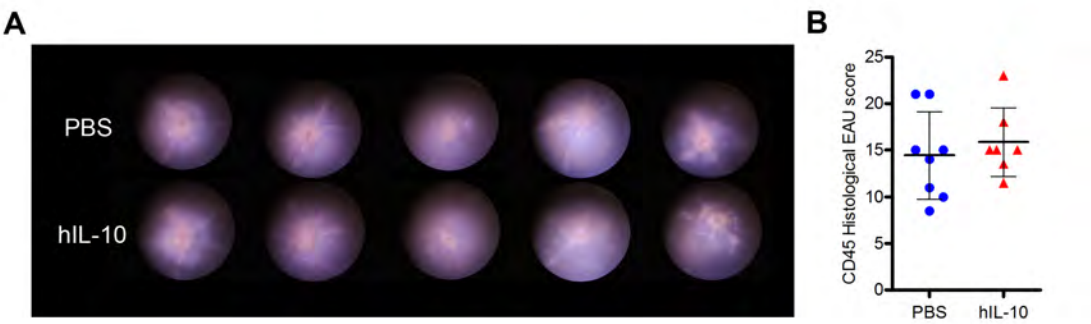

Figure 53. Administration of intravitreal recombinant human IL-10 at peak EAU fails to suppress EAU. PBS or 200ng in 2µl was injected into the vitreous cavity at days 17 and 21-post induction of EAU. **A)** TEFI of paired eyes at peak disease on day 26 fails to demonstrate significant reduction in disease. **B)** Masked CD45-stained histology EAU scores confirm this finding. Paired T-test, P=0.19. n=8. Mean + SD shown.

As a result of this experiment, the assertion that local treatment with IL-10 in the effector phase of EAU is effective was examined. The new findings of efficacy in EIU led to the use of human rather than mouse IL-10. To gauge its effect upon EAU in the absence of confounding factors from AAV itself, 200ng recombinant human IL-10 in a 2µl intravitreal injection was

administered to mice at day 17 and 21 post-induction. At peak disease on day 26 TEFI was performed **(Figure 53A)**. No reduction in EAU disease appearance or histological disease score was evident **(Figure 53B)**. This result combined with the preceding experiments implies that IL-10 does not readily suppress EAU, even before the issue of viral-mediated transfer arises.

6.9 Chapter summary

In conclusion, the lack of robust effects upon EAU and EIU suggest that IL-10 is unlikely to offer an option to pursue for therapeutic purposes. Whilst several publications have reported suppression using murine IL-10, we were unable to reproduce the results using lentivirus, AAV2 or modern AAV serotypes including AAV9, AAV8 and ShH10. Recombinant human IL-10 was shown to be effective in attenuating EIU but required a bolus dose of 200ng. The same effective ocular concentrations could be matched and even exceeded using ShH10, but through this route of delivery no suppression of EIU was attained. The disparity may be a function of the dynamics of IL-10 signalling or more likely due to the nature of viral gene delivery.

7 Results 5: Targeting TNF to suppress ocular inflammation by AAV-mediated gene transfer of soluble receptors

TNF is central to the disease process in EAU, through the recruitment and licencing of inflammatory macrophages within the retina to produce nitric oxide and mediate tissue damage.[127,187] Furthermore, its role in human disease is underscored by the potent effect of TNF inhibitors used widely in clinical practice for uveitis.[10,11]

There are two receptors for TNF and soluble forms occur naturally. Soluble TNF-receptor 1 (known also as p55) preferentially binds soluble TNF whilst soluble TNF-receptor 2 (known as p75) preferentially binds transmembrane TNF.[188] Systemic administration of recombinant human p55 fusion protein has been used to successfully attenuate murine EAU.[133] Other groups have also reported successful attenuation of EAU in the Lewis rat following the expression of soluble TNF receptors from non-viral gene transfer to the ciliary muscle.[60]

Monomeric murine soluble TNF receptor 1 and 2 (p55 and p75 respectively) sequences were already available within the group and had been sub-cloned into the pD10 CMV-promoter plasmid followed by an IRES-eGFP fragment. Whilst TNF is biologically active as a trimer, it was envisaged that monomeric soluble receptor binding could still block its ligand interaction with viable membrane bound receptors. As it had been reported that monomeric soluble TNF receptors were able to block the cytotoxic activity of TNF *in vitro*,[189] it was felt that this would be a reasonable target to over-express in the eye and test the principle of gene transfer in uveitis using recently developed pseudotyped AAV vectors.

In EAU the major source of tissue damage arises from the reactive oxygen species produced by macrophages. Different signals are required which converge upon the induction of nitric oxide synthetase (iNOS). Typically in EAU it is IFNγ that triggers macrophages to produce TNF, which then acts in

an autocrine manner leading to iNOS production. Other signals including TLR4 activation by lipopolysaccharide also lead to activation. To confirm the presence of nitric oxide production from macrophages in the EAU model in our facility, slides were stained with an anti-nitrotyrosine antibody **(Figure 54)**. The antibody detects 3-nitrotyrosine residues that arise from the action of peroxinitrite – a reactive oxygen species generated by nitric oxide and superoxide anions from macrophages.[190] Nitrotyrosine was detected throughout the diseased retina and only in areas where CD11b+ cells were co-located.

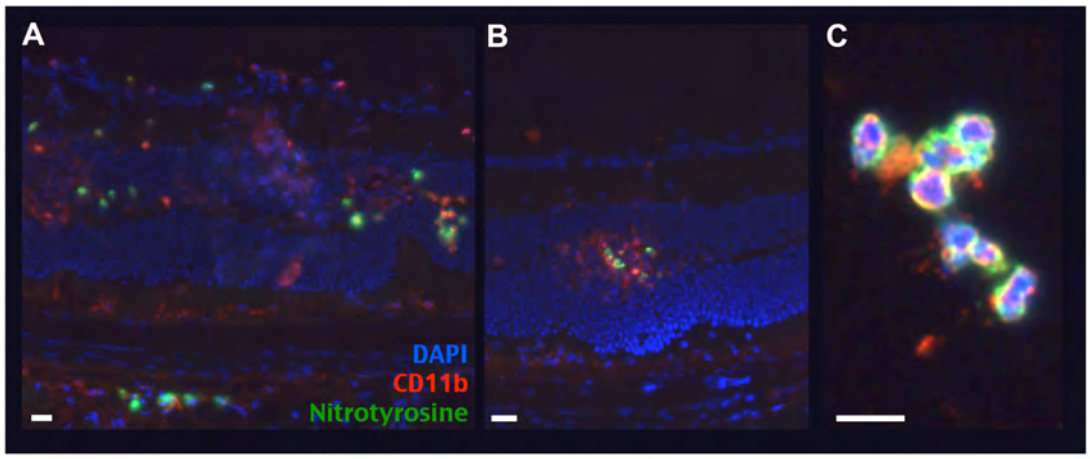

Figure 54. TNF-licenced nitric oxide synthetase induction in myeloid cells during EAU leads to detectable nitrotyrosine residues and structural damage. Cryosections from eyes at peak C57BL/6 EAU were stained for Nitrotyrosine (green), CD11b (red) and DAPI (blue). **A)** Widespread retinal destruction is accompanied by nitrotyrosine staining. Regions of choroidal signal are also present. **B)** Staining is limited to regions of CD11b+ cell infiltration, where peroxinitrite is produced and damaged adjacent retinal cells. **C)** CD11b+ vitreous cells also produce nitrotyrosine staining on surrounding debris. Scale bars = 25μm.

7.1 Gene transfer of monomeric soluble TNF receptors by AAV8 fails to attenuate EAU

Following refinement of AAV8 production, $1x10^{10}$ genome copies (gc) of CMV promoter-soluble p55-IRES-eGFP expressing vector was injected prophylactically into the subretinal space to test its effect upon EAU. At peak disease, TEFI shows multiple discrete lesions and visible GFP signal in the control group (**Figure 55A**). These lesions appeared to correlate with retinal

folds containing CD11b+ cells and have been seen before in EAU without gene transfer, though not frequently. Histological scoring of an independently repeated experiment, failed to demonstrate a difference in EAU disease score **(Figure 55B)**.

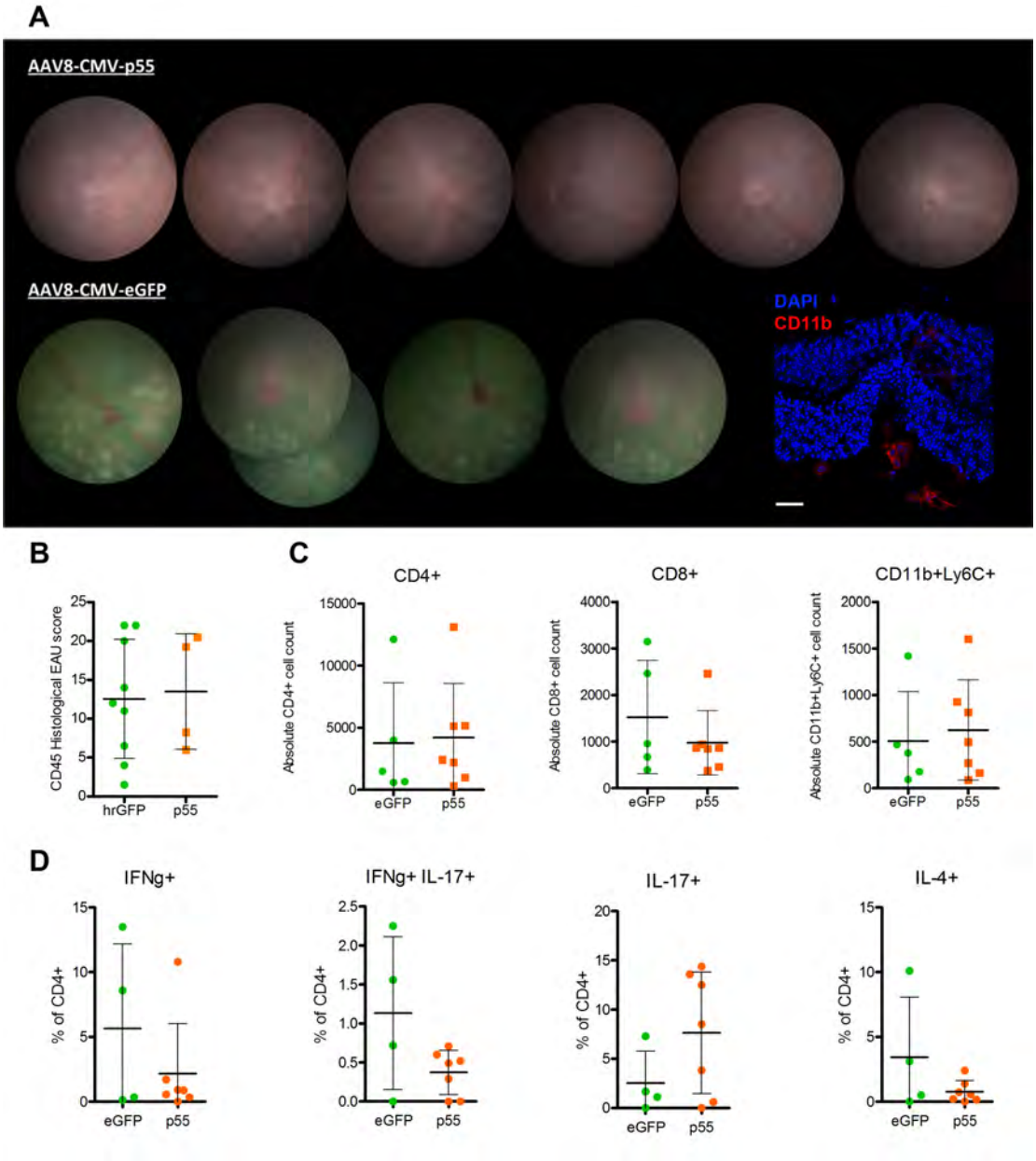

Figure 55. AAV8 expression of soluble p55 monomeric receptor does not affect infiltration or CD4 polarisation in EAU compared to GFP control. A cohort of eyes received 2µl subretinal injections of $1x10^{10}$gc AAV8-CMV-GFP or AAV8-CMV-p55 a week prior to EAU induction. **A)** Representative TEFI images at day 26 show GFP in the visible spectrum and multiple retinal lesions, shown to be CD11b+ cell-containing outer nuclear layer folds by histology (inset). **B)** An independent cohort scored by histology fails to demonstrate suppression. **C)** Absolute cell counts as analysed by flow cytometry in another cohort, does

not differ between groups. **D)** Intracellular cytokine staining of CD4+ cells. The trends did not reach statistical significance. Mann-Whitney U test. Mean and SD shown.

When absolute cell counts for each combined retina, vitreous and anterior chamber were assessed by flow cytometry, there was no significant difference in lymphocyte or inflammatory monocyte number between the groups (**Figure 55C**). Intracellular cytokine staining showed only a slight trend towards increased IL-17A+ helper T-cell polarization (**Figure 55D**), but the absolute number of cells was low, so this finding should be interpreted cautiously. Any true increase in T_H17 polarisation could be explained if there is paradoxical stabilization or enhancement of TNF signaling as a result of p55 overexpression.[130] Increased TNF activity might be expected to enhance T_H17 cell numbers, as evidence from anti-TNF therapy in human autoimmune disease demonstrates a reduction in T_H17 cell counts.[191,192]

The possibility of differential effects between the subtypes of soluble TNF receptor was raised and so the AAV8-CMV-p75-IRES-eGFP was tested. It would be expected to have a greater affinity for binding transmembrane TNF, but might also trigger reverse-signaling through TNF. The effect this might have locally in the eye has not been studied. Publications looking at effects on human monocytes are unclear and demonstrate either stimulatory or inhibitory effects dependent on context.[193,194] In T-cell interactions with monocytes, tmTNF appears to mediate activation. In endothelial cell co-cultures with monocytes, reverse-signaling appears to prevent monocyte activation and secondary cell death.

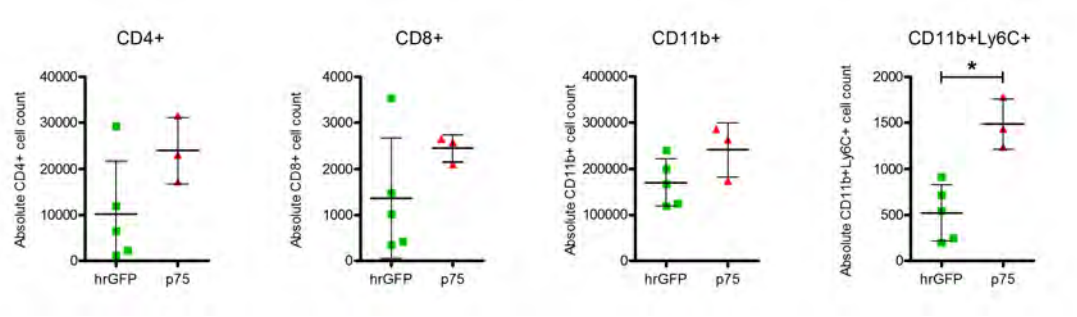

Figure 56. Expression of p75 fails to suppress EAU and increases the number of CD11b+Ly6C+ cells in the eye. One week following subretinal injection of 1x10^{9}gc titre-matched AAV8 CMV-p75-IRES-eGFP or CMV-hrGFP, EAU was induced. At peak disease (day 26) the eyes were analysed by flow cytometry. A trend towards greater numbers of cells was evident in the p75 group, which reached statistical significance for CD11b+Ly6C+ cells. Mann-Whitney U test, P = 0.03.

Following subretinal injection of titre-matched p75-expressing vector and GFP control, EAU was induced and eyes again analysed by flow cytometry. A generalized trend towards greater numbers of infiltrate was present and this was statistically significant for CD11b+Ly6C+ monocytes **(Figure 56)**. Due to the potential worsening of disease, the experiment was not repeated. One hypothesis was that reverse signaling on the RPE could have led to increased chemokine or indeed TNF production. sTNFR could bind to tmTNF expressed by RPE cells and deliver a pro-inflammatory reverse-signal, worsening the outcome of EAU. Obtaining an accurate measure of active TNF in the context of soluble p55 and p75 may have been helpful, but is technically challenging.[195] As neither monomeric soluble TNF receptor suppressed EAU, before concluding that these were ineffective targets, other confounding factors were considered.

7.2 Neither immunological differences between eGFP and hrGFP, nor the presence of the IRES construct explains the failure to suppress EAU

As suppression had not been achieved using p55 or p75, or using IL-10 (see **results chapter 4**) alternative factors were sought prior to further EAU experiments. At this stage a report emerged in the field highlighting specific issues with eGFP expressing AAV in the macaque eye, where progressive

inflammation occurred.[196] Supported by studies from other fields, eGFP has been shown to possess a highly antigenic eight amino acid H2-K^d restricted region at the C-terminus.[197,198] It was thought to be potentially responsible for many of the observed findings.

In the constructs tested thus far, all therapeutic transgenes were tagged with an IRES-eGFP, whilst due to availability, the control vector always used hrGFP. To exclude the confounding factor of an adaptive immune response specific to eGFP abrogating any suppressive effect of the therapeutic vector a separate experiment was commenced. Two weeks following subretinal injection with 1x10^{10}gc AAV8-CMV-eGFP or AAV8-CMV-hrGFP, EAU was induced and scored at peak disease by CD45 immunolabelled histology **(Figure 57A)**. No difference was detected and so this was not felt to be a significant factor.

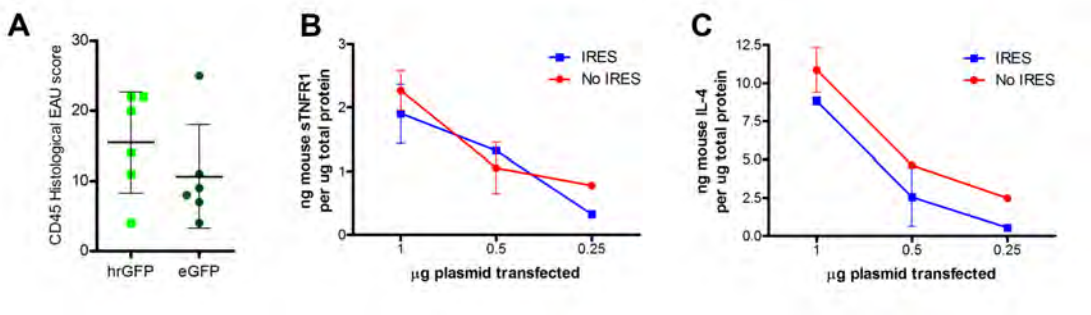

Figure 57. eGFP compared with hrGFP expression does not significantly alter the severity of EAU and the presence of an IRES-GFP segment does not markedly reduce the level of the preceding transgene. Mice were injected with 1x10^{9}gc titre-matched AAV8-CMV-eGFP or AAV8-CMV-hrGFP. **A)** Two weeks later EAU was induced and eyes scored by histology in a masked fashion. No statistically significant difference was seen between the two groups. n=6 eyes, Wilcoxon matched pairs test P=0.15. pD10 plasmid encoding either **B)** CMV-sTNFR1 (p55) or **C)** CMV-mouse IL-4 with and without an IRES-eGFP segment were transfected into HEK-293T cells at three different concentrations. 48 hours later supernatants were tested by ELISA for the transgene products at three dilutions and in triplicate. Total protein was corrected for by BCA protein assay. Whilst a trend towards lower levels with an IRES-eGFP present, the effect is not large or statistically significant by Two-way ANOVA. Data are from two independent experiments. n=5 minimum per group.

Another potential factor was the presence of the IRES-eGFP tag. It was repeatedly observed that the amount of eGFP produced was inversely

proportional to the size of the preceding gene (Dr S. Barker, personal communication). As the IRES results in a longer, single mRNA transcript it was unclear if this reduced the overall expression of the preceding transgene. This could lead to reduced levels of therapeutic protein which might result in lack of efficacy.

To test this hypothesis, the IRES-eGFP tag was cloned out from several plasmid constructs for comparison. Each pair was then matched by spectrophotometry and transfected into HEK-293T cells at a range of concentrations. 48 hours later supernatants were tested by ELISA with total protein correction. Secreted protein was chosen as the final endpoint to account for any confounding post-transcriptional or post-translational factors. No marked difference was identified using either matched p55 **(Figure 57B)** or IL-4 constructs **(Figure 57C)**. Despite these findings, where eminently possible the IRES-eGFP tag was removed to avoid any uncertainty.

7.3 Avoiding retinal detachment by using ShH10 vector still does not permit the suppression of EAU by monomeric p55

It is known that detachment of the retina by subretinal injection is highly inflammatory, with elevated TNF, IL-1β and CCL2 detectable in the eye by 48hrs.[179] The subretinal route is favoured for AAV delivery due to the cell transduction characteristics and well-established lack of systemic immune response. However, in terms of local immunomodulation, the widespread microglial activation, gliosis and structural trauma caused by subretinal injection may alter the balance too far to overcome, let alone permit immunosuppression. Other cotemporaneous experiments using subretinal delivery had also failed to yield suppression, and so an alternative route was sought.

One solution pursued was to employ a newly available AAV serotype - ShH10. This was engineered to specifically transduce Muller glia following intravitreal injection.[57] In our hands it was found to transduce ciliary

epithelium and corneal endothelium, with occasional Muller cell transduction around vessels (see **results chapter 3**). CMV-p55 monomer without IRES-eGFP was produced with the ShH10 capsid and titre-matched to an ShH10-CMV-eGFP control vector.

2µl intravitreal injections of ShH10 vectors were performed one week before induction of EAU. At peak disease on day 26, eyes were imaged by TEFI **(Figure 58A)** before the aqueous, vitreous and retina were dissected, dissociated and analysed by flow cytometry **(Figure 58B)**. The pooled supernatants following dissociation of each eye in 200µl PBS were tested by p55 receptor ELISA **(Figure 58C)**.

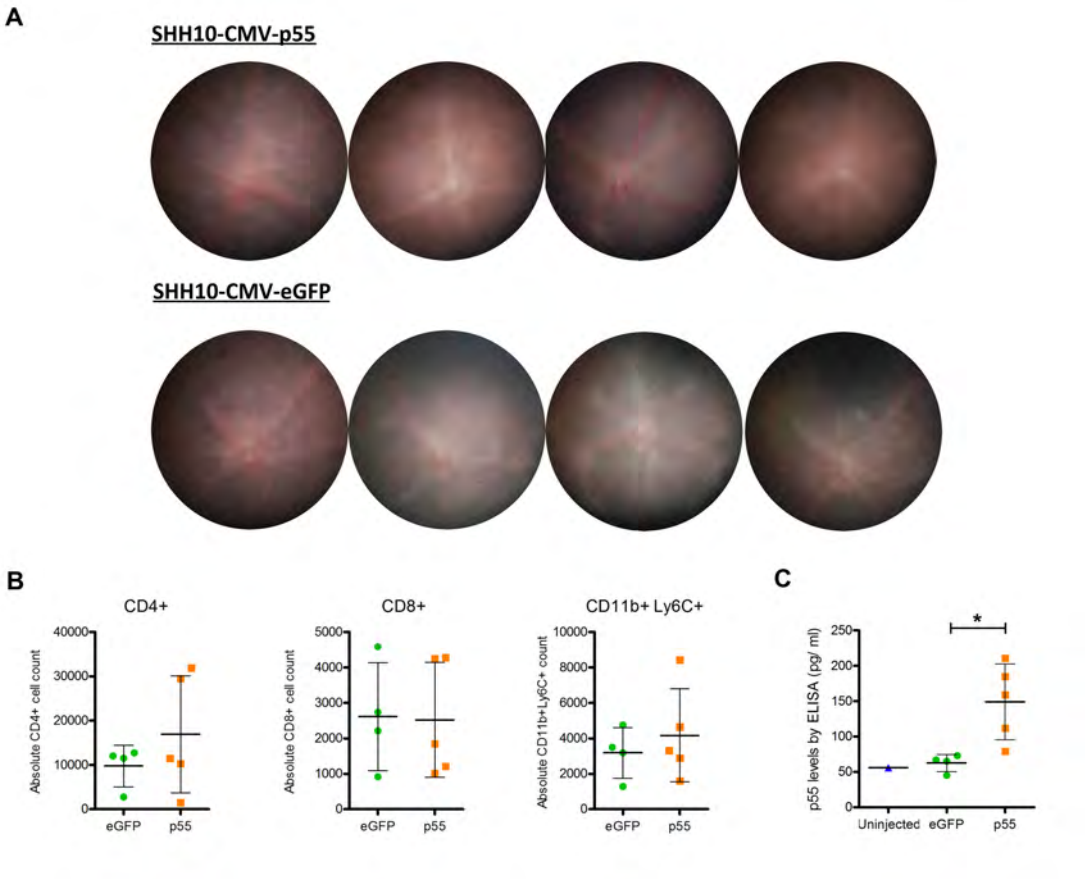

Figure 58. Prophylactic ShH10 mediated expression of monomeric p55 receptor does not affect infiltration in EAU compared to GFP control, despite detectably elevated levels in the tissue. Eyes received 2µl intravitreal injections of $2x10^{10}$gc ShH10-CMV-p55 or ShH10-CMV-eGFP virus a week before EAU induction. **A)** TEFI images at day 26 show minimal differences between the two groups, reflected in **B)** Absolute cell counts by flow cytometry from dissociated retina and AC fluid. This is despite **C)** an approximate 3-fold increase in p55

levels compared to GFP control virus detected in retinal supernatants by ELISA. Mann-Whitney U test. *=P=0.016. Mean +SD shown.

TEFI revealed equivalent appearances and there was no difference in lymphocyte or monocyte cell counts between control and the p55 monomer. ELISA confirmed the production of p55, although levels were elevated by approximately three-fold only compared to GFP. The maximum titre possible had been administered ($1x10^{10}$gc), but only left for 1 week prior to induction of EAU. It would have been possible to increase the levels allowing full Muller cell transduction at 3 weeks. It was decided to first test the approach using a different inflammatory model.

7.4 Endotoxin-induced uveitis is not suppressed by ShH10-mediated soluble p55 and TNF inhibition can cause worsened infiltration

Endotoxin-induced uveitis was selected as a rapid and alternative model to test the approach of AAV mediated TNF inhibition. It is essentially only a TLR4 mediated acute inflammatory insult and so might be more amenable to suppression than the multiple pathway orchestrated disease of EAU. It also is used as a model of anterior uveitis, with minimal retinal involvement and so if the anterior ocular compartment is more amenable to successful gene therapy this might be apparent.

Whilst controversy exists, with some groups reporting TNF inhibition worsens EIU severity,[199] others claim that it results in suppression of disease.[32,176] Effects are context-dependent and although systemic inhibition is likely beneficial, the effect of local therapy remains unclear. It has been shown that non-viral gene transfer of p55-Ig fusion protein can suppress EIU in rats.[107] and so this approach was felt to be reasonable.

ShH10 was chosen as ciliary body and corneal endothelial transduction are attained after one week. These tissues are closer to the anterior chamber and so it was envisaged that a greater concentration of therapeutic protein would be obtained in that region. ShH10-CMV-p55 monomer without IRES

tag was produced and $1x10^{10}$gc injected into the vitreous cavity. A matched ShH10-CMV-eGFP control was used. Seven days later intravitreal injection of 1ng LPS was performed. The eyes were dissected and analysed by flow cytometry at the 18-hour timepoint. No difference in either neutrophil **(Figure 59A)** or monocyte **(Figure 59B)** infiltration could be identified between groups. A two-fold increase in concentration of p55 protein in the ocular supernatants compared to GFP control was obtained **(Figure 59C)** and successful transduction of the ciliary epithelium was confirmed in the GFP cohort by histology **(Figure 59D)**.

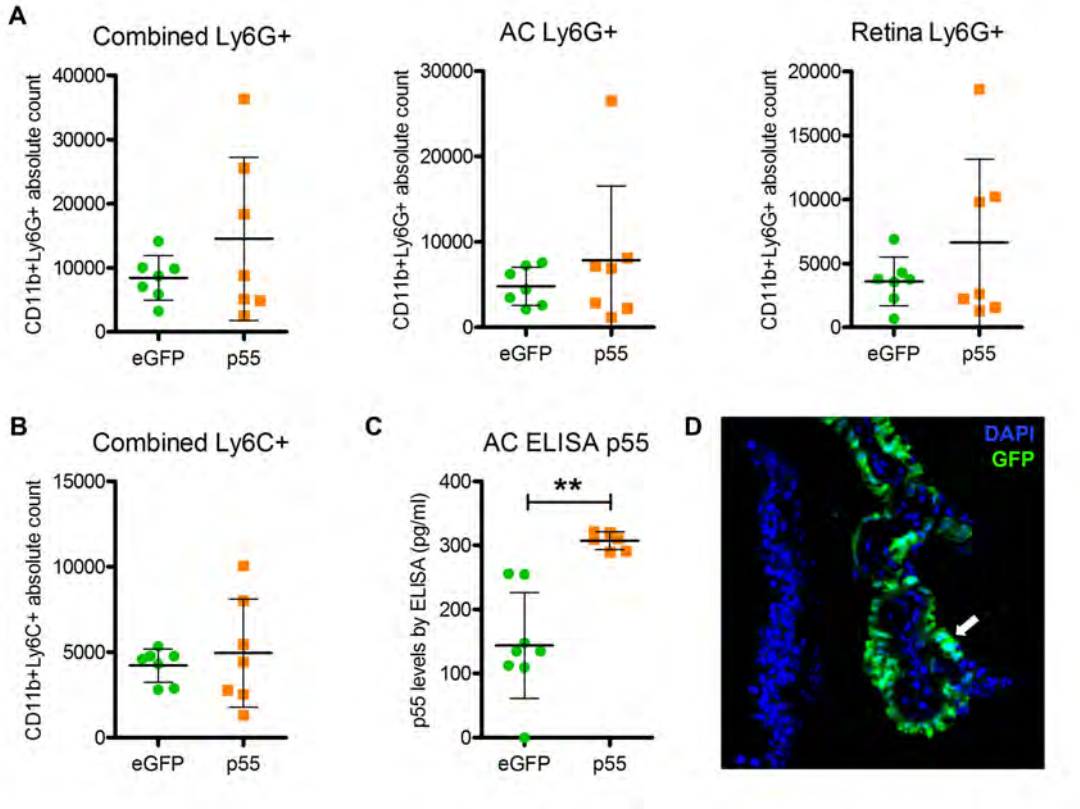

Figure 59. ShH10 expression of monomeric p55 receptor does not affect EIU at double the control level. Eyes received 2µl intravitreal injections of $2x10^{10}$gc ShH10-CMV-p55 or ShH10-CMV-eGFP virus one week before EIU induction and analysis at 16hr. **A)** There was no statistically significant difference in the number of CD11b+Ly6G+ or **B)** CD11b+Ly6C+ cells compared to the GFP control. This is despite **C)** AC levels of p55 were approximately double the GFP control by ELISA. Mann-Whitney U test, P=0.0024. **D)** Successful transduction of the ciliary epithelium (white arrow) was confirmed by confocal microscopy on sectioned ShH10-CMV-eGFP injected eyes. Mean + SD shown.

It was concluded that either the p55 levels attained were not sufficient, or EIU was not amenable to therapy by the modulation of TNF with soluble p55 in this context. Recombinant soluble p55 was not easily available, and so to determine if any degree of inhibition was possible, a limited amount of recombinant human p55-Ig fusion protein was obtained (A kind gift of D Copland, University of Bristol). This is quite different from the monomer, consisting of two human p55 receptors linked by an Fc region, but might still provide evidence to support the use of TNF inhibition in EIU. p55-Ig was injected concurrently with the induction of EIU in a limited set of mice and terminated at 18-hours. Upon dissection, it was discovered that all eyes (4/4) had diffuse, large haemorrhages throughout the retina **(Figure 60A)** an observation not seen in any EIU eyes before.

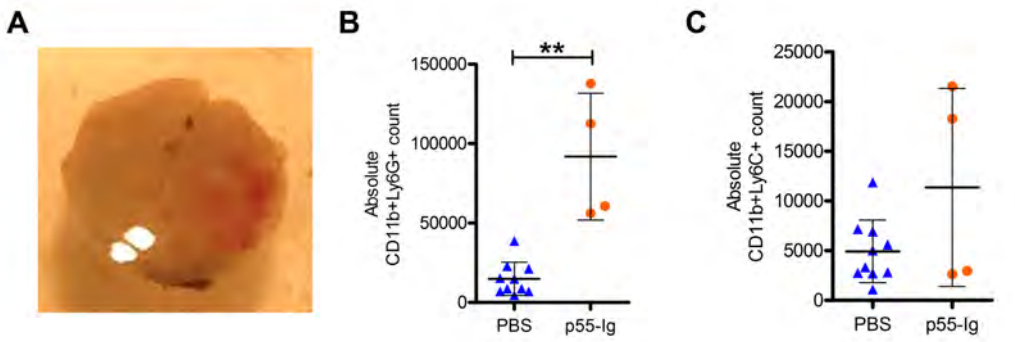

Figure 60. Administration of recombinant human p55-Ig at the induction of EIU leads to retinal haemorrhage and worsened infiltration. Mice were injected in the vitreous cavity with 1ng LPS mixed with either PBS or 4µg recombinant human p55-Ig fusion protein. Eyes were analysed by flow cytometry 18hr later. **A)** In the p55-Ig group, all 4 eyes had diffuse retinal haemorrhages, as shown dissected and viewed from the subretinal space. **B)** A significant increase in the number of infiltrating CD11b+Ly6G+ cells was seen, without change in **C)** the CD11b+Ly6C+ compartment. Mann-Whitney U test, P=0.002. Means + SD shown.

Flow cytometry confirmed worsened EIU with a significantly elevated number of neutrophils compared to contemporaneously injected PBS controls **(Figure 60B)**. There was no difference in the number of CD11b+Ly6C+ cells **(Figure 60C)**. Explaining these findings is challenging. The dose of recombinant protein delivered was high to ensure a response, but may have been non-specifically toxic. Alternatively, potent TNF inhibition may indeed be detrimental and lead to increased disease. The findings point toward the

presence of biological activity from the p55-Ig fusion, albeit detrimental in this experiment. It was decided to reassess the monomeric forms *in vitro* before continuing further and check their activity with a functional readout.

7.5 In vitro assessment confirms the superior efficacy of soluble p75-Ig fusion dimer over the monomeric form

All experiments had demonstrated either no improvement in disease scores or a worsened outcome with p75 overexpression. Returning to the literature, several publications using plasmids encoding multimeric variants of p55 had been shown to suppress EAU in the rat.[60,107] Whilst the most widely used target is one conjugated to a murine IgG Fc fragment, isolated soluble p55 receptor was shown to suppress EAU.[107] One difference is that the human receptor was used in this study, which has only around 64% homology to the murine protein (UCSD Signalling gateway). There may also be an issue of dosage, as measurement in intraocular fluid showed that 5ng/ml was able to suppress disease, whereas we obtained around 0.15 ng/ml with murine p55.

The presence or absence of the Fc-fusion may provide another explanation for the discrepancy between study results. There are reports that human sTNFR have a dose-dependent effect upon TNF activity, acting to neutralise, buffer and stabilise active trimers.[130] In that study, p75 had a greater effect upon preventing recombinant TNF induced cytotoxicity than an equivalent dose of p55. In a model of lethal sepsis in mice triggered by systemic endotoxin, the human p75 monomer was compared to the Fc-linked dimer.[200] The dimer had a 50-fold stronger affinity and a 1000 times greater efficiency at preventing TNF induced cell death *in vitro*. Unlike the monomer, it could prevent endotoxaemic death when administered at doses as low as 10µg. When the monomer was administered, even up to 260µg, it failed to provide any benefit over control IgG. Furthermore, unlike the dimer, it actually increased circulating serum TNF levels ten-fold, possibly due to the stabilising effect upon the active TNF trimers as had been described in vitro.[130]

To interrogate these issues further, a soluble TNF fusion protein was sought. The only freely available sequence for cloning into the pD10 plasmid for AAV production, was that of a murine p75-Ig dimer.[161] This was prepared and compared to the murine p75 monomer using an *in vitro* WEHI-164 cytotoxicity assay. This mouse fibrosarcoma cell line rapidly undergoes cytotoxic cell death in response to active TNF. Recombinant protein was obtained by transfecting equal amounts of the plasmids encoding the p75 variants into HEK-293T cells. The conditioned medium from these cells were mixed with recombinant murine TNF and then added to the WEHI-164 cells. Cell death was accurately calculated by flow cytometry with the fluorescent live-dead dye 7AAD **(Figure 61)**.

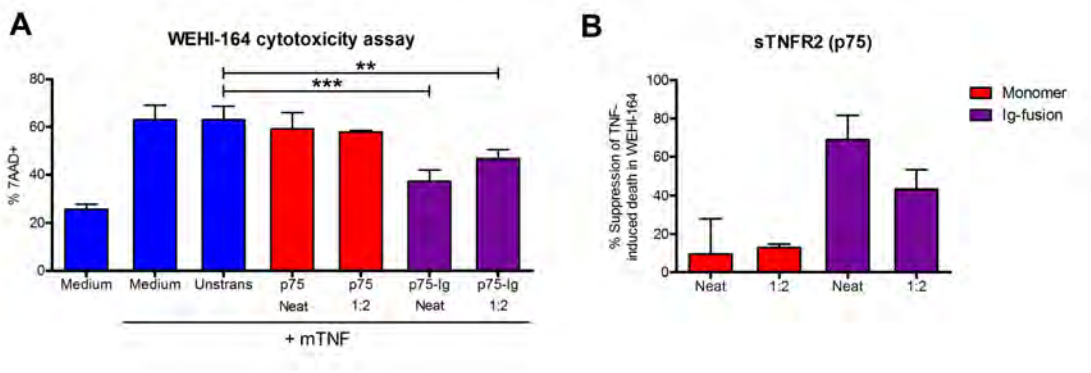

Figure 61. WEHI-164 cytotoxicity assays confirm the neutralising effect of p75-Ig *in vitro* and the negligible action of monomeric p75. 1µg of CMV-p75 or CMV-p75-Ig plasmid was transfected into HEK-293T cells, the supernatant collected after 48hrs and 0.22µm filtered. 2.5ng recombinant murine TNF was combined with this conditioned media or that from un-transfected HEK-293T cells for 30mins at room temperature. This was added to 80% confluent wells of the WEHI-164 cell line. 24 hours later wells were spun down and 7AAD added to stain dead cells. Flow cytometry was performed and 10,000 events collected for each sample. **A)** Medium lacking TNF and with TNF alone define the range of the assay from ~25% to ~60%. Neat medium from un-transfected cells has no effect upon the assay. Neat p75 monomer (red) and 1:2 dilution are no different to the control. Neat p75-Ig (purple) and 1:2 dilution however both significantly suppress cell death from TNF. One-way ANOVA with Tukey's multiple comparison test. **=P<0.01, ***=P<0.001. **B)** The same data expressed as percentage suppression in cell death. Technical triplicates performed. n=4, pooled from two independent experiments. Means + SD shown.

The data describes the superior effect of the p75-Ig dimer on preventing WEHI-164 cell death compared to the p75 monomer, implying more effective

suppression of TNF. It was not possible to easily determine if the p75 monomer enhanced TNF effects, as cytotoxicity was already at the upper limit of the assay. This clear result, which was independently repeatable led to the production of AAV8 and ShH10 encoding CMV-p75-Ig with no IRES tag.

7.6 Prophylactic AAV8 mediated p75-Ig dimer delivery to the eye still fails to detectably suppress EAU

Though the subretinal route was not favoured initially, it was required to reliably achieve higher levels of transgene. This was felt to be important as the therapeutic mechanism involved neutralising TNF and so a greater amount of p75-Ig would be assumed to lead only to improved blockade. Two weeks following prophylactic AAV8 delivery of either p75-Ig or eGFP control, EAU was induced and scored by histology at peak disease **(Figure 62)**. By CD45-labeled histology, no suppression could be seen compared to GFP control virus. TNF was below the level of detection in both groups using ELISA on pooled ocular fluid from six mice. One possibility is that TNF does not contribute to the same degree in the *C57BL/6* model, compared to other models of EAU and so any beneficial effect would not be seen.

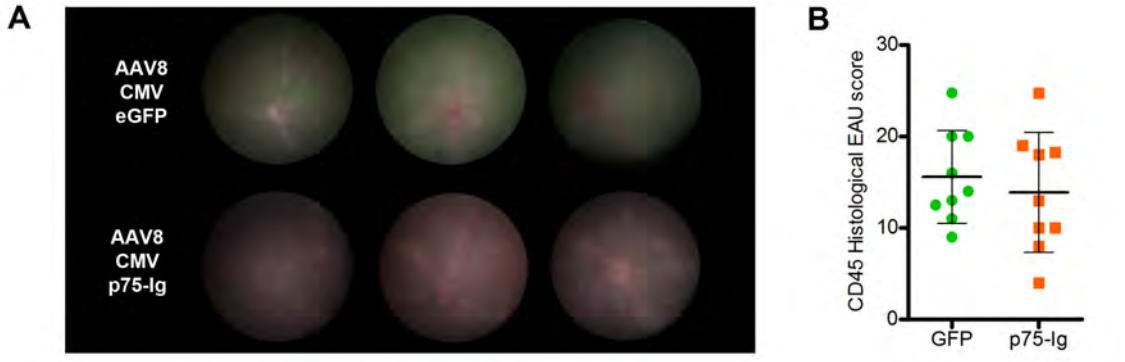

Figure 62. Prophylactic p75-Ig expression from subretinal delivery of AAV8 fails to suppress histological EAU scores. Two weeks after subretinal injection of $1x10^{10}$gc of AAV8-CMV-p75-Ig or AAV8-CMV-eGFP, EAU was induced. **A)** TEFI images at day 19 do not show obvious differences aside from high levels of GFP that spill into the visible spectrum. **B)** At day 26 of EAU the eyes were taken for sectioning, staining and masked scoring. No significant difference was evident between the groups, even by paired analysis. Wilcoxon signed rank test, P=0.55.

7.7 Using the highly TNF driven *B10.RIII* strain model of EAU does not improve suppression by gene delivery of p75-Ig

The *B10.RIII* model of EAU is known to be more severe than that induced in *C57BL/6* mice. In particular, levels of TNF are documented to be higher and animals respond dramatically to systemic TNF inhibition.[129,164] The expectation was that both more severe and TNF-driven disease would provide the best opportunity to observe suppression by gene transfer. Subretinal injection of AAV8-CMV-p75-Ig and PBS control were delivered prophylactically and EAU induced three weeks later. This timepoint was chosen to allow maximal expression of p75-Ig and for any retinal detachment induced inflammation to reduce. Eyes were scored by H&E stained histology **(Figure 63)**.

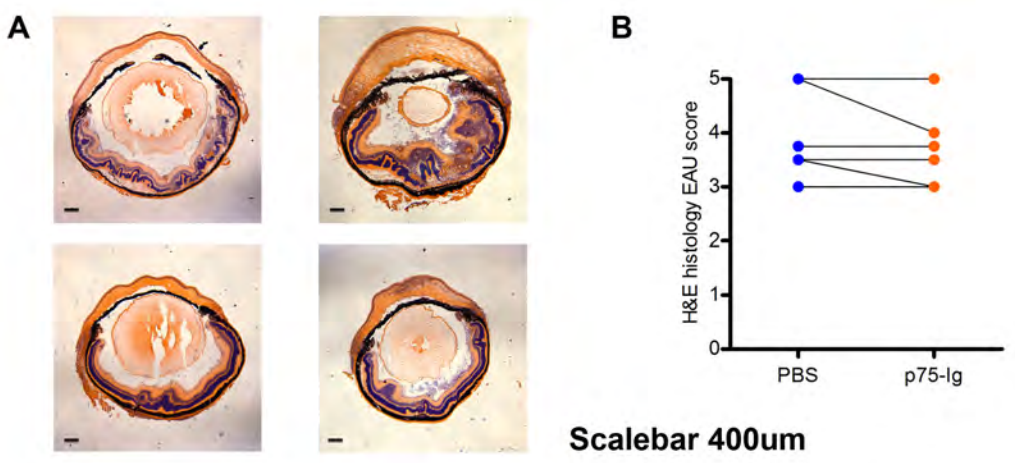

Figure 63. Prophylactic intraocular p75-Ig expression fails to suppress disease in the *B10.RIII* model of EAU. Subretinal injection of 1x10^{10}gc AAV8-CMV-p75-Ig in 2µl or PBS was performed three weeks prior to the induction of EAU. At day 12 eyes were harvested and H&E histological EAU scores determined. **A)** Representative histological images of extensive retinal folding and damage, with PBS on left and AAV8-p75-Ig on right. x2.5 magnification. Scale bars = 400µm. **B)** Paired analysis shows no significant suppression of disease. Wilcoxon signed rank test, P=0.203. n=6 mice. TNF was below the level of detection in both groups using ELISA on pooled ocular fluid from six mice.

Severe disease with extensive retinal folding was seen in most eyes, but no significant suppression was evident in the p75-Ig group compared to PBS controls. It is possible that the disease was too severe, or there is an intrinsic

issue when using the subretinal route. The immune environment might also compensate for the continuous inhibition of TNF resulting from prolonged production of p75-Ig. Alternatively local neutralisation of TNF with p75-Ig may not be an effective therapy.

7.8 Gene delivery of p75-Ig during established EAU demonstrates a trend towards reduced structural damage

Following the lack of effect in either prophylactic experiment, it was decided to trial an interventional approach, delivering p75-Ig only during established disease **(Figure 64)**. This might minimise any adaptation of the local immune environment to persistent suppression of TNF. The approach requires the use of ShH10, as a subretinal injection was not thought to be advisable due to the increased technical difficulty in an inflamed eye and the increased potential to exacerbate inflammation itself.

Whilst some groups have reported changes in cell number in EAU as a result of TNF neutralization, others show the main effect is upon limiting structural damage from myeloid cell activation.[201] It was felt that subtle preservation in structure might not be clearly observed on cryosections. As a result eyes were analysed by paraffin sectioning and H&E staining.

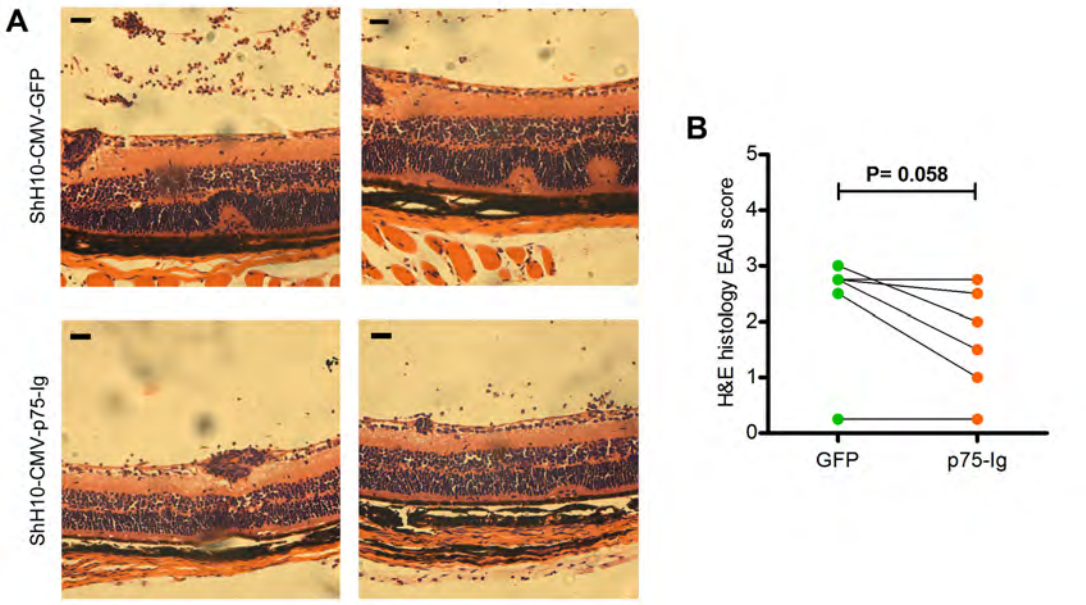

Figure 64. Interventional p75-Ig expression by ShH10 trends towards a mild reduction of structural changes in EAU. *C57BL/6J* mice at day 17 post-induction of EAU were injected with $2x10^{10}$gc ShH10-CMV-eGFP or p75-Ig. Eyes were harvested for paraffin sections at day 26pi. **A)** Representative images of histology from paired eyes, illustrating the presence of vasculitis in both, but reduced retinal folding in the p75-Ig group. Scale bars = 50µm. **B)** The mean scores of two masked assessors are plotted for paired eyes. Whilst they do not reach statistical significance, a strong trend is seen. Wilcoxon signed rank test, P=0.058. n=6 mice.

Whilst no statistically significant difference could be demonstrated, a strong trend was seen and no eyes from the p75-Ig group showed worsened appearances compared to GFP controls. In general retinal folds were less frequent and less pronounced in the p75-Ig group. It is possible that the effect size may be real but small and so this pilot experiment would not have been powered adequately to detect this. This experiment is intended to be independently repeated as part of future work using other readouts including ELISA and flow cytometry.

7.9 Chapter summary

TNF is known to be a critical pro-inflammatory cytokine in both human uveitis and EAU. Nitrotyrosine residues were identified in our EAU model, suggesting the final effector action of macrophage licencing by TNF was present. Monomeric soluble TNF-receptors p55 and p75 were delivered by subretinal AAV8, but were shown to have either no effect, or to worsen infiltration respectively. The potential confounding roles of eGFP vs hrGFP and the addition of an IRES-sequence in constructs were addressed and it was considered unlikely that they contributed to therapeutic failure. Avoiding retinal detachment using prophylactic ShH10 delivery of monomeric p55 also failed to suppress EAU. Testing in the EIU model, no attenuation was seen delivering monomeric p55. Injecting high dose recombinant p55-Ig in EIU though worsened the disease. Returning to *in vitro* investigation, the monomeric p75 TNF receptor was found to be inferior in its capacity to neutralise TNF compared its Ig-fusion dimer. This p75-Ig dimer failed to improve EAU when delivered by prophylactic subretinal AAV8 injection. Using the more severe *B10.RIII* model of EAU did not expose any potential suppressive effect either. ShH10 mediated delivery during established EAU showed a strong trend towards reduced structural damage, but this did not reach statistical significance. Local TNF neutralisation by gene transfer does not appear to be an optimal target to suppress EAU.

8 Results 6: An inflammation-responsive promoter can intrinsically regulate AAV-mediated transgene expression in the eye

Most promoters used in gene therapy for uveitis have been strong and constitutively active, such as the Chicken β-actin or CMV immediate-early promoters. However, some form of control is important. Tonic expression of most anti-inflammatory proteins is a risk for tolerance induction and likely down-regulation of the target pathway, rendering the treatment ultimately ineffective or at worse detrimental. Anti-viral or transgene directed responses are also suspected to be dose-dependent, particularly if AAV is delivered via the subretinal route.[76] Limiting production of the target protein with an inducible, rather than continuously active promoter should therefore only be of additional benefit.

Whilst some groups have used 'tet-on' and 'tet-off' exogenous tetracycline inducible systems, these are not self-regulating and inefficient as they are never fully silenced and often provide only low levels of expression.[93] Additionally they are based on prokaryotic DNA sequences and would be unlikely to be approved by regulators for human therapy. The ideal mechanism would intrinsically self-regulate, driving the expression of therapeutic transgene only in the presence of - and in proportion to - an acute inflammatory state.

Interferon gamma (IFNγ) and tumour necrosis factor alpha (TNF) are key pro-inflammatory cytokines identified in both human uveitis and EAU. They are elevated during active disease and levels fall during resolution.[129] An ideal inflammation-responsive promoter would respond to both cytokines synergistically. Interferon regulatory factor 1 (IRF1) is a protein that stimulates the transcription of many interferon responsive genes. The enhancer of the IRF1 promoter has been characterised and possesses both gamma-activated sequences and NFκB motifs which can activate transcription downstream of both IFN and TNF signalling respectively.[162] As

a parallel strand, an NFκB-motif enhanced minimal SV40 promoter construct was also tested.

The pGL4.Luc2 reporter plasmid was used to assess promoter activity. The full human IRF1 promoter sequence was amplified from genomic DNA by PCR. The characterised 195bp enhancer region was then cloned in front of the minimal SV40 promoter and duplicated several times in an attempt to enhance the magnitude of transcriptional response. As a control, the main enhancer region of the CMV promoter was cloned in front of the minimal SV40 promoter. A pre-synthesised 5-copy NFκB-response element enhancing the same SV40 minimal promoter was obtained in a plasmid encoding the luciferase gene. The plasmid schematics are shown in **Figure 65**.

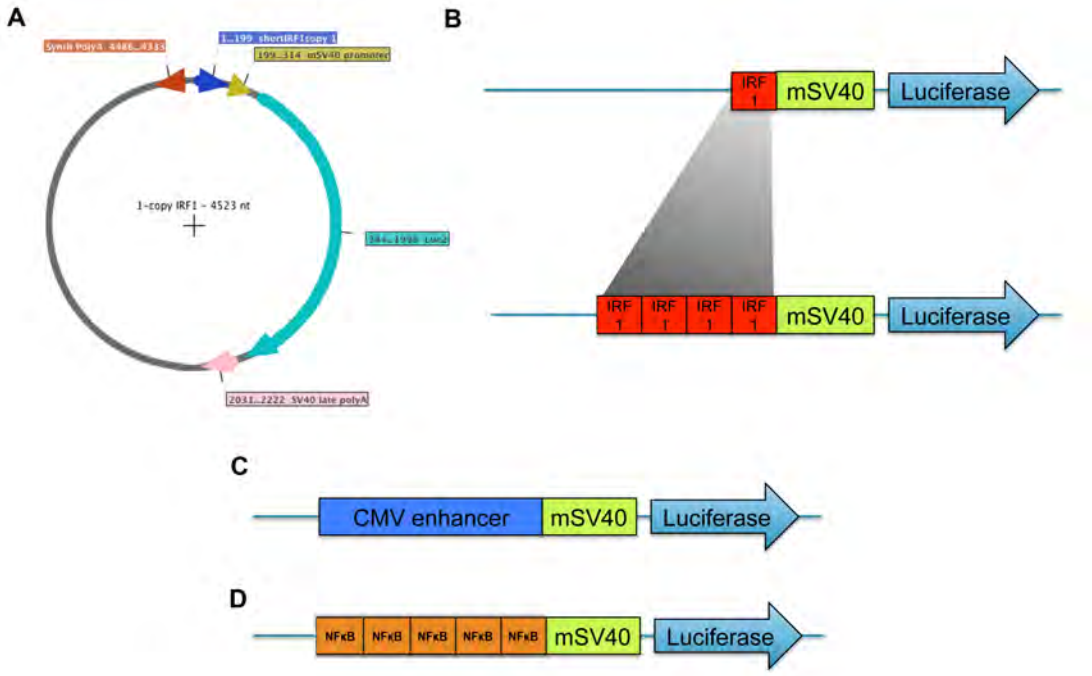

Figure 65. Schematics of Luciferase plasmids to test inflammation-responsive promoters. The pGL4-Luc2 plasmid schematic is shown with a single copy IRF1 enhancer, (blue) minimal SV40 promoter (yellow) and Luciferase (turquoise) gene **(A)**. A range of constructs with multiples of the IRF1 enhancer region (one to four) was generated to determine the number required for optimal transcription **(B)**. The control consisted of the CMV immediate-early response element placed upstream of the same SV40 minimal promoter **(C)**. The NFκB construct was arranged in a similar fashion **(D)**.

Plasmids were initially tested *in vitro* by Lipofectin transfection into HEK-293T cells for 48hrs, prior to different conditions of stimulation with human recombinant IFNγ and TNF. Following this, the cells were lysed and substrate added in order to measure Luciferase activity. A TK-Renilla luciferase plasmid with constitutive activity was co-transfected to control for transfection efficiency.

8.1 Interferon Regulatory Factor 1 promoter

IFNγ-responsive promoters were identified as candidates for an inflammatory-inducible promoter, as IFNγ is a key pro-inflammatory cytokine, known to increase early in EAU, before rapidly reducing as disease ceases. A robust quantification of the concentration of IFNγ within the retina during murine uveitis is lacking. In rat EAU, levels between 50-150 pg/ml have been obtained from ocular homogenates at peak disease,[202] whilst 10 pg/ml has been measured in human aqueous fluid during acute uveitis.[203] Extrapolating from these tissue values to an *in vitro* dose on cell lines is inaccurate and unreliable, so a range of doses required testing.

Identification of a cell type that responds to IFNγ was the initial step, as it is unclear from the literature which cell types these are in the retina aside from RPE. According to RT-PCR data, IRF1 is expressed in human RPE, which is itself known to respond to IFNγ.[204] This is encouraging as it is the predominant cell type transduced by most serotypes of AAV. Staining sections from eyes at peak EAU, revealed the presence of the IFNγ-receptor 1 (IFNγR1) predominantly on astrocytes and Muller glia **(Figure 66A)**. This receptor was chosen as a marker as it is the ligand-binding alpha chain and tends to be constitutively expressed, unlike its heterodimeric counterpart IFNγR2.[205] The co-localisation of IFNγR1 staining with GFAP, a cytoskeletal protein specific to these two cell types and produced during activation, affirmed this association. Sections of eyes without EAU from CFA control animals resulted in staining for IFNγR1 in astrocytes only **(Figure 66B)**. It is likely that in EAU the receptor is up-regulated on Muller glia in response to

other inflammatory stimuli, consistent with work has shown the response of rat Muller glia to exogenous IFNγ.[206]

To reinforce the evidence for co-localisation with GFAP on sections, Muller glia cultures derived from a CRALBP-GFP mouse line (a gift of Dr Claire Hippert) were successfully stained for IFNγR1 **(Figure 66C)**. RT-PCR on these cells also confirmed the presence of transcript **(Figure 66D)**. Splenocytes were extracted from a WT mouse as a positive control. Adult mouse cortex and the 3T3 mouse fibroblast cell line also were positive for IFNγR1.

Testing different repeat number IRF1 constructs by Luciferase assay in HEK-293T cells, revealed that whilst IRF1 could respond to TNF stimulation, (predominantly NFκB signalling) no response to IFNγ was observed **(Figure 66E)**. This was the case over a wide range of doses, using cytokine from several manufacturers (Biolegend and Invitrogen Life Sciences) and no additive effect could be seen when combined with TNF. Compared to unstimulated cells, all IRF1 constructs above a single copy led to approximately three-fold higher inducible responses with TNF.

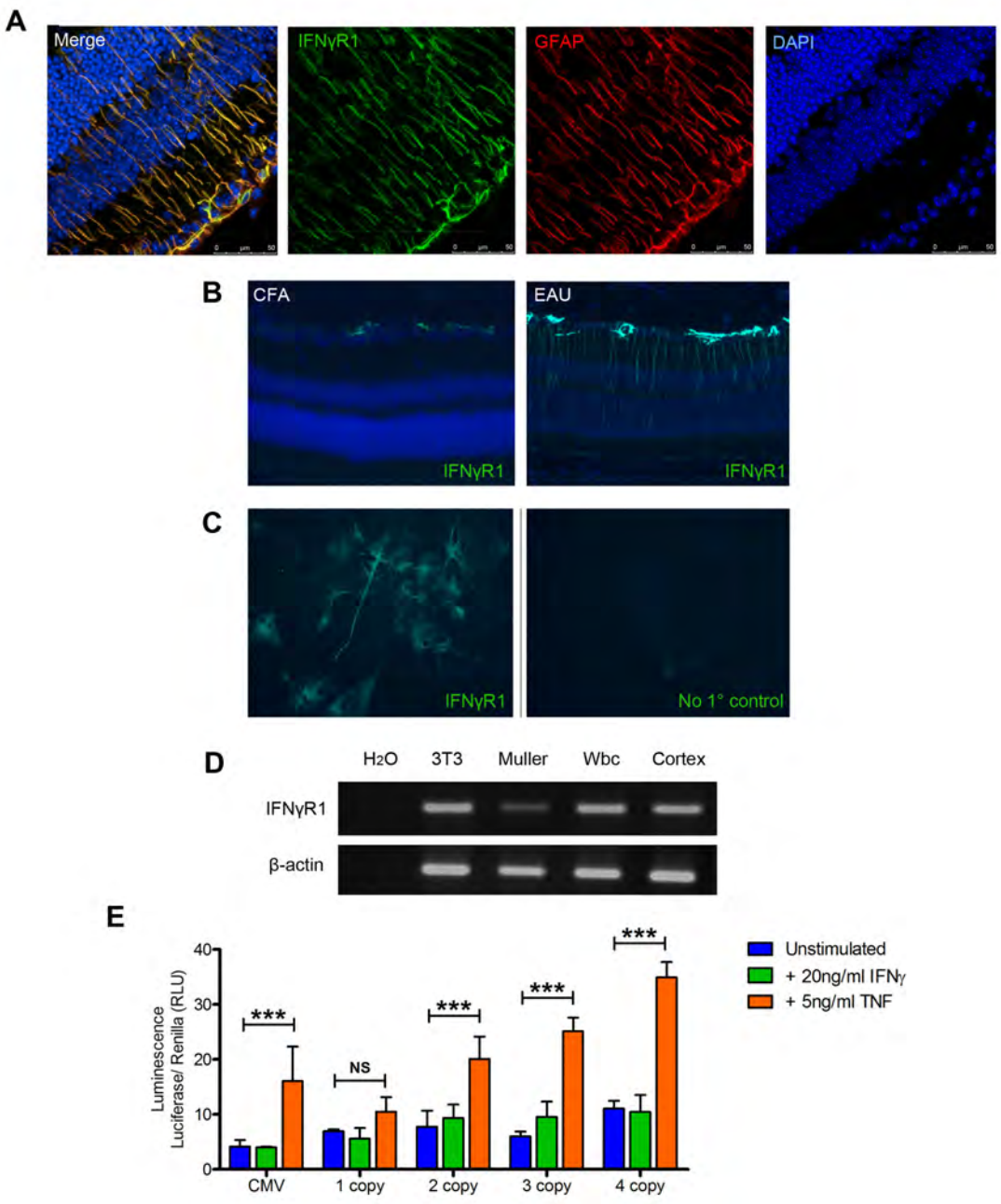

Figure 66. IFNγ-receptor 1 was identified on Muller cells but the IRF1 promoter construct fails to respond to IFNγ. Immunohistochemistry on eyes from **A)** d26 EAU were imaged by confocal microscopy for IFNγR1 and shown to co-localise with GFAP - a marker of astrocytes and Muller cells. Microscope filters were adjusted to ensure minimal bleed-through between colours, with similar staining apparent on single colour stained slides. **B)** Using CFA control eyes, without inflammation, staining was only detected on astrocytes, implying upregulation of the receptor on Muller cells. **C)** To confirm Muller cell expression, explant cultures from *Rlbp1-GFP* mice also stained for IFNγR1. **D)** RT-PCR confirms the presence of IFNγR1 in these cultures (Muller), as well as other tissues including mouse 3T3 fibroblasts, mouse splenocytes (wbc) and mouse cortex. **E)** The IRF1 promoter constructs fail to respond to IFNγ, but do respond to TNF. Representative example of one of two independent

experiments performed. Two-way ANOVA with Bonferroni post-tests. ***=P<0.001. Mean + SD shown.

For multiple reasons the IRF1 construct was not pursued further. No IFNγ response could be identified, despite the published characterisation.[162] Compared to unstimulated cells the response to TNF, even with the 4-copy promoter was moderate at best. The main population expressing IFNγR1 is also the Muller cells, which are difficult to transduce with AAV. At the time of initial investigation only AAV9 was available, which can transduce Muller cells only following subretinal injection at exceptionally high titres (Claire Hippert, personal communication). A degree of toxicity at this level was also suspected from observed loss of photoreceptors in some treated eyes. Subsequently ShH10 became available within the lab (see **results chapter 3**), which was reported to transduce Muller cells across the eye following intravitreal injection in mouse pups. In the adult it was identified that only patches of transfected populations of Muller cells could be achieved. This was not thought to be of sufficient extent for effective therapy and hence not pursued.

8.2 NFκB-motif promoter

NFκB forms the archetypal pro-inflammatory signalling pathway, involved in both adaptive and innate immunity. The canonical activation pathway is activated by a variety of stimuli including TNF, Interleukin-1 and Toll-like receptor activation. Ultimately these act to phosphorylate and target IκB to the proteosome, which typically liberates p65/RelA dimers to enter the nucleus and stimulate transcription at NFκB-consensus motifs.[207] Furthermore similar NFκB-based constructs have been used during AAV therapy of the brain and so application in the eye should be feasible.[96]

A construct with five repeats of the binding motif GGGAATTTCC at the 5' end of the SV40 minimal promoter was obtained and tested by Luciferase reporter assay with a Renilla luciferase encoding plasmid to control for transfection efficiency. As a benchmark, it was tested against a construct

with the enhancer region of the CMV immediate-early promoter 5' to the SV40 minimal promoter as described **(Figure 65)**.

Firstly, the dose-response curve to TNF was delineated over a wide *in vitro* range, as the intraocular concentration attained during murine EAU has not been published. In the rat, 83.5pg/ml TNF has been detected at peak EAU, but again how this translates to an equivalent *in vitro* dose is unclear.[202] A strong trend for increasing dose-response was evident and even at 2ng/ml TNF the response was greater than CMV **(Figure 67A)**.

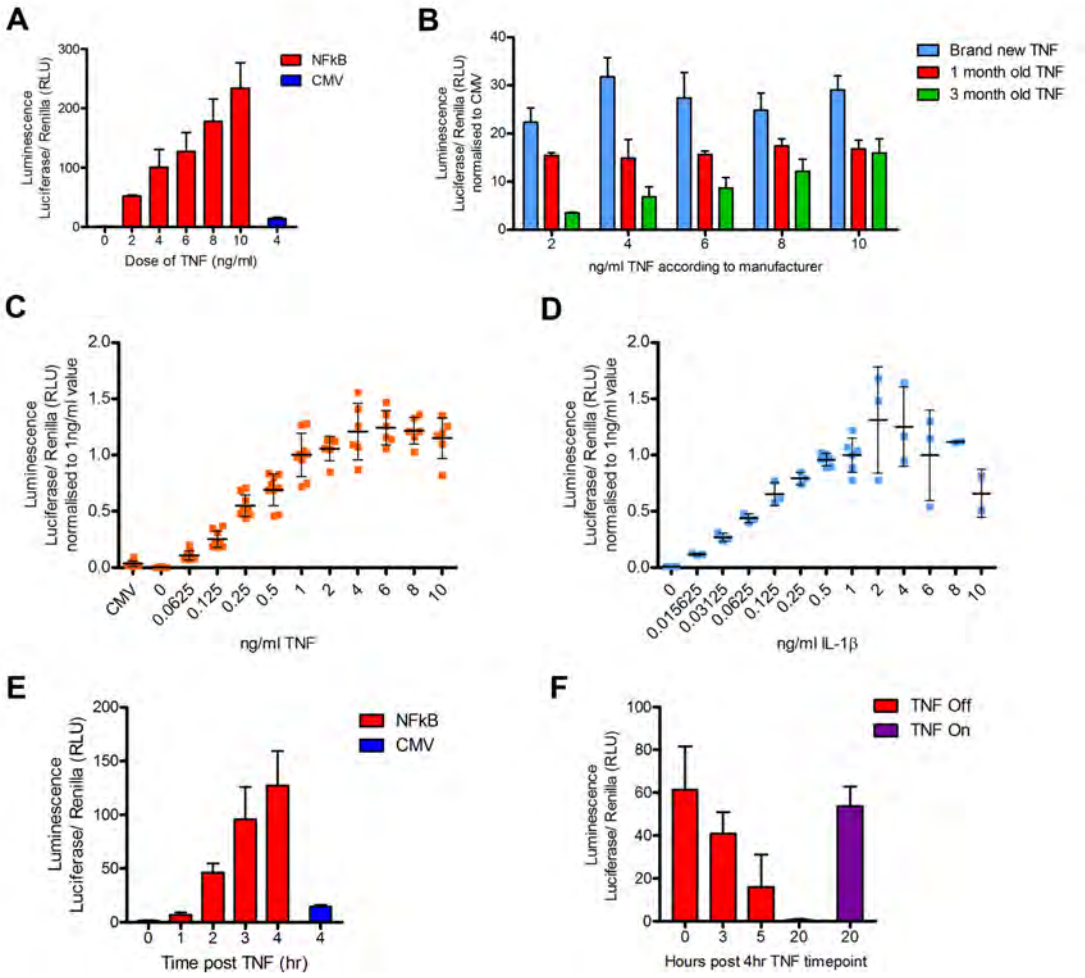

Figure 67. The NFκB-motif promoter rapidly responds in a dose-dependent manner, with low background activity and a detectable decrease in activity after withdrawal of stimulation. A Luciferase reporter construct driven by the five copy NFκB-motif promoter was used to assess activity. 30,000 HEK-293T cells were used with a Renilla plasmid to control for transfection efficiency. **A)** Dose-response of TNF as a stimulant of NFκB at 4hr, compared to CMV enhancer. During independent repeats, highly variable results were obtained. **B)** The age of recombinant TNF following reconstitution - despite optimal storage under

manufacturer's recommendations - was found to be important. Three different batches illustrate different results, despite supposed equal doses. **C)** By normalising to the 1ng dose result, whilst absolute TNF activity varies, relative effect of dose clearly demonstrates the pattern of response from the NFκB-promoter. There is a linear increase until plateau around 6ng. Note that even at small doses, the response is greater than the CMV enhancer. **D)** A similar pattern of response is obtained using recombinant IL-1β, demonstrating that the response is NFκB and not TNF-specific. **E)** Following the addition of 5ng/ml TNF, Luciferase production is detectable above baseline at an hour and continues to increase. **F)** Following 4hr stimulation of 5ng/ml TNF, the media is changed and TNF removed. A trend towards reduced promoter activity is seen by 5 hours onwards. At 20hrs, activity has returned to baseline, unlike the activity of the matched sample where TNF was left on. All experiments were performed with technical triplicates and repeated independently at least once. **C** and **D** contain pooled results from three and two independent experiments respectively. Mean + SD shown.

During subsequent experimentation, large variation was seen. Much of this was identified as a degradation in potency of the recombinant human TNF, despite storage at -20°C as per manufacturer recommendation. Results from different aliquots of either freshly purchased TNF, or after storage for 1 or 3 months were compared **(Figure 67B)**. It is probable that no dose-response can be seen in the newer aliquots, as they were maximally stimulated. As a result, data from independent experiments were normalised to the 1ng/ml TNF value. This allowed the results to be pooled and demonstrate the pattern of a linear range of response and plateau **(Figure 67C)**. To confirm the response was NFκB specific and not an off-target effect of TNF, the same experiment was performed, but using recombinant human IL-1β **(Figure 67D)**. IL-1β is known to activate NFκB after binding to IL-1R and signalling via MyD88.[208] A similar dose response was identified.

Finally, the activation and deactivation kinetics of the NFκB-promoter were assessed. TNF was applied at 5ng/ml and Luciferase activity determined across the first few hours **(Figure 67E)**. This shows that even by 2 hours after stimulation, a detectable increase in Luciferase can be seen. Following removal of TNF from the cell culture medium, Luciferase activity decreased, such that a large reduction in activity was evident after 5 hours and almost undetectable by 20 hours **(Figure 67F)**. These temporal characteristics are encouraging and therefore could be viable for translational therapy.

The NFκB-SV40 promoter was cloned in place of the CMV promoter in the pD10-CMV-eGFP plasmid. Using this a viral preparation of AAV8-NFκB-eGFP was produced and tested by application on HEK 293T cells. After 72 hours, 5ng/ml TNF was applied in the culture medium. As it is likely that translation of GFP to a detectable level would take longer than Luciferase, yet would have a stable half-life of 26 hours, assessments were made at 24 and 48 hours. Following trypsin dissociation the cells were analysed by flow cytometry **(Figure 68).** A clear shift in the number of cells expressing GFP was seen at 48hr compared to the unstimulated controls, with the 24hr timepoint providing intermediate values. On the basis of these results, *in vivo* testing was progressed to.

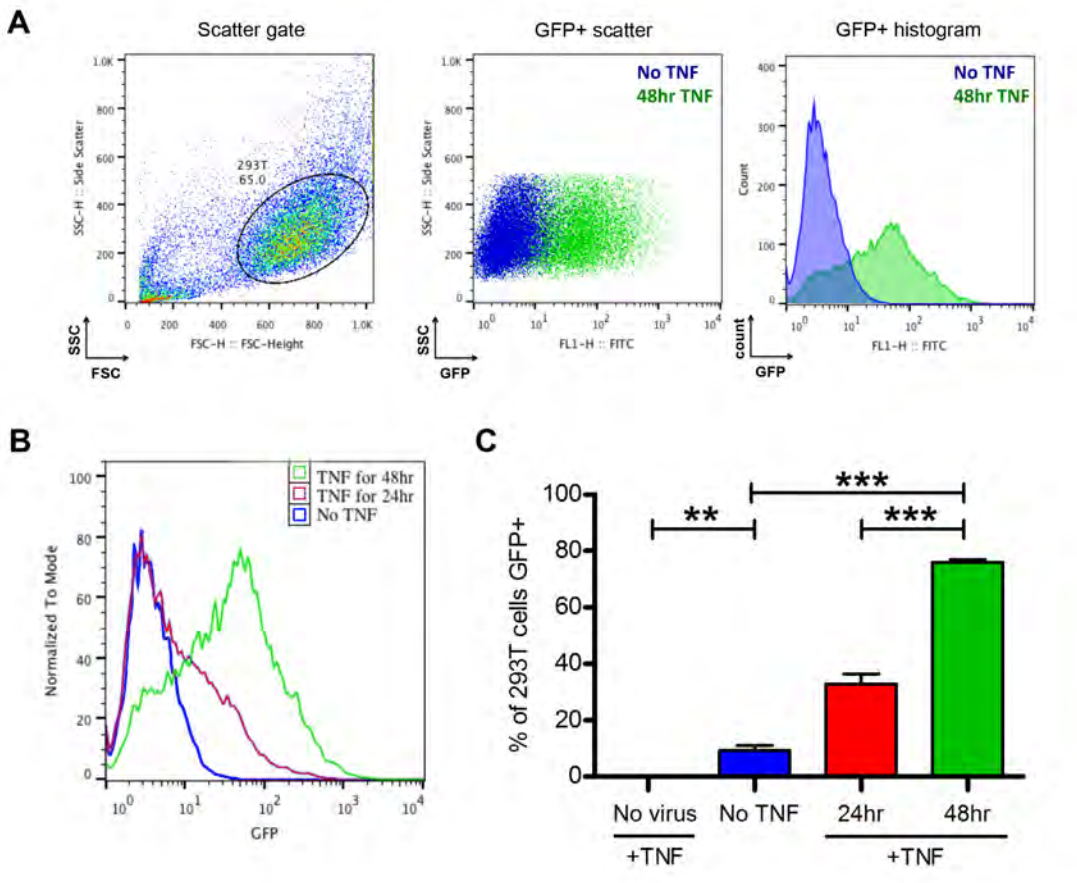

Figure 68. HEK-293T cells infected with AAV8-NFκB-eGFP *in vitro* respond to stimulation by TNF. 30,000 293T cells were plated into 96-well plates and infected with AAV8-NFκB-eGFP for 48hrs at an MOI of 20000. 5ng/ml Human recombinant TNF in fresh D10 medium was added to the wells then analysed by flow cytometry at different timepoints. **A)** Representative flow cytometry plots gated by scatter profile first. No TNF (blue) and 48hrs

TNF (green) groups are displayed with GFP signal either against SSC or as a histogram. **B)** Histograms normalised to the mode for different samples including 24hrs TNF (red). **C)** Summary graph shows the increase in percentage of cells expressing GFP with TNF over time. Statistically significant differences between all groups were evident, with a selection illustrated. One-way ANOVA **=P<0.01, ***=P<0.001. Mean + SD shown. The No TNF group was analysed at 48hrs. 10,000 events were collected for each sample. Data are representative of two independent experiments with technical triplicates in each group.

Two independent cohorts of mice underwent subretinal injection with $1x10^{10}$ vector genomes in 2µl of either AAV8-CMV-eGFP or AAV8-NFκB-eGFP. Two weeks later a subset of the mice was induced with EAU. Following anaesthesia and dilation with 1% Tropicamide, slit-lamp fundal fluorescent imaging was performed at key timepoints and representative images shown in **Figure 69**.

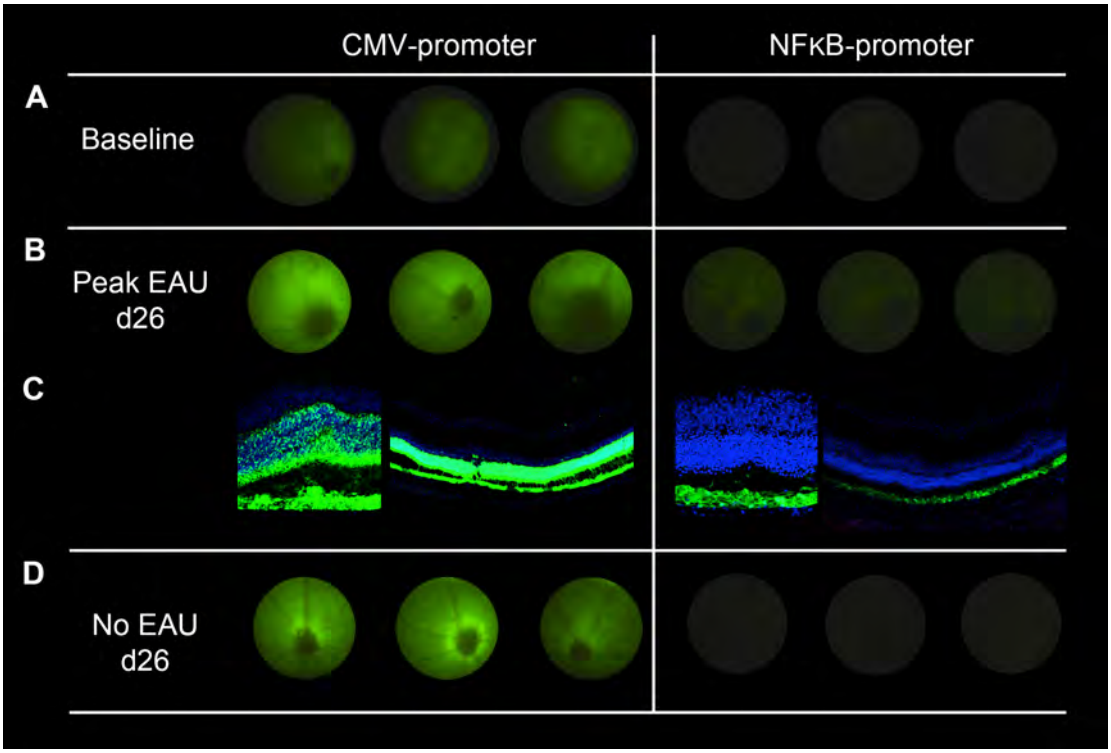

Figure 69. Unlike the CMV promoter, which is constitutively active, the NFκB-promoter only leads to expression following the induction of EAU. Two independent cohorts of mice were injected with $1x10^{10}$ vector genomes of titre-matched AAV8-CMV-eGFP or AAV8-NFκB-eGFP in the subretinal space. Three representative slit-lamp fundal fluorescence images from an eye of three different mice are shown for each condition. Exposure time standardised at 30.2s. **A)** At the baseline timepoint, two weeks post-injection, only the CMV promoter demonstrates activation, though small amounts of GFP can be seen in the NFκB promoter eyes around the traumatic site of injection. **B)** At peak EAU, the NFκB-promoter is active,

although the signal is less than the CMV-promoter. **C)** Histology confirms that NFκB signal is exclusively in the RPE (n=4) reflecting the presence of NFκB signalling, whilst the CMV-promoter is constitutively active in both photoreceptors and RPE. Images acquired with identical confocal settings. **D)** To demonstrate that increased time is not responsible for the activation of NFκB, control eyes without EAU at day 26 were imaged and showed to lack GFP signal.

At the baseline timepoint two weeks post-injection of AAV, but prior to the induction of EAU, the CMV promoter showed GFP signal. At this timepoint AAV8 would be expected to be generating high levels of expression in RPE and photoreceptors, but would not peak until several weeks. There was however, no signal in the NFκB-promoter injected eyes, except occasionally around the area of the needle track where traumatic inflammation may be occurring following injection **(Figure 69A)**. At peak EAU on day 26, imaging was repeated. At this point the NFκB-promoter was active and GFP detectable **(Figure 69B)**. Compared to CMV, the intensity was less. This was partially explained by histology, which revealed expression only in the RPE with the NFκB-promoter **(Figure 69C)**. This is as potentially expected as NFκB signalling is robustly documented in RPE, whereas there are no published reports clearly demonstrating canonical NFκB signalling in photoreceptors. Additionally greater numbers of AAV particles are likely to infect the RPE. Groups reporting NFκB expression have found the signal to arise from microglia, rather than the photoreceptors themselves.[209] However, microglial transduction by AAV8 has neither been seen nor reported in the literature. Total GFP signal from the CMV promoter is significantly greater, as photoreceptors also account for over ten-fold more cells than the RPE. Comparing the GFP fluorescence in the RPE alone, the signal does not appear substantially different between the groups.

To control for the possibility of late expression from the NFκB promoter as a consequence of the AAV transduction kinetics, mice injected with AAV8, but not induced with EAU were examined at the same timepoint as peak EAU, a full 40 days post-injection **(Figure 69D)**. Reassuringly, no signal was seen in the NFκB group. The CMV-promoter cohort did not appear to differ from

those with EAU, indicating a lack of induction or suppression as a result of inflammation with this promoter.

8.3 Flow cytometric quantification establishes the dose-response of the NFκB-promoter in EAU

To objectively demonstrate the inflammation-inducible nature of the NFκB-promoter, sixteen mice from two independent cohorts were analysed by flow cytometry. Following the same protocol used for histology and fundal imaging, mice were culled at day 26 EAU having been injected with titre-matched AAV8-CMV-eGFP or AAV8-NFκB-eGFP two-weeks prior to disease induction.

It was established earlier that the key cell type able to facilitate expression from the NFκB-motif promoter construct is the RPE. Previous work using flow cytometry to quantify CD45+ infiltrating cells in EAU from dissociated retina alone, confirmed that it reflected structural damage and is a valid measure of disease severity.[159] Given that murine EAU is the closest model of human uveitis widely available, if the CD45+ cell count correlated with the degree of GFP induction in the RPE, this would be the closest possible validation prior to a clinical trial.

For each eye the matched retina, vitreous and aqueous humour were dissected from the RPE/choroidal complex. This is typically a clear separation along the subretinal space. The retinal mix and RPE were mechanically dissociated as separate samples to achieve single cell suspensions. The RPE was analysed by flow cytometry for intrinsic GFP signal, whilst the dissociated retinal sample was stained with anti-CD45 first **(Figure 70)**.

There is intrinsic variability between animals and eyes during EAU, which naturally provides a wide range of inflammatory stimuli to test the responsiveness of the NFκB-promoter. Taking two eyes with mild and severe EAU based on TEFI, the fundal fluorescence image shows a proportionately

greater GFP signal with increased severity **(Figure 70A)**. The matched flow cytometry plots outline the gating strategy for analysis and further show the association between increased CD45+ cells and GFP+ RPE cells.

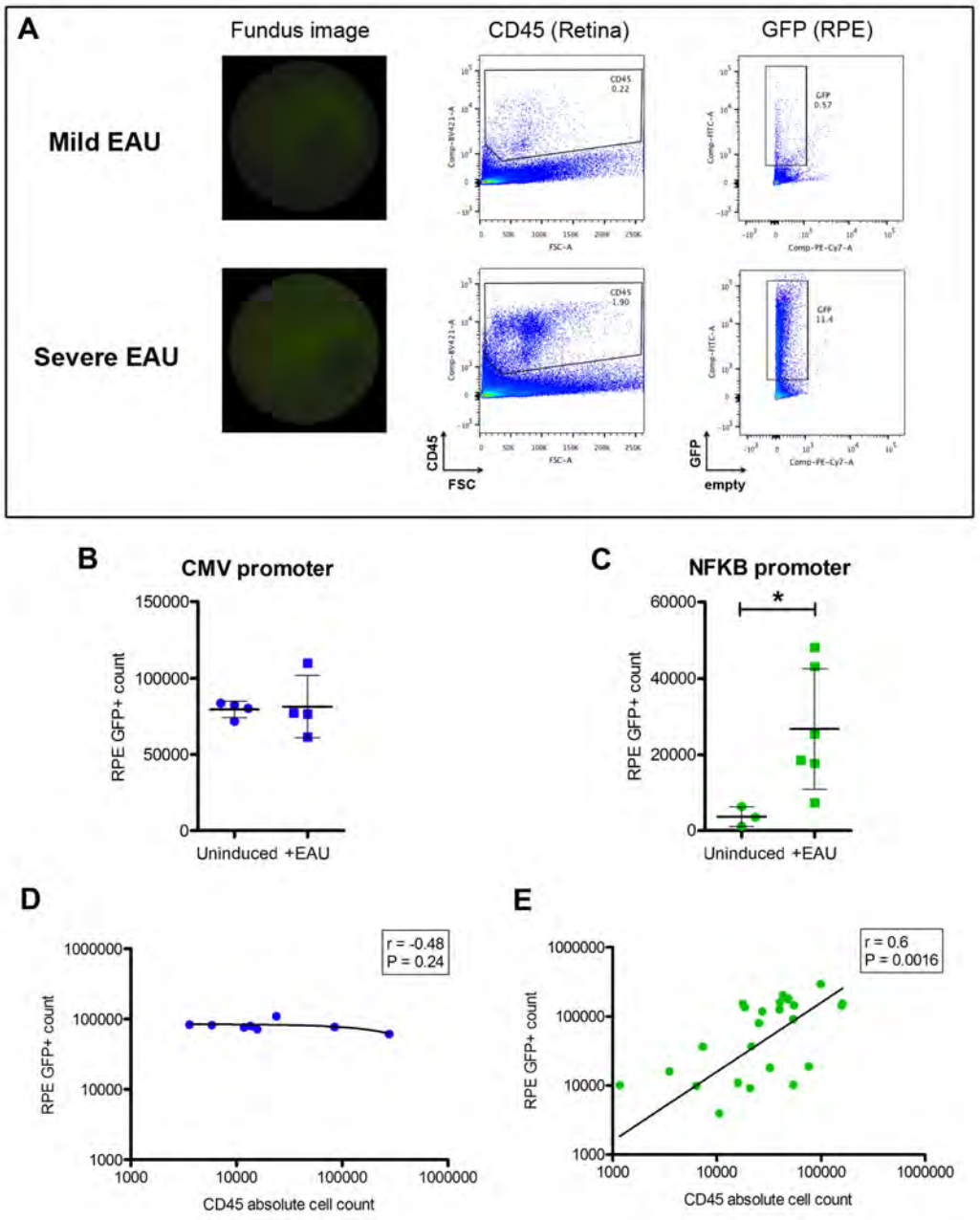

Figure 70. Flow cytometry of GFP signal and CD45+ cell infiltration confirms activation the NFκB-motif promoter in proportion to the degree of inflammation caused by EAU. Mice were injected with $1x10^{10}$ vector genomes of either AAV8-NFκB-eGFP or AAV8-CMV-eGFP into the subretinal space. Two weeks later, EAU was induced, and the eyes were harvested for flow cytometry at d26. The retina and vitreous were dissected as one sample for CD45 staining, with the RPE/choroid as another. **A)** Representative fundal images and flow cytometry plots from the eyes of mice with different degrees of EAU severity, indicated by the different numbers of CD45+ cells in each eye and reflective of the overall inflammatory

environment. As a result, the eye with more CD45+ cells has a greater GFP+ RPE cell count. **B)** Induction of EAU does not affect GFP+ RPE cell counts in eyes injected with AAV8-CMV-eGFP. **C)** The NFκB-motif promoter produces a low level of GFP that increases when EAU is induced. P<0.01, Mann-Whitney U. Mean + SD shown. **D)** Using the CMV promoter, there is no correlation between CD45+ count and GFP+ count. n=8 eyes. **E)** The NFκB-motif promoter demonstrates a significant correlation between increasing CD45+ cell count and GFP+ RPE count, implying it is regulated by inflammation. n=23 eyes from two independent experiments. Linear regression (black line) and Spearman correlation (boxes) shown.

To look at the induction potential of both the CMV **(Figure 70B)** and NFκB-motif **(Figure 70C)** promoters, the RPE GFP+ counts were plotted for eyes with and without the induction of EAU. This shows a lack of further increase in GFP+ signal resulting from EAU upon CMV-driven transcription, whereas the activating effect of inflammation upon the NFκB promoter is evident.

The GFP+ RPE count was correlated with the corresponding CD45+ cell count for each eye. Again, the CMV promoter shows no correlation, with most cells expressing the transgene regardless of the degree of cellular infiltration **(Figure 70D)**. The NFκB-promoter in contrast shows a statistically significant correlation. As the CD45 count increases, so does the GFP+ RPE count **(Figure 70E)**. This quantitatively demonstrates the action of the NFκB promoter as a mechanism for self-regulated production of potential anti-inflammatory transgenes, in the closest available model to human uveitis. Furthermore, expression increases in direct proportion to the degree of inflammatory cellular infiltrate.

As outlined in the previous chapters, AAV mediated delivery of a suitable anti-inflammatory cytokine to treat EAU remains problematic. Incorporation of the NFκB promoter may aid successful suppression when a suitable target is identified in future work. At the end of this project, particularly as no target transgene driven by a constitutive promoter has been identified as effective, the promoter has not yet been incorporated and tested in an interventional study. Pending further work this will be performed. Aside from therapy, one alternative application is to use the construct for *in vivo* monitoring of the inflammatory environment.

8.4 The NFκB promoter can be used as an *in vivo* reporter to examine aspects of the EAU model itself.

An area of debate exists around the post-peak, so-called 'resolution' phase of murine EAU. The inducible disease in the *C57BL/6* mouse was classically regarded as monophasic, regressing to quiescence. It is now increasingly recognised that EAU does not resolve completely and at late timepoints is still highly dynamic. Several groups have reported vascular remodelling [25,160] and changes in cellular infiltrate, with evidence of progressive accumulation of exhausted phenotype CD8+ T-cells.[24]

To answer this question, several mice underwent subretinal injection of AAV8-NFκB-eGFP and then were followed through the course of EAU out to day 87. Representative slit lamp fluorescent fundal images are shown for four mice in **Figure 71**. As expected, there is no GFP before EAU is induced, but expression is seen at peak disease on day 26. By day 38, EAU usually has the appearance of clinical resolution, with apparent scarring around areas of prior vasculitis and the resolution of disc oedema. GFP intensity reflecting NFκB signalling in the RPE is however, undiminished and arguably slightly increased.

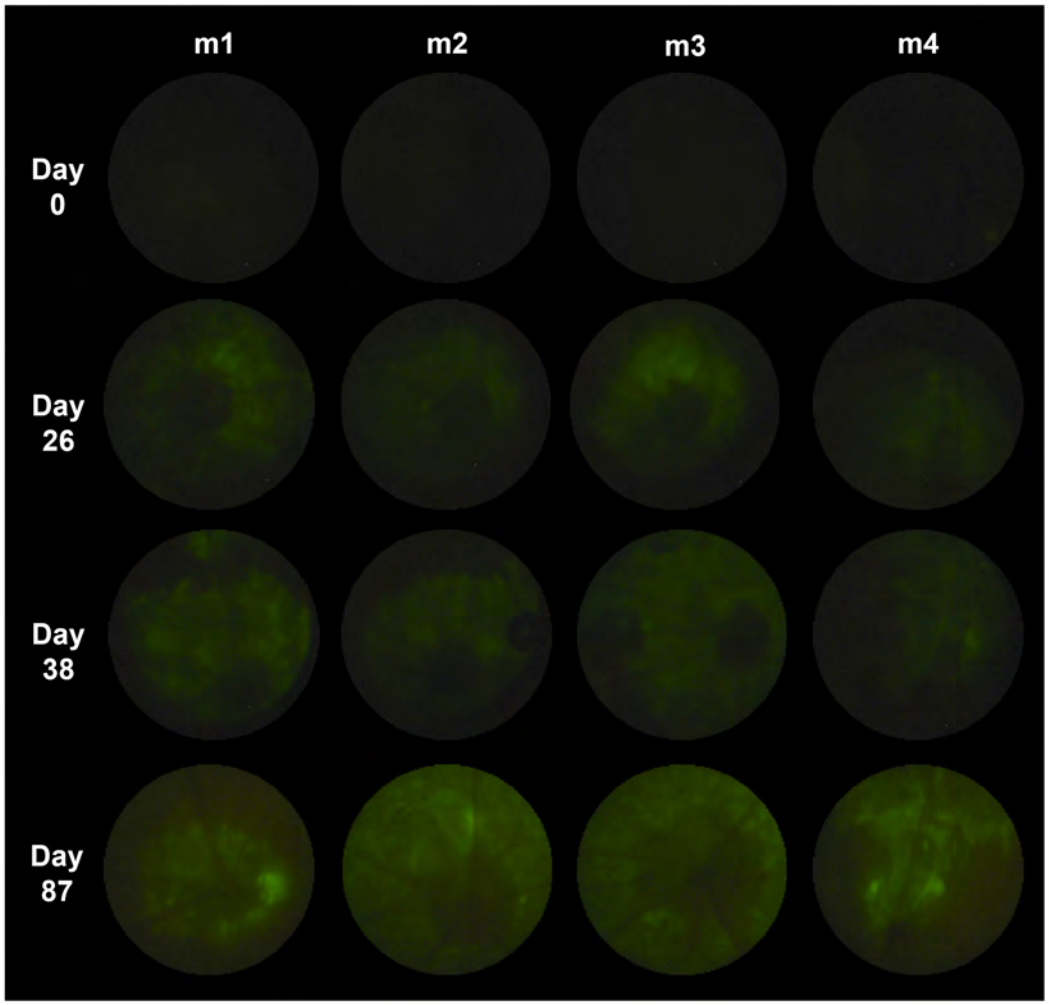

Figure 71. The NFκB-GFP construct confirms the presence of persistent inflammatory activity in the eye at timepoints classically labelled as resolved disease. Representative images of four eyes from a cohort of C57BL/6 mice (m1-4) that underwent EAU induction two weeks after subretinal injection of AAV8-NFκB-GFP. Slit-lamp fundal fluorescence images are shown for the same eye over four timepoints – baseline (day 0), peak disease (day 26), early post-peak (day 38) and late (day 87).

EAU is rarely run as far as day 87 and would be expected to be quiescent at this stage. Occasionally though deep retinal folds are seen at late stages, which have been documented to contain a mixture of myeloid and lymphoid cell types.[25] In the eyes injected with AAV8-NFκB-GFP, GFP signal is certainly not diminished at day 86 and appears more intense than at any other stage **(Figure 71)**. Regions of approximately the same size as the aforementioned retinal folds appear to form foci where the GFP signal is greatest, particularly in eye m3. This could reflect local activation of NFκB in

the underlying RPE in a process that is not yet clear. Certainly these findings support the emerging consensus that a form of continued inflammatory activity occurs in post-peak EAU.

One caveat is the possibility of an anti-viral response to AAV, which could trigger a late stage response and inflammation that would perpetuate NFκB activation. Certainly in the absence of EAU, eyes injected with AAV8-NFκB-eGFP did not express detectable levels even after four weeks, making a general response unlikely **(Figure 69)**. Whilst possible that the addition of EAU might exacerbate a response, data in the prior chapters failed to detect systemic neutralising antibody or CD8 T-cell responses following subretinal AAV8 administration during EAU. NFκB is involved in processes other than inflammation, including angiogenesis. The promoter as designed would not be able to respond to pro-inflammatory signalling specifically and so could respond to these stimuli, if arising late in EAU. An antigen-directed reaction to eGFP or direct cellular toxicity also cannot be excluded. Publications have identified a strongly antigenic eight amino acid H2-K^d restricted region at the C-terminus of eGFP.[197] Whilst this was not tested for by ELISPOT in these cohorts, as shown previously a head-to-head experiment against hrGFP failed to identify any difference in inflammation in the context of EAU. It is thus unlikely to have a large effect upon these results.

8.5 Chapter summary

The successful translation of gene therapy for uveitis to clinical trial will undoubtedly require refinements enabling self-regulated production of the therapeutic target. Based on our understanding of the key pro-inflammatory cytokines involved in experimental models of uveitis, IFNγ and NFκB signalling pathway-based promoters were chosen. Whilst the IRF1-based promoter failed to respond appropriately to IFNγ, the NFκB promoter demonstrated favourable characteristics. Strong dose-response, rapid onset and termination were identified *in vitro* using a Luciferase reporter assay. The promoter was then tested as AAV8-NFκB-eGFP *in vitro* and *in vivo*. It was inactive in the absence of disease, but led to expression in the RPE at peak

EAU. Using flow cytometry, the promoter was quantitatively shown to respond in direct proportion to the severity of inflammation, measured by CD45+ cell infiltration. This capacity was then used as a reporter to show that persistent NFκB activation occurs in the RPE during late post-peak stages of EAU.

9 Discussion

This project aimed to advance the field of gene therapy for uveitis using new AAV serotypes, known to achieve superior levels of expression and wider cellular tropism. IL-10 and TNF inhibitors, two of the most commonly used anti-inflammatory targets were investigated but did not appear to be effective at suppressing intraocular inflammation in the mouse when delivered using AAV. An inflammatory responsive promoter was trialled for the first time in the eye and activated only in the presence of and in proportion to the degree of inflammation. New approaches for the analysis of the two commonly used mouse models of ocular inflammation, EAU and EIU, were developed using OCT and flow cytometry respectively.

9.1 OCT can be used to assess and score EAU

In **results chapter 1**, OCT was proposed as a viable method for evaluating mouse EAU and quantifying disease *in vivo*. A minimally subjective OCT-based scoring system has been described, which correlates well with existing histology and TEFI based analyses. Additionally OCT provides a tool for following dynamic intraretinal changes and will permit the reconciliation of mounting functional and cellular data arising from the EAU model **(Table 12)**.

Benefits	Limitations
Can detect intraretinal changes in real-time	Expensive hardware limits availability
Allows repeated scoring of the same eye over a time-course	Large initial learning curve of user skill required to acquire good quality scans
Can detect oedema *in vivo*, a characteristic otherwise lost by histological processing	Severe disease (*B10.RIII*) with vitritis and posterior synaechiae can prevent adequate imaging.
Enables correlation of OCT with matched immunohistochemistry that might inform the interpretation of human OCT images from patients with Uveitis.	
Requires less overall time compared to histology when processing, sectioning and staining are accounted for.	
Can result in less mice needed for experiments (3R's)	

Allows exactly matched eyes to proceed for alternative tissue analysis such as flow cytometry or multiplex ELISA, instead of surrogate severity scores from a parallel cohort.	

Table 12. A summary of benefits and limitations of the novel OCT scoring system compared to conventional assessment of EAU.

9.1.1 OCT Correlates with current EAU scoring methods and has distinct advantages

In *C57BL/6* mice, for the range of pathology historically used to score EAU severity – vitreous, disc, vessel and retinal structural changes – discrimination is possible using OCT. OCT can therefore be considered as a technique used for disease assessment, and substituted for post-mortem histology where appropriate will allow reduction and refinement of animal usage. Histology will inevitably still be performed for first describing novel findings and corroborative phenotyping, but could otherwise be widely replaced by OCT. This is because OCT remains conceptually analogous to and using our scoring system, is shown to be directly correlated to post-mortem histology scores. The overall time per eye required for imaging and scoring is in general less once processing, sectioning and staining for histology are accounted for. For OCT scoring, it would take approximately 30 minutes per eye, including scanning, processing and scoring. Histology would take at least 40 minutes per eye to embed, section and score, not including the time required for staining, which would be several hours, though could be performed in batches.

A further advantage is that OCT can be used to observe directly features *in vivo* such as oedema and vascular leakage, which are seldom detectible on histology due to the dehydrating nature of tissue processing techniques. This platform has the additional ability to simultaneously perform fluorescein angiography, scanning at the exact location of any lesion. However, we noted that OCT was able to distinguish specific signals in tissue surrounding leaking vessels that could be used as surrogates to avoid unnecessary angiography.

OCT permits repeated *in vivo* examination of the same animal, allowing the progression of features, or intraretinal response to therapy to be closely monitored and examined. OCT also delivers a closer substitute for histology than TEFI. Whilst current *in vivo* monitoring with TEFI can detect disc and vessel alterations, it cannot detect intraretinal or vitreous changes.[159] OCT avoids the disadvantages of intense light exposure, corneal contact and appears not to overestimate disc involvement to the same degree. Nevertheless, TEFI still has a role as a useful and quick screening step, identifying animals for subsequent detailed OCT scoring, or matching disease stage for other assessments.

Wide inter- and intra-animal variation in disease severity in the *C57BL/6* EAU model means many mice are often required to obtain reproducible data from functional or cellular analysis. The data implies that OCT will allow accurate intraretinal synchronisation of disease stage within experimental groups prior to any therapeutic intervention during established EAU. This should consequently narrow biological variation and allow the significant detection of interventions with smaller numbers of animals. By scoring disease without post-mortem histology, animals can also be repurposed to other analyses (flow cytometry, qPCR, cytokine ELISA) with additional knowledge of the exact disease stage of each eye.

9.1.2 OCT can guide the discovery and characterisation of novel retinal features

It has been demonstrated by employing OCT that vitreous and intraretinal changes can not only be evaluated in more detail, but can also identify and assess previously unrecognised features of the inflamed retina in a more targeted way. Using our platform, vessels can be imaged with combined FFA and OCT to localise leakage and analyse surrounding tissue in the associated areas. Deep retinal folds can be imaged and importantly, distinguished on OCT from other changes such as the abnormal vascular telangiectasia prior to neovascular outgrowths. This feature in EAU was

identified by FFA and OCT from day 36 onwards showing vascular re-modelling to occur earlier in disease than indicated by similar vascular membranes recently observed only from day 60 post-induction.[160]

The vascular lesions share some similarities with those described in degenerative models with low-grade chronic inflammatory components, such as rhodopsin kinase knockout mice[210] or those carrying the *rd8* mutation.[30] The mice used in our study carry neither defect and thus the lesion may represent a more widespread feature of tissue re-modelling in response to degenerative or inflammatory processes in the retina. Our data illustrates such changes, with vessels extending through the outer nuclear layer and under the RPE, before reconnecting with superficial retinal vasculature. The vessels are unlikely to represent choroidal neovascularisation as neither FFA findings nor the irregular, yet ordered splay of the abnormal vessels are characteristic of this. The pathogenesis is likely linked through the development of glial activation, which both degeneration and EAU would trigger. Further analysis including 3D-scanning electron microscopy to prove the integrity of Bruch's membrane would be required to confirm this assertion.

9.1.3 OCT scoring and future directions

Construction of the OCT scoring system proved complex and retaining adequate capture of detail had to be balanced against simplicity of use. Our system was designed purposely to remove subjectivity where possible and unlike histological and TEFI scoring systems does not use imprecise stratification such as 'mild, moderate or subtotal'. The structural sub-score, calibrated for broad overview and time efficiency does not distinguish between subtypes of retinal changes. As such it remains necessary to carefully study specific structural features as required for the precise purpose of each experiment.

As EAU in rats and B10.RIII mice is more severe[17,171], the current data is based on C57BL/6 mice since the model permits detailed imaging of the retina at critical stages. The largest constraint is the limitation of the degree

of optical resolution. Further refinements in both the hardware and optics for rodent imaging will inevitability increase the quality of data obtained, which will allow progressively improved scoring accuracy and characterisation. Detailed analysis of choroidal changes may be possible using long wavelength, enhanced depth imaging OCT, whilst employing emerging adaptive optics technology may eventually allow the observation of dynamic processes on a single cell level *in vivo*.[169] More work to further precisely delineate with OCT temporal changes and responses to therapeutic intervention are the likely next steps to be taken and could also include the development of algorithms and segmentation improvement to increase accuracy.

In back-to-back publications, submitted to the same journal a week after our work, another group has presented an OCT-based analysis and scoring system for use in the *B10.RIII* mouse.[174] Their use of both different hardware and strain is excellent validation of the approach of using OCT in EAU. As noticed during our own assessment of *B10.RIII* disease imaging quality in the system used by Chen *et al* was impeded by vitritis and posterior synaechiae. Whilst features could be identified, the final scoring system was based primarily only upon retinal thickness. Though this is a rapid and simple method, it may miss subtle changes in morphology and takes no account of which layer pathology may occur in.

9.1.4 Interpreting OCT changes in human intraocular inflammatory disease by correlation of histopathology and OCT in murine EAU

Several of the features we have described in EAU mirror OCT changes seen in some human posterior segment inflammatory diseases.[211,212] An additional significant benefit of using our approach lies in the ability to directly correlate scan features with matched tissue, which can be directly analysed to identify immune cell composition and altered function. Due to the paucity of human material for histology, an identical human study is not feasible. OCT is however, already being used in clinical practice to phenotype and monitor posterior uveitis.[213] By further examining other preclinical animal models,

including humanised and spontaneous EAU in mice, more accurate correlations might be drawn.[37] Conversely, screening new EAU models with OCT for retinal changes closest to those of human disease, will allow selection and refinement during development. In the clinic, it remains challenging to judge the remission of posterior segment inflammatory disease or to detect early recurrence and relapse. Quantification and analysis of OCT features other than macular oedema, as we have used here in EAU, could distinguish remission versus low-grade chronic inflammation as well as tissue re-modelling in order to guide clinical decision-making.

9.2 Flow cytometry provides a more comprehensive and quantitative assessment of the EIU model

Whilst EIU is not an accurate model of human anterior uveitis, it is a useful tool for the interrogation of innate-triggered inflammation in the eye and mechanisms of cellular infiltration.[32] Since its first proposal as an ocular model in 1980, use has not fallen over the last thirty years **(Figure 72)**. This is likely to be a result of the simplicity and speed of the model that suits early *in vivo* drug screening, as well as initial interrogation of innate responses in many newly developed transgenic mice. Changing research interests and priorities are likely to only increase the use of EIU. Recent studies into age-related macular degeneration (AMD), a highly active area of research, have highlighted the importance of the inflammasome.[214] This is a key signalling mechanism engaged by EIU. As robust animal models of AMD are lacking, initial acute testing of several therapeutics directed against the inflammasome is already being performed in EIU. Microglial contributions to AMD are also becoming apparent and the model has also been used to examine this.[215]

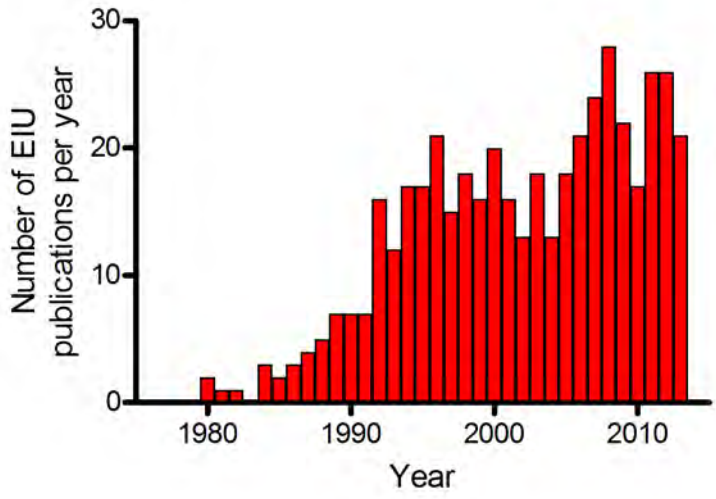

Figure 72. Despite the limitations of the EIU model its use has not fallen since introduction in 1980. Publications for each year listed on MEDLINE containing search terms: [endotoxin] AND [induced] AND [uveitis]. Metrics obtained from Medline trend: automated yearly statistics of PubMed results for any query, 2004. Web resource at http://dan.corlan.net/medline-trend.html.

EIU has historically been assessed by histology with paraffin sections stained with H&E. Subjective counts of haematoxylin-staining cells in the AC and vitreous are then performed across a limited cross-section of the eye. This count is used as a measure of disease severity and therapeutic attenuation derived from this. It seems almost counterintuitive that flow cytometry is regularly used to assess EAU, where structural changes are important and mandate the additional use of histology, while in EIU only histology has been regularly employed, where it is widely acknowledged that structural damage seldom occurs and only the amount of infiltrate is important.[31] In this setting flow cytometry seems an ideal assessment method for EIU, providing rapid, accurate and objective quantification of cell number.

In **results chapter 2**, the evidence for the use of flow cytometry to score EIU was presented, alongside our technique, which allows efficient processing of multiple samples. Other aspects of the EIU model were explored. The ratio of anterior and posterior/vitreous infiltrate was shown to be approximately equivalent, with cells seen entering through the iris and optic disc respectively. The time-course of infiltration, divided into neutrophils and monocytes was determined and the two patterns of initial neutrophil (6-12hr)

then monocyte (18hr) ingress were identified.[32] A similar observation has previous been made following systemic induction of EIU in the rat and analysis with immunohistochemistry.[216] In that study, the first peak of iNOS+ cell infiltrate occurred at 12hrs, compared to 6hrs we identified with intravitreal delivery. This probably reflects the quicker initiation of chemotactic signals following local LPS delivery. We induced EIU by intravitreal injection of LPS, but the flow cytometry technique could be applied to either footpad or intraperitoneal induced systemic EIU models. These are likely to result in lower intraocular cell counts however.

Flow cytometry	Histology
Fully quantitative and objective.	Semi-quantitative and requires a subjective assessor.
Ocular tissue is homogenised so sample evenly reflects the entire eye.	Discontinuous sections provide only a limited cross-sectional sample of the eye.
Up to 18 different markers can be assessed simultaneously dependent upon flow cytometer.	Only 1-2 markers can be stained for on each paraffin section.
Live-Dead discrimination feasible with vital dyes.	Not possible as tissue fixed.
Remaining RPE/iris/ciliary body tissue can be used for other analyses, as can cellular supernatants e.g. ELISA, qPCR.	The whole eye must be used for histology.
Rapid – as there are no long incubation steps, results can be obtained on the same day.	Processing and embedding typically require several days.
Allows large-scale processing – setup allows 96 samples to be scored in one run.	Manual sectioning and scoring is time-consuming and labour intensive. Limits throughput.
Higher cost (flow cytometer & antibodies). Limited availability of dissecting microscopes and flow cytometry facility.	Histology facilities widespread and cost-effective.
Unexpected structural changes will not be detected.	Unexpected structural changes will be detected.

Table 13. Advantages and disadvantages of EIU assessment by flow cytometry compared to traditional histological analysis. Advantages are highlighted with green text and disadvantages in red text.

As summarised in **Table 13**, there are many additional benefits over histology by using flow cytometry. For new experiments, it is still recommended to check a sample of eyes by histology for unexpected structural changes. However, subsequent assessment performed by flow cytometry would allow rapid and large-scale processing of samples,

particularly suited to for example, high-throughput drug screening. Furthermore, simultaneous detection of subset specific changes and analysis of matched tissue samples and supernatants will maximise the opportunity to identify novel effects. The additional cost and access to a flow cytometer are potential barriers to widespread application, though it is available in most immunology labs, with commercial availability and price constantly improving.

A final validation of the technique would be to directly correlate histology and flow cytometric counts. This is not possible directly using identical eyes, as the same tissue is required for both analyses. Comparison of the mean and spread of two simple EIU cohorts could be used. Alternatively observing the same pattern of dose-response to an interventional therapy could provide further support. Both would be time-consuming and it was felt that the techniques were likely to coincide, as we have detected the same responses to recombinant human IL-10 in EIU as were published by another group using histology.[177] Further validation could be undertaken in the future. One advance that was described recently, is the use of OCT to image vitreous cells and retinal oedema in EIU.[217] This could uniquely be used for repeated quantification of cellular infiltration *in vivo*, though no scoring structure has yet been proposed in the literature. No discrimination between the subtype of infiltrating cell would be possible currently, though with enhanced resolution and adaptive optics this may be feasible in the future. Additionally, the sedimentation effect of gravity may lead to artificially low cell counts, as the single-slice OCT might not sample all the cells in the AC. It is likely that both techniques could be combined ultimately for the most comprehensive analysis of EIU.

9.3 Refinement of AAV production and the effect of Endotoxin contamination

Minimal attention has been placed upon the refinement of AAV production for immunologically sensitive applications within the eye. Examination of published methods suggests that most research-grade preparations are not even checked routinely for endotoxin contamination, which would be

expected to be widespread.[87] This project is the first to specifically address the effects of endotoxin in relation to intraocular use of AAV. Endotoxin contamination of AAV8-CMV-GFP injected into the subretinal space resulted in an increase in the number of CD11b+Ly6G+ cells in the eye. These cells are likely to be neutrophils and whilst not high in number are capable of releasing damaging free radicals. Direct activation of TLR4 as the receptor for endotoxin, has been implicated in photoreceptor oxidative stress, so in combination these two processes may have effects upon long-term photoreceptor cell survival.[218] Use of the subretinal route curtailed some effects of LPS, with reduced numbers of infiltrating cells seen within the eye compared to intravitreal injection. It is unclear if this is purely due to compartmentalisation, preventing systemic or responsive cell type exposure to LPS, or some other active phenomenon of suppression unique to the subretinal space.

It may be that many of the effects of endotoxin are not obvious in mice, which are generally less sensitive than many other animals.[219] Dog eyes injected by one of the group using an AAV preparation found subsequently to be heavily contaminated with endotoxin, developed florid clinically apparent inflammation. Reinjection of the same vector testing negative at 2.5EU/ml endotoxin in a different dog did not result in any clinically detectable changes.[220] In terms of endotoxin specifically confounding the effects of AAV, it was identified that in the short-term, there was no increase in expression as one study indirectly suggested.[181]

It was hypothesised that endotoxin may be responsible for the discrepancy between the transduction pattern of ShH10 we observed in adult mice and the widespread transduction reported in publications. The ShH10 vector was used in adult mice and shown to transduce ciliary epithelium, corneal endothelium but only columns of Muller cells, rather than widespread transduction.[57] Our vector was purified differently using an AVB column and certified as below 2.5EU/ml endotoxin. The discrepancy in results was thought to arise from the lack of contaminants or endotoxin, degrading the inner limiting membrane to allow improved ShH10 penetration of the retina.

Spiking vector with purified LPS however did not reproduce the original results. It remains possible however, that purified LPS alone may not be sufficient and it is contaminating cellular debris or mixed bacterial population derived endotoxins that are required.

The degree of contamination with debris from HEK-293T cells used to produce AAV varies significantly dependent upon purification strategy. It would be expected to contain highly inflammatory intracellular components that whilst not apparently problematic for monogenic rescue applications, could affect therapeutic immunomodulation by AAV-mediated gene therapy. Using an AVB column to purify vectors markedly reduced the degree of cellular protein contaminants compared to the previous Sephacryl-Poros method. These impurities could be examined in the future by processing untransfected HEK-293T cells according to various AAV purification protocols and investigating the effects of the resultant samples upon the eye.

A new protocol for enriching the number of active, full AAV capsids was trialled and found to be successful for AAV5, but not robust enough for AAV8, though subsequent work appears to suggest this is possible. Capsid enrichment as a final step was not employed, as the main strategy used AAV8 and ShH10. Theoretically the reduction in antigen load, in the form of unnecessary empty AAV capsids, could prevent the loss of subretinal deviation that has been reported to be antigen dose dependent.[76] Another concern is that intraocular inflammation might negate the subretinal immune deviation to AAV, and EAU appears to cause loss of immune deviation in the vitreous cavity.[221] Inducing EAU after the injection of subretinal AAV8 however did not appear to lead to systemic adaptive immune responses when judged by ELISPOT and neutralising antibody assays.

9.4 Suppressing autoimmunity using interleukin-10 is complex

IL-10 was chosen as the initial target transgene as it has been widely used and is regarded as the archetypal anti-inflammatory cytokine. Specifically,

several publications from our group and others showed that gene transfer using IL-10 was able to suppress both EAU and EIU.[34,93,110] In these initial publications, AAV2 and lentivirus were used to express IL-10 at relatively low levels compared to that achieved with AAV9 and AAV8 in this project. Additionally in this project, new methods of assessment such as OCT and CD45-immunolabelled EAU scores, or flow cytometry for EIU were employed to provide potentially more accurate and efficient measures. PBS controls were also included for the first time as a higher translational hurdle and a more consistent comparator, than potentially variable GFP expressing viral preparations.

Using a variety of modern AAV vectors and routes murine IL-10 could not be shown to suppress EAU or EIU over a wide range of dose. Species differences were addressed by using viral and human IL-10, but again these did not obviously suppress disease. To obtain a strong positive control, recombinant human IL-10 was used in EIU with success. Using ShH10-CMV-human IL-10, levels known to suppress EIU were matched and confirmed by ELISA. No reduction in cell count was seen, implying that either the delivery mechanism of AAV, or the dynamics of IL-10 production in the intraocular environment could be responsible for the difference. Future experiments to address this issue could involve injecting GFP and hIL-10 expressing vectors prior to the induction of EIU with simultaneous administration of 200ng recombinant human IL-10. This dose is known to suppress EIU and so if suppression is no longer seen in the GFP control, then the presence of AAV is responsible. If only seen in the hIL-10 expressing vector, it would be more likely due to induction of a refractory state to the effects of IL-10.

Strong evidence for the therapeutic effect of IL-10 in the effector phase of EAU is lacking and our data using AAV-derived and recombinant IL-10 further support this assertion. In other models of autoimmune disease, close examination of the literature reveals that several therapeutic IL-10 studies have demonstrated a lack of effect or even worsening of inflammation.[222] This is probably an under-representation due to publication bias towards positive results and may go some way towards explaining the striking failure

of clinical trials using recombinant IL-10.[223] It is perhaps not surprising that IL-10 is complexly regulated as a result of many millennia of evolution, to counter the known hijack of IL-10 by viruses and parasites.

Significant suppression is clearly affected by dose, route of administration, timing of intervention in the disease course and the target tissue. [222] It looks likely that IL-10 is capable of blocking initial systemic T-cell activation through reduced MHCII and co-stimulation on APCs. This appears to be the mechanism through which systemic IL-10 has an effect in prophylactic treatment of animal models and is the case in EAE when disease is induced by subcutaneous immunisation.[224] Adoptive transfer models of EAE, where T-cells are already activated, fail to reduce and show a trend to worsen when recombinant hIL-10 is given at any stage.[225] Much of our basic understanding of IL-10 arises from genetically deficient mice so at disease initiation there is already an effect upon antigen presentation. Further use of conditional knockout lines will clarify the exact action of IL-10 in the effector phase, with one study showing attenuated EAE following T-cell specific deletion of the IL-10 receptor.[226] Target tissue may prove critical as in rheumatoid arthritis models; IL-10 appears to cause almost universal suppression, unlike the eye or CNS.[223]

In work using EAU, transgenic lines expressing IL-10 under either T-cell (CD2 and IL-2) or macrophage (CD68) promoters, initiation was attenuated through reduced antigen presentation to naïve T-cells.[227] However, *IL-10*$^{-/-}$ mice show a strong trend towards reduced disease severity. Recombinant IL-10 could also inhibit EAU initiation, but no data upon intervention was shown, suggesting the absence of effect.[126]

Our experiments using IL-10 appeared to be highly variable. ShH10-vIL-10 and ShH10-hIL-10, achieved suppression to a significant (and substantial) level in an experiment each, but the second-time did not show the effect to be repeatable. This is unlikely to be due to normal inter-experiment variation, and could be explained more by a narrow therapeutic window or small effect size. The improved methods of analysis and extra PBS controls, in concert

with this narrow window, may explain the previous work showing suppression. It is possible a change in systemic immune responses due to undetected parasitic infection or microbiome changes, could explain differences between cohorts of mice being alternately responsive and apparently refractory to IL-10.

Interestingly, following high-level expression of human IL-10 from subretinal injection of ShH10, a significant increase in intraocular CD8+ cells was seen. This was not present in the control group. These may be cytotoxic T-cells functioning in an anti-viral response, though this was not observed with subretinal AAV8-IL-10. IL-10 however has been shown to stimulate the proliferation and activation of effector CD8+ T-cells and the high levels may have contributed to the local increase in cell number.[228]

Future work could trial the use of hIL-10 under an inflammation-inducible promoter such as NFκB. There is some evidence that regulated expression might lead to different effects. Enhanced pancreatic islet destruction in the NOD mouse was seen when transgenic IL-10 was constitutively expressed, but a mild protective effect was seen when IL-10 was placed under the control of the IL-2 promoter in T-cells.[229]

EAU as a more complex disease model may not be as likely to suppress with one agent alone, albeit one as pleiotropic as IL-10. It is clearly important in uveitis pathogenesis, evidenced by the association with genetic polymorphisms in the IL-10 promoter.[117] The potentially narrow therapeutic window and multiplicity of variables involved in successful deployment of this target will however make translation difficult. Considering the current data, it is probably prudent to pursue other transgenes as gene therapy for uveitis.

9.5 Local inhibition of TNF by p75-Ig may have a mild effect upon EAU

Targeting TNF is a common approach to many autoimmune diseases including uveitis. Monomeric soluble TNF-receptors p55 and p75 were

already available within the lab and so they chosen for delivery by gene transfer but shown to have either no effect, or to even worsen the infiltration of CD11b+Ly6C+ cells in EAU. These findings led to a reappraisal of evidence and *in vitro* testing, which highlighted the inferior efficacy of monomeric soluble p75 compared to its Ig-fusion dimer. Extrapolating from published work, it is possible that soluble TNF receptors may actually stabilise and buffer the formation of active TNF trimers, except at very high doses.[130] Returning to *in vitro* investigation, the p75-Ig construct was shown to functionally inhibit the effects of TNF. Despite this, no clear evidence of the suppression of EAU could be seen.

TNF inhibitors are now widely used in clinical practice for uveitis and have been shown to be effective when administered systemically.[15] In many patients however, they are not sufficient and disease remains uncontrolled. Formulations include Adalimumab, a humanised monoclonal IgG1 antibody and Etanercept, a dimeric Ig-fusion protein of the human p75 TNF receptor. Whilst both successfully treat rheumatoid arthritis, evidence is emerging that Etanercept is less effective than Adalimumab in uveitis and granulomatous inflammation.[230] This is thought to result from the different way TNF is neutralised, with less stable binding of Etanercept to TNF trimers. [231] In this project, mouse p75-Ig fusion dimer was used, which would be closer to Etanercept in its action than Adalimumab. Any underlying idiosyncratic effect specific to TNF inhibition in uveitis, might have affected the ability of p75-Ig to suppress EAU. In retrospect, a construct based upon Adalimumab, human p55-Ig or newer generation antibodies specific to transmembrane or soluble forms of TNF such as XPro1595 might have been preferable.[129] These are commercially sensitive however and their coding sequences are undisclosed, so they were unavailable for use.

Whilst systemic blockade of soluble TNF alone clearly appears to attenuate EAU and cellular infiltration into the eye, local inhibition requires both soluble and transmembrane TNF neutralisation.[129] Even then the magnitude of suppression appears to be small. Most reports suggest that infiltration is only mildly affected, whilst common to most is the delayed onset and reduction in

structural damage mediated through macrophage activation.[133,201] Some groups have reported successful therapy of EAU with prophylactic local non-viral expression of human p55-Ig from the ciliary muscle in the rat.[60] Others used intravitreal Etanercept in the afferent phase of EAU, which results in a marginal reduction in severity.[232] No suppression was seen however when given in the efferent phase, after the establishment of EAU. This potentially bodes poorly for anti-TNF therapy as a local treatment, as all human intervention would occur in established disease only. It could equally prove a limitation of the animal model itself however, as TNF inhibition might be still effectively used during remission to prevent cycles of relapse instead, as seen in human uveitis. This cannot be modelled and thus detected in EAU.

Some reports have shown systemic TNF inhibition to worsen infiltration in systemically induced EIU.[199] Certainly it is possible for TNF inhibitors to cause potential toxicity and worsen infiltration, as seen in the small number of eyes injected with recombinant human p55-Ig in this project. Elevated TNF transcripts in the RPE, iris and ciliary body were identified during intravitreally induced EIU suggesting its pathogenic importance. Other groups however have shown suppression with both systemic administration of Etanercept[176] and local inhibition of TNF by p55-Ig expressed from the ciliary muscle in EIU.[107] These discrepancies highlight more difficulties and variables involved in targeting TNF, even when attempting to suppress a relatively simple model of ocular inflammation.

In aggregate the studies may partly explain why suppression of EAU was not achieved. Local inhibition of TNF in EAU may not be efficacious, as the site of peripheral activation in the immunised skin and draining lymph nodes will be untreated and T-cells continue to be activated. It may be that the dose of p75-Ig was too low, as near complete neutralisation of TNF might be required for any effect even if suppression in the efferent phase can occur. A key action of TNF is to degrade the blood-retinal barrier partly by acting on endothelial cells, so if cells are already activated and infiltrated, then the effects of inhibition are limited to preventing macrophage activation. This reduction may not be sufficient or widespread enough to counter the damage

from simultaneous, widespread infiltration of peripherally activated cell types. It may be effective as mentioned however, to maintain remission between active episodes, if used in a more faithful animal model of human uveitis that has repeated cycles of activation.

9.6 The NFκB-motif promoter drives inflammation-responsive transcription in proportion to the severity of EAU

Initial investigation used the IRF1-promoter as a dual response enhancer, as it had been characterised as responsive to both NFκB and IFNγ signaling.[162] Whilst NFκB activation triggered by recombinant TNF caused a response in proportion to the number of copies, no response at all could be obtained using a range of doses of IFNγ from two different suppliers. The relative change compared with baseline expression was higher using a pure five-repeat NFκB-motif fused to the minimal SV40 promoter and so this construct was taken forward.

Delivered in AAV8 and driving the expression of GFP, it was first confirmed that *in vitro* activation of the promoter occurred in response to TNF, a pro-inflammatory cytokine known to be critical in EAU. *In vivo* examination revealed minimal activation following subretinal injection itself, with eyes remaining free of GFP signal for over 33 days. At peak EAU, expression of GFP is seen in the RPE consistent with the well-known presence of NFκB signalling in this cell type.[233] AAV8 transduces photoreceptors efficiently, but only rarely were seen to express GFP in each eye. Evidence in the literature is scant and does not unequivocally support the presence of canonical NFκB signaling in photoreceptors. It is likely that these occasional transduced cells could represent low-level contamination with AAV8-CMV-GFP from the production process. It is also possible that lower levels of transcription from the NFκB-motif promoter, combined with less genome copies of AAV transducing photoreceptors compared to RPE, could lead to below detection levels of GFP.

The NFκB-motif promoter, apparently restricted to RPE only, appears to generate lower levels of GFP compared to the CMV promoter. Whilst the NFκB-motif promoter is undoubtedly weaker, this could be compounded as RPE cells are less numerous than photoreceptors. The positive findings however, are that the NFκB-motif promoter is not active in the absence of inflammation and when it is triggered, the degree of transcription appears to be directly proportional to the severity of disease. Uniquely, this was demonstrated with flow cytometry upon matched tissues from the same eye, analysing the RPE for GFP signal and other ocular tissues for infiltrating CD45+ leukocytes known to be responsible for disease pathogenesis in EAU. It has been reported that AAV may use non-canonical NFκB signalling in its life cycle, as levels increase following infection and inhibition prevents AAV-mediated gene expression *in vitro*.[181] Our construct would be expected to respond to non-canonical signalling, though this is usually at a lower level than fast IκB-complex mediated signals.[234] It is possible that the NFκB requirement is only during initial infection and so any signal would be missed by the two-week baseline.

This is the first intrinsic inflammation-regulated promoter to be used with gene therapy in the eye. Similar promoters have been used in other organ systems, but the same degree of assessment is not possible and *ex vivo* histology is required.[96,235] The eye is suited to *in vivo* monitoring and baseline, peak and post-peak responses could be repeatedly gauged for the same eye. One group looking at an animal model of rheumatoid arthritis used repeated invasive sampling of articular fluid and ELISA for the transgene product.[94] This could detect responses to stimulation, but the procedure may in itself have contributed to the inflammation.

The CMV promoter has been reported to be silenced following delivery by AAV in different tissues and in response to inflammation.[236]
Whilst not designed specifically to address this question, a marked reduction in GFP signal was not observed in RPE during the presence of EAU after subretinal delivery of AAV8-CMV-eGFP.

The NFκB-motif promoter was not employed in any therapeutic experiments to suppress EAU. This was due to the absence of a robust therapeutic target, with both IL-10 and soluble TNF-receptors failing to suppress disease under the constitutive CMV promoter. It was intended that once a treatment had been established, it could be tested to see if the therapeutic effect was maintained or enhanced under a responsive promoter. In terms of future work, it may be that for some targets such as IL-10, only regulated production will result in successful suppression.[222] It is likely however that using a different therapeutic transgene, effective under both constitutive and regulated expression would be more robust and likely to translate to clinical therapy.

The NFκB-motif promoter driving the expression of eGFP was used as a reporter to assess the activation status of the RPE during the post-peak stages of EAU. Whilst possible that the promoter fails to deactivate, it is more likely that as has been increasingly suspected, there is no true resolution of inflammation and so continued NFκB signaling in the RPE.[24] It is not known if NFκB activation at this point results in pro-inflammatory cytokine synthesis, as NFκB could be equally involved in proliferative, survival or angiogenic stimuli.[105] Future work will use small molecule NFκB inhibitors and activators to delineate the capacity to terminate transcription from the promoter. The approach of *in vivo* monitoring using this promoter could be deployed in other models such as laser-induced CNV and models of dry AMD or retinal degenerations, to assess the localization and magnitude of RPE activation.

9.7 Reconciling the failure to suppress intraocular inflammation and implications to future gene therapy for uveitis

During this project, modern AAV serotypes such as AAV9, AAV8 and ShH10 were used to overexpress IL-10 variants and block TNF with soluble TNF-receptors in uveitis models. The assumption was that faster onset and higher levels of therapeutic transgene compared to AAV2 would only improve efficacy. No other studies to date have used these vectors for modulation of

intraocular inflammation. Novel readouts such as OCT for EAU and flow cytometry for EIU were used alongside traditional measures to improve the reliability and detection of therapeutic suppression. Unfortunately the suppression seen in previous published literature with lentivirus and AAV2 could not be achieved using these modern serotypes.[34,93,110]

There are many possible reasons why previous results could not be replicated or matched using modern AAV serotypes. It is possible that the attenuation in disease previously seen was small in magnitude and with more objective readouts is not repeatable. The use of IL-10 as examined in current work, is affected by many variables and has a narrow therapeutic window, so prior positive results might have occurred by chance. There could also be confounding features specific to modern AAV serotypes themselves.

9.7.1 Vectors

Modern serotypes efficiently infect cell types that AAV2 could not. Perhaps uniquely perturbing and activating cells such as Muller glia resulted in a greater pro-inflammatory stimulus than the degree of suppression by encoded transgenes. High levels of viral expression and corresponding levels of cellular transcriptional stress may themselves potentially have an adverse effect upon the inflammatory environment, though techniques to determine this are likely to be imprecise. Support for this hypothesis comes from the observation that in many cases GFP-expressing vectors showed worsened disease than PBS injected controls. Given potential worsening with GFP vector alone, the absence of PBS or uninjected controls as in several previous studies could result in the misinterpretation of suppression from an interventional vector that is transcriptionally less efficient.

It could be envisaged that the use of new serotypes such as ShH10 would be beneficial by avoiding retinal detachment. This is known to be inflammatory and for several weeks results in photoreceptor dysfunction as measured by ERG.[179,180] The reduced trauma may have been countered though by the increased likelihood of adaptive systemic responses to intravitreally delivered

AAV.[77] Any response to ocular transduction by AAV is likely to be additionally dependent upon coincident innate stimuli such as endotoxin.[92]

9.7.2 Dose

It is hard to draw direct comparisons of dose as no other studies showed matched *in vivo* levels of transgene product. One showed protein levels of AAV2 delivered IL-4 by ELISA during treatment, but without data from any control group, so it is hard to ascertain what the background level was and therefore the degree of elevation.[113] In one study reporting successful attenuation of EAU with AAV2, ELISA upon eyes without disease did not show a statistically significant elevation in murine IL-10 levels.[110] If this truly caused suppression, then the implication is that a near undetectable level of elevation is required. As significantly increased levels were confirmed in present experiments using modern serotypes, this could explain the lack of disease attenuation.

To address one aspect of dosage the positive control of human recombinant IL-10 was used in the EIU model. Exact levels were matched between recombinant protein and ShH10-delivered IL-10 after 6hrs. No inhibition was seen with virally mediated IL-10 delivery at doses that did show inhibition using recombinant protein. Either a direct effect of the presence of AAV or the dynamics of IL-10 administration are likely to be responsible. For example, if microglia are a key target of IL-10 induced suppression by preventing chemokine release, then prior activation through a response to AAV might render them insensitive to deactivation.

A future experiment could be to inject AAV8 or ShH10 carrying GFP and IL-10 one week before EIU induction and simultaneous administration of a dose of recombinant human IL-10 known to suppress disease. If suppression is no longer achieved, the effects of either prior AAV transduction or tolerance to persistently elevated levels of IL-10 might be distinguished. It will also be worthwhile to re-visit non-viral methods of gene transfer to examine if these effects are confined to delivery by vectors such as AAV.

9.7.3 Therapeutic transgenes

In view of the present findings, it appears that neither IL-10 nor TNF inhibitors are ideal therapeutic transgenes for several aforementioned reasons and success may have been achieved by delivering other targets. The data obtained suggests that murine IL-10 is ineffective in EIU, in contrast to human IL-10. This difference makes is hard to reconcile many published studies and may go some way to explaining the mixed results seen using different species of IL-10 interchangeably in approaches across multiple organ systems.[223,225,226] Whilst systemic TNF inhibition clearly affects the recruitment of infiltrating cells, it is less firmly established whether local inhibition will suppress disease. If it does the degree of suppression is likely to be small.[187] It may be that other methods of neutralising TNF in the eye are required, such as with encoded recombinant antibody F_{ab} domains or the p55-Ig fusion protein, as it will have a greater effect upon soluble TNF.

Future work should consider other targets that ideally are beneficially pleiotropic, effective at low levels, but with a wide therapeutic window. IL-27 appears to be one such target and has been effectively used to treat EAU expressed from AAV2, but it is unusual that no further progress towards clinical trial has been forthcoming.[114] Combining targets is an appealing strategy and was intended once effective transgenes had been identified. Given that none reliably performed it was not felt appropriate to empirically attempt combination of different vectors.

9.7.4 Local versus systemic therapy

The gene therapy approach in uveitis relies upon the assumption that local modulation of the immune environment can treat disease, deactivating, killing or preventing initial entry of infiltrating cells. Systemic TNF inhibition and IL-10 have been shown to inhibit disease when given prior to the initiation of *C57BL/6* EAU, though this is likely due to prevention of induction and down-regulation of peripheral antigen presentation. In the effector phase of disease, local therapy with IL-10 has not convincingly been shown to prevent tissue damage in EAU.

Local ocular TNF inhibition with Etanercept has a very mild protective effect upon *C57BL/6* EAU in the afferent phase. This is possibly due to pre-conditioning and preventing subsequent blood-retinal barrier degradation as no effect is seen when delivered in the efferent phase when cells have already entered the eye.[232] Gene delivery when tested in this project however was given prophylactically so expression was occurring in the afferent phase of EAU, and the possibility to suppress disease should have existed.

A strong local mechanism action for any successful future target transgene may be required, particularly as T-cells that are already activated can be resistant to IL-10 and other forms of suppression.[222] A more effective treatment might involve triggering an anergic state or cell death in infiltrating activated cells. Fas ligand might serve this function and was considered, though not trialled as there is evidence of the Fas receptor expression on normal ocular tissues.[237] Another alternative target could be CD200, a member of the immunoglobulin superfamily expressed ubiquitously by neurons including those in the retina. The CD200 receptor (CD200R), in contrast, is restricted to cells of the myeloid lineage and likely contributes to the immune-privilege of the eye. Ligation of CD200R acts to deliver a constitutive inhibitory signal on retinal microglial cells, preventing the induction of NOS and IL-6 in response to IFNγ. An agonist antibody to CD200R has been used successfully to delay and attenuate murine EAU in the effector phase. Conceivably, a strategy to overexpress CD200 across the retina could decrease the activation of resident and infiltrating myeloid cells to reduce disease, even once established.

Even local modulation by IL-10 or TNF inhibition might work if the target organ (i.e. the eye) were the site of primary or even secondary antigen presentation. In terms of human and mouse biology, this is still a contentious issue. Regardless the choice of experimental model could be critical if this were the case, as inducible models in the *C57BL/6* and *B10.RIII* strains will undergo antigen presentation artificially in the inguinal lymph nodes when

typically subcutaneous injected. With an established reservoir of antigen presentation in the periphery, even an reasonably effective local therapy might soon be overwhelmed by the constant flow of cells from such a peripheral site of activation.

9.7.5 Animal models

Using a spontaneous model of EAU could enable local gene therapy to be effective if the primary site of antigen presentation is in the eye, such as IRBP promoter-HEL transgenic mice.[22] In this instance IL-10 and TNF blockade might prevent initiation of disease. Whether this will ultimately translate to humans with pre-existing pathology though is debatable but slowly being clarified through the use of spontaneous mouse models transgenic for RBP-3 as found in human uveitis.[23]

Pertussis toxin is used in most inducible models of EAU, but publications suggest it may have long-lasting underappreciated effects upon T-cell polarisation and activation that could render them resistant to subsequent modulation and suppression.[238] One group reporting successful modulation of EAU with AAV2 used the *B10.RIII* strain, which they were able to induce without pertussis toxin. This is a difference that could explain why suppression in the *C57BL/6* model has not been possible.

9.7.6 Immune privilege and implications for ocular gene therapy

The identified trends for worsening inflammatory disease scores even in GFP control vector treated eyes, raises the possibility that trauma from the route of delivery or the vector itself, could abrogate the constitutive immune privilege of the eye and immune deviation mechanisms. Precedence arises from work looking at ACAID, which is lost in the contralateral eye following even the relatively mild stimulus of a retinal laser burn.[239] Further experiments to look at worsening of contralateral disease and loss of immune privilege following AAV-mediated gene delivery, could have implications for the expanding number of trials for ocular diseases affected by inflammation, such as diabetic retinopathy and choroidal neovascularization.

9.8 Conclusion

This project has highlighted the complexity of using viral-mediated gene transfer to suppress intraocular inflammation. Perhaps it is unsurprising that the eye is potentially hostile to the presence of viral vectors, as many viruses such as CMV, Herpes simplex and Varicella zoster are all evolutionarily well-established ocular pathogens. In a similar manner, microbes are engaged in a continuing battle to overcome the immune system often subverting targets such as the IL-10 pathway. Again the eye may have evolved tight regulatory mechanisms that make intervention challenging. Few other local approaches for chronic uveitis are upon the horizon and emerging systemic therapies still require long-term administration and have numerous side effects. Gene therapy for uveitis is still a promising goal but as this project has demonstrated, several hurdles remain and further work will be needed to resolve the many variables and factors impeding progress towards clinical trial.

10 Figure and table titles

- Table 1. Common mouse models of inducible and spontaneous experimental autoimmune uveoretinitis.
- Table 2. Immunological cell surface markers used in flow cytometry of mouse EAU
- Table 3. Comparison of the different methods of gene transfer used in ocular gene therapy
- Table 4. A comparison of gene therapy against other treatment approaches for uveitis.
- Table 5. Inflammation-regulated promoters published for use in gene therapy.
- Table 6. Published preclinical studies of gene therapy for uveitis.
- Table 7. Oligonucleotides synthesised by Sigma Aldrich
- Table 8. Primary antibodies used in immunohistochemistry.
- Table 9. Primary conjugated antibodies used for flow cytometry.
- Table 10. Range and processing of final OCT scores.
- Table 11. Endotoxin status of several vectors, reagents and equipment used for AAV production in the lab.
- Table 12. A summary of benefits and limitations of the novel OCT scoring system compared to conventional assessment of EAU.
- Table 13. Advantages and disadvantages of EIU assessment by flow cytometry compared to traditional histological analysis.

- Figure 1. Immunological mechanisms of initiation and effector pathways active in the inducible EAU model.
- Figure 2. Schematic of recombinant AAV.
- Figure 3. Strategy of viral vector-mediated gene therapy for uveitis.
- Figure 4. TNF forms and their binding receptors.
- Figure 5. An anatomical comparison between an OCT optical section and histology.
- Figure 6. Pilot OCT images of mouse EAU and matched TEFI photographs.
- Figure 7. Vitreous condensation at the interface between the posterior hyaloid face and inner retinal surface is consistent with clinical vitritis.
- Figure 8. EAU induces distinct optic nerve head changes on OCT.
- Figure 9. OCT imaging and matched histology identify deep retinal structural changes and an associated cellular infiltrate.
- Figure 10. OCT identifies vascular changes in EAU with appearances altered by depth and degree of infiltration.
- Figure 11. OCT imaging assists the identification and characterisation of novel features developed during the EAU model.

- Figure 12. OCT can track the development of tissue changes over time during the course of EAU.
- Figure 13. An example of the standard scoring series.
- Figure 14. A worked example of the OCT-based scoring system.
- Figure 15. OCT-based scoring correlates well with established measures.
- Figure 16. The OCT-based scoring system was validated in an interventional experiment.
- Figure 17. The scotopic electroretinogram shows reduced b-wave amplitude during *C57BL/6* EAU, but this may be a result of the induction protocol.
- Figure 18. OCT can detect pathology during the severe form of EAU induced in the *B10.RIII* mouse strain.
- Figure 19. Characterisation of EIU using quantitative flow cytometry.
- Figure 20. Composition of the infiltrate in EIU can be distinguished by flow cytometry whilst qPCR on matched tissues can assess the transcription of multiple chemokines.
- Figure 21. Compartmental sub-analysis of the EIU model is possible using flow cytometry.
- Figure 22. Examples of flow cytometry applied to interventional EIU experiments.
- Figure 23. Alterations leading to the refined AAV production process.
- Figure 24. Intravitreal and subretinal delivery of ShH10 lead to different patterns of cell transduction in the adult mouse.
- Figure 25. Endotoxin positive AAV8 leads to acute neutrophil infiltration, but no changes in transgene expression.
- Figure 26. Histological differences are evident between responses to intravitreal and subretinal delivery of endotoxin.
- Figure 27. Spiking ShH10-CMV-eGFP with endotoxin does not overtly affect the extent or type of retinal cells expressing GFP.
- Figure 28. An enrichment of genome-containing capsids is possible using Sepharose Q_{XL} medium and AAV5.
- Figure 29. The genome-containing-capsid enrichment process using a Sepharose Q_{XL} column is not able to separate full and empty AAV8 capsids.
- Figure 30. High dose systemic Dexamethasone at the time of subretinal injection does not alter the degree of EIU induced a week later.
- Figure 31. No systemic antigen-specific immune responses are detected after EAU induction following subretinal delivery of AAV8.
- Figure 32. Subretinal Lentivirus-mIL-10 delivery provides support for the successful secretion of transgene product from RPE into retina and vitreous.
- Figure 33. Polarised human ES and iPS-derived RPE confirm apical secretion of murine IL-10 and p75-Ig protein following ShH10 transduction.
- Figure 34. Local parameters of the *C57BL/6* EAU model.
- Figure 35. The effect of EAU upon AAV transduced retina.

- Figure 36. AAV9 mediated expression of *mIL-10* leads to increased severity of EAU and associated retinal cell loss.
- Figure 37. The AAV9-mIL-10 vector induces dose-dependent retinal changes and T-cell infiltration.
- Figure 38. Refined production process AAV8-CMV-mIL-10 still fails to suppress EAU.
- Figure 39. Intravitreal injection of ShH10-viral IL-10 during established EAU does not change final disease outcome.
- Figure 40. Subretinal administration of AAV8-CMV-mIL-10-IRES-eGFP does not affect EIU.
- Figure 41. Murine *IL-10* expressed from different AAV serotypes fails to suppress EIU at any dose achieved.
- Figure 42. Intracameral Lentivirus expressing murine *IL-10* attenuated AC cell counts only during EIU when analysed by flow cytometry.
- Figure 43. The experimental repeat and addition of a PBS control demonstrates no significant suppression of EIU by Lenti.*mIL-10*, despite detection of elevated mIL-10 protein levels in the eye.
- Figure 44. ShH10 delivered viral IL-10 does not reliably suppress EIU.
- Figure 45. Unlike recombinant murine IL-10, human IL-10 suppresses EIU in a dose-dependent manner.
- Figure 46. ShH10-mediated transfer of mouse, human or viral *IL-10* does not suppress EIU at 18-hours following injection one-week prior.
- Figure 47. A comparative timecourse of recombinant protein demonstrates comparable levels at 18-hours post injection to ShH10-derived human IL-10 in the eye.
- Figure 48. ShH10-derived human IL-10 suppresses EIU at the 6-hour timepoint, with corresponding reduction in key neutrophil chemokines.
- Figure 49. Repeat experiment of ShH10-human IL-10 with additional controls fails to reproduce the suppression of EIU at the 6hr timepoint.
- Figure 50. Levels of human IL-10 comparable to suppressive recombinant protein doses can be obtained using subretinal ShH10, but no therapeutic effect is seen upon EIU. Furthermore, a local infiltration of CD8+ cytotoxic T-cells is detected.
- Figure 51. Extending the time to three weeks following intravitreal injection of ShH10-human IL-10 achieves higher transgene levels, but still does not suppress EIU.
- Figure 52. Repeat of AAV2 mediated delivery of *mIL-10* with the addition of flow cytometric analysis fails to reproduce the reported suppression.
- Figure 53. Administration of intravitreal recombinant human IL-10 at peak EAU fails to suppress EAU.
- Figure 54. TNF-licenced nitric oxide synthetase induction in myeloid cells during EAU leads to detectable nitrotyrosine residues and structural damage.
- Figure 55. AAV8 expression of soluble p55 monomeric receptor does not affect infiltration or CD4 polarisation in EAU compared to GFP control.

- Figure 56. Expression of p75 fails to suppress EAU and increases the number of CD11b+Ly6C+ cells in the eye.
- Figure 57. eGFP compared with hrGFP expression does not significantly alter the severity of EAU and the presence of an IRES-GFP segment does not markedly reduce the level of the preceding transgene.
- Figure 58. Prophylactic ShH10 mediated expression of monomeric p55 receptor does not affect infiltration in EAU compared to GFP control, despite detectably elevated levels in the tissue.
- Figure 59. ShH10 expression of monomeric p55 receptor does not affect EIU at double the control level.
- Figure 60. Administration of recombinant human p55-Ig at the induction of EIU leads to retinal haemorrhage and worsened infiltration.
- Figure 61. WEHI-164 cytotoxicity assays confirm the neutralising effect of p75-Ig *in vitro* and the negligible action of monomeric p75.
- Figure 62. Prophylactic p75-Ig expression from subretinal delivery of AAV8 fails to suppress histological EAU scores.
- Figure 63. Prophylactic intraocular p75-Ig expression fails to suppress disease in the *B10.RIII* model of EAU.
- Figure 64. Interventional p75-Ig expression by ShH10 trends towards a mild reduction of structural changes in EAU.
- Figure 65. Schematics of Luciferase plasmids to test inflammation-responsive promoters.
- Figure 66. IFNγ-receptor 1 was identified on Muller cells but the IRF1 promoter construct fails to respond to IFNγ.
- Figure 67. The NFκB-motif promoter rapidly responds in a dose-dependent manner, with low background activity and a detectable decrease in activity after withdrawal of stimulation.
- Figure 68. HEK-293T cells infected with AAV8-NFκB-eGFP *in vitro* respond to stimulation by TNF.
- Figure 69. Unlike the CMV promoter, which is constitutively active, the NFκB-promoter only leads to expression following the induction of EAU.
- Figure 70. Flow cytometry of GFP signal and CD45+ cell infiltration confirms activation the NFκB-motif promoter in proportion to the degree of inflammation caused by EAU.
- Figure 71. The NFκB-GFP construct confirms the presence of persistent inflammatory activity in the eye at timepoints classically labelled as resolved disease.
- Figure 72. Despite the limitations of the EIU model its use has not fallen since introduction in 1980.

11 References

1. Jabs, D. A., Nussenblatt, R. B., Rosenbaum, J. T.Standardization of Uveitis Nomenclature (SUN) Working Group. Standardization of uveitis nomenclature for reporting clinical data. Results of the First International Workshop. *American Journal of Ophthalmology.* **140,** 509–516 (2005).
2. Suhler, E. B., Lloyd, M. J., Choi, D., Rosenbaum, J. T. & Austin, D. F. Incidence and prevalence of uveitis in Veterans Affairs Medical Centers of the Pacific Northwest. *American Journal of Ophthalmology* **146,** 890–6.e8 (2008).
3. Durrani, O. M., Meads, C. A. & Murray, P. I. Uveitis: A Potentially Blinding Disease. *Ophthalmologica* **218,** 223–236 (2004).
4. Chiang, Y. P., Bassi, L. J. & Javitt, J. C. Federal budgetary costs of blindness. *Milbank Q* **70,** 319–340 (1992).
5. Gritz, D. Incidence and prevalence of uveitis in Northern California The Northern California Epidemiology of Uveitis Study. *Ophthalmology* **111,** 491–500 (2004).
6. Rathinam, S. R. *et al.* Population-based prevalence of uveitis in Southern India. *British Journal of Ophthalmology* **95,** 463–467 (2011).
7. Acharya, N. R. *et al.* Incidence and Prevalence of Uveitis: Results From the Pacific Ocular Inflammation Study. *JAMA Ophthalmology* 131(11): 1405-1412. (2013).
8. Murphy, C. C. *et al.* Validity of using vision-related quality of life as a treatment end point in intermediate and posterior uveitis. *British Journal of Ophthalmology* **91,** 154–156 (2007).
9. Tomkins-Netzer, O. *et al.* Treatment with Repeat Dexamethasone Implants Results in Long-Term Disease Control in Eyes with Noninfectious Uveitis. *Ophthalmology* 121(8): 1649-1654 (2014).
10. Imrie, F. R. & Dick, A. D. Biologics in the treatment of uveitis. *Current Opinion in Ophthalmology* **18,** 481–486 (2007).
11. Cordero-Coma, M., Yilmaz, T. & Onal, S. Systematic review of anti-tumor necrosis factor-alpha therapy for treatment of immune-mediated uveitis. *Ocular Immunology & Inflammation* **21,** 19–27

(2013).

12. Lee, R. W. J. & Dick, A. D. Current concepts and future directions in the pathogenesis and treatment of non-infectious intraocular inflammation. *Eye (Lond)* **26,** 17–28 (2012).
13. Rothova, A., Berendschot, T. T. J. M., Probst, K., van Kooij, B. & Baarsma, G. S. Birdshot chorioretinopathy: long-term manifestations and visual prognosis. *Ophthalmology* **111,** 954–959 (2004).
14. Tugal-Tutkun, I., Onal, S., Altan-Yaycioglu, R., Huseyin Altunbas, H. & Urgancioglu, M. Uveitis in Behçet disease: an analysis of 880 patients. *American Journal of Ophthalmology* **138,** 373–380 (2004).
15. Sharma, S. M., Nestel, A. R., Lee, R. & Dick, A. D. Clinical Review: Anti-TNFα Therapies in Uveitis: Perspective on 5 Years of Clinical Experience. *Ocular Immunology & Inflammation* **17,** 403–414 (2009).
16. Schewitz-Bowers, L. P., Lee, R. W. & Dick, A. D. Immune mechanisms of intraocular inflammation. *Expert Reviews in Ophthalmology* **5,** 43–58 (2010).
17. Caspi, R. R., Grubbs, B. G., Chan, C. C., Chader, G. J. & Wiggert, B. Genetic control of susceptibility to experimental autoimmune uveoretinitis in the mouse model. Concomitant regulation by MHC and non-MHC genes. *The Journal of Immunology* **148,** 2384–2389 (1992).
18. Silver, P. B. *et al.* Identification of a major pathogenic epitope in the human IRBP molecule recognized by mice of the H-2r haplotype. *Investigative Ophthalmology & Visual Science* **36,** 946–954 (1995).
19. Pennesi, G. *et al.* A humanized model of experimental autoimmune uveitis in HLA class II transgenic mice. *Journal of Clinical Investigation.* **111,** 1171–1180 (2003).
20. Anderson, M. S. *et al.* Projection of an immunological self shadow within the thymus by the aire protein. *Science* **298,** 1395–1401 (2002).
21. Lambe, T. *et al.* CD4 T Cell-Dependent Autoimmunity against a Melanocyte Neoantigen Induces Spontaneous Vitiligo and Depends upon Fas-Fas Ligand Interactions. *The Journal of Immunology* **177,** 3055–3062 (2006).

22. Lambe, T. *et al.* Limited peripheral T cell anergy predisposes to retinal autoimmunity. *The Journal of Immunology.* **178,** 4276–4283 (2007).
23. Horai, R. *et al.* Breakdown of immune privilege and spontaneous autoimmunity in mice expressing a transgenic T cell receptor specific for a retinal autoantigen. *Journal of Autoimmunity.* 44: 21-33 (2013).
24. Boldison, J. *et al.* Tissue-Resident Exhausted Effector Memory CD8+ T Cells Accumulate in the Retina during Chronic Experimental Autoimmune Uveoretinitis. *The Journal of Immunology* **192,** 4541–4550 (2014).
25. Chu, C. J. *et al.* Assessment and in vivo scoring of murine experimental autoimmune uveoretinitis using optical coherence tomography. *PLoS ONE* **8,** e63002 (2013).
26. Horai, R. & Caspi, R. R. Cytokines in Autoimmune Uveitis. *Journal of Interferon & Cytokine Research* 31 (10): 733-744 (2011).
27. Fujino, Y. *et al.* Immunopathology of experimental autoimmune uveoretinitis in primates. *Autoimmunity* **13,** 303–309 (1992).
28. Szpak, Y. Spontaneous retinopathy in HLA-A29 transgenic mice. *Proceedings of the National Academy of Sciences* **98,** 2572–2576 (2001).
29. Mattapallil, M. J. *et al.* The rd8 mutation of the Crb1 gene is present in vendor lines of C57BL/6N mice and embryonic stem cells, and confounds ocular induced mutant phenotypes. *Investigative Ophthalmology & Visual Science* (2012). doi:10.1167/iovs.12-9662
30. Luhmann, U. F. O. *et al.* Differential modulation of retinal degeneration by ccl2 and cx3cr1 chemokine signalling. *PLoS ONE* **7,** e35551 (2012).
31. Rosenbaum, J. T., McDevitt, H. O., Guss, R. B. & Egbert, P. R. Endotoxin-induced uveitis in rats as a model for human disease. *Nature* **286,** 611–613 (1980).
32. Smith, J. R., Hart, P. H. & Williams, K. A. Basic pathogenic mechanisms operating in experimental models of acute anterior uveitis. *Immunology & Cell Biololgy.* **76,** 497–512 (1998).
33. Rosenbaum, J. T., Woods, A., Kezic, J., Planck, S. R. & Rosenzweig,

H. L. Contrasting ocular effects of local versus systemic endotoxin. *Investigative Ophthalmology & Visual Science* **52,** 6472–6477 (2011).

34. Trittibach, P. *et al.* Lentiviral-vector-mediated expression of murine IL-1 receptor antagonist or IL-10 reduces the severity of endotoxin-induced uveitis. *Gene Therapy* **15,** 1478–1488 (2008).
35. Egwuagu, C. E., Charukamnoetkanok, P. & Gery, I. Thymic expression of autoantigens correlates with resistance to autoimmune disease. *The Journal of Immunology.* **159,** 3109–3112 (1997).
36. Sakaguchi, S., Miyara, M., Costantino, C. M. & Hafler, D. A. FOXP3+ regulatory T cells in the human immune system. *Nature Reviews Immunology* **10,** 490–500 (2010).
37. Caspi, R. R. *et al.* Mouse models of experimental autoimmune uveitis. *Ophthalmic research* **40,** 169–174 (2008).
38. Caspi, R. R. A look at autoimmunity and inflammation in the eye. *Journal of Clinical Investigation.* **120,** 3073–3083 (2010).
39. Raveney, B. J. E., Copland, D. A., Calder, C. J., Dick, A. D. & Nicholson, L. B. TNFR1 signalling is a critical checkpoint for developing macrophages that control of T-cell proliferation. *Immunology* **131,** 340–349 (2010).
40. Xu, H. *et al.* A clinical grading system for retinal inflammation in the chronic model of experimental autoimmune uveoretinitis using digital fundus images. *Experimental Eye Research.* **87,** 319–326 (2008).
41. Kerr, E. C., Copland, D. A., Dick, A. D. & Nicholson, L. B. The dynamics of leukocyte infiltration in experimental autoimmune uveoretinitis. *Progress in Retinal and Eye Research* **27,** 527–535 (2008).
42. Kerr, E. C., Raveney, B. J. E., Copland, D. A., Dick, A. D. & Nicholson, L. B. Analysis of retinal cellular infiltrate in experimental autoimmune uveoretinitis reveals multiple regulatory cell populations. *Journal of Autoimmunity.* **31,** 354–361 (2008).
43. Rose, S., Misharin, A. & Perlman, H. A novel Ly6C/Ly6G-based strategy to analyze the mouse splenic myeloid compartment. *Cytometry* **81A,** 343–350 (2011).
44. Geissmann, F. *et al.* Development of monocytes, macrophages, and

dendritic cells. *Science* **327,** 656–661 (2010).

45. Foxman, E. F. *et al.* Inflammatory mediators in uveitis: differential induction of cytokines and chemokines in Th1- versus Th2-mediated ocular inflammation. *The Journal of Immunology.* **168,** 2483–2492 (2002).
46. Ali, R. R. Ocular gene therapy: introduction to the special issue. *Gene Therapy* **19,** 119–120 (2012).
47. London, A. *et al.* Functional Macrophage Heterogeneity in a Mouse Model of Autoimmune Central Nervous System Pathology. *The Journal of Immunology* 190(7): 3570-3578 (2013).
48. Bainbridge, J. W. B. *et al.* Effect of Gene Therapy on Visual Function in Leber's Congenital Amaurosis. *New England Journal of Medicine* **358,** 2231–2239 (2008).
49. Cideciyan, A. V. *et al.* Human gene therapy for RPE65 isomerase deficiency activates the retinoid cycle of vision but with slow rod kinetics. *Proceedings of the National Academy of Sciences.* **105,** 15112–15117 (2008).
50. Maguire, A. M. *et al.* Age-dependent effects of RPE65 gene therapy for Leber's congenital amaurosis: a phase 1 dose-escalation trial. *The Lancet* **374,** 1597–1605 (2009).
51. Pang, J. *et al.* Efficiency of lentiviral transduction during development in normal and rd mice. *Molecular Vision* **12,** 756–767 (2006).
52. Ali, R. R. *et al.* Gene transfer into the mouse retina mediated by an adeno-associated viral vector. *Human Molecular Genetics* **5,** 591–594 (1996).
53. Buie, L. K. *et al.* Self-complementary AAV virus (scAAV) safe and long-term gene transfer in the trabecular meshwork of living rats and monkeys. *Investigative Ophthalmology & Visual Science* **51,** 236–248 (2010).
54. Natkunarajah, M. *et al.* Assessment of ocular transduction using single-stranded and self-complementary recombinant adeno-associated virus serotype 2/8. *Gene Therapy* **15,** 463–467 (2008).
55. Petrs-Silva, H. *et al.* High-efficiency Transduction of the Mouse Retina by Tyrosine-mutant AAV Serotype Vectors. *Molecular Therapy*

17, 463–471 (2008).

56. Allocca, M. *et al.* Novel Adeno-Associated Virus Serotypes Efficiently Transduce Murine Photoreceptors. *Journal of Virology* **81,** 11372–11380 (2007).
57. Klimczak, R. R., Koerber, J. T., Dalkara, D., Flannery, J. G. & Schaffer, D. V. A novel adeno-associated viral variant for efficient and selective intravitreal transduction of rat Müller cells. *PLoS ONE* **4,** e7467 (2009).
58. Balaggan, K. S. & Ali, R. R. Ocular gene delivery using lentiviral vectors. *Gene Therapy* **19,** 145–153 (2012).
59. de Kozak, Y. *et al.* Inhibition of experimental autoimmune uveoretinitis by systemic and subconjunctival adenovirus-mediated transfer of the viral IL-10 gene. *Clinical & Experimental Immunology* **130,** 212–223 (2002).
60. Kowalczuk, L. *et al.* Local ocular immunomodulation resulting from electrotransfer of plasmid encoding soluble TNF receptors in the ciliary muscle. *Investigative Ophthalmology & Visual Science* **50,** 1761–1768 (2009).
61. Lee, D. J., Biros, D. J. & Taylor, A. W. Injection of an alpha-melanocyte stimulating hormone expression plasmid is effective in suppressing experimental autoimmune uveitis. *International Immunopharmacol.* **9,** 1079–1086 (2009).
62. Rajala, A. *et al.* Nanoparticle-Assisted Targeted Delivery of Eye-Specific Genes to Eyes Significantly Improves the Vision of Blind Mice In Vivo. *Nano Letters* (2014).
63. Bloquel, C. Plasmid electrotransfer of eye ciliary muscle: principles and therapeutic efficacy using hTNF- soluble receptor in uveitis. *The FASEB Journal* 20(2): 389-391 (2005).
64. Liu, M. M., Tuo, J. & Chan, C.-C. Gene therapy for ocular diseases. *British Journal of Ophthalmology* 95(5): 604-612 (2010).
65. Daya, S. & Berns, K. I. Gene Therapy Using Adeno-Associated Virus Vectors. *Clinical Microbiology Reviews* **21,** 583 (2008).
66. Lock, M. *et al.* Characterization of a Recombinant Adeno-Associated Virus Type 2 Reference Standard Material. *Human gene therapy* **21,**

1273–1285 (2010).

67. Nonnenmacher, M. & Weber, T. Intracellular transport of recombinant adeno-associated virus vectors. *Gene Therapy* **19,** 649–658 (2012).
68. McCarty, D. M., Monahan, P. E. & Samulski, R. J. Self-complementary recombinant adeno-associated virus (scAAV) vectors promote efficient transduction independently of DNA synthesis. *Gene Therapy* **8,** 1248–1254 (2001).
69. Reich, S. J. *et al.* Efficient trans-splicing in the retina expands the utility of adeno-associated virus as a vector for gene therapy. *Human gene therapy* **14,** 37–44 (2003).
70. Kaeppel, C. *et al.* A largely random AAV integration profile after LPLD gene therapy. *Nature Medicine* **19,** 889–891 (2013).
71. Rivera, V. M. *et al.* Long-term pharmacologically regulated expression of erythropoietin in primates following AAV-mediated gene transfer. *Blood* **105,** 1424–1430 (2005).
72. Acland, G. M. *et al.* Long-term restoration of rod and cone vision by single dose rAAV-mediated gene transfer to the retina in a canine model of childhood blindness. *Molecular Therapy* **12,** 1072–1082 (2005).
73. Boye, S. E., Boye, S. L., Lewin, A. S. & Hauswirth, W. W. A Comprehensive Review of Retinal Gene Therapy. *Molecular Therapy* **21,** 509–519 (2013).
74. Gao, G. *et al.* Clades of Adeno-Associated Viruses Are Widely Disseminated in Human Tissues. *Journal of Virology* **78,** 6381–6388 (2004).
75. Nayak, S. & Herzog, R. W. Progress and Prospects: Immune Responses to Viral Vectors. *Gene Therapy* **17,** 295 (2010).
76. Barker, S. E. *et al.* Subretinal delivery of adeno-associated virus serotype 2 results in minimal immune responses that allow repeat vector administration in immunocompetent mice. *Journal of Gene Medicine* **11,** 486–497 (2009).
77. Li, Q. *et al.* Intraocular route of AAV2 vector administration defines humoral immune response and therapeutic potential. *Molecular Vision* **14,** 1760–1769 (2008).

78. Mingozzi, F. & High, K. A. Immune responses to AAV in clinical trials. *Current Gene Therapy* **11,** 321–330 (2011).

79. Boutin, S. *et al.* Prevalence of Serum IgG and Neutralizing Factors Against Adeno-Associated Virus (AAV) Types 1, 2, 5, 6, 8, and 9 in the Healthy Population: Implications for Gene Therapy Using AAV Vectors. *Human gene therapy* **21,** 704–712 (2010).

80. Yuasa, K. *et al.* Adeno-associated virus vector-mediated gene transfer into dystrophin-deficient skeletal muscles evokes enhanced immune response against the transgene product. *Gene Therapy* **9,** 1576–1588 (2002).

81. Manno, C. S. *et al.* Successful transduction of liver in hemophilia by AAV-Factor IX and limitations imposed by the host immune response. *Nature Medicine* **12,** 342–347 (2006).

82. Wang, L., Figueredo, J., Calcedo, R., Lin, J. & Wilson, J. M. Cross-presentation of adeno-associated virus serotype 2 capsids activates cytotoxic T cells but does not render hepatocytes effective cytolytic targets. *Human gene therapy* **18,** 185–194 (2007).

83. Willett, K. & Bennett, J. Immunology of AAV-Mediated Gene Transfer in the Eye. *Frontiers in Immunology* **4,** (2013).

84. Faust, S. M. *et al.* CpG-depleted adeno-associated virus vectors evade immune detection. *Journal of Clinical Investigation* 123(7): 2994-3001 (2013).

85. Beutler, B. & Rietschel, E. T. Timeline: Innate immune sensing and its roots: the story of endotoxin. *Nature Reviews Immunology* **3,** 169–176 (2003).

86. Poltorak, A. *et al.* Defective LPS signaling in C3H/HeJ and C57BL/10ScCr mice: mutations in Tlr4 gene. *Science* **282,** 2085–2088 (1998).

87. Gorbet, M. B. & Sefton, M. V. Endotoxin: the uninvited guest. *Biomaterials* **26,** 6811–6817 (2005).

88. Wright, J. F. Manufacturing and characterizing AAV-based vectors for use in clinical studies. *Gene Therapy* **15,** 840–848 (2008).

89. Yi, H., Patel, A. K., Sodhi, C. P., Hackam, D. J. & Hackam, A. S. Novel Role for the Innate Immune Receptor Toll-Like Receptor 4

(TLR4) in the Regulation of the Wnt Signaling Pathway and Photoreceptor Apoptosis. *PLoS ONE* **7,** e36560 (2012).

90. Wang, M., Ma, W., Zhao, L., Fariss, R. N. & Wong, W. T. Adaptive Müller cell responses to microglial activation mediate neuroprotection and coordinate inflammation in the retina. *Journal of Neuroinflammation* **8,** 173 (2011).
91. Shi, G. *et al.* Differential Involvement of Th1 and Th17 in Pathogenic Autoimmune Processes Triggered by Different TLR Ligands. *The Journal of Immunology* **191,** 415–423 (2013).
92. Zinkernagel, M. S., McMenamin, P. G., Forrester, J. V. & Degli-Esposti, M. A. T cell responses in experimental viral retinitis: mechanisms, peculiarities and implications for gene therapy with viral vectors. *Progress in Retinal and Eye Research* **30,** 275–284 (2011).
93. Smith, J. R. *et al.* Tetracycline-inducible viral interleukin-10 intraocular gene transfer, using adeno-associated virus in experimental autoimmune uveoretinitis. *Human gene therapy* **16,** 1037–1046 (2005).
94. Geurts, J. *et al.* Application of a disease-regulated promoter is a safer mode of local IL-4 gene therapy for arthritis. *Gene Therapy* **14,** 1632–1638 (2007).
95. Henningsson, L. *et al.* Disease-Dependent Local IL-10 Production Ameliorates Collagen Induced Arthritis in Mice. *PLoS ONE* **7,** e49731 (2012).
96. Chtarto, A. *et al.* An Adeno-Associated Virus-Based Intracellular Sensor of Pathological Nuclear Factor-κB Activation for Disease-Inducible Gene Transfer. *PLoS ONE* **8,** e53156 (2013).
97. Yang, T. *et al.* Development of an inflammation-inducible gene expression system using helper-dependent adenoviral vectors. *Journal of Gene Medicine* **12,** 832–839 (2010).
98. Khoury, M. *et al.* Inflammation-inducible anti-TNF gene expression mediated by intra-articular injection of serotype 5 adeno-associated virus reduces arthritis. *Journal of Gene Medicine* **9,** 596–604 (2007).
99. Pan, R. Y. *et al.* Disease-inducible transgene expression from a recombinant adeno-associated virus vector in a rat arthritis model.

Journal of Virology **73,** 3410–3417 (1999).

100. Miagkov, A. V., Varley, A. W., Munford, R. S. & Makarov, S. S. Endogenous regulation of a therapeutic transgene restores homeostasis in arthritic joints. *Journal of Clinical Investigation.* **109,** 1223–1229 (2002).
101. Garaulet, G. *et al.* IL10 Released by a New Inflammation-regulated Lentiviral System Efficiently Attenuates Zymosan-induced Arthritis. *Molecular Therapy* **21,** 119–130 (2012).
102. Platanias, L. C. Mechanisms of type-I- and type-II-interferon-mediated signalling. *Nature Reviews Immunology* **5,** 375–386 (2005).
103. Linossi, E. M., Babon, J. J., Hilton, D. J. & Nicholson, S. E. Suppression of cytokine signaling: The SOCS perspective. *Cytokine & Growth Factor Reviews* 24(3): 241-248 (2013).
104. Khera, T. K., Dick, A. D. & Nicholson, L. B. Mechanisms of TNFα regulation in uveitis: Focus on RNA-binding proteins. *Progress in Retinal and Eye Research* **29,** 610–621 (2010).
105. Ruland, J. Return to homeostasis: downregulation of NF-κB responses. *Nature Immunology* **12,** 709–714 (2011).
106. Dick, A. D. *et al.* Control of myeloid activity during retinal inflammation. *Journal of Leukocyte Biology* **74,** 161–166 (2003).
107. Touchard, E. *et al.* Effects of ciliary muscle plasmid electrotransfer of TNF-alpha soluble receptor variants in experimental uveitis. *Gene Therapy* **16,** 862–873 (2009).
108. Verwaerde, C. *et al.* Ocular transfer of retinal glial cells transduced ex vivo with adenovirus expressing viral IL-10 or CTLA4-Ig inhibits experimental autoimmune uveoretinitis. *Gene Therapy* **10,** 1970–1981 (2003).
109. Fang, I.-M. *et al.* Inhibition of experimental autoimmune anterior uveitis by adenovirus-mediated transfer of the interleukin-10 gene. *Journal of Ocular Pharmacology & Therapeutics* **21,** 420–428 (2005).
110. Broderick, C. A. *et al.* Local administration of an adeno-associated viral vector expressing IL-10 reduces monocyte infiltration and subsequent photoreceptor damage during experimental autoimmune uveitis. *Molecular Therapy.* **12,** 369–373 (2005).

111. Tsai, M.-L. *et al.* Suppression of experimental uveitis by a recombinant adeno-associated virus vector encoding interleukin-1 receptor antagonist. *Molecular Vision.* **15,** 1542–1552 (2009).

112. Tian, L. *et al.* AAV2-Mediated Subretinal Gene Transfer of hIFN-α Attenuates Experimental Autoimmune Uveoretinitis in Mice. *PLoS ONE* **6,** e19542 (2011).

113. Tian, L. *et al.* AAV2-Mediated Combined Subretinal Delivery of IFN-α and IL-4 Reduces the Severity of Experimental Autoimmune Uveoretinitis. *PLoS ONE* **7,** e37995 (2012).

114. Shao, J. *et al.* AAV2-Mediated Subretinal Gene Transfer of mIL-27p28 Attenuates Experimental Autoimmune Uveoretinitis in Mice. *PLoS ONE* **7,** e37773 (2012).

115. Chan, C. C. *et al.* Recombinant adenovirus encoding gp100 modulates experimental melanin-protein induced uveitis (EMIU). *Journal of Autoimmunity.* **11,** 111–118 (1998).

116. Asseman, C., Mauze, S., Leach, M. W., Coffman, R. L. & Powrie, F. An essential role for interleukin 10 in the function of regulatory T cells that inhibit intestinal inflammation. *Journal of Experimental Medicine.* **190,** 995–1004 (1999).

117. Atan, D. *et al.* Punctate inner choroidopathy and multifocal choroiditis with panuveitis share haplotypic associations with IL10 and TNF loci. *Investigative Ophthalmology & Visual Science* **52,** 3573–3581 (2011).

118. Tan, J. C., Indelicato, S. R., Narula, S. K., Zavodny, P. J. & Chou, C. C. Characterization of interleukin-10 receptors on human and mouse cells. *Journal of Biological Chemistry.* **268,** 21053–21059 (1993).

119. Moore, K. W., de Waal Malefyt, R., Coffman, R. L. & O'Garra, A. Interleukin-10 and the Interleukin-10 Receptor. *Annual Reviews in Immunology* **19,** 683–765 (2001).

120. Redpath, S., Ghazal, P. & Gascoigne, N. R. Hijacking and exploitation of IL-10 by intracellular pathogens. *Trends in Microbiology* **9,** 86–92 (2001).

121. Saraiva, M. & O'Garra, A. The regulation of IL-10 production by immune cells. *Nature Reviews Immunology* **10,** 170–181 (2010).

122. Pot, C., Apetoh, L. & Kuchroo, V. K. Type 1 regulatory T cells (Tr1) in

autoimmunity. *Seminars in Immunology* **23,** 202–208 (2011).

123. Calder, C. J., Nicholson, L. B. & Dick, A. D. A selective role for the TNF p55 receptor in autocrine signaling following IFN-gamma stimulation in experimental autoimmune uveoretinitis. *The Journal of Immunology* **175,** 6286–6293 (2005).

124. Calder, V. L. *et al.* Increased CD4+ expression and decreased IL-10 in the anterior chamber in idiopathic uveitis. *Investigative Ophthalmology & Visual Science* **40,** 2019–2024 (1999).

125. Sun, B., Sun, S. H., Chan, C. C. & Caspi, R. R. Evaluation of in vivo cytokine expression in EAU-susceptible and resistant rats: a role for IL-10 in resistance? *Experimental Eye Research.* **70,** 493–502 (2000).

126. Rizzo, L. V., Xu, H., Chan, C. C., Wiggert, B. & Caspi, R. R. IL-10 has a protective role in experimental autoimmune uveoretinitis. *International Immunology.* **10,** 807–814 (1998).

127. Dick, A. D., Forrester, J. V., Liversidge, J. & Cope, A. P. The role of tumour necrosis factor (TNF-alpha) in experimental autoimmune uveoretinitis (EAU). *Progress in Retinal and Eye Research* **23,** 617–637 (2004).

128. Bradley, J. R. TNF-mediated inflammatory disease. *Journal of Pathology* **214,** 149–160 (2008).

129. Khera, T. K. *et al.* Tumour necrosis factor-mediated macrophage activation in the target organ is critical for clinical manifestation of uveitis. *Clinical & Experimental Immunology* **168,** 165–177 (2012).

130. Aderka, D., Engelmann, H., Maor, Y., Brakebusch, C. & Wallach, D. Stabilization of the bioactivity of tumor necrosis factor by its soluble receptors. *Journal of Experimental Medicine* **175,** 323–329 (1992).

131. Murphy, C. C., Duncan, L., Forrester, J. V. & Dick, A. D. Systemic CD4(+) T cell phenotype and activation status in intermediate uveitis. *British Journal of Ophthalmology* **88,** 412–416 (2004).

132. Raveney, B. J. E., Copland, D. A., Dick, A. D. & Nicholson, L. B. TNFR1-dependent regulation of myeloid cell function in experimental autoimmune uveoretinitis. *The Journal of Immunology.* **183,** 2321–2329 (2009).

133. Dick, A. D. *et al.* Inhibition of tumor necrosis factor activity minimizes target organ damage in experimental autoimmune uveoretinitis despite quantitatively normal activated T cell traffic to the retina. *Eur. The Journal of Immunology.* **26,** 1018–1025 (1996).

134. Levy-Clarke, G. *et al.* Expert Panel Recommendations for the Use of Anti-Tumor Necrosis Factor Biologic Agents in Patients with Ocular Inflammatory Disorders. *Ophthalmology* 121(3): 785-796 (2013).

135. Rosenbaum, J. T. Future for biological therapy for uveitis. *Current Opinion in Ophthalmology* **21,** 473–477 (2010).

136. Sicotte, N. L. & Voskuhl, R. R. Onset of multiple sclerosis associated with anti-TNF therapy. *Neurology* **57,** 1885–1888 (2001).

137. Wu, L. *et al.* intravitreal tumor necrosis factor inhibitors in the treatment of refractory diabetic macular edema: a pilot study from the Pan-American Collaborative Retina Study Group. *Retina (Philadelphia, Pa.)* **31,** 298–303 (2011).

138. Androudi, S., Tsironi, E., Kalogeropoulos, C., Theodoridou, A. & Brazitikos, P. Intravitreal adalimumab for refractory uveitis-related macular edema. *Ophthalmology* **117,** 1612–1616 (2010).

139. Zhang, X. *et al.* IFN-beta1a inhibits the secretion of Th17-polarizing cytokines in human dendritic cells via TLR7 up-regulation. *The Journal of Immunology* **182,** 3928–3936 (2009).

140. Plskova, J., Greiner, K., Muckersie, E., Duncan, L. & Forrester, J. V. Interferon-alpha: a key factor in autoimmune disease? *Investigative Ophthalmology & Visual Science* **47,** 3946–3950 (2006).

141. Deuter, C. M. E. *et al.* Efficacy and tolerability of interferon alpha treatment in patients with chronic cystoid macular oedema due to non-infectious uveitis. *British Journal of Ophthalmology* **93,** 906–913 (2009).

142. Bodaghi, B. *et al.* Efficacy of interferon alpha in the treatment of refractory and sight threatening uveitis: a retrospective monocentric study of 45 patients. *British Journal of Ophthalmology* **91,** 335–339 (2007).

143. Onal, S. *et al.* Long-term Efficacy and Safety of Low-Dose and Dose-Escalating Interferon Alfa-2a Therapy in Refractory Behcet Uveitis.

Archives of Ophthalmology. **129,** 288 (2011).

144. Kertes, P. J., Britton, W. A. & Leonard, B. C. Intravitreal interferon alpha-2b for the treatment of neovascular age-related macular degeneration: a pilot study. *Canadian Journal of Ophthalmology.* **32,** 185–188 (1997).
145. Porter, R. Uveitis in association with multiple sclerosis. *British Journal of Ophthalmology* **56,** 478–481 (1972).
146. Becker, M. D. Interferon as a treatment for uveitis associated with multiple sclerosis. *British Journal of Ophthalmology* **89,** 1254–1257 (2005).
147. Wong, J., Gomes, T., Mamdani, M., Manno, M. & O'Connor, P. W. Adherence to multiple sclerosis disease-modifying therapies in Ontario is low. *Canadian Journal of Neurological Sciences.* **38,** 429–433 (2011).
148. Shih, C.-S. *et al.* AAV-mediated local delivery of interferon-beta for the treatment of retinoblastoma in preclinical models. *Neuromolecular Medicine.* **11,** 43–52 (2009).
149. Hu, D.-N. *et al.* Interleukin-1{beta} increases baseline expression and secretion of interleukin-6 by human uveal melanocytes in vitro via p38 MAPK/NF-{kappa}B pathway. *Investigative Ophthalmology & Visual Science* (2011). doi:10.1167/iovs.10-6908
150. Ikeda, M., Ikeda, U., Shimada, K., Minota, S. & Kano, S. Regulation of ICAM-1 expression by inflammatory cytokines in rat mesangial cells. *Cytokine* **8,** 109–114 (1996).
151. Arend, W. P. The balance between IL-1 and IL-1Ra in disease. *Cytokine & Growth Factor Reviews.* **13,** 323–340 (2002).
152. Teoh, S. C. B. *et al.* Tailoring biological treatment: anakinra treatment of posterior uveitis associated with the CINCA syndrome. *British Journal of Ophthalmology* **91,** 263–264 (2007).
153. Botsios, C., Sfriso, P., Furlan, A., Punzi, L. & Dinarello, C. A. Resistant Behçet disease responsive to anakinra. *Annals of Internal Medicine* **149,** 284–286 (2008).
154. Lim, W.-K. *et al.* Suppression of immune-mediated ocular inflammation in mice by interleukin 1 receptor antagonist

administration. *Archives of Ophthalmology* **123,** 957–963 (2005).

155. Stein-Streilein, J. & Taylor, A. W. An eye's view of T regulatory cells. *Journal of Leukocyte Biology* **81,** 593–598 (2006).

156. Li, D. & Taylor, A. W. Diminishment of alpha-MSH anti-inflammatory activity in MC1r siRNA-transfected RAW264.7 macrophages. *Journal of Leukocyte Biology* **84,** 191–198 (2008).

157. Pappu, R., Ramirez-Carrozzi, V. & Sambandam, A. The interleukin-17 cytokine family: critical players in host defence and inflammatory diseases. *Immunology* **134,** 8–16 (2011).

158. Agarwal, R. K. *et al.* Retroviral gene therapy with an immunoglobulin-antigen fusion construct protects from experimental autoimmune uveitis. *Journal of Clinical Investigation.* **106,** 245–252 (2000).

159. Copland, D. A. *et al.* The clinical time-course of experimental autoimmune uveoretinitis using topical endoscopic fundal imaging with histologic and cellular infiltrate correlation. *Investigative Ophthalmology & Visual Science* **49,** 5458–5465 (2008).

160. Chen, M. *et al.* Persistent inflammation subverts thrombospondin-1-induced regulation of retinal angiogenesis and is driven by CCR2 ligation. *The American Journal of Pathology* **180,** 235–245 (2012).

161. Doll, F., Schwager, K., Hemmerle, T. & Neri, D. Murine analogues of etanercept and of F8-IL10 inhibit the progression of collagen-induced arthritis in the mouse. *Arthritis Research & Therapy* **15,** R138 (2013).

162. Pine, R. Convergence of TNFalpha and IFNgamma signalling pathways through synergistic induction of IRF-1/ISGF-2 is mediated by a composite GAS/kappaB promoter element. *Nucleic Acids Research* **25,** 4346–4354 (1997).

163. Dick, A. D., Cheng, Y. F., Liversidge, J. & Forrester, J. V. Immunomodulation of experimental autoimmune uveoretinitis: a model of tolerance induction with retinal antigens. *Eye (Lond)* **8** (Pt 1), 52–59 (1994).

164. Gardner, P. J. *et al.* SIRT1 activation protects against autoimmune T cell-driven retinal disease in mice via inhibition of IL-2/Stat5 signaling. *Journal of Autoimmunity.* **42,** 117–129 (2013).

165. Dick, A. D., Duncan, L., Hale, G., Waldmann, H. & Isaacs, J.

Neutralizing TNF-alpha activity modulates T-cell phenotype and function in experimental autoimmune uveoretinitis. *Journal of Autoimmunity.* **11,** 255–264 (1998).

166. Chan, C.-C. *et al.* Pathology of experimental autoimmune uveoretinitis in mice. *Journal of Autoimmunity.* **3,** 247–255 (1990).
167. Wenzel, A., Grimm, C., Samardzija, M. & Remé, C. E. Molecular mechanisms of light-induced photoreceptor apoptosis and neuroprotection for retinal degeneration. *Progress in Retinal and Eye Research* **24,** 275–306 (2005).
168. Gabriele, M. L. *et al.* Optical coherence tomography: history, current status, and laboratory work. *Investigative Ophthalmology & Visual Science* **52,** 2425–2436 (2011).
169. Wojtkowski, M., Kaluzny, B. & Zawadzki, R. J. New directions in ophthalmic optical coherence tomography. *Optometry & Vision Science* **89,** 524–542 (2012).
170. Fischer, M. D. *et al.* Noninvasive, in vivo assessment of mouse retinal structure using optical coherence tomography. *PLoS ONE* **4,** e7507 (2009).
171. Gadjanski, I. *et al.* Correlation of optical coherence tomography with clinical and histopathological findings in experimental autoimmune uveoretinitis. *Experimental Eye Research.* **93,** 82–90 (2011).
172. Xu, H., Dawson, R., Forrester, J. V. & Liversidge, J. Identification of Novel Dendritic Cell Populations in Normal Mouse Retina. *Investigative Ophthalmology & Visual Science* **48,** 1701–1710 (2007).
173. Van Dop, C. *et al.* ADP-ribosylation of transducin by pertussis toxin blocks the light-stimulated hydrolysis of GTP and cGMP in retinal photoreceptors. *Journal of Biological Chemistry.* **259,** 23–26 (1984).
174. Chen, J., Qian, H., Horai, R., Chan, C.-C. & Caspi, R. R. Use of optical coherence tomography and electroretinography to evaluate retinal pathology in a mouse model of autoimmune uveitis. *PLoS ONE* **8,** e63904 (2013).
175. McMenamin, P. G. & Crewe, J. Endotoxin-induced uveitis. Kinetics and phenotype of the inflammatory cell infiltrate and the response of the resident tissue macrophages and dendritic cells in the iris and

ciliary body. *Investigative Ophthalmology & Visual Science* **36,** 1949–1959 (1995).

176. Avunduk, M. C. *et al.* Etanercept treatment in the endotoxin-induced uveitis of rats. *Experimental Eye Research.* **79,** 357–365 (2004).
177. Rosenbaum, J. T. & Angell, E. Paradoxical effects of IL-10 in endotoxin-induced uveitis. *The Journal of Immunology.* **155,** 4090–4094 (1995).
178. Grimm, D., Kern, A., Rittner, K. & Kleinschmidt, J. A. Novel tools for Production and purification of recombinant Adenoassociated virus vectors. *Human gene therapy* **9,** 2745–2760 (1998).
179. Nakazawa, T. *et al.* Characterization of cytokine responses to retinal detachment in rats. *Molecular Vision.* **12,** 867–878 (2006).
180. Pearson, R. A. *et al.* Restoration of vision after transplantation of photoreceptors. *Nature* **485,** 99–103 (2012).
181. Jayandharan, G. R. *et al.* Activation of the NF-kappaB pathway by adeno-associated virus (AAV) vectors and its implications in immune response and gene therapy. *Proceedings of the National Academy of Sciences.* **108,** 3743–3748 (2011).
182. Lock, M., Alvira, M. R. & Wilson, J. M. Analysis of particle content of recombinant adeno-associated virus serotype 8 vectors by ion-exchange chromatography. *Human Gene Therapy Methods* **23,** 56–64 (2012).
183. Annear, M. J. *et al.* Gene therapy in the second eye of RPE65-deficient dogs improves retinal function. *Gene Therapy* **18,** 53–61 (2010).
184. Novogrodsky, A., Ravid, A., Rubin, A. L. & Stenzel, K. H. Hydroxyl radical scavengers inhibit lymphocyte mitogenesis. *Proceedings of the National Academy of Sciences.* **79,** 1171–1174 (1982).
185. Lei, B., Zhang, K., Yue, Y., Ghosh, A. & Duan, D. Adeno-associated virus serotype-9 efficiently transduces the retinal outer plexiform layer. *Molecular Vision.* **15,** 1374–1382 (2009).
186. Matsumura, N. *et al.* Low-dose lipopolysaccharide pretreatment suppresses choroidal neovascularization via IL-10 induction. *PLoS ONE* **7,** e39890 (2012).

187. Khera, T. *et al.* TNF-mediated macrophage activation in the target organ is critical for clinical manifestation of uveitis. *Clinical & Experimental Immunology* 168(2): 165-177 (2012).

188. Grell, M. *et al.* The transmembrane form of tumor necrosis factor is the prime activating ligand of the 80 kDa tumor necrosis factor receptor. *Cell* **83,** 793–802 (1995).

189. Engelmann, H., Aderka, D., Rubinstein, M., Rotman, D. & Wallach, D. A tumor necrosis factor-binding protein purified to homogeneity from human urine protects cells from tumor necrosis factor toxicity. *Journal of Biological Chemistry.* **264,** 11974–11980 (1989).

190. Beckman, J. S. & Koppenol, W. H. Nitric oxide, superoxide, and peroxynitrite: the good, the bad, and ugly. *American Journal of Physiology.* **271,** C1424–37 (1996).

191. Liu, C. *et al.* Anti-tumour necrosis factor therapy enhances mucosal healing through down-regulation of interleukin-21 expression and T helper type 17 cell infiltration in Crohn's disease. *Clinical & Experimental Immunology.* **173,** 102–111 (2013).

192. Xueyi, L. *et al.* Levels of Circulating Th17 Cells and Regulatory T Cells in Ankylosing Spondylitis Patients with an Inadequate Response to Anti−TNF-α Therapy. *Journal of Clinical Immunology* **33,** 151–161 (2012).

193. Rossol, M. *et al.* Interaction between transmembrane TNF and TNFR1/2 mediates the activation of monocytes by contact with T cells. *The Journal of Immunology.* **179,** 4239–4248 (2007).

194. Eissner, G. *et al.* Reverse Signaling Through Transmembrane TNF Confers Resistance to Lipopolysaccharide in Human Monocytes and Macrophages. *The Journal of Immunology.* **164,** 6193–6198 (2000).

195. Moreau, E., Philippé, J., Couvent, S. & Leroux-Roels, G. Interference of soluble TNF-alpha receptors in immunological detection of tumor necrosis factor-alpha. *Clinical Chemistry.* **42,** 1450–1453 (1996).

196. Dalkara, D. *et al.* In Vivo-Directed Evolution of a New Adeno-Associated Virus for Therapeutic Outer Retinal Gene Delivery from the Vitreous. *Science Translational Medicine* **5,** 189ra76–189ra76 (2013).

197. Gambotto, A. *et al.* Immunogenicity of enhanced green fluorescent protein (EGFP) in BALB/c mice: identification of an H2-Kd-restricted CTL epitope. *Gene Therapy* **7,** 2036–2040 (2000).

198. Stripecke, R. *et al.* Immune response to green fluorescent protein: implications for gene therapy. *Gene Therapy* **6,** 1305–1312 (1999).

199. Kasner, L., Chan, C. C., Whitcup, S. M. & Gery, I. The paradoxical effect of tumor necrosis factor alpha (TNF-alpha) in endotoxin-induced uveitis. *Investigative Ophthalmology & Visual Science* **34,** 2911–2917 (1993).

200. Mohler, K. M. *et al.* Soluble tumor necrosis factor (TNF) receptors are effective therapeutic agents in lethal endotoxemia and function simultaneously as both TNF carriers and TNF antagonists. *The Journal of Immunology..* **151,** 1548–1561 (1993).

201. Robertson, M., Liversidge, J., Forrester, J. V. & Dick, A. D. Neutralizing tumor necrosis factor-alpha activity suppresses activation of infiltrating macrophages in experimental autoimmune uveoretinitis. *Investigative Ophthalmology & Visual Science* **44,** 3034–3041 (2003).

202. Okada, A. A., Sakai, J., Usui, M. & Mizuguchi, J. Intraocular cytokine quantification of experimental autoimmune uveoretinitis in rats. *Ocular Immunology & Inflammation.* **6,** 111–120 (1998).

203. Lacomba, M. S. *et al.* Aqueous and Serum Interferon {gamma}, Interleukin (IL) 2, IL-4, and IL-10 in Patients With Uveitis. *Archives of Ophthalmology.* **118,** 768 (2000).

204. Li, W., Nagineni, C. N., Hooks, J. J., Chepelinsky, A. B. & Egwuagu, C. E. Interferon-gamma signaling in human retinal pigment epithelial cells mediated by STAT1, ICSBP, and IRF-1 transcription factors. *Investigative Ophthalmology & Visual Science* **40,** 976–982 (1999).

205. Schroder, K., Hertzog, P. J., Ravasi, T. & Hume, D. A. Interferon-gamma: an overview of signals, mechanisms and functions. *Journal of Leukocyte Biology* **75,** 163–189 (2004).

206. Cotinet, A., Goureau, O., Hicks, D., Thillaye-Goldenberg, B. & de Kozak, Y. Tumor necrosis factor and nitric oxide production by retinal Müller glial cells from rats exhibiting inherited retinal dystrophy. *Glia*

20, 59–69 (1997).

207. Li, Q. & Verma, I. M. NF-κB regulation in the immune system. *Nature Reviews Immunology* **2,** 725–734 (2002).

208. Beg, A. A., Finco, T. S., Nantermet, P. V. & Baldwin, A. S. Tumor necrosis factor and interleukin-1 lead to phosphorylation and loss of I kappa B alpha: a mechanism for NF-kappa B activation. *Molecular and Cellular Biology* **13,** 3301–3310 (1993).

209. Zeng, H.-Y., Tso, M. O. M., Lai, S. & Lai, H. Activation of nuclear factor-kappaB during retinal degeneration in rd mice. *Molecular Vision.* **14,** 1075–1080 (2008).

210. Jaissle, G. B. *et al.* Bone spicule pigment formation in retinitis pigmentosa: insights from a mouse model. *Graefes Archives of Clinical & Experimental Ophthalmology.* **248,** 1063–1070 (2010).

211. Vance, S. K., Khan, S., Klancnik, J. M. & Freund, K. B. Characteristic spectral-domain optical coherence tomography findings of multifocal choroiditis. *Retina (Philadelphia, Pa.)* **31,** 717–723 (2011).

212. Forooghian, F., Gulati, N. & Jabs, D. A. Restoration of retinal architecture following systemic immunosuppression in birdshot chorioretinopathy. *Ocular Immunology & Inflammation* **18,** 470–471 (2010).

213. Gallagher, M. J., Yilmaz, T., Cervantes-Castañeda, R. A. & Foster, C. S. The characteristic features of optical coherence tomography in posterior uveitis. *British Journal of Ophthalmology.* **91,** 1680–1685 (2007).

214. Doyle, S. L. *et al.* IL-18 attenuates experimental choroidal neovascularization as a potential therapy for wet age-related macular degeneration. *Science Translational Medicine* **6,** 230ra44 (2014).

215. Couturier, A. *et al.* Anti-vascular endothelial growth factor acts on retinal microglia/macrophage activation in a rat model of ocular inflammation. *Molecular Vision.* **20,** 908–920 (2014).

216. McMenamin, P. G. & Crewe, J. M. Cellular localisation and dynamics of nitric oxide synthase expression in the rat anterior segment during endotoxin-induced uveitis. *Experimental Eye Research.* **65,** 157–164 (1997).

217. Rageh, A. *et al.* In Vivo Scoring of the Endotoxin-Induced Uveitis Model using Optical Coherence Tomography: Comparison with Fundus Imaging and Histology. *Investigative Ophthalmology & Visual Science* E–Abstract 2876 (2014).

218. Ko, M. K., Saraswathy, S., Parikh, J. G. & Rao, N. A. The role of TLR4 activation in photoreceptor mitochondrial oxidative stress. *Investigative Ophthalmology & Visual Science* **52,** 5824–5835 (2011).

219. Prashker, D. & Wardlaw, A. C. Temperature responses of mice to Escherichia coli endotoxin. *British Journal of Experimental Pathology.* **52,** 36–46 (1971).

220. Annear, M. J. *et al.* Gene therapy in the second eye of RPE65-deficient dogs improves retinal function. *Gene Therapy* **18,** 53–61 (2011).

221. Sonoda, K.-H. *et al.* The analysis of systemic tolerance elicited by antigen inoculation into the vitreous cavity: vitreous cavity-associated immune deviation. *Immunology* **116,** 390–399 (2005).

222. Roncarolo, M.-G., Battaglia, M. & Gregori, S. The role of interleukin 10 in the control of autoimmunity. *J. Autoimmun.* **20,** 269–272 (2003).

223. Marlow, G. J., van Gent, D. & Ferguson, L. R. Why interleukin-10 supplementation does not work in Crohn's disease patients. *World Journal of Gastroenterology.* **19,** 3931–3941 (2013).

224. Rott, O., Fleischer, B. & Cash, E. Interleukin-10 prevents experimental allergic encephalomyelitis in rats. *European Journal of Immunology.* **24,** 1434–1440 (1994).

225. Cannella, B., Gao, Y. L., Brosnan, C. & Raine, C. S. IL-10 fails to abrogate experimental autoimmune encephalomyelitis. *Journal of Neuroscience Research.* **45,** 735–746 (1996).

226. Liu, X. *et al.* The T cell response to IL-10 alters cellular dynamics and paradoxically promotes central nervous system autoimmunity. *The Journal of Immunology* **189,** 669–678 (2012).

227. Agarwal, R. K. *et al.* Abrogation of anti-retinal autoimmunity in IL-10 transgenic mice due to reduced T cell priming and inhibition of disease effector mechanisms. *The Journal of Immunology..* **180,** 5423–5429 (2008).

228. Groux, H., Bigler, M., de Vries, J. E. & Roncarolo, M. G. Inhibitory and stimulatory effects of IL-10 on human CD8+ T cells. *The Journal of Immunology.* **160,** 3188–3193 (1998).

229. Pauza, M. E., Neal, H., Hagenbaugh, A., Cheroutre, H. & Lo, D. T-cell production of an inducible interleukin-10 transgene provides limited protection from autoimmune diabetes. *Diabetes* **48,** 1948–1953 (1999).

230. Marotte, H. & Cimaz, R. Etanercept - TNF receptor and IgG1 Fc fusion protein: is it different from other TNF blockers? *Expert Opinion in Biological Therapeutics* **14,** 569–572 (2014).

231. Tynjälä, P., Lindahl, P., Honkanen, V., Lahdenne, P. & Kotaniemi, K. Infliximab and etanercept in the treatment of chronic uveitis associated with refractory juvenile idiopathic arthritis. *Annals of the Rheumatic Diseases* **66,** 548–550 (2007).

232. Busch, M. *et al.* Effects of systemic and intravitreal TNF-α inhibition in experimental autoimmune uveoretinitis. *Investigative Ophthalmology & Visual Science* **54,** 39–46 (2013).

233. Faure, V., Hecquet, C., Courtois, Y. & Goureau, O. Role of interferon regulatory factor-1 and mitogen-activated protein kinase pathways in the induction of nitric oxide synthase-2 in retinal pigmented epithelial cells. *Journal of Biological Chemistry.* **274,** 4794–4800 (1999).

234. Fusco, A. J. *et al.* NF-κB p52:RelB heterodimer recognizes two classes of κB sites with two distinct modes. *EMBO Reports.* **10,** 152–159 (2008).

235. Rachakonda, P. S., Rai, M. F. & Schmidt, M. F. G. Application of inflammation-responsive promoter for an in vitro arthritis model. *Arthritis & Rheumatism* **58,** 2088–2097 (2008).

236. Paterna, J. C., Moccetti, T., Mura, A., Feldon, J. & Büeler, H. Influence of promoter and WHV post-transcriptional regulatory element on AAV-mediated transgene expression in the rat brain. *Gene Therapy* **7,** 1304–1311 (2000).

237. Wahlsten, J., Gitchell, H., Chan, C. C., Wiggert, B. & Caspi, R. Fas and Fas Ligand Expressed on Cells of the Immune System, not on the Target Tissue, Control Induction of Experimental Autoimmune

Uveitis. *The Journal of Immunology.* **165,** 5480–5486 (2000).

238. Fujimoto, C. *et al.* Pertussis Toxin Is Superior to TLR Ligands in Enhancing Pathogenic Autoimmunity, Targeted at a Neo-Self Antigen, by Triggering Robust Expansion of Th1 Cells and Their Cytokine Production. *The Journal of Immunology.* **177,** 6896–6903 (2006).

239. Lucas K *et al.* Retinal laser burn-induced neuropathy leads to substance P-dependent loss of ocular immune privilege. *The Journal of Immunology*. **189**(3): 1237-42 (2012).

12 Published papers

Chu CJ, Barker SE, Dick AD & Ali RR.

Gene Therapy for Noninfectious Uveitis

Ocular Immunology and Inflammation (2012) 20(6), 394–405.

Chu CJ, Herrmann P, Carvalho LS, Liyanage SE, Bainbridge JWB, Ali RR, Dick AD & Luhmann UFO

Assessment and *In Vivo* Scoring of Murine Experimental Autoimmune Uveoretinitis Using Optical Coherence Tomography.

PLoS ONE (2013) 8(5): e63002.